The Anodic Behaviour of Aluminium Alloys in Alkaline Solutions

A thesis presented for the degree of

Doctor of Philosophy in Chemical Engineering

at the University of Canterbury

Christchurch, New Zealand

By

D.J.McPhail

January, 1993

Acknowledgements

Throughout this work many people have given me help and encouragement for which I am eternally grateful.

I would like to thank my supervisor Associate Professor W.B.Earl for his time, assistance and guidance. The many hours of fruitful discussion and the occasional "cracking of the whip" provided the stimulus required to complete this work.

Thanks are also due to the Comalco Research Centre, Melbourne, Australia whose financial support and supply of aluminium alloys made this work possible.

To all the members of the technical staff of the chemical and process engineering department, my expressed thanks; for without your help many of the "hills" would have been "mountains".

I am very grateful to Dr. John Smaill of the mechanical engineering department for arranging the metallurgical testing of some of the aluminium electrodes, and for the many hours of valuable discussion.

I would also like to thank the technical staff of the mechanical engineering department, who carried out the metallurgical testing on some of the electrodes.

Many thanks to all my friends and colleagues, who have supported, encouraged and helped me throughout this learning adventure.

Last, but not least, I would like to thank my parents, who have not only financially assisted me in times of hardship, but have supported me in all that I have done.

If a little knowledge is dangerous,
where is the man who has so much as
to be out of danger ?

T.H.Huxley (1825 - 95)

Table of Contents

Abstract

The electrochemical behaviour of aluminium in alkaline solutions, with small amounts (<0.1wt%) of indium, magnesium and gallium as alloying constituents, and the identification of the parameters that will most effect an operating Al / air battery system have been investigated. The alloys investigated were suggested by Comalco Research Laboratories, Melbourne and had the following analysis:

Pure Aluminium (better than 99.995%)
Al - 0.046%Ga
Al - 0.067%Ga
Al - 0.110%Ga
Al - 0.1%Mg - 0.1%In
Al - 0.016%In
Al - 0.045%In
Al - 0.10%In
Al - 0.1%Mg
Al - 0.085%In - 0.09%Ga

It has been found that the peak potential, using the fast cut technique, is independent of indium concentration for indium alloys of less than 0.1%In, and that the reaction kinetics for the aluminium dissolution at the peak potential change as the aluminate concentration in the alkaline solution is increased.

The steady state potential shows a logarithmic relationship to the indium content of the binary alloys and this showed that there is little advantage in using an indium content of greater than 0.04%.

The flowcell experiments showed that the indium containing alloys become coated with a black film, and that onset of significant polarization coincided with the disappearance of this film. X-ray analysis has confirmed that both indium and gallium concentrate on the reaction surface during polarization.

This work has shown the ternary Al - 0.1%Mg - 0.1%In alloy to be the best from those tested. The magnesium in the alloy has been shown to refine the electrode grain structure and to significantly reduce the parasitic corrosion rate.

The effects of aluminate accumulation in the electrolyte on polarization were measured and increasing the flowrate and temperature have been shown to increase the maximum current density attainable.

Chapter.1 - Introduction

1.1 General

Aluminium is the most plentiful metal available to man, occurring as aluminium oxide in an ore called bauxite. The most common method of aluminium production is via the Heroult-Hall process. This process involves the electrolytic reduction of the aluminium oxide using carbon anodes to form molten aluminium, carbon monoxide and carbon dioxide.

Thermodynamically, aluminium is a very energy intensive material, with a gibbs free energy of formation for the Al^{3+} ion of -485 KJ/mol, and a theoretical energy density of 8.1 kWh/kg. Aluminium has a face centred cubic structure, a low density (2.7 g/cm^3), with standard electrode potentials (versus SHE) of -1.662 V in acid solutions, and -2.33 V in alkaline solutions. Despite the protective oxide layer which is inherent on aluminium, it is subject to severe corrosion if solution pH is above 8 or below 5 @ 25°C (67).

Aluminium is widely used as a construction material, especially in the aircraft industry, but is to soft and weak in its pure state. It is alloyed with various elements (Cu, Mg, Mn, Si , etc) to give it strength and durability under physical loading, and has become pre-eminent as a conductor of electricity. The electrical conductivity of aluminium is approximately 65% that of copper on a volume basis.

1.2 Review of Previous work

1.2.1 Aluminium / Aluminium alloys in acid to neutral solutions

Most of the early work (1 - 12, 21 - 23) carried out on aluminium has been done in acid solutions, due to the ease with which the oxide layer is removed. Earl & Hagyard (1) showed that using a fast cut technique, in which a fresh aluminium surface is exposed to an electrolyte, the theoretical aluminium potential can be measured directly. It was shown that the peak potential obtained immediately after cutting, showed that the aluminium is in equilibrium with its ions in aqueous solution. Further these workers showed that the peak potential was independent of pH in solutions of pH < 5. The subsequent decay in potential to a mixed potential is due to the onset of the hydrogen evolution reaction.

Other workers (4,6,7,20) have studied the role of various cations and anions on the dissolution behaviour of aluminium, with the chloride ion being of particular importance with respect to the breakdown of the oxide film. Garreau et al (4) showed that adding perchlorate to solutions which normally damage aluminium, protected the metal from further damage. Khedr & Lashien (20) studied the effect of depositing transition / heavy metal cations on the aluminium surface in chloride containing solutions. These workers found that at low cation concentration inhibition of the corrosion reaction is observed, but at high concentrations, the galvanic coupling effects accelerated the corrosion. Pitting corrosion near the metal deposits was observed. They found that the addition of the binary mixtures of chromate - benzotriazole and chromate - sulfanilic acid to the solution showed synergistic inhibition, stopping the dissolution of aluminium. The chromate ion repairs the oxide film defects and strongly adsorbs on to the electrode surface.

The theoretical potential - pH diagrams for the aluminium - water system proposed by Pourbaix have been extended by Macdonald & Butler (8) and Brook (5) to elevated temperatures. The most significant point concerning this work is the increased stability range of the aluminate ion with increasing temperature, with the decreased domain of the aluminium ion. The diagram below (taken from Brook (5)) illustrates these points.

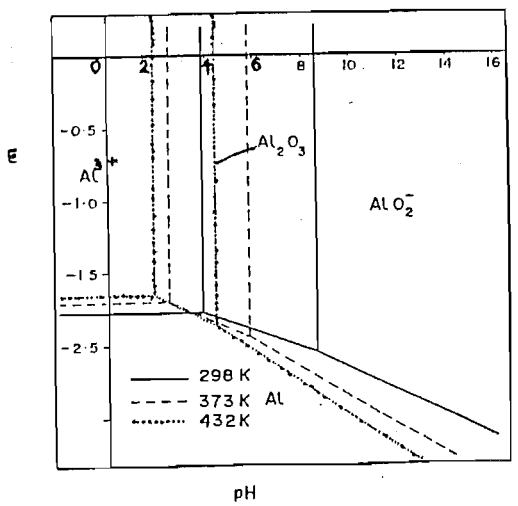

Potential-pH diagram for the Al-H_2O system. Concentration of soluble species 10^{-6}M.

Fig.1

More recently workers (21 - 26) have investigated the use of alloying components such as indium, magnesium, mercury, etc, to decrease the polarisability of aluminium. Cheng (3) found that the addition of indium and magnesium to the lithium - aluminium electrode in a LiCl-KCl euteutic electrolyte caused the electrode to have a more dendritic surface, which resulted in a higher lithium utilization.

Some of the earliest work using alloys to improve the anodic behaviour (decrease the polarization) of aluminium was carried out by Keir et al (21,22). These workers found that the aluminium - tin alloy gave the best results as a sacrificial anode of the group IV elements when galvanicly coupled to a mild steel cathode in 0.1N NaCl.

This alloy also exhibited potentials more negative than -1.0V v.s SHE, with a very low oxide resistivity which has been attributed to the Sn^{4+} ion entering the oxide, thus creating cation vacancies. These workers then investigated several ternary alloys based on the aluminium - tin binary alloy. The classes of metals added to the binary aluminium - tin alloy were considered in three groups, those that expand the aluminium lattice (Bi,Zr,Mg and Ag), which stabilizes the aluminium - tin solid solution; those that contract the lattice (Si,Zn,Cu and Mn), thus rejecting tin from solid solution; and those that have no effect on the lattice (Co,Ni,Fe and As), as they are generally insoluble in aluminium. The main result from their work was that the lattice expanders either increase dissolution (e.g. Bismuth increases the galvanic current) or have little or no effect on the galvanic current that flowed when coupled to the mild steel cathode.

Several workers (23 - 25) have investigated the aluminium - indium, - thallium, - gallium, and - phosphorous binary alloys in salt solutions. Despic et al (23) used indium, gallium and thallium in binary and ternary alloys with aluminium, testing the alloys in neutral $1Mol.l^{-1}$ NaCl at 25°C. Their work showed that these alloys caused:
(1) a shift in the rest potential in the negative direction,
(2) an increase in the workable current density (i.e. an increase in the current density attainable for a specific overpotential) and
(3) a decrease in the Negative Difference Effect (NDE) as compared to pure aluminium.
[The NDE is the linear increase in the rate of hydrogen evolution with increasing dissolution current density.]

The alloys, except for gallium, decreased the rate of corrosion in the neutral salt solution. These workers found the NDE to depend strongly on the electrolyte concentration and cation species present, but was independent of pH (over the range 1.4 - 11).

Mance et al (25) investigated the effect of indium and thallium as binary additions to high purity and technically pure (99.5%) aluminium in sea water. They found that the anodic dissolution rate by alloying with technically pure aluminium was considerably worse than by alloying with super pure aluminium. They also found that increased corrosion along grain boundaries was unavoidable in alloys used in the as-cast state, due to segregation of alloying elements to the grain boundary. This resulted in the use of an annealing process at about 560°C, which produces a more uniform dissolution, by decreasing the amount of segregation present. The addition of thallium to aluminium had little effect on the electrochemical properties, which is due to thallium's insolubility in

aluminium. There is however a marked difference when thallium is added to the aluminium - indium alloy, which is attributed to thallium's solubility in indium.

These same workers (24) then investigated the effect of gallium and phosphorous alloys in NaCl solution. They found, like other workers, that the gallium alloys had high corrosion rates, but this can be decreased by the addition of phosphorous. The corrosion rate, whilst being effected by the alloying additions, is also affected by the insoluble intermetallic compounds which contain both alloying components and impurities.

1.2.2 Aluminium / Aluminium alloys in alkaline solutions

The use of alkaline solutions not only gives aluminium a more negative electrode potential, but also improves the performance of the air cathode (53), compared to using acid solutions. There is still however significant hydrogen production via the parasitic corrosion reaction on the aluminium electrode.

Many workers (13 - 20) have investigated the properties of aluminium in alkaline solutions, while others (27 - 34) have reported the effects of alloying components on the electrochemical behaviour in alkaline solutions.

A stepwise dissolution model has been proposed by Macdonald et al (17) for aluminium in 4M KOH @ 25°C, which requires the stepwise addition of hydroxyl ions to the surface, until aluminium hydroxide is formed, which finally chemically reacts to form aluminate. This anodic process competes with the cathodic hydrogen evolution reaction for surface sites. Analysis of the impedance data gave transfer coefficients of <0.1 for the elementary charge transfer reactions, which is possible for very reactive species like aluminium and the hydroxyl ion. The Macdonald mechanism is supported by Plumb & Swain (14) who found that at $pH < 12.4$ the electrode potential depended on the aluminate concentration and pH, but with $pH > 12.4$ the electrode potential is determined by the direct reaction between the hydroxyl ions in solution and the metal ions from the metal.

Heusler et al (16) has also investigated the dissolution kinetics of aluminium in alkaline solutions, and showed that the dissolution rate of aluminium increases with increasing flow velocity, and is proportional to the hydroxide ion concentration.

Koshel et al (18) investigated the electrode kinetics of aluminium with varying solution temperature. These workers showed that the electrode kinetics were weakly dependent on flow velocity (1.4 - 15.9 cm/s), which was said to show the existence of a dynamic protective film on the metal surface, and that the anodic dissolution current density and corrosion rate increase with temperature. The anodic dissolution rate was found to have a maximum for a KOH concentration between 7 - 9 mole / litre.

Work by Brown & Whitley (27) supported assertions by Heusler that a metal surface free of oxide or hydroxide cannot be obtained in alkaline solutions. These workers attributed the fall in aluminium dissolution rate, and rise in hydrogen evolution rate with decreasing electrode potential, to a thinning and hydration of the oxide layer.

Even though most workers have tried to reduce the amount of gasing (i.e. H_2 production) when aluminium is placed in alkaline solutions, there has been some interest (15) in aluminium as a hydrogen source. It was found, that if aluminium were to be used as a hydrogen source, it was best in atomized powder form, providing as high a surface area as possible, with a purity no greater than 99.8%.

An important result from this work was that the regeneration reaction of hydroxyl ions (below) is the limiting factor in the overall long term hydrogen production rate.

$$NaAl(OH)_4 \text{ --------> } Al(OH)_{3\,(s)} + NaOH$$

The fact that this regeneration step limits the hydrogen production reaction, makes this method of hydrogen generation impractical as a possibility for use in a fuel cell.

Aluminium in its pure state is unacceptable for use in most battery systems, thus workers turned to low level alloying in an attempt to try to reduce the parasitic corrosion which takes place, whilst trying to reduce the polarization occurring on aluminium.

Most workers (27 - 34) have found that the most promising alloys were those that contained indium in solid solution in hydroxide electrolytes at elevated temperatures. Macdonald et al (31) carried out an in depth study of several possible alternative battery anode alloys, with a view to reducing the corrosion rate under open circuit conditions. Using 4M KOH @ 50°C these workers measured the following corrosion rates:

Table .1 Comparison of possible anode alloys

Alloy	O.C.P * (mV Hg/HgO)	Corrosion Rate ($mg/cm^2/min$)	Corrosion Rate (mm/yr)
Al - 99.99%	-1678	0.515	1002
Zn	-1400	0.0014	1
Al -0.1%In -0.2%Ga-0.1%P -0.01%Tl	-1750	0.058	113
Al - 0.1%In	-1740	1.965	3825
Al - 0.1%Bi	-1840	0.593	1154

(From Macdonald et al (31))

* O.C.P = open circuit potential

The above table clearly shows how the aluminium potential can be shifted in the negative direction by various alloys. The addition of indium alone, whilst making the rest potential much more negative, increases the corrosion rate. By higher order alloying the corrosion rate can be made an order of magnitude lower than that of pure aluminium and still maintain the more negative rest potential.

Even though these workers have shown bismuth to give a more negative potential than the indium alloy, and to have a corrosion rate equivalent to that of pure aluminium, no further work has been published concerning bismuth.

These results are encouraging, but for an electrode to be considered as a replacement for zinc in a primary battery it would need to have a corrosion rate of at least the same order of magnitude.

These workers also investigated the effect of cold working, and have shown there to be little effect on the corrosion rate, except for the Al - 0.5%Ga alloy which showed a minimum at 50% cold worked.

The polarization data for several alloys in 4M KOH @ 25,50 and 80°C has been presented by Macdonald et al (19,28,32). They showed aluminium to exhibit passivity in concentrated potassium hydroxide solution at 25 and 50°C, with an active to passive transition being evident at 25°C. At potentials more positive than the open circuit potential they found the current / potential curve to be almost linear. The low level alloying components (In, Ga, Tl, Mn and Mg) were found to produce a passivating protective layer on the aluminium. Activation of the alloys occurred when this layer had been oxidised into soluble products; for example those alloys containing gallium become active at the potential which corresponds to gallium going into solution as $Ga(OH)_4^-$. The alloying elements inhibit the hydrogen evolution by decreasing the exchange current density for the cathodic reaction.

The diagram below shows that activation / passivation mechanism that has been put forward by Macdonald. The passive state (A) shows aluminium dissolution to be solely due to the parasitic corrosion reaction in the no load condition. The passive to active transition (B) occurs when the alloying element (M), which helps form the protective surface film, is oxidised. Thus the active state (C), for the significantly polarised electrode, shows both aluminium and the alloying element(s) passing into solution. This mechanism supports the existence of an oxide / hydroxide layer on the electrode, showing the final dissolution step to be chemically controlled. The active to passive transition (D), which occurs as polarization decreases, is due to the alloying element(s) either plating out of solution onto the aluminium surface, or remaining on the electrode surface as aluminium further dissolves.

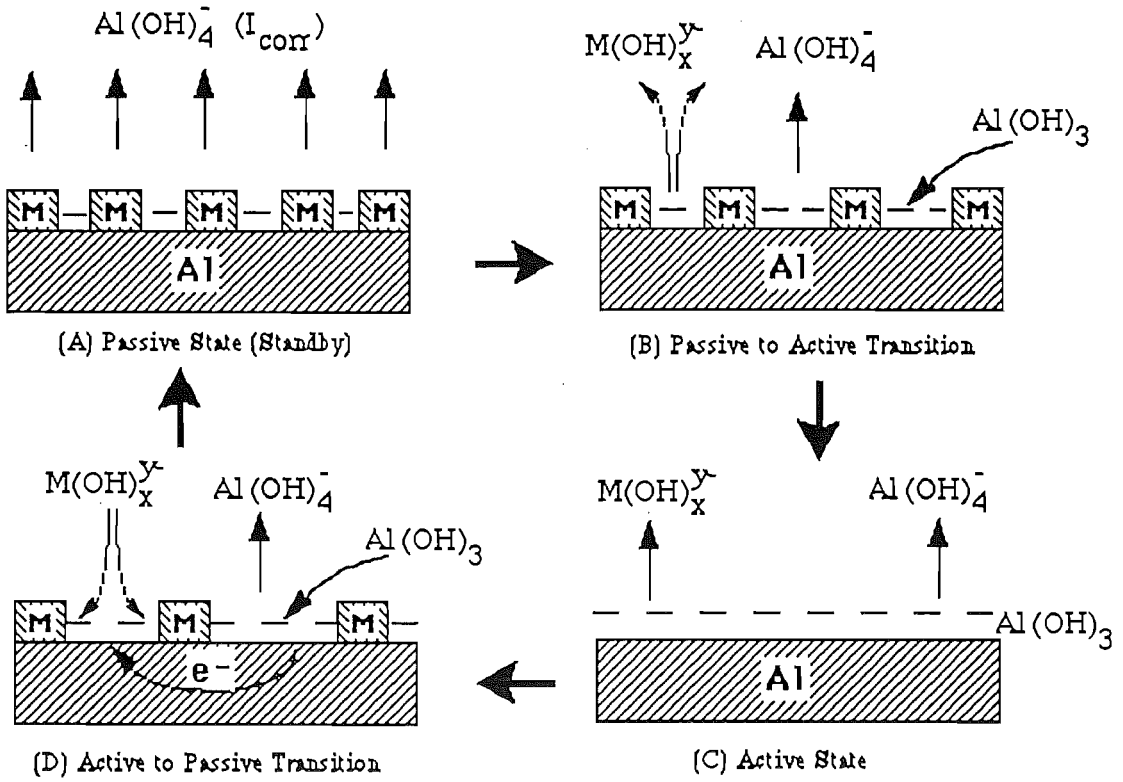

Schematic Model of events that occur on the activation and deactivation of an aluminium alloy anode

Fig.2
Macdonald et al (32)

Macdonald has proposed that the effect of the minor alloying elements in reducing the no load corrosion rate is not strongly dependent on the composition of the bulk alloy, but more to the presence of the alloying elements, which form the passive film. This is supported by the findings of Pickering et al (75,76) for the dissolution of binary alloys.

Jeffrey & Halliop (34) carried out some optimization experiments in 4M NaOH at 60°C, for the aluminium -indium -magnesium -manganese alloy, and also investigated the effect of adding stannate to the electrolyte. They found that using a base aluminium of 99.995%, that their preferred alloy was Al -0.05%In -0.1%Mg -0.03%Mn.

Aluminium - manganese and aluminium - manganese - magnesium alloys have a high resistance to corrosion. Manganese forms sub-microscopic particles, but also some large particles, $Al_6(Mn,Fe)$ and $Al_{12}(Mn,Fe)_3Si$. Both of these larger particles have solution potentials equal to that of the solid solution matrix. Manganese also forms intermetallic compounds with iron which are less active from a hydrogen evolution standpoint, hence increasing the coulombic efficiency. Magnesium also reduces the rate of hydrogen evolution, but is less effective than manganese.

They found that the alloys containing gallium, with or without tin, benefitted from the presence of stannate in the electrolyte, which reduced corrosion. These workers, as well as Macdonald, proposed that magnesium and manganese present in the indium - activated alloys further reduces the parasitic corrosion.

Some recent work has been carried out by Hunter (33) using aluminium-indium, aluminium-gallium and aluminium-tin binary alloys,and several ternary alloys. He found that the aluminium-indium alloys exhibited the NDE, and suggested an alloy dominance regime,where one of the alloying components for ternary and higher order alloys dominates the polarization characteristics (i.e. shows behaviour similar to that of the dominant binary alloy). The dominance ordering suggested from this work, which relates to the melting points of the elements and their theoretical mobilities, is tin > indium > gallium.

Hunter identified two active states for the alloys, firstly the superactive state, where the alloy is more active than pure aluminium, and secondly the hyperactive state, which is an extremely active electrochemical condition, attributed to the formation of gaseous hydrides on the reaction surface. Hyperactivity was found to exist only for alloys in dilute concentrations which form hydrides at potentials above the Al / Al^{3+} reversible potential, e.g. In, Sn, Si, C, Cd, Zn, etc. Hunter's assertions of alloy dominance and of the hyperactive state have not yet been confirmed by other workers.

1.2.3 Influence of Solution Modification

Several workers (35 - 44) have investigated the possibility of modifying the solution parameters to obtain the same effect as when alloying aluminium, but more importantly to reduce the parasitic corrosion rate.

Bockstie et al (44) carried out some of the earliest work on corrosion inhibition of aluminium in caustic solutions. Their work showed several fundamental facts; corrosion can be accelerated by addition of S^{2-} or SH^- ; corrosion can be inhibited via surface amalgamation (i.e. zinc deposition), especially zinc oxide - saturated solutions and / or alkyldimethyl- benzylammonium salts; and that corrosion is reduced at high anodic current densities. The zinc oxide reacts to give a layer of zinc on the aluminium surface, but this tends to flake off with continual immersion.

Roebuck & Pritchett (37) investigated different aspects of corrosion inhibitors for aluminium; (1) chemical classification, organic or inorganic; and (2) surface reactivity, adsorption types or surface reaction types. The general results of their work showed that the inorganic inhibitors help to reform the damaged oxide layer, whereas the organic inhibitors tend to either polarize the cathodic reaction or form a protective layer by adsorption onto the metal surface via polar linkage. These workers found that the choice of cationic species can also have a dramatic effect, e.g. the corrosion rate in sodium chromate was 13 times higher than in magnesium chromate solution.

Several other worker (38 - 42) have investigated the inhibition of varying grades of aluminium in modified alkaline solutions. Sarangapani et al (42) showed that a 4N NaOH electrolyte with 0.4% calcium oxide and 20% sodium citrate (base electrolyte) gave the best inhibition efficiency over other electrolytes containing these additives plus different cations. They found that some additives which formed anions in solution, when added to the base electrolyte could further inhibit the corrosion on 2S (>99%) aluminium, e.g. aluminium and zinc.

Paramasivam et al (41) investigated different grades of aluminium and different levels of zinc oxide added to 4N NaOH solution. They found that the 3S (98.7%Al, 1.2%Mn) and 57S (97.5%Al, 2%Mg, 0.25%Mn) alloys were best suited as anode materials, with 4N NaOH containing 0.6M zinc oxide as the best electrolyte.

The same aluminium grades as for (41) were investigated by Albert et al (39) in alkaline citrate solution. These workers found the 57S aluminium to be the most promising anode in 4N NaOH with 20% sodium citrate and 2.5%wt / vol $CaCl_2.2H_2O$.

The use of polymer chlorides has been investigated by Hirai et al (40), these were found to inhibit the cathodic reaction by increasing the double layer thickness of polymer cations. The two polymers investigated were polyvinylbenzyltrimethyl-ammonium chloride (PVBA) and polydiallyldimethylammonium chloride (PDDA).

Cathodic inhibition by these polymers gave a negative shift in the corrosion potential, with a reduction in corrosion current to about 5 mA / cm^2 .

There has been some work (36,43) carried out using some of the alloying elements (In,Zn,Ga) as electrolyte additives, to investigate whether they produce similar effects to when they are in the metal alloy. Böhnstedt (43) has used gallium and indium ions in 7N KOH solution, with an Al - 0.5%Mg electrode at 60°C. He has shown that some ions (Zn,Sn,Pb,B) have little to no effect on the rest potential, whereas others (Tl,As,Sb) significantly shift the potential in a negative direction. The more important ions (Hg,In and Ga) are those that shift the entire current - potential curve in the negative direction.

Gallium ions showed the most distinguishable difference from the pure solution, which can be seen in figures 3 and 4 below. The addition of 1g Ga / l results in an approximately 250 mV shift in the rest potential and an improvement in polarization characteristics. The addition of the same quantity of indium only gave a 100mV shift. It is however clear that the hydrogen evolution rate increases with increasing gallium content. This work showed similar results to those of Hunter (33), i.e. gallium concentrates at the grain boundary, resulting in the grain boundary areas being enlarged, thus increasing the effective surface area, which causes a shift in the current - potential curve.

Burri et al (36) has carried out work similar to that of Böhnstedt, but added indium and zinc into a weakly acidic sodium chloride solution, with pure aluminium test electrodes. The results of their work showed that adding indium chloride and zinc chloride to the electrolyte caused a 300 mV negative shift in rest potential, and an increase in the faradaic efficiency to approximately 95% at a pH of 2 - 3 .

The next step in the study of solution modification was to investigate the aluminium alloys in inhibited and uninhibited solutions. Macdonald & English (35) have tested two quaternary alloys in solutions containing SnO_3^{2-} , $In(OH)_3$, BiO_3^{3-}, $Ga(OH)_4^-$ and MnO_4^{2-} . There were two significant results from this work. At high discharge rates (400 mA / cm^2) both K_2MnO_4 and Na_2SnO_3+$In(OH)_3$ are effective inhibitors, but at low discharge rates only the potassium permanganate is effective and still maintains good coulombic efficiency over uninhibited solution.

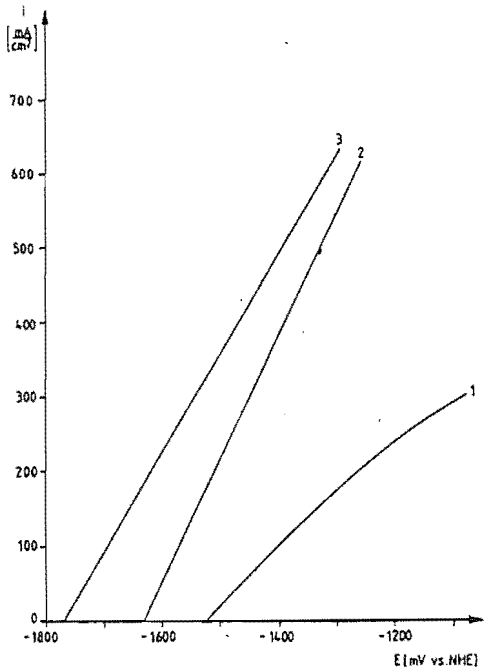

Anodic polarization curves for aluminum electrodes in different electrolytes: (1) 7N KOH, (2) 7N KOH + 1 g In^{3+}/l, (3) 7N KOH + 1 g Ga^{3+}/l. Electrode: Al 99.9 alloyed with Mg 0.5%. Temperature: 60 °C. Scan rate: 10 mV/s.

Fig.3
Böhnstedt (43)

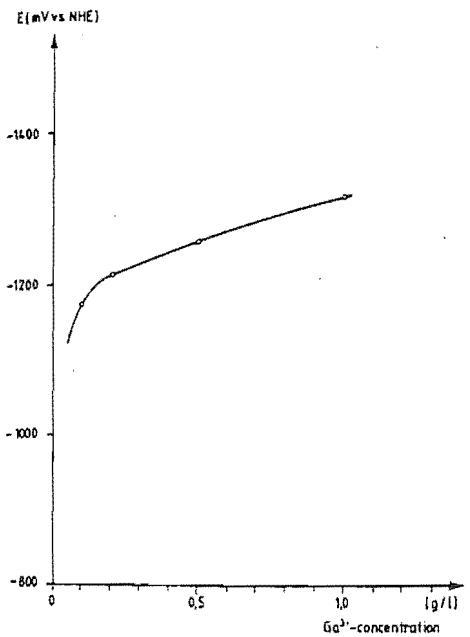

Potential of Al 99.9 alloyed with Mg 0.5% electrode under load 600 mA/cm^2. Temperature: 60 °C. Electrolyte: 7N KOH + Ga^{3+} addition.

Fig.4
Böhnstedt (43)

1.2.4 Al / Air Battery technology

There are literally hundreds of different battery systems available today, but only a few have incorporated aluminium anodes into them. Aluminium has always been an extremely favourable anode material, given its high electrochemical potential and low equivalent weight, which produces a theoretical energy density of 8.1 kWh/kg Al. Aluminium would be an ideal anode material if it did not produce such a stable oxide film and undergo parasitic corrosion. There have been attempts (55) to replace zinc in the Zn / C and Zn / MnO_2 cells with aluminium, but these have only had limited success, mainly due to the self corrosion of the aluminium.

The initial range of Al / air batteries were for general use, based on a sea-water electrolyte, but in 1986 Alcan (63) started the development of an Al / air battery for standby / reserve applications, which could replace diesel - powered generators in emergency situations. This latest development provided greater than 360 Wh/kg Al (62).

Apart from Alcan's intensive work on the Al / air system there has been much interest from other workers (45 - 63). Zaromb (48) and Zaromb & Foust (46) carried out some of the earliest work on the alkaline Al / air system. Zaromb (48) proposed that the best replacement for zinc is an alkaline aluminium primary battery using a 3M KOH self - regenerating electrolyte for a greater than 1kW load. He suggests the use of a porous-carbon or even better a porous- nickel air cathode, along with the use of some corrosion inhibitors in the electrolyte, and elimination of corrosion accelerators such as sulphides.

The feasibility of electrolyte regeneration was the subject of (46), given the reactions:

Cell reaction

$$Al + 3/4\,O_2 + OH^- + 1/4\,H_2O \text{ -----> } Al(OH)_4^- \qquad \text{(reaction 1.1)}$$

Regeneration reaction

$$Al(OH)_4^- \text{ ------> } Al(OH)_3 \text{ (solid)} + OH^- \qquad \text{(reaction 1.2)}$$

The main requirement for a cell operating under regeneration conditions is that reaction 1.2 occurs at a sufficiently fast rate to maintain the bulk hydroxide ion concentration.

These workers found that most previous current drain experiments with self - regeneration were impeded by the buildup of $Al(OH)_3$ reaction product near the 'Al' electrodes, thus proving that reaction 1.2 occurs at a sufficiently fast rate. By improving

the anode design and collecting the $Al(OH)_3$ in an electrolyte recycle system, these workers showed that their cell could obtain 3 times the discharge of a cell without regeneration.

Chen & Savinell (56) have recently modelled the Al - air cell in caustic solution, developing an algorithm, which includes a kinetic expression for not only the cathodic and anodic reactions, but the parasitic corrosion reaction as well. Other effects such as mass transfer, gas evolution, migration, etc have also been included in their model.

Blurton & Sammells (53) have reviewed the most promising metal / air cells and summarised the possible systems into two categories, the non-rechargeable and the rechargeable cells. Lithium, aluminium and magnesium occur in the first, with various zinc and iron cells in the second. The zinc and iron cells, whilst being easily produced and controlled, have energy densities of less than half that of the lithium and aluminium cells. Magnesium appears to have no advantage over aluminium, and lithium appears unlikely to show any commercial application according to these workers.

The table below has been taken from Scamans(49) which compares various theoretical properties of prospective metals for metal / air cells.

Table .2 Comparison of metal / air cell systems

Metal	Electrochemical equivalent (Ah / g)	Theoretical cell voltage * (V)	Theoretical specific energy (Wh / g)	Operating voltage (V)
Li	3.86	3.4	13	2.4
Al	2.98	2.7	8.1	1.6
Mg	2.20	3.1	6.8	1.4
Ca	1.34	3.4	4.6	2.0
Zn	0.82	1.6	1.3	1.2
Fe	0.96	1.3	1.2	1.0

* cell voltage with oxygen cathode

Scamans (49) points out that the specific energy and power density of a cell depends largely on which electrolyte is used, in saline solution both low specific energy (220 Wh/kg) and low power density (30 W/kg) can be expected, whereas the alkaline Al / air system developed by Alcan (63) has a specific energy of 4200 Wh/kg. The huge difference in specific energy is due to the use of highly caustic solution compared to a mildly acid saline solution.

A basic representation of the Al / air cell is given in figure.5 below taken from (49), showing the aluminium anode, which may or may not be alloyed, and the air cathode, which is permeable to the oxygen in air, but not to the electrolyte.

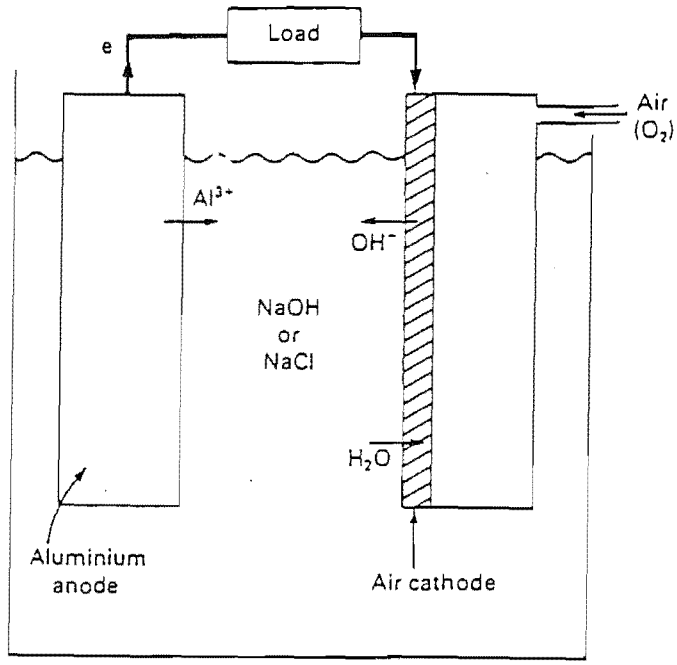

Net reaction: $4Al + 6H_2O + 3O_2 \rightarrow 4Al(OH)_3$

Schematic of a simple aluminium/air cell

Fig.5

Scamans (49)

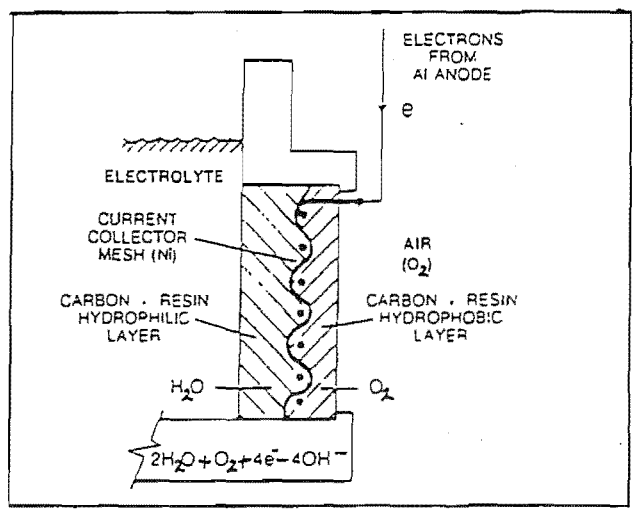

Principles of the Air Cathode

Fig.6

Fitzpatrick et al (50)

The principles behind the cathode are shown in figure .6 above from (50), which shows the cathode to be a carbon resin, but it could also be made from porous nickel.

Mosley (52) has reviewed the aluminium / air fuel cell with respect to its development and applicability to use in private cars. The two diagrams below have been taken from this work. Figure.7 shows the fuel life - cycle comparison between that of the internal combustion engine and that of the aluminium / air fuel cell. The aluminium / air fuel cell cycle shows the advantages of being recyclable and environmentally cleaner. Figure.8 shows the aluminium / air process replacement of the internal combustion engine.

Some of the problems which have arisen from this system are :

(1) Improving the efficiency and lowering the manufacturing cost of the aluminium alloy anodes,

(2) Improving the reliability and lowering costs of the air cathodes,

and (3) Development of a crystalliser to operate within the volume constraints of a vehicle.

The efficiency of the anodes have been increased by alloying magnesium and manganese with the aluminium. The manganese is thought to form intermetallic compounds with the iron impurity present in the aluminium, which have a lower hydrogen overpotential than the bulk alloy. The current density for normal driving conditions is approximately 1 - 2 KA/m^2 (100 - 200 mA/cm^2).

The cathodes presently available have equivalent lifetimes of 2 - 3 years, and are either steam - activated carbon blacks, or activated carbons, with a cobalt tetra methoxy phenyl porphyrin.

A reliable crystalliser is still the essence to successful cell operation. It has been reported that one has been developed by workers at Lawrence Livermore Laboratories (57), but due to commercial sensitivity little is known of it.

Problems which have not yet been fully solved are, the deposition of hydrargillite on fuel cell manifolds and pipework, and the plating out of tin from the stannate corrosion inhibitor onto valves and pipework. It is possible that the first problem might be solved by the use of a coating that the aluminium hydroxide can adhere to. The second problem might be overcome by the use of modern plastics technology.

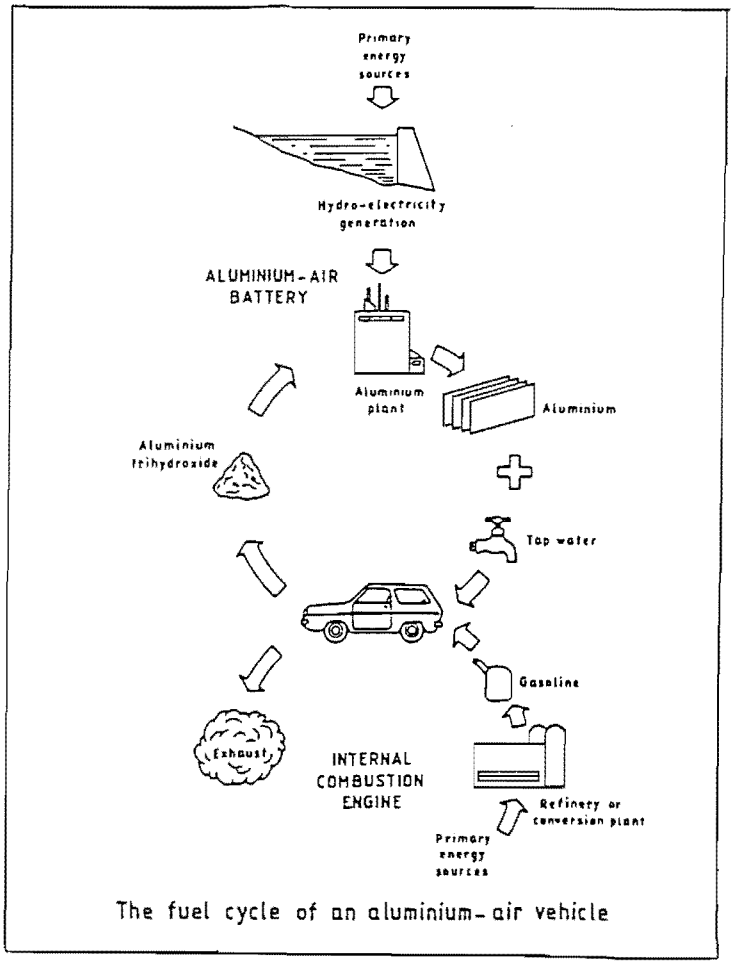

The fuel cycle of an aluminium-air vehicle

Fig.7
Mosley (52)

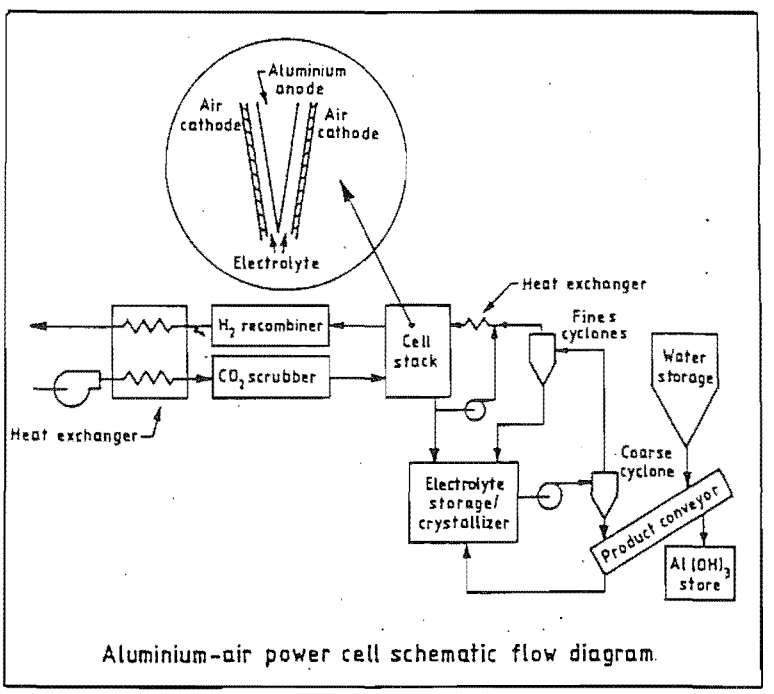

Aluminium-air power cell schematic flow diagram.

There are three independent circulation flows: (1) incoming air enters cell stack after CO_2 removal, preheating, and humidifying, (2) cell-stack-electrolyte circulation loop goes through a heat exchanger to remove excess heat from system, and (3) cell-crystallizer exchanger flow goes through particle-size separation devices for final hydrargillite product removal and removal of most of the particles from the electrolyte before return to cell.

Fig.8
Mosley (52)

Despic et al (47) have developed a large - capacity medium - power (24 W) saline aluminium - air battery. This battery consists of two - 10 cell packs, which has aluminium-gallium-tin-magnesium anodes, and a capacity of 2590 Ah, with an open circuit voltage of 13.4V. They found that the reaction product tended to clog between plates after long periods of discharge, and sometimes needed to be mechanically removed.

Alupower (a subsidiary of Alcan aluminium) has designed a saline Al / air battery pack (58), which operates at 6V and 2.5A (15W).

British Telecom contracted Alcan International in November 1986 to build an Al /air battery that could be used as an emergency supply, this needed to supply 600 W of electricity continuously over 48 hours. The battery system that was developed (59), showed one Al / air battery to produce over 36 kWh of energy, replacing the lead - acid battery back-up system of 24 batteries producing 32 kWh.

1.3 Aluminium Alloys

The main alloying elements that have been used to modify the electrochemical behaviour of aluminium are indium, magnesium, gallium, thallium, manganese and tin The binary phase diagram for each of the alloying elements will be presented in this section, followed by a short discussion on the general properties of the alloy, with particular attention given to alloying at low levels (<0.2%).

Gallium, indium and Thallium are all group III elements with a +3 oxidation state; magnesium a group II element has a +2 oxidation state. Tin is a group IV element with +4 and +2 oxidation states. Manganese is a transition element with stable oxidation states of +7,+6,+4,+3, +2.

Al - indium

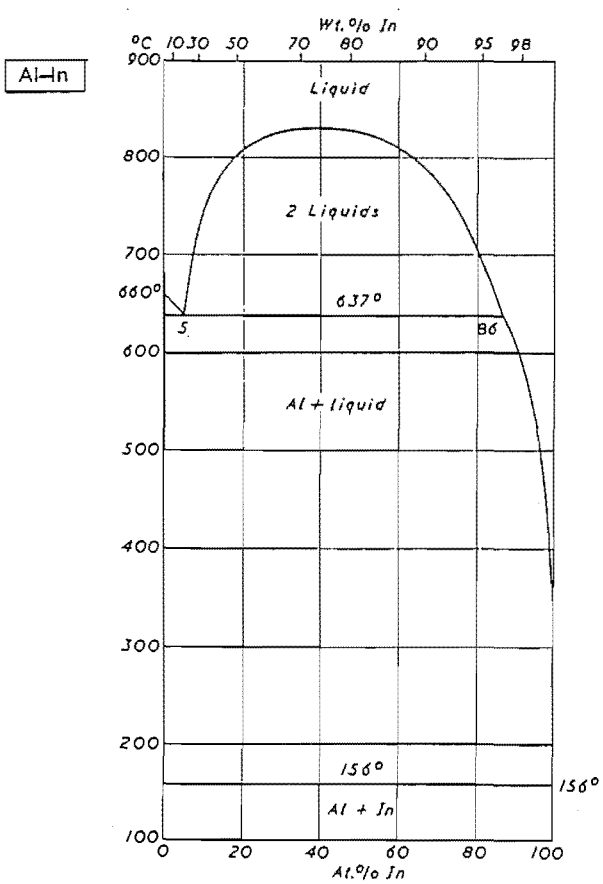

Indium, a soft silvery - white metal, has an atomic number of 49, atomic weight of 114.82, and a melting point of 156.61°C.

The binary phase diagram given left (68), shows indium to be insoluble in the face centred cubic Al - solid solution. It has been found (70), that the maximum amount of indium that can be present in solid solution is 0.045 at% In. This diagram also shows that very little aluminium dissolves into high percentage indium alloys.

The Al - In system shown, is characterised by the immiscible liquid phases below the critical point, the monotectic reaction of Al with the two liquids, and the eutectic reaction where the In - rich phase solidifies to give solid aluminium and solid indium.

Al - Magnesium

Magnesium is a light , silvery - white and tough metal. It has an atomic number of 12, atomic weight of 24.305 and a melting point of 649 °C .

The binary phase diagram (below) shows that magnesium is soluble in aluminium forming an α – phase, which contains 1.9wt% Mg at 100 °C. The phase diagram becomes reasonably complex for the 35 - 67.7 wt% Mg region, but this is not relevant for this work.

Al - Manganese

Manganese has an atomic number of 25, an atomic weight of 54.938, and a melting point of 1244 °C.

The binary phase diagram (below) shows the Al-Mn system to be very temperature and composition sensitive. This diagram shows that the maximal equilibrium solubility of manganese into aluminium to be approximately 1.4wt%. By using very rapid quenching of the melt, a supersaturated solid solution with a manganese content as high as 9.2 wt% is possible.

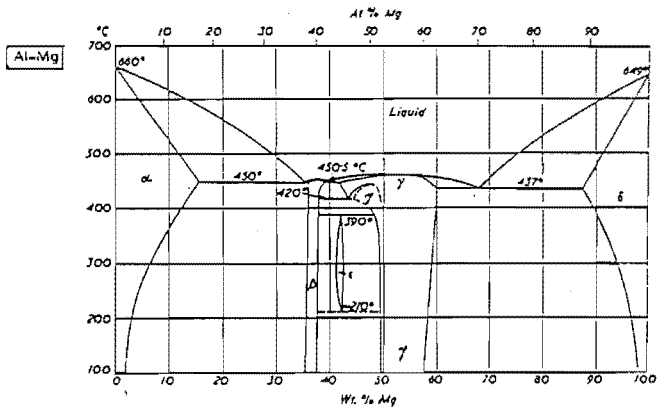

Al - Gallium

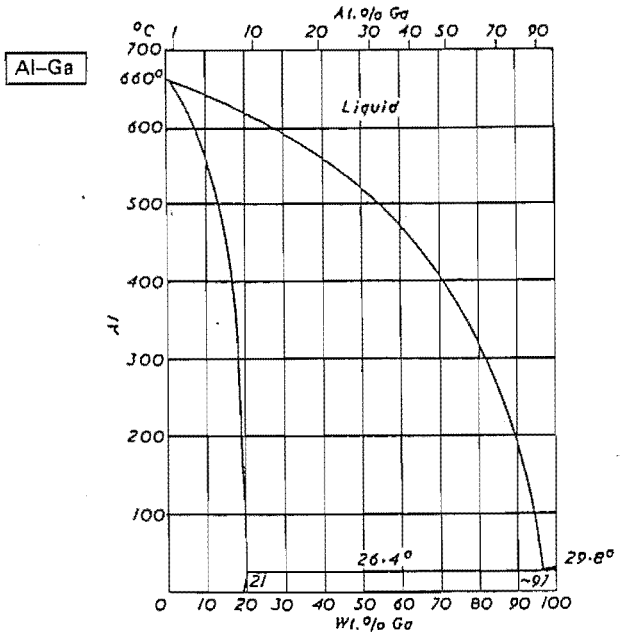

Gallium has an atomic number of 31, an atomic weight of 69.737, and melting point of 29.78 °C.

The Al - Ga binary phase diagram left, shows gallium to be soluble in aluminium upto a maximum of 21 wt% at 26.4 °C. However the solubility of aluminium in gallium is very low.

It has been reported in (71) that the lattice parameters for an Al - 0.53 at% Ga alloy were practically the same as those of pure aluminium.

Al - Thallium

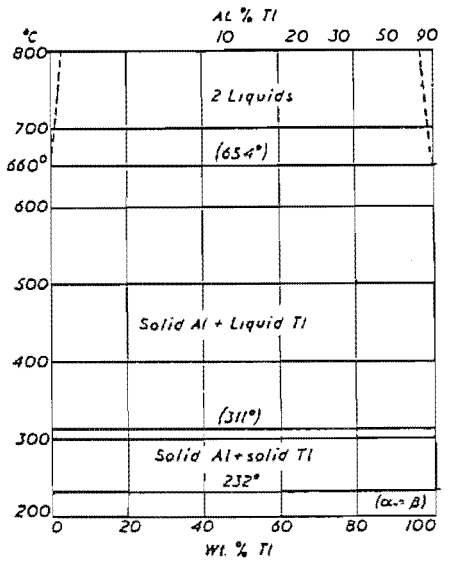

Al-Tl

Thallium has an atomic number of 81, an atomic weight of 204.37, and a melting point of 303.5 °C. This metal is very soft and malleable, showing a metallic luster when freshly exposed to air , but quickly develops a bluish - grey tinge.

Aluminium and Thallium are entirely insoluble in each other, which is supported by the fact that the melting points of either Al or Tl are not affected by additions of the other component.

Al - Tin

Tin has an atomic number of 50, an atomic weight of 118.69, and a melting point of 231.9681 °C.

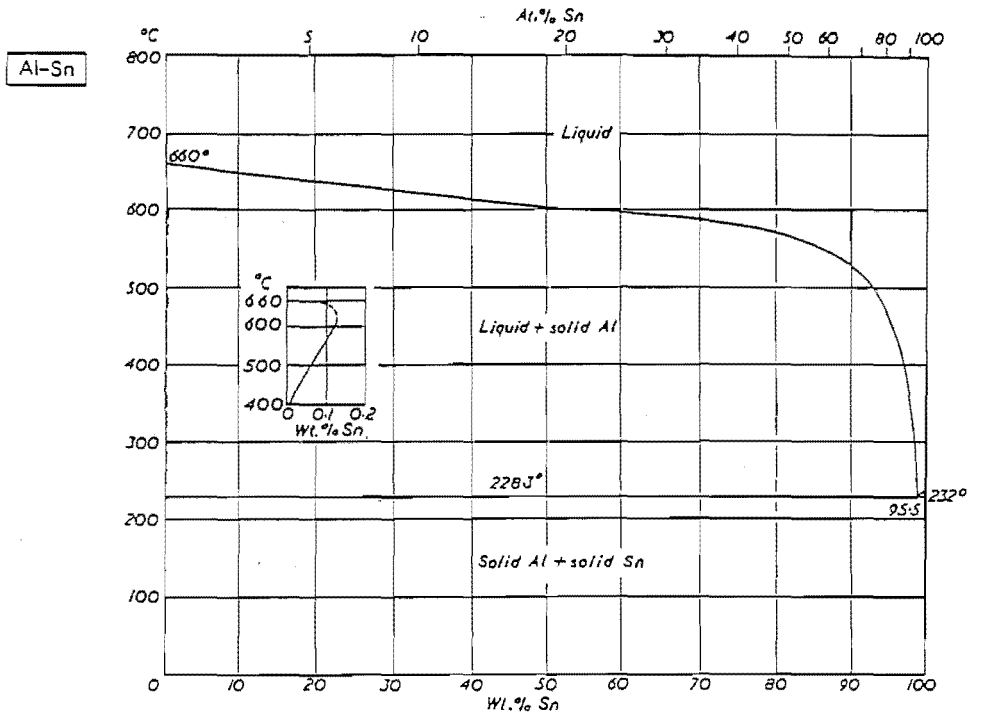

The solid solubility of tin in aluminium is very low, but from the above diagram a maximal amount of approximately 0.14% Sn at 650 °C is possible, which would give a supersaturate solid solution at room temperature if rapidly quenched. Likewise, it is evident from the above diagram, that aluminium is also insoluble in tin.

Chapter.2 - Experimental

2.1 General

The experimental techniques used for this research have been based on techniques already developed within this department. Developments or modifications of any technique are discussed in the appropriate section.

The technique used for the fast cut work follows that of Hagyard and Williams(2), and later modified by Earl (1,9,10). The flowcell was initially designed from the work carried out by Kirkpatrick (11).

All potentials are reported with respect to the hydrogen scale, unless otherwise stated, and have generally been corrected for the solution IR drop. The IR drop due to solution resistance was measured using the current interupt method, as outlined in (66).

The fast cut work was carried out using the saturated calomel electrode as the reference electrode, seperated from the cell via a salt bridge and cellophane membrane. The reference electrode used for the flow cell experiments was the mercury / mercuric oxide electrode.

Experimental outline:

The experimental program can be divided into two sections, that using the fast cut technology (Hagyard & Williams(2), Earl (1,9,10)), and that using a development of the Kirkpatrick flowcell (11) to operate at elevated temperatures.

The fast cut work was restricted to investigating various alloys at room temperature under no load conditions, in highly alkaline solutions, with and without aluminate. The aim of these experiments was to measure the anode activation characteristcs for a freshly created metal surface (i.e. oxide free surface).

The flow cell which more closely emulates an operating battery, was used to obtain polarization curves for the alloys, for varying temperatures, flow rates and solutions. This section serves two purposes, (1) to identify how a prospective battery anode will operate under load, and (2) to test the predictive ability of the fast cut work for operating anodes.

Alloys:

All the aluminium and aluminium alloys in this work were supplied by Comalco Research Centre, Melbourne, Australia, with the base aluminium having a purity of better than 99.99%.

Analysis of the alloys supplied by Comalco showed the main impurites to be in the following ranges:

Si < 0.01%

Fe < 0.01% - 0.0003% (min)

Cu < 0.01% - 0.0017% (min)

Other impurities such as Cr,Mn,Ti,Zr, etc are present at < 0.005% and in most cases < 0.002%.

The alloys as supplied were:

(1) Super Pure Aluminium (better than 99.99%)

(2) Al - 0.016% In

(3) Al - 0.045% In

(4) Al - 0.10% In

(5) Al - 0.046% Ga

(6) Al - 0.067% Ga

(7) Al - 0.110% Ga

(8) Al - 0.1% Mg

(9) Al - 0.1% Mg - 0.1% In

(10) Al - 0.085%Ga - 0.09%In

The aluminium samples had been cast into molds held at 200°C, then allowed to cool.

The electrodes were machined out of this material, using a lathe and a tungsten - carbide tool. The electrodes were then placed in their holders and submitted to an acetone reflux to remove any grease and dirt.

Electrolytes:

All electrolytes were prepared using " Analar " grade reagents dissolved in distilled water. For the fast cut solutions no pre - electrolysis was thought necessary, which is supported by work carried out by Earl (9,10) and Watson (12). Watson showed that after increasing the impurity level to many times that normally found, that there was no observable effect on the potential or mean kinetic parameters.

The aluminate solutions were prepared by dissolving super pure aluminium in the hydroxide solutions, and adding extra hydroxide to allow for that used in the dissolution, thus maintaining the required hydroxide concentration. Dissolution is via the parasitic corrosion reaction below.

$$Al + OH^- + H_2O \text{ -------> } AlO_2^- + 3/2\, H_2 \qquad \text{(reaction.2.1)}$$

The hydroxyl ion concentration of the solutions were checked via standard titration (Vogel (78)), whilst the aluminate concentrations were checked using EDTA titration (Vogel (79)).

2.2 Fast Cut Cell

The experimental layout of equipment (similiar to that of Earl (10)) is shown in fig 2.1. The oscilloscope shown in fig 2.1 is a " Hewlett - Packard" 1740A (100 MHz), and the frequency generator an "Exact" model 7030 generator. The cathode follower fig 2.3 was redesigned using modern circuitry, and shown to have a rise time roughly equivalent to that of Earl's of 0.1 μsec and input impedance > 10^{12} Ω .

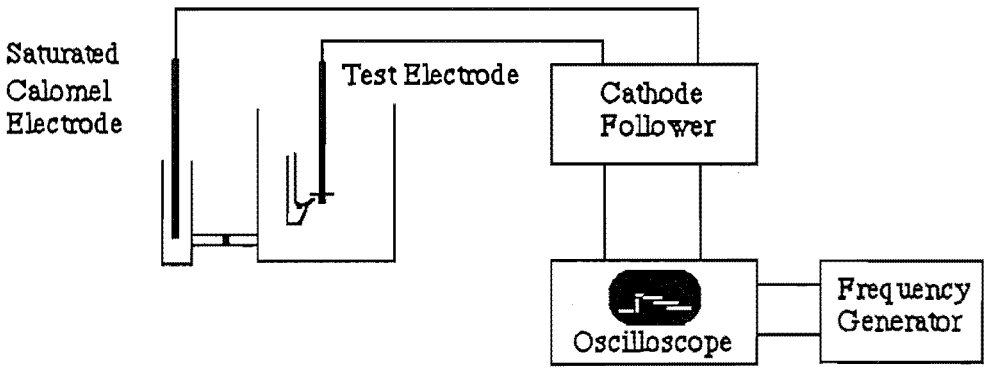

Fig.2.1 Fast Cut Equipment Layout

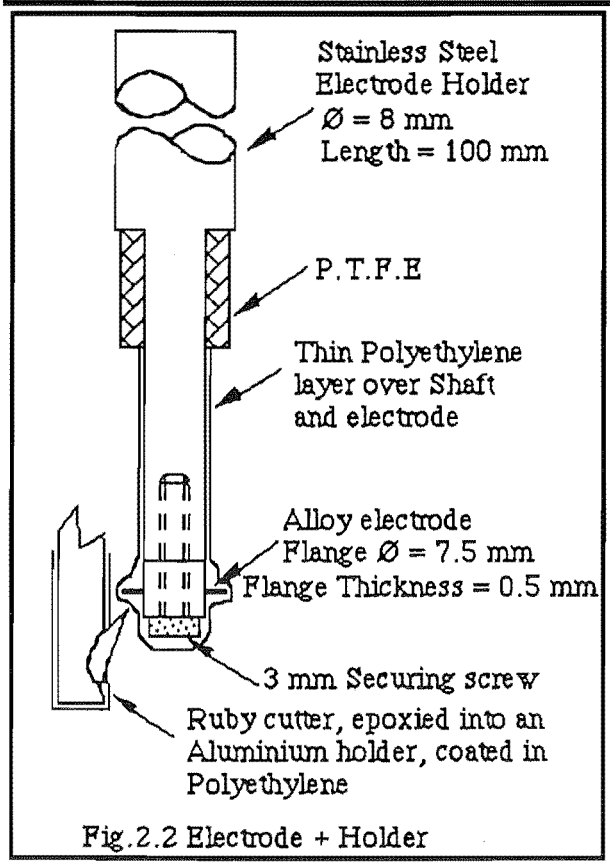

Fig.2.2 Electrode + Holder

The electrode and electrode holder Fig 2.2 are similiar to that used by Earl (9). The alloy electrode was threaded so that it could be firmly attached to the holding screw that is then screwed tightly onto the holder shaft. The thread provides better electrical contact between the electrode and the electrode holder.

After acetone degreasing the electrode and holder are heated to approximately 120°C, then covered in polythene powder and placed back into the oven to allow the powder to fuse onto the metal surface. This process is carried out several times until the electrode and holder are sufficiently coated with polythene .

Polythene was found in earlier work (80) to be the most appropriate material to coat the electrode.

The electrode is driven past the ruby cutter into the solution, creating a fresh metal surface.

Cathode Follower (rise time 0.1 μs, impedance $>10^{12}\Omega$)

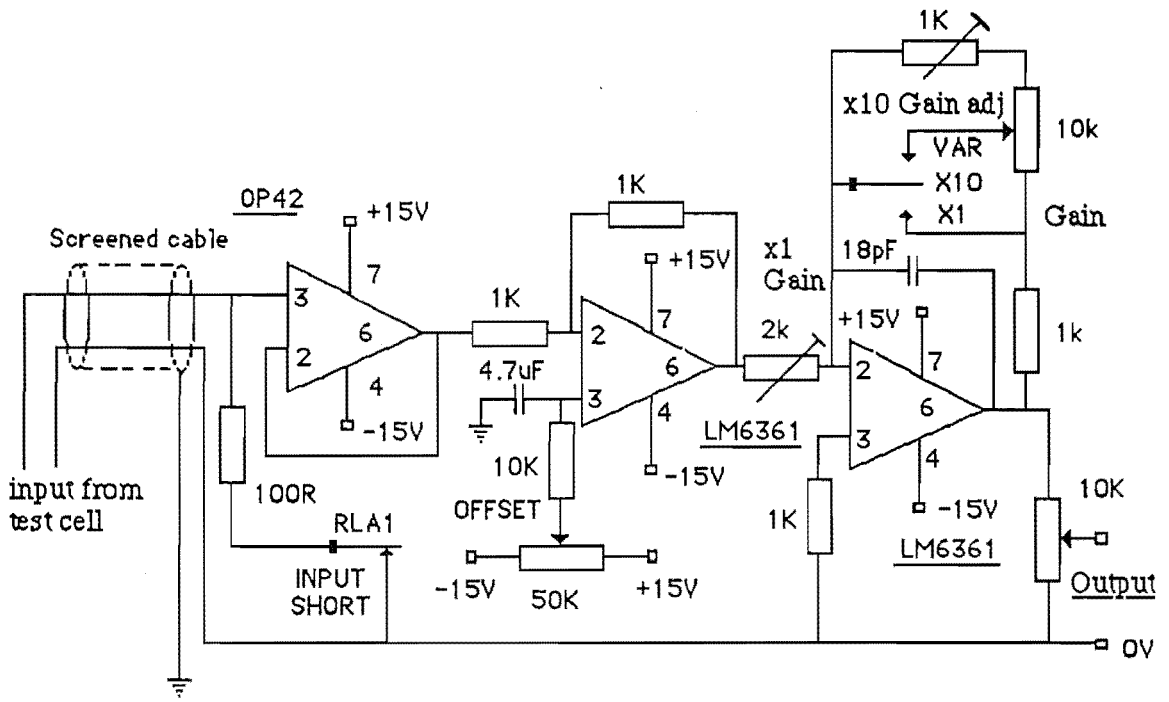

Fig 2.3

The cathode follower as represented in the above circuit diagram, fig 2.3, is a device that tracks the potential change of the freshly cut electrode. A trigger debouncer was also used to avoid double triggering due to vibrations or stray electrical pulses at cut initiation, thus once the trigger has been activated it must then be reset via the relay switch.

2.3 Flow cell

The flowcell design, fig 2.5, was based on Kirkpatrick's (11) earlier work, with major improvements specifically for this work. The experimental conditions for this work involved using solutions of 1- 6 M KOH at temperatures as high as 80 ^{0}C. The equipment layout is shown below in fig 2.4 .

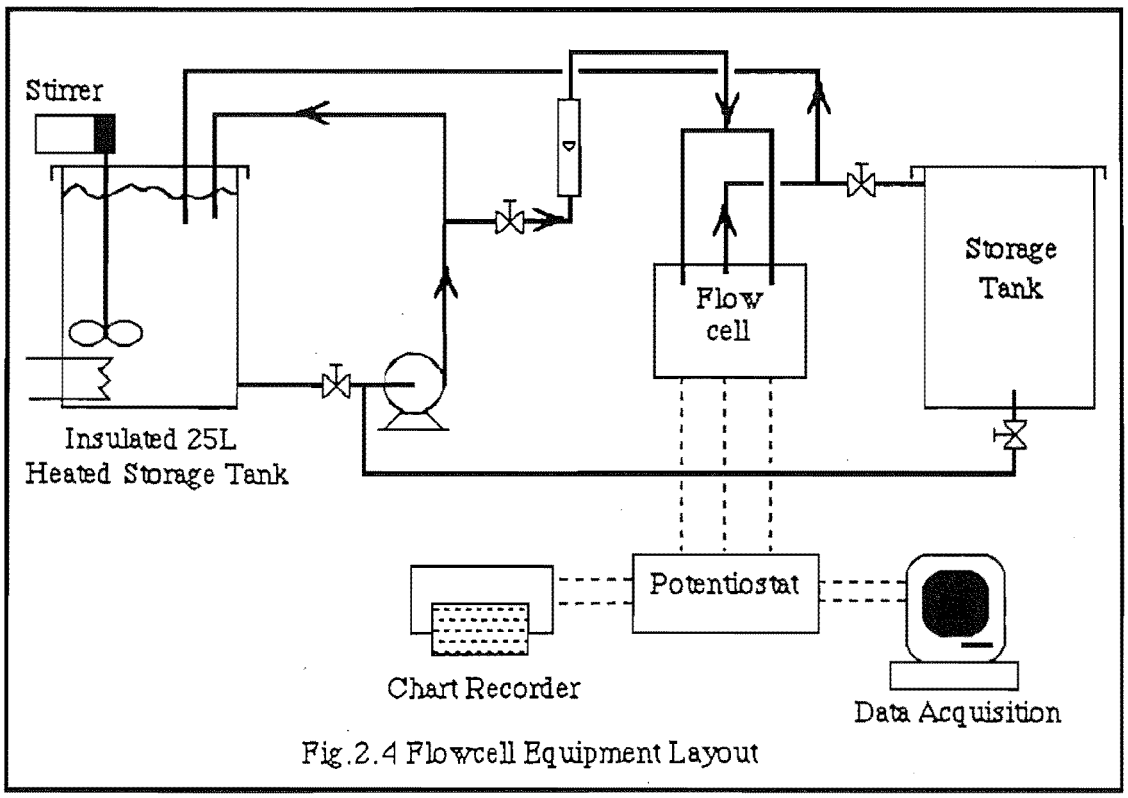

Fig.2.4 Flowcell Equipment Layout

The solution is heated in a stirred 25 L insulated polypropylene tank, and then pumped via a " March " model AC - 3D - MD magnetically coupled pump around the system. Most of the solution is recycled back to the heated tank directly, with a drawoff leg controlling the required amount of solution to the cell, which is metered via a " Gemü " 855 / 20 - 400 l / h rotameter. The solution once past the flowcell is recycled back to the heated tank. A " EG & G Princeton Applied Research " model 362 scanning potentiostat is used to polarise the electrodes both potentiostatically and galvanostatically, with data acquisiton via a " Strobes " signal acquisition system model 901, which is coupled to a Mackintosh Plus computer model M0001 AP. The chart recorder, a " Graphtec " servocorder SR6312, supplies a continuous hardcopy of the potential and current throughout the experiment.

Some advantages of the flowcell (fig 2.5) used in this work over that originally made by Kirkpatrick (11) are:

(1) It is a composite structure made to withstand the hydroxide solutions upto 80°C.

(2) The rate at which the electrode is raised could be varied in this work to maintain the dissolving electrode surface parallel with the flow profile, whereas it remained constant in the Kirkpatrick flowcell.

(3) The lower part of the outlet tube (part (1.1)) is threaded, so that allowances for expansions and contractions of the cell at different temperatures can be made. This means the electrode - outlet gap is relatively constant for all experiments.

(4) Rubber O-rings are used in many places in the flowcell, giving more effective seals, than in the Kirkpatrick design.

(5) A capillary connection so that a reference electrode may be used, was also implemented.

The entire flowcell system has been made so that the only metal in contact with the solution is the electrode under examination, and the platinum counter electrode.

As the electrode can be made an appropriate length to allow for the high current densities used and advanced as the electrode dissolves, the flowcell can be operated for longer periods as could a conventional rotating disc electrode system.

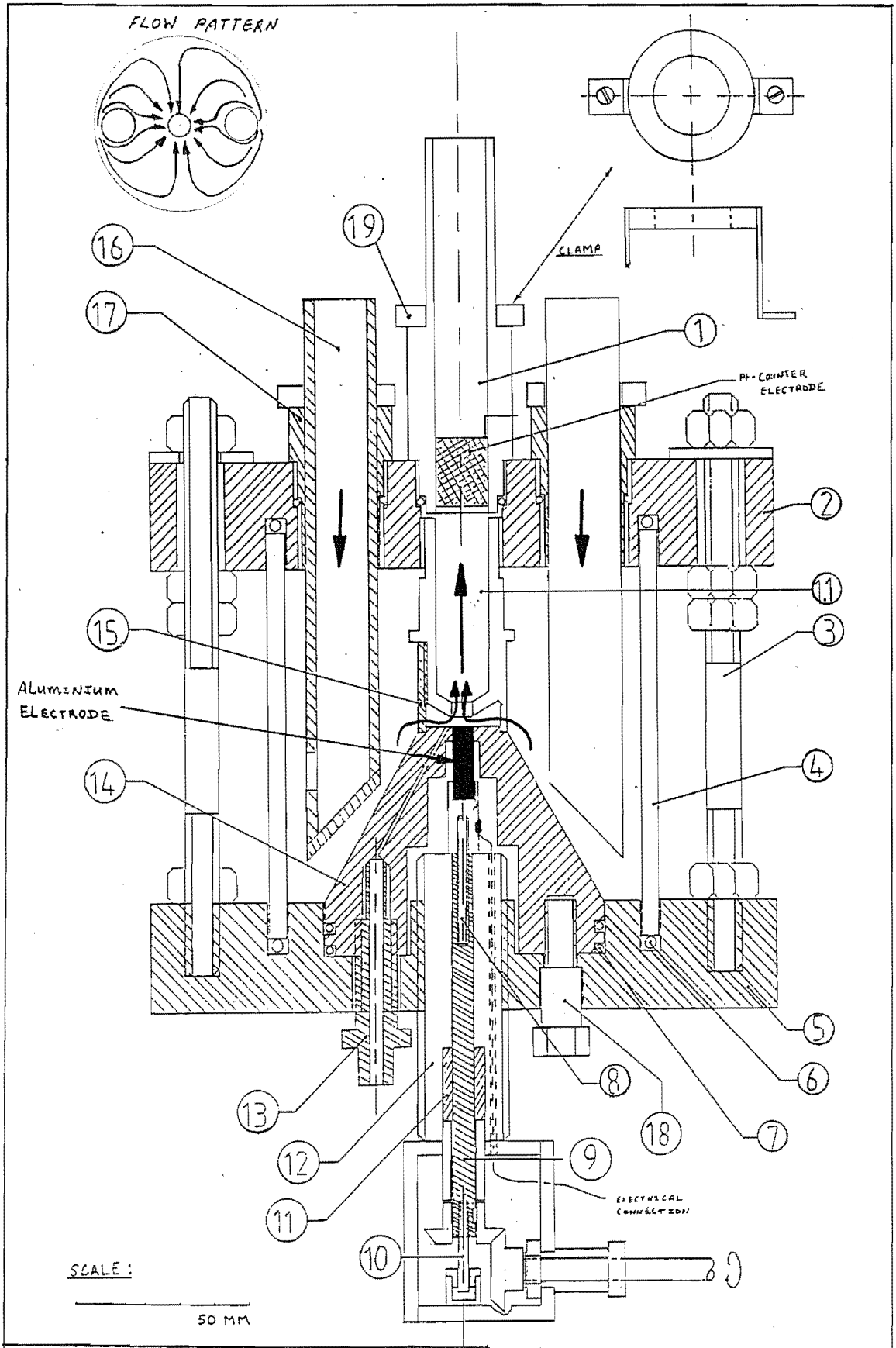

Parts List:	
1 - ABS outlet tube	10 - electrical connection
2 - ABS cell cap	11 - brass bush
3 - S/Steel cell supports	12 - PTFE mounting screw
4 - Perspex cell wall	13 - ABS connection
5 - PVC cell bottom	14 - PTFE cell base
6 - O-Ring	15 - ABS flow aligner
7 - O-Ring	16 - ABS inlet tube
8 - electrode connector	17 - ABS inlet bush
9 - central shaft	18 - PVC bolts
	19 - S/Steel clamp

ELECTROCHEMICAL FLOW CELL	DEPT OF CHEMICAL AND PROCESS ENGINEERING
	DWG No. 1
By: D.J.McPhail	Date: 9/1/91

Fig. 2.5

Chapter.3
Results and Discussion of Fast Cut Experiments

3.1 Introduction

Before any experimentation in alkaline solutions could be carried out, it was pertinent to attempt to reproduce some of the results shown by other workers (1,2,9,10). This was not only to show that the experimental apparatus operated correctly, but also to improve experimental technique where possible.

The trace shown below (Photo 3.1) is typical of the traces obtained from photographing the single oscilloscope trace just before and after the electrode cut had occurred, when using KCl solutions.

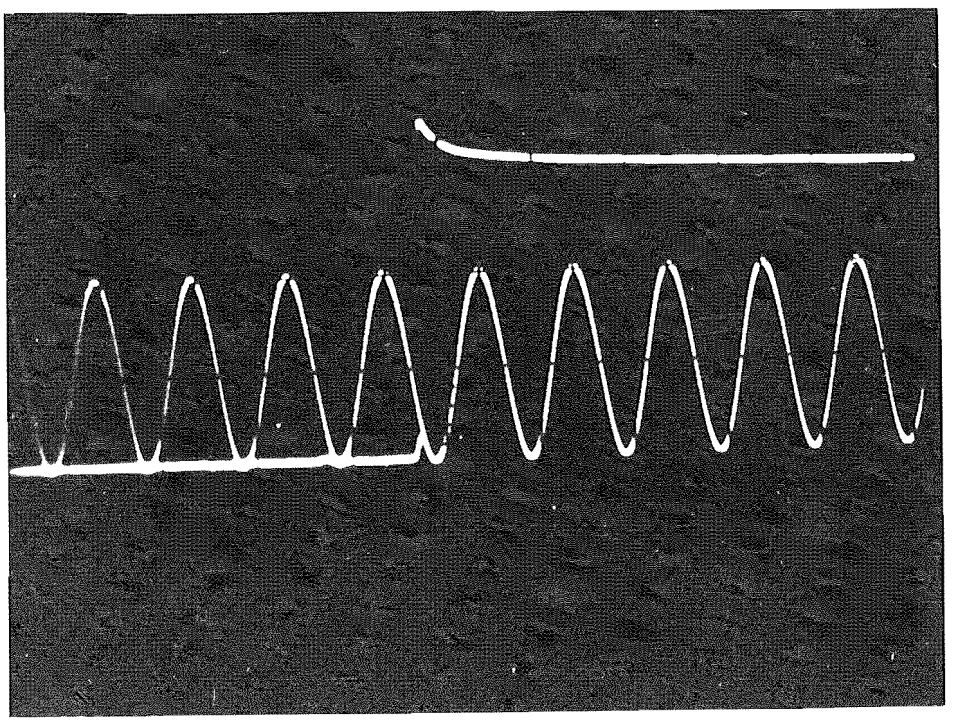

Photo 3.1 Pure Aluminium (5N) in 1.0 M KCl pH = 3.0 @ 20 °C versus Saturated Calomel Electrode (SCE)

The sine wave in the photograph has a frequency of 1 KHz and amplitude equal to a standard western cell (i.e. 1.018V).

The results of this preliminary work in 1M KCl, showed the peak potential (as shown in the table below) to be independent of pH in the pH range 3 to 5.5, and the mixed potential to be dependent on pH, as shown by other workers (2). The cutting speed was measured as 1000 ±50 cm / s, which is similar to that previously used.

Table 3.4.1 A comparison of Peak Potential data in 1M KCl solution @ 20°C

Solution pH	This Work ±20 mV	Hagyard & Williams (2) ±40 mV
3	-1588	
5.5	-1590	
3.2		-1590
3.2		-1600
5.2		-1600

3.2 Alkaline solution traces

The traces obtained using the hydroxide solutions were quite different to those of the KCl solutions, because the delay before the onset of the cathodic reaction was much longer than previously observed. Photos 3.2 and 3.3 below illustrate this point. The sine wave in each photo is the same as previously mentioned (i.e. 1 KHz), but a split time basis was used on the oscilloscope in an effort to obtain more information from the traces.

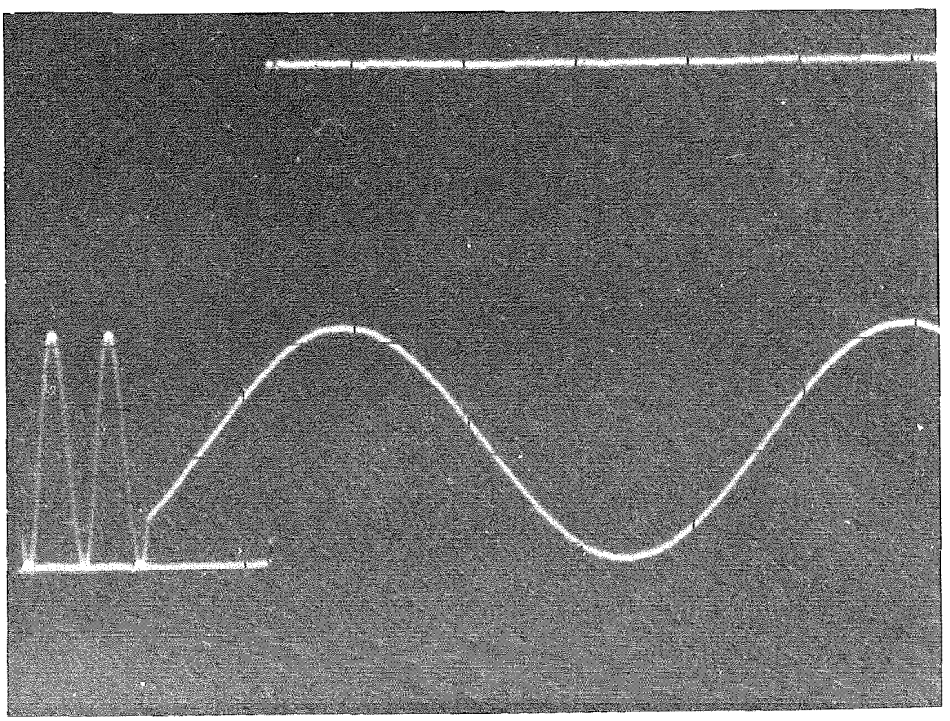

Photo 3.2 Pure Aluminium (5N) in 3M KOH at 25°C versus SCE

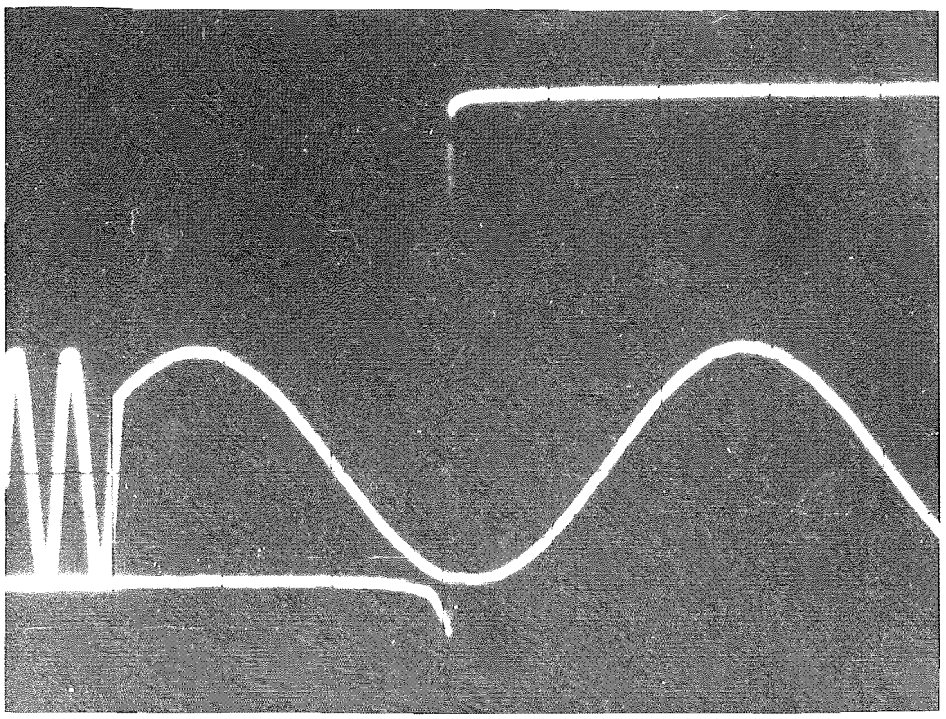

Photo 3.3 Pure Aluminium (5N) in 1M KOH at 25°C versus SCE

The above photographs show that the peak potential holds at a plateau for some time after the cut has occurred. The main difference between these two results is that the electrode in photo 3.3 appears to have a small tail leading to the plateau. This has no effect on the peak potential and is due to the cut being slower than normal. Once the cathodic reaction has begun the potential falls in a similar exponential, but slower, manner as observed earlier by other workers (2,9).

3.3 The Peak potential and decay to steady state

It has been established that the peak potential remains for a longer period in KOH solutions, than in the KCl solutions. This result would indicate that there is a larger delay in the onset of the cathodic reaction. Following Earl's analysis (9),this observation could be due to the lower availability of hydrogen ions at the electrode surface.

In hydroxide solutions there are two possible cathodic reactions. The first is the more familiar reaction involving hydrogen ions,

$2H^+ + 2e^-$ ---------> H_2 (g) (reaction 3.1)

$E^o = 0.0V$

which is directly controlled by the availability of hydrogen ions to the electrode surface. It can be shown that the hydrogen ion concentration for the trace in photo 3.2 (KOH solution) is approximately 10^{12} times lower than for photo 3.1 (KCl pH = 3 solution), which would support the observed results.

The second cathodic reaction, as detailed by Macdonald (32), is a two step adsorption model, which follows the Langmuir adsorption isotherm. The steps are :

$$H_2O + e^- + M \Leftrightarrow MH + OH^- \quad \text{(step.1)}$$

$$MH + e^- + H_2O \xrightarrow{\text{rds}} H_2 + OH^- \quad \text{(step.2)}$$

rds = rate determining step

However, Macdonald points out that the experimental results for pure aluminium show a high exchange current density, and a tafel slope which is higher than is consistent with this simple mechanism. He concludes that the differences between the theoretical and experimental results could be due to the assumption of the transfer coefficient being 0.5, use of the Langmuir isotherm and the surface actually being covered in corrosion product (i.e. an oxide / hydroxide layer).

A full analysis of the fast cut curves was made by Earl (9), who showed that the surface of the electrode was fully anodic just after cutting, and that there was a 20 μsec delay before the onset of the cathodic hydrogen evolution reaction in acid solutions. He postulated an area change-over from fully anodic (immediately after cutting) to mainly cathodic (at steady state). Earl showed in earlier work (10) that the cathodic area is approximately 200 times the anodic area at steady state. The possibility of a very much slower changeover of areas in alkaline solutions is possible, and as considered by Earl, the anodic to cathodic area ratio changes as a second or higher order exponential type function.

The observed results are likely to be a combination of the factors discussed above, of which this work has not set out to prove or disprove.

3.4 Aluminium & In / Ga / Mg alloys

This work will be discussed in two sections, (1) the peak potential trends and (2) the mixed potential trends. Only a few graphs will be presented here to illustrate the main points, whilst all others can be found in appendix (B).

3.4.1 The Peak Potential

The graph below is a plot of the Al - In alloy peak potential dependence on the KOH concentration.

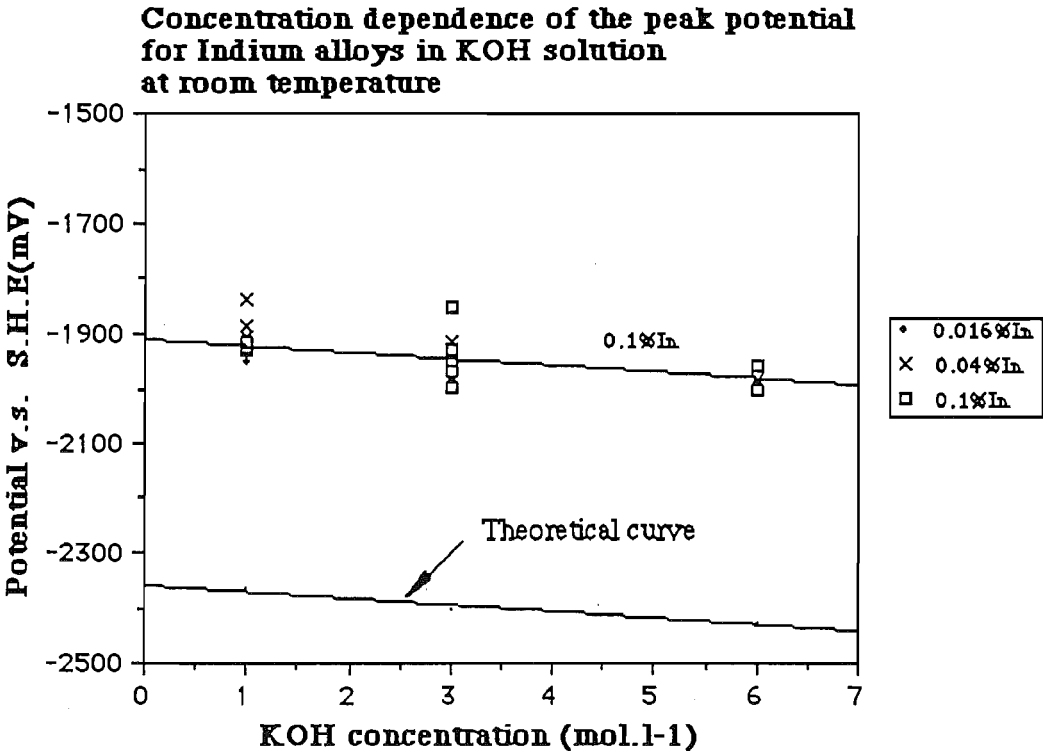

Graph 3.1 Concentration dependence of the peak potential for indium alloys; on KOH concentration in solutions at room temperature (20°C)
Standard deviation = 26 mV

This graph suggests that the Al - In alloys peak potential is linearly dependent on KOH concentration. It has been shown in appendix B that the potential is also linearly dependent on pH, due to the narrow pH range investigated (14 to 14.8), as expected from equation 3.2 below.

Pourbaix (56) proposed the following dissolution reactions:

In acid to neutral solutions aluminium dissolution is via

$$Al \text{ ----------> } Al^{3+} + 3e^- \quad \text{(reaction 3.4)}$$

$$E^o = -1.663 + 0.0197 \log (Al^{3+}) \quad \text{(equation 3.1)}$$

and for alkaline solutions dissolution is via

$$Al + 2H_2O \text{ ----------> } AlO_2^- + 4H^+ + 3e^- \quad \text{(reaction 3.5)}$$

$$E^o = -1.262 - 0.0788\ pH + 0.0197 \log (AlO_2^-) \quad \text{(equation.3.2)}$$

The theoretical curve shown in graph 3.1 above corresponds to equation 3.2, assuming an aluminate activity of one. It is clearly seen that the experimental curve is approximately 400 mV more positive than the theoretical curve. This suggests that the peak potential that has been measured is a transient mixed potential, and that the cathodic reaction also occurs immediately are cutting. It is still expected that the freshly created electrode surface is mainly anodic, and that the eventual decay to the steady state mixed potential is due in part to an area changeover from anodic to mainly cathodic as postulate by Earl (9).

The linear relationship shown between potential and KOH concentration in graph 3.1 suggests that the hydrogen dissolution kinetics are independent of KOH concentration.

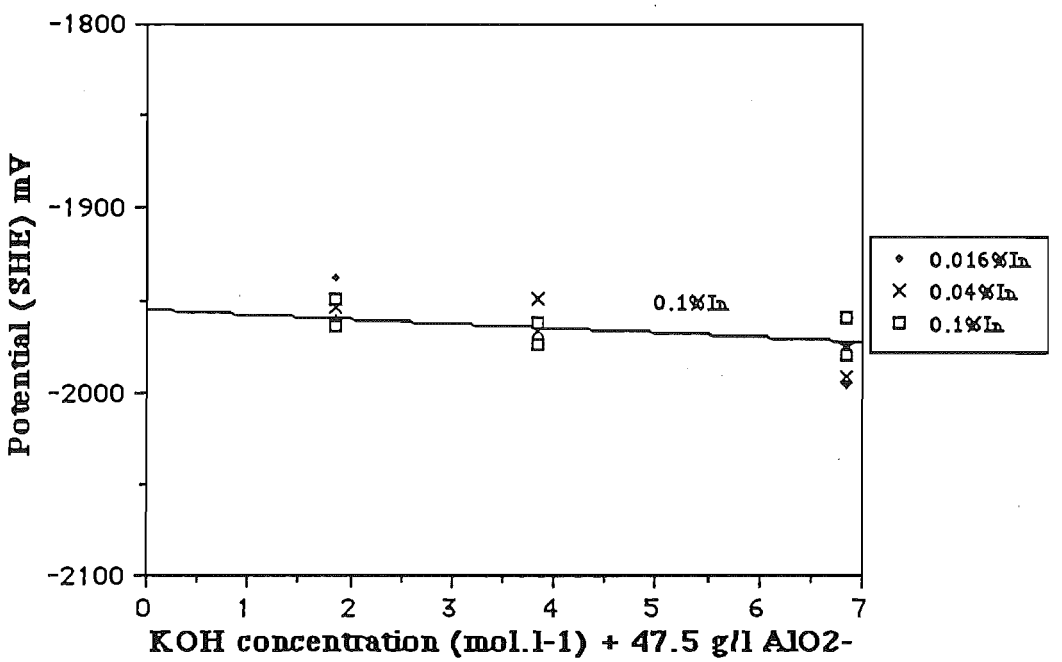

Graph 3.2 Concentration dependence of the peak potential for indium alloys; on KOH concentration in solutions containing aluminate, at room temperature (20°C)

This trend of a more positive peak potential than is theoretically expected was observed for all the alloys investigated, and is quite different to the results found using acidic solutions by other workers (1,2,9,10).

Reaction 3.4 above, was used by earlier researchers, using acid to neutral solutions to explain the observation of no peak potential dependence on pH, but a dependence on the aluminium ion concentration in solution, which can be explained by Nernst theory.

The graph 3.2 above shows the effect of adding aluminate to the solution. As the aluminate concentration increases the peak potential becomes less dependent on hydroxide concentration (i.e. the slope of the concentration versus potential graph decreases). The slope of the potential - pH diagram for the data in graph 3.2 is 0.0244 V/pH unit. This slope is much less than that given in equation 3.2, suggesting that the aluminium dissolution kinetics and / or the hydrogen evolution kinetics have changed. If the rate determining step for aluminium dissolution is reaction 3.6 , this yields a potential - pH slope of 0.0197, which is close to that of the above data.

$$Al + H_2O \text{ ---------> } AlOH^{++} + H^+ + 3e^- \text{ (reaction 3.6)}$$

However this is unlikely to be the case as the $AlOH^{++}$ ion is very reactive, and would rapidly react in the alkaline solution to form the aluminate ion. Thus it is more likely that there is a change in the hydrogen evolution kinetics when aluminate is present in solution, but is still independent of the KOH concentration.

It appears from graphs 3.1 and 3.2 that within experimental error the peak potential is independent of the indium content of the alloy.

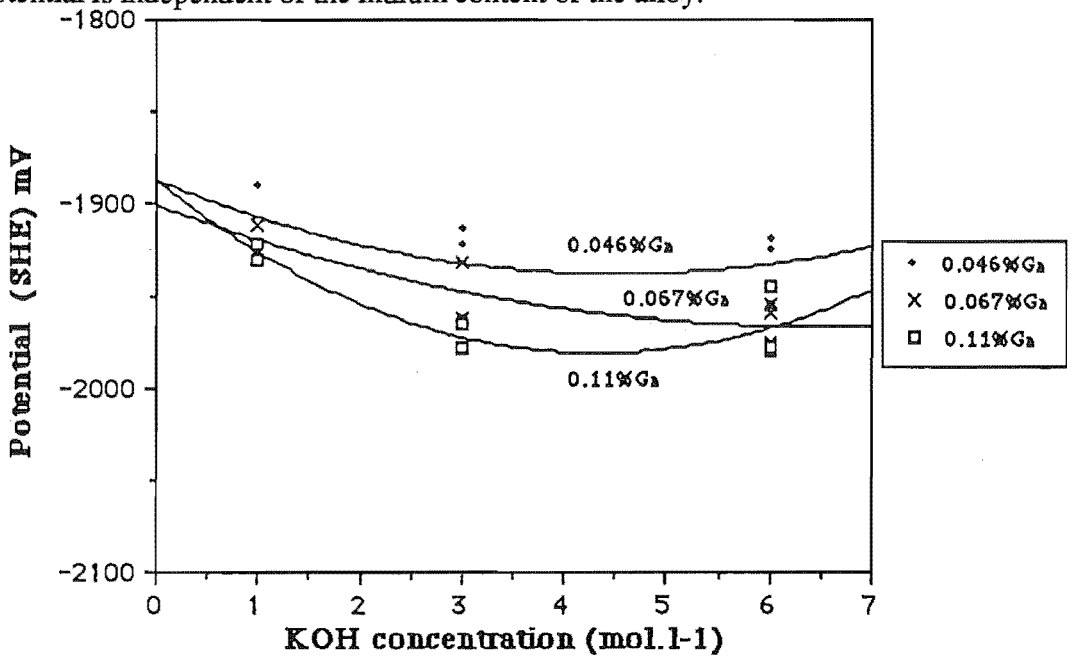

Graph 3.3 Concentration dependence of the peak potential for gallium alloys; on KOH concentration in solutions at room temperature (20°C)

Graph 3.3 above, shows the dependence of the Al - Ga alloys on hydroxide concentration. The gallium alloys show an increasingly negative peak potential with increasing gallium content, and do not show the linear behaviour with increasing hydroxide concentration as found for the indium alloys. The slight curvature shown can not yet be adequately explained

Hunter(33) found that for gallium levels greater than 0.026wt% and temperatures above 20 °C that gallium "superactivated" aluminium (i.e. the alloys become more active than pure aluminium) at steady state. The observed peak potential behaviour is in many ways similar to Hunter's findings. The effect of gallium on the peak potential can be more clearly seen below in graph 3.4.. This graph shows that the potential becomes more negative with increasing gallium content above 0.04wt% , as would be expected following Hunter's results. The peak potentials for the gallium containing alloys are however more positive than that of pure aluminium, thus showing no superactivation. This suggests that gallium only superactivates aluminium by modifying any oxide layer that is formed at steady state.

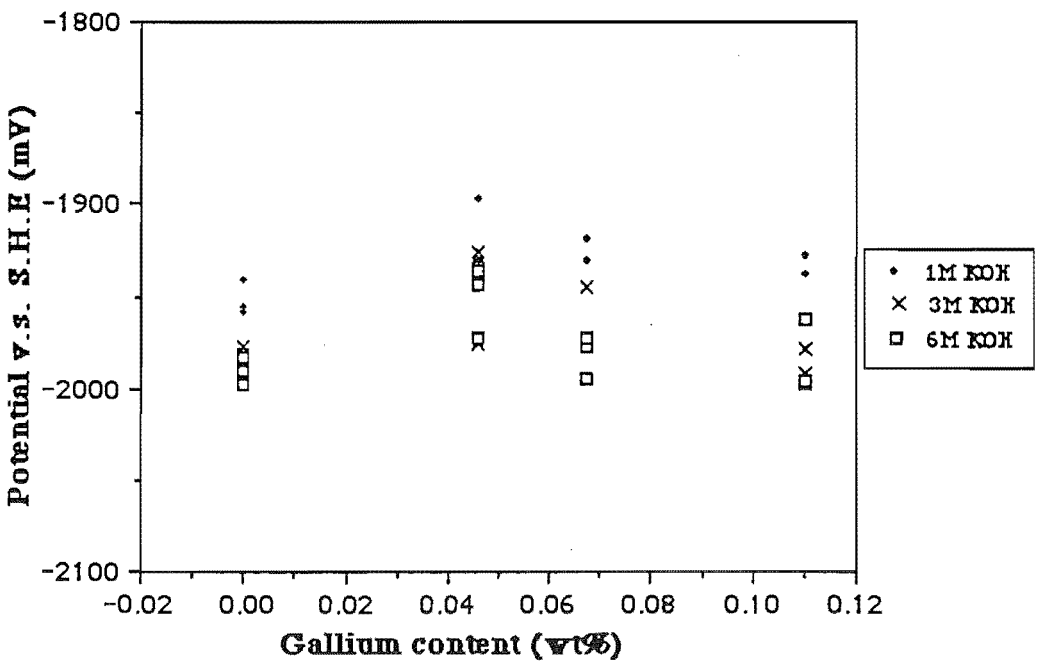

Graph 3.4 Alloy influence on peak potential
in KOH solution, at room temperature (20°C)

The nature of this experimental technique produces an inherent spread of data, but by inspection of the fast cut graphs it is evident that reproducibility increases with increasing hydroxide concentration and increasing aluminate concentration. This is best illustrated by comparing graphs 3.1 and 3.2 .

3.4.2 The Steady State Potential

The steady state potential is defined as the potential of the electrode 3 minutes after the cut has been made under no load conditions. The graph below, graph 3.5, shows that indium is quite effective in making the steady state potential more negative (super-active) than for pure aluminium.

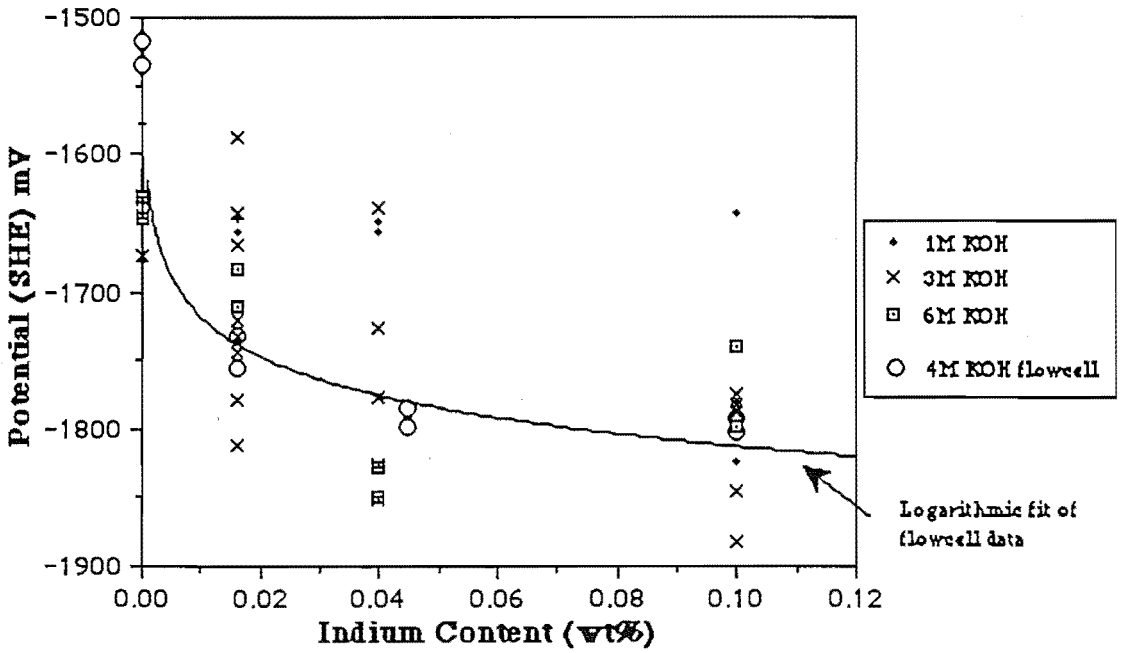

Graph 3.5 Indium influence on potential 3 minutes after cut;
on KOH concentration in solutions at room temperature (20°C).
Equation of best fit : Potential = -1906.9 - 94.22*Log(wt%In)
Least Squares Regression Coefficient: $r^2 = 0.985$

The steady state potential of the 4M KOH flowcell data has also been plotted and fitted logarithmically on to graph 3.5. The steady state potentials of the flowcell data correspond to the electrode potential 30 minutes after initial immersion in solution, and/or 30 mins after loading has ceased. This data fits well with the data from the fast cut cell, thus illustrating that the potential 3 minutes after cutting is representative of the true steady state potential.

The logarithmic fit of the flowcell data in graph 3.5 describes how effective indium is in inhibiting the cathodic electrode process, by either inhibiting cathodic sites and/or increasing the hydrogen discharge overvoltage.

This graph brings out two major points, (1) it is clearly advantageous to use hydroxide solution of greater than $1 mol.l^{-1}$ concentration to make the electrode potential more negative, and (2) that there is little advantage in using an indium alloy content of greater than 0.04wt%. This second point is supported by Jeffery and Halliop's (34) optimization experiments using Al - Mg - In - Mn quaternary alloys.

A plot of the solution concentration versus potential for the different indium containing alloys is given below. This graph would suggest that an optimum solution concentration of about 4M KOH should be used.

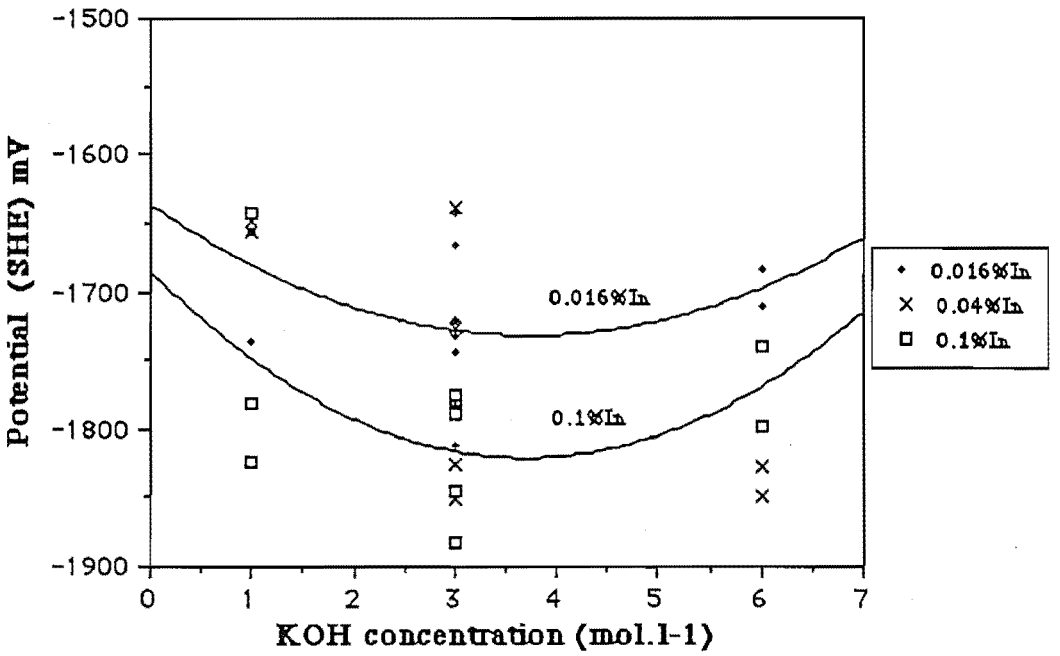

Graph 3.6 Concentration dependence of the 3 minute potential for indium alloys; on KOH concentration in solutions at room temperature (20°C)

The potential - concentration curves shown become more negative up to 4 mol.l^{-1}, this is due to thinning of the surface film as the hydroxide concentration increases (67, 77). As the concentration increases above 4 mol.l^{-1} the cathodic (hydrogen evolution) rate further increases, with little corresponding thinning of the surface film, thus the electrode potential becomes more positive, explaining the observed optimum.

The observed trend held in general for all the indium containing alloys, for solutions with and without aluminate. However the gallium alloys behaved quite differently, as shown in graph 3.7 below.

The steady state potential for the gallium alloys, unlike indium alloys, continued to become more negative with increasing hydroxide concentration. The potential of the 0.046%Ga alloy is more negative than that of the 0.11%Ga alloy, which is a reversal of the trend found for the peak potential, and can be directly attributed to the cathodic effect of gallium preferentially segregating to the grain boundary and assisting hydrogen evolution.

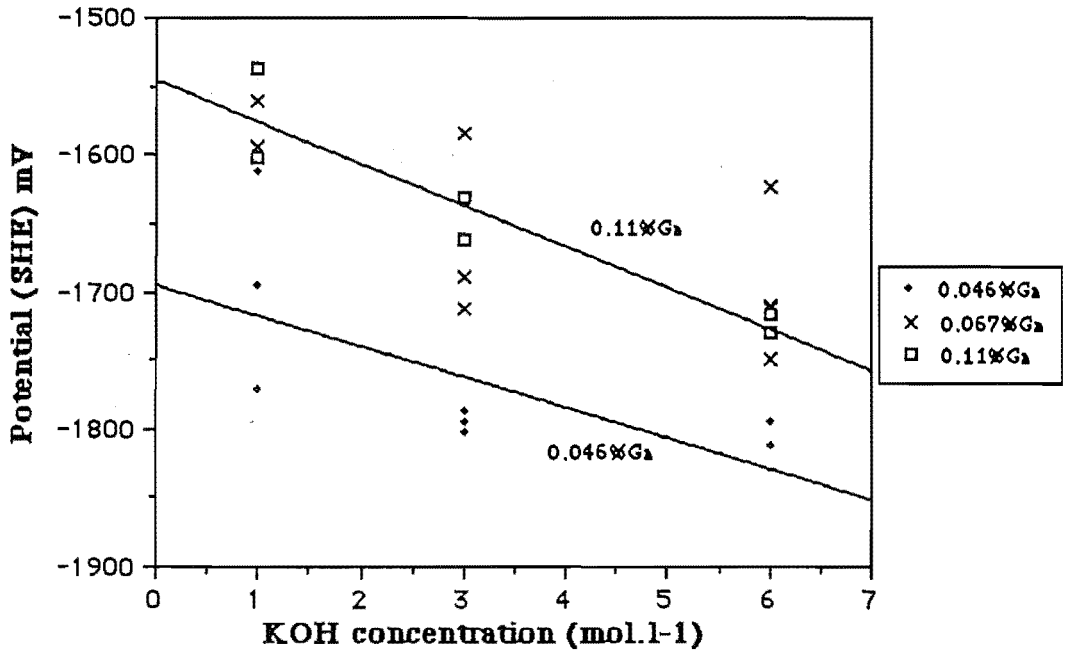

Graph 3.7 Concentration dependence of the 3 minute potential for gallium alloys; on KOH concentration in solutions at room temperature (20°C)

Gallium segregation is discussed later in section 4.2.

The super - activating effect of gallium can be better comprehended in graph 3.8, where the mixed potential of the Al-0.046%Ga alloy is more negative than for pure aluminium and the higher gallium containing alloy electrodes. This supports the results of Hunter(33), who found gallium containing alloys of greater than 0.026 wt% superactivated aluminium at steady state. It is concluded that an electrode of gallium content between 0.026% and 0.046% could be effective as an anode for battery purposes.

This graph further illustrates the effectiveness of solutions with a hydroxide concentration greater than 1mol.l^{-1} in obtaining more negative mixed potentials.

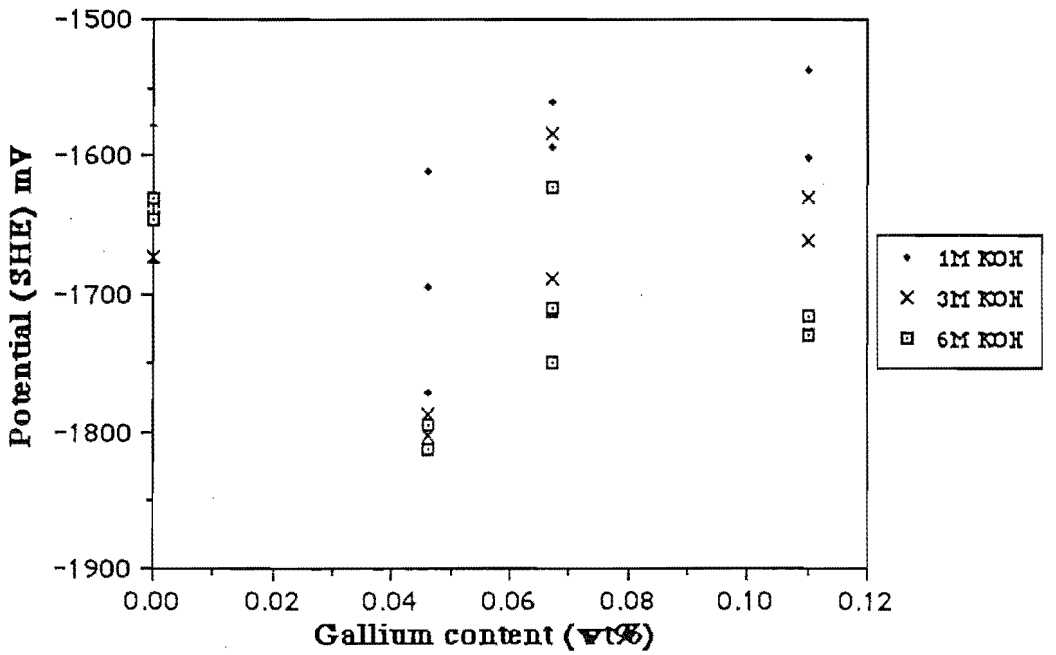

Graph 3.8 Gallium influence on potential 3 minutes after cut; on KOH concentration in solutions at room temperature (20°C)

A comparison of graphs 3.8 (gallium content) and 3.5 (indium content) shows the relative effect of the gallium and indium on the steady state potential. At an alloying level of approximately 0.04% the potentials are the same, but at higher alloy contents the gallium steady state potential is always positive to that of its indium counterpart, atleast upto the 0.1% alloy level investigated, this shows indium to be of greater value.

The effect on potential due to aluminate in the hydroxide solutions is illustrated in the tables below.

Table 3.4.2 The Aluminate effect on Potential for Al - 0.1%In

Solution: 3M KOH @ 25°C

Aluminate content g/l	Steady State Potential mV	Peak Potential mV
0.0	-1825	-1950
9.5	-1760	-1965
47.5	-1760	-1960

Table 3.4.3 The Aluminate effect on Potential for Al - 0.11%Ga

Solution: 3M KOH @ 25°C

Aluminate content g/l	Steady State Potential mV	Peak Potential mV
0.0	-1650	-1965
9.5	-1660	-1975
47.5	-1640	-1975

It can be clearly seen from the tables above that within experimental error aluminate has no significant effect on the peak potential for either alloy. The steady state potential for the gallium alloy also appears independent of aluminate concentration, but there does appear to be an effect for the indium alloy, when going from 0.0 g/l to 9.5 g/l, which follows Nernst theory, but this does not continue for further increases in aluminate concentration, possibly due to the polymeric nature of aluminate (14).

Chapter .4
Results and Discussion of Flowcell Experiments

4.1 Introduction - Flowcell operation

The flowcell used in this work has been described in detail in chapter .2.

The flowcell gives similar results to what might be obtained using a rotating disc electrode, with the advantage that the flowcell can be operated for longer periods, at much higher current densities.

The flow profile in the cell under operating conditions can be seen by the dark fluid in the photograph below, with a gap Reynolds Number of 4650 which would suggest turbulent flow conditions.

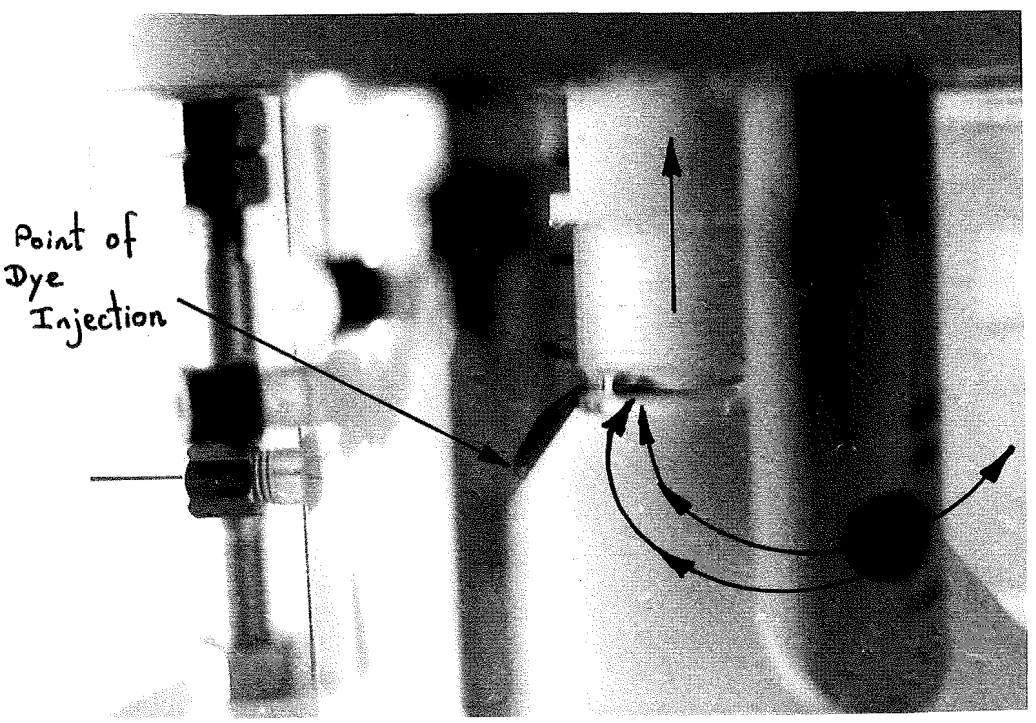

Photo 4.1 Elevation photograph showing dye injection into the flowcell from the needle on the left, with maximum solution velocity across the electrode surface of 1.5 m/s, Reynolds No. = 4650

The experimental program carried out was to investigate aluminium alloy electrodes in electrolytes, (1) at temperatures from 20 to 80 ^{o}C, (2) using 1 to 6 mol.l^{-1}

hydroxyl ion concentrations, (3) with varying cation species (i.e. K^+ and Na^+), and (4) with varying dissolved aluminate concentrations (i.e. 0 to 70 g/l AlO_2^-). The polarization dependence on flow velocity was also investigated.

4.2 Electrode dissolution morphology

All the electrodes that have been tested are in the as cast state as received from Comalco Research Centre, Melbourne, with no further heat treatment being carried out.

The electrodes dissolved in a uniform manner, with slight differences in their surface appearance. The dissolution behaviour supports Macdonald's (32) theory of a passive - active transition, which is related to the film formed on the electrode surface.

Scanning Electron Micrographs (S.E.M) have been carried out for the following aluminium samples,

(1) Pure Aluminium
(2) Al - 0.1%In
(3) Al - 0.1%Mg - 0.1%In

all of which were polarised in a solution initially at 4M KOH with aluminium dissolved into it to give an aluminate concentration of 9.5 g/l (0.161M AlO_2^-). The solution hydroxyl ion concentration remained depleted after the aluminium dissolution (solution concentration approx. 3.84M KOH). The solution temperature was held constant at 50°C, with a flow velocity of 1.47 m/s.

The following alloy samples were highly polished, and etched, then microscopically examined,

(1) Al.- 0.1%In
(2) Al - 0.1%Mg - 0.1%In
(3) Al - 0.085%In - 0.09%Ga
(4) Al - 0.11%Ga

The micrographs below (photos 4.2.1 - 3) show the relatively even dissolution of the alloy electrodes, and varying surface appearance. The electrodes have undergone a greater amount of dissolution at their edge, which is due in part to the highest flow velocity being at this point.

As expected each electrode shows a small degree of pitting. The pure aluminium electrode appears to have a smoother surface (photo 4.2.5) than the two alloys, and is covered with a film which from Hunter (33) and Macdonald's(32) work would seem to be oxide or hydroxide. The two indium containing alloys are both covered in a film, with the evenness of the Al - 0.1%In alloy surface suggesting that the indium is relatively evenly distributed. The Al - Mg - In electrode however has a large crater on its surface, which will be discussed later in this section.

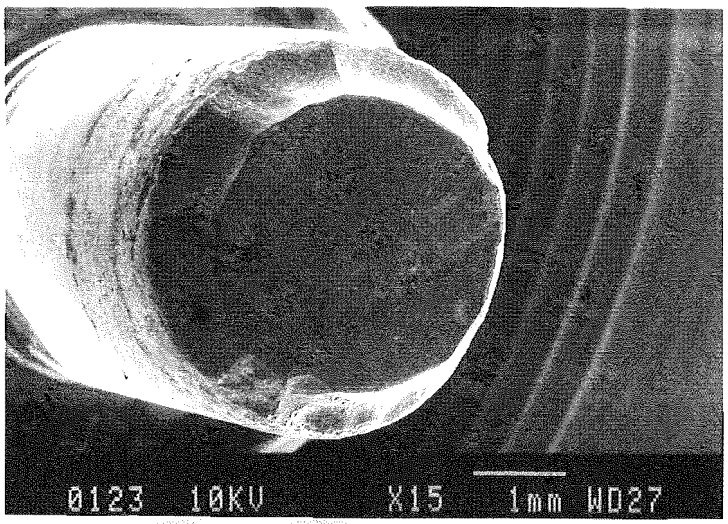

Photo 4.2.1-Pure Aluminium

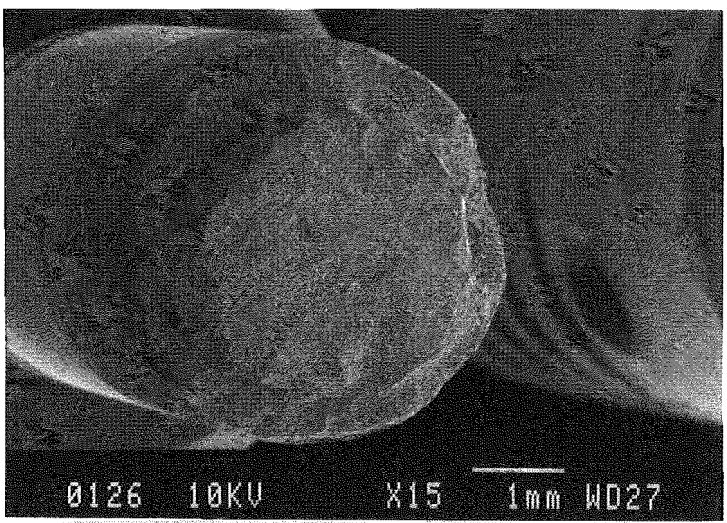

Photo 4.2.2- Al - 0.1%In

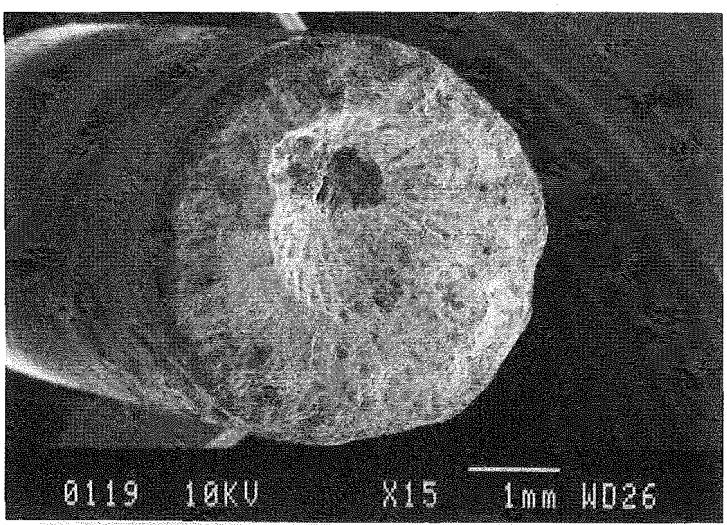

Photo 4.2.3- Al - 0.1%Mg - 0.1%In

A closer inspection of the electrode surfaces (photos 4.2.5 - 7) shows three different aspects. The pure aluminium electrode (photo 4.2.5) has a smooth amorphous layer which shows a few small pit sites generally smaller than 5μm in diameter, whereas the Al - 0.1%In electrode (photo 4.2.6) has a relatively uniform film. The general surface micrograph (photo 4.2.7) for the ternary alloy shows a very open / porous surface structure, which explains the occurrence of dendritic (whisker) growth from the electrode surface after experimentation, even after the electrode has been thoroughly washed with distilled water to remove residual hydroxide solution. The growth was similar in nature to that which occurs when mercury comes into contact with aluminium. The dendritic growth observed on the Al - 0.1%Mg - 0.1%In electrode makes this alloy less favourable for use in an Al / air battery system, under present operating regimes, due to possible electrical shorting between electrode plates, and blocking of the electrolyte flow paths.

Inspection of the ternary alloy crater (photo 4.2.4 below) showed preferential corrosion to have occurred, possibly due to low melting point species concentrating near this region. As the low melting point species have not concentrated at the centre, as would be expected from crystalization theory, it is suggested that the coolling rate of the casting was higher than the diffusion rate of the low melting point species through the lattice, thus trapping them at some distance from the centre of the electrode. The trapped low melting point species would create a region having a higher concentration of cathodic sites, thus making the centre more anodic to the surrounding material. The observed preferential dissolution at the centre of the electrode is thus explained, given the galvanic cell that would occur between the anodic and cathodic regions.

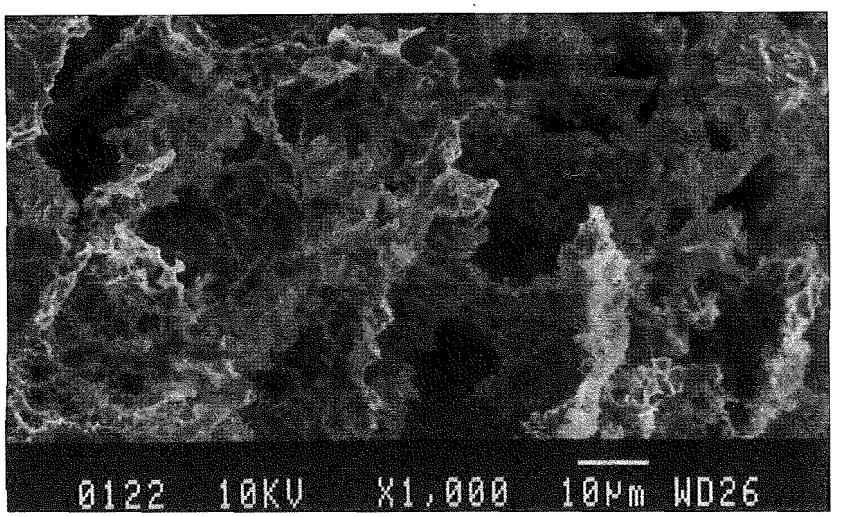

Photo 4.2.4 -Al -0.1%Mg -0.1%In

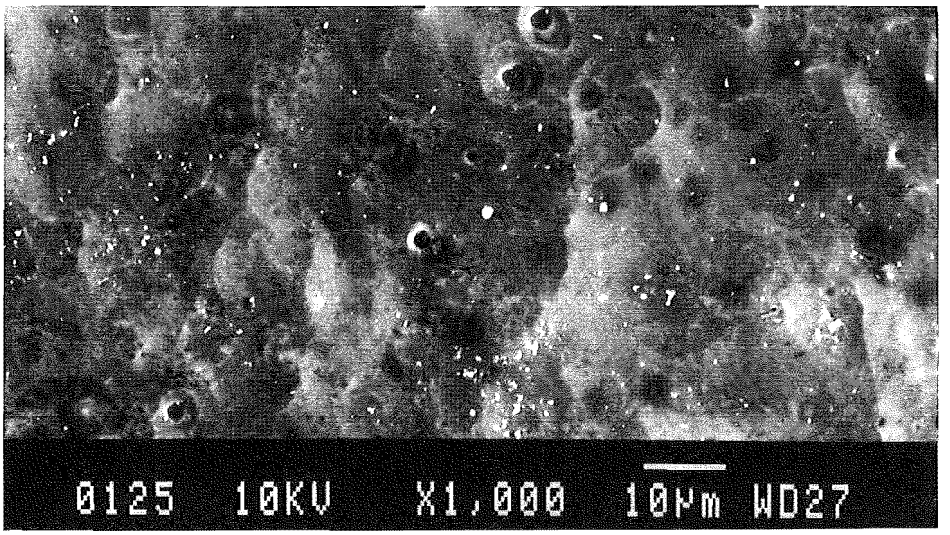

Photo 4.2.5-Pure Aluminium

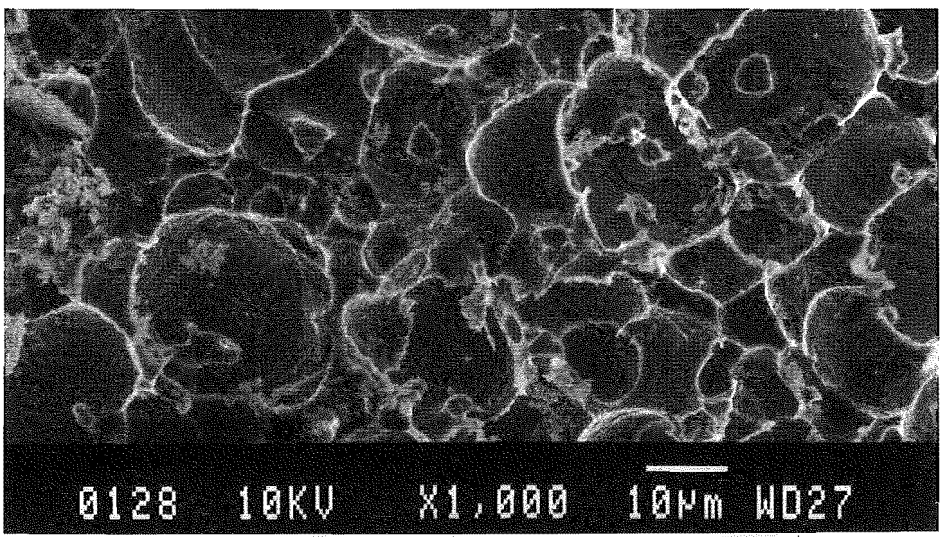

Photo 4.2.6- Al - 0.1%In

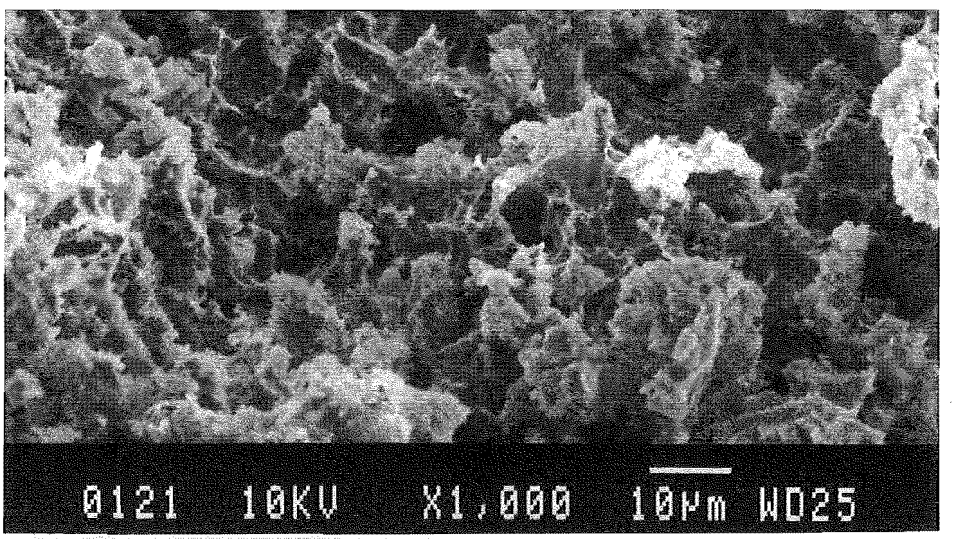

Photo 4.2.7- Al - 0.1%Mg - 0.1%In

Photographs 4.2.8 - 4.2.11 (below) show the surfaces of the highly polished, then etched Al - 0.1%In and Al - 0.1%Mg - 0.1%In samples at varying magnifications. Photos 4.2.8 and 4.2.9 show that both samples have a definite radial appearance. The radial appearance is also evident for pure aluminium, as seen in photos 4.2.12 and 4.2.13, and is directly attributable to the columnar growth pattern of the as cast samples, which may vary slightly with casting cooling rate.

The Al - 0.1%In electrode (photo 4.2.8) shows a significant amount of second phase, generally situated on or close to grain boundaries, which is relatively evenly distributed over the electrode surface. A second phase formation at a grain boundary is clearly seen in photo 4.2.10. Hunter (33) has showed that the presence of second phase particles has little effect on the polarization characteristics of the Al - In alloys and this work confirms his observations.

The Al - 0.1%Mg - 0.1%In alloy (photo 4.2.9) shows a similar radial appearance to the Al - In alloy. The grain structure is however much finer, with a segregation zone at the grain boundary being apparent. The dispersion, which is better seen in photo 4.2.11, means that there is a concentration gradient between the bulk alloy and the grain boundary. The existence of the radial appearance would suggest that any low melting point species formed will concentrate at or close to the centre of the casting, depending on the casting coolling rate, which is supported by the surface appearance shown in photo 4.2.3 earlier.

Any concentration gradient that is formed while casting can easily be removed via a solution heat treatment stage, which homogenises the electrodes, to produce a uniform solid solution.

It is yet to be proved that there is any difference in macroscopic polarisation behaviour due to an alloys heat treatment history. This is partially supported by the findings of this work and Macdonald (32), who used homogenized alloys, that the polarization of indium containing alloys, depended generally on the presence of indium and not quantity.

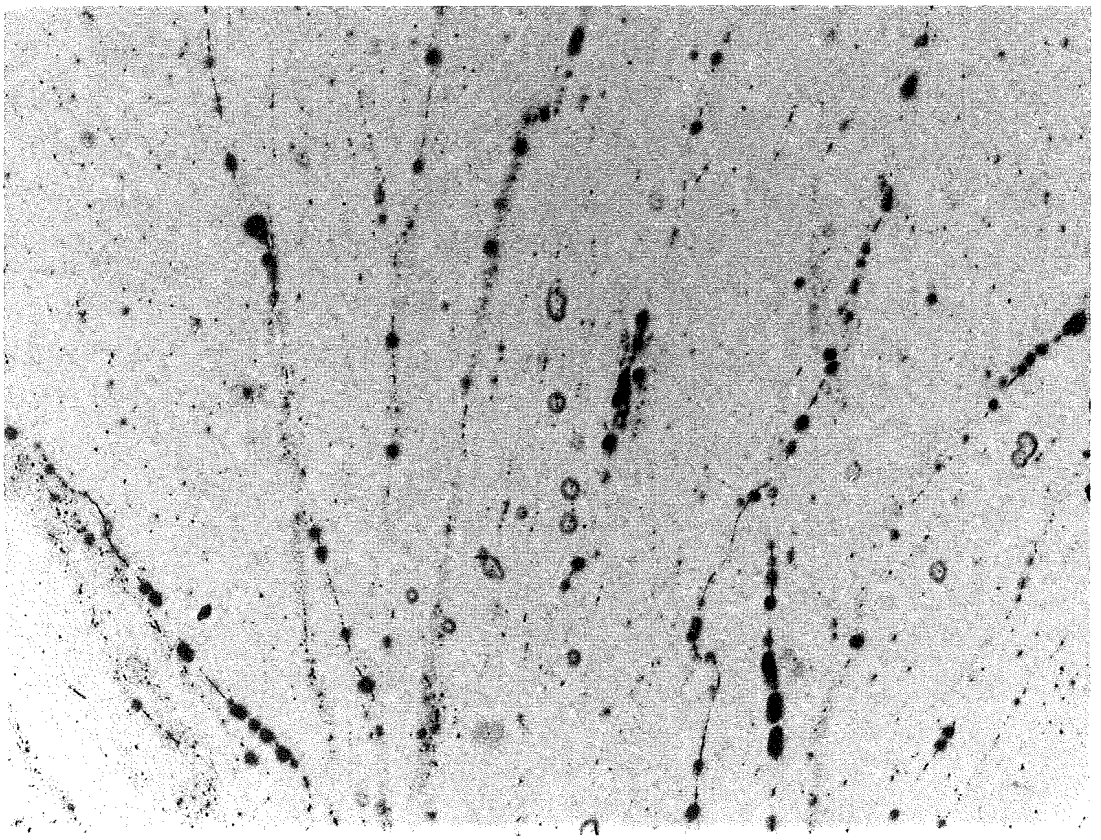

Photo 4.2.8 - Al - 0.1%In
Magnification 65x

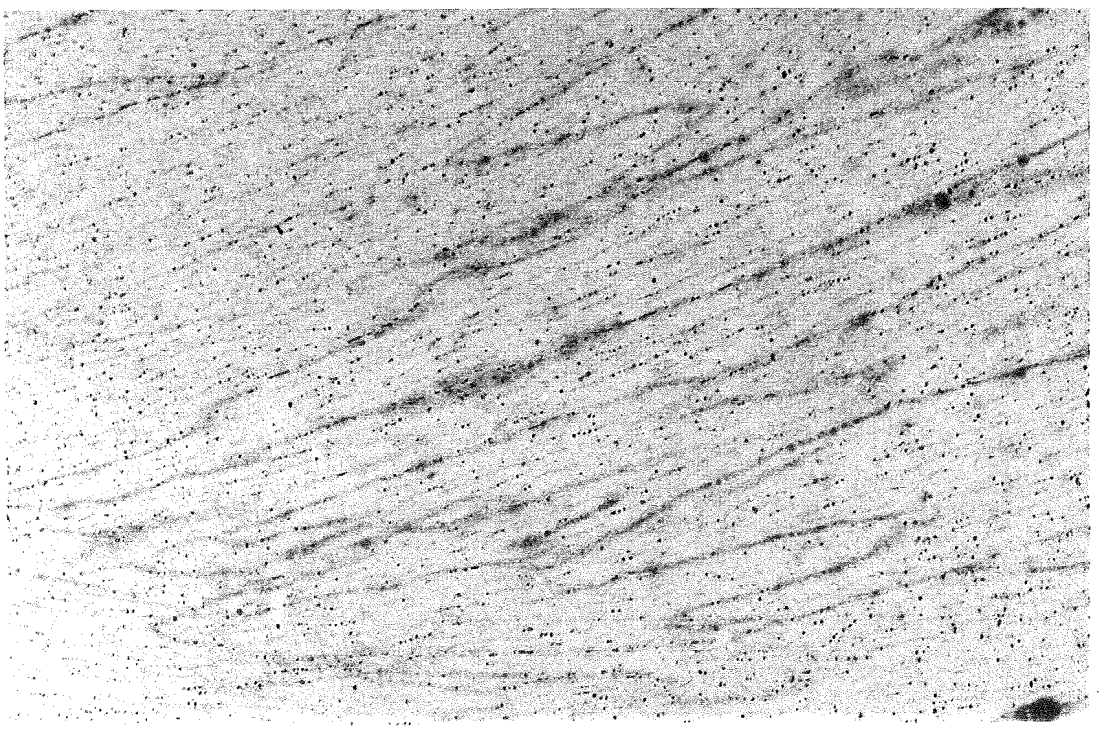

Photo 4.2.9 - Al -0.1%Mg - 0.1%In
magnification 65x

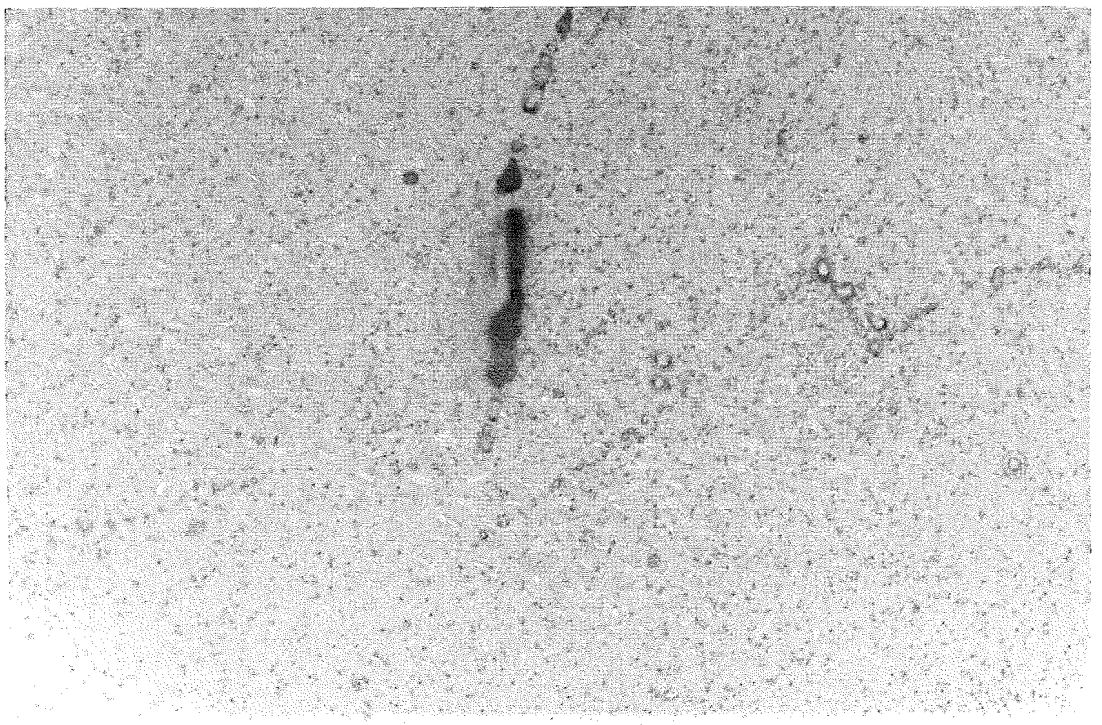

Photo 4.2.10 - Al - 0.1%In
Magnification 645x

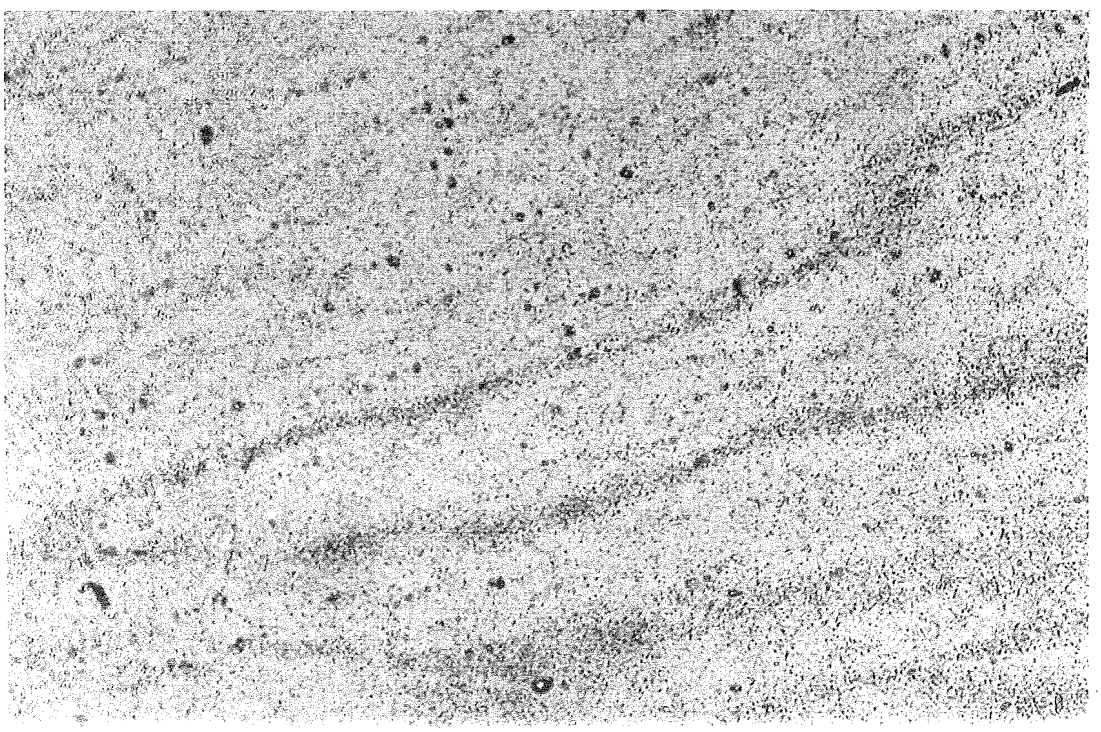

Photo 4.2.11 - Al -0.1%Mg - 0.1%In
magnification 260x

The radial appearance, mentioned previously, as shown below in photo 4.2.12 for pure aluminium polarised in 2M KOH at 60°C and 1.47 m/s, is very similar to the electrode shown in photo 4.2.13, which is for pure aluminium in 4M NaOH at 75°C and 1.47 m/s, with this electrode showing a heavily etched surface structure.

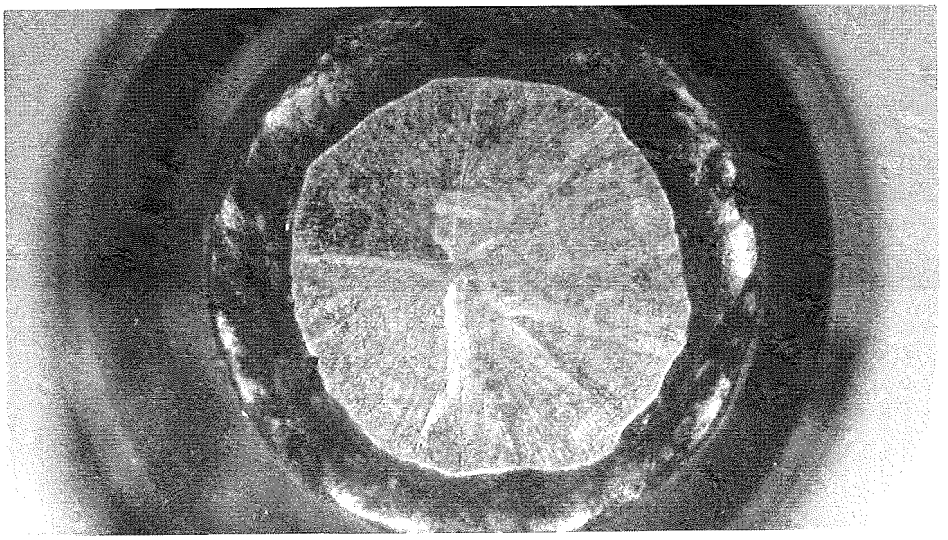

Photo 4.2.12 - Pure Aluminium - 2M KOH

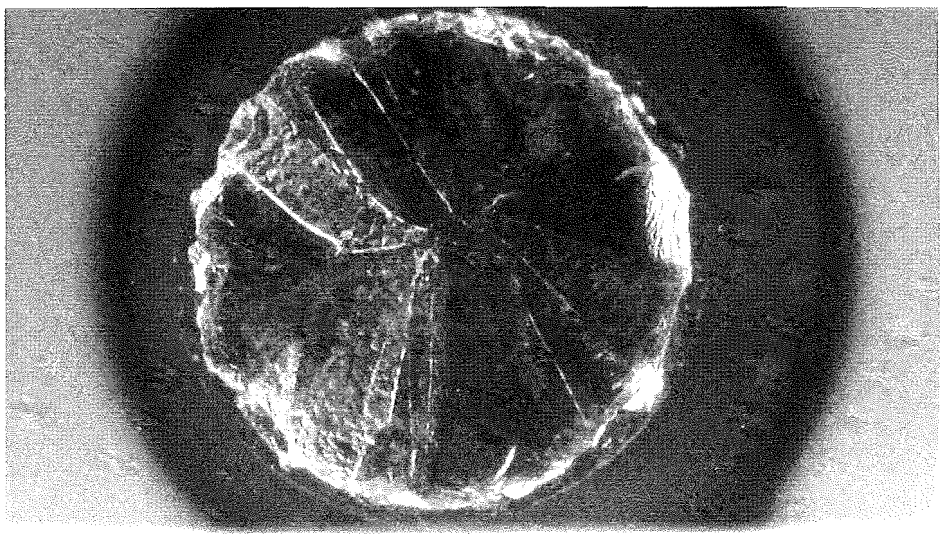

Photo 4.2.13 - Pure Aluminium - 4M NaOH

The radial formation is due to a columnar grain boundary growth, which occurs at right angles to the isotherms on cooling of the casting.

X-ray analysis of an Al - 0.045%In electrode polarized in 4M KOH + 9.5 g/l AlO_2^- at 50°C has given support to Macdonald's (32) theory that the alloy electrodes in the passive state are protected by a thin layer of metallic alloying element(s). Figure 4.2.1 shows the X-ray intensity curve for the polished electrode surface, and figure 4.2.2 that of the etched surface. Comparing these two figures clearly shows that there is a much higher surface concentration of indium on the electrode surface after polarization than before.

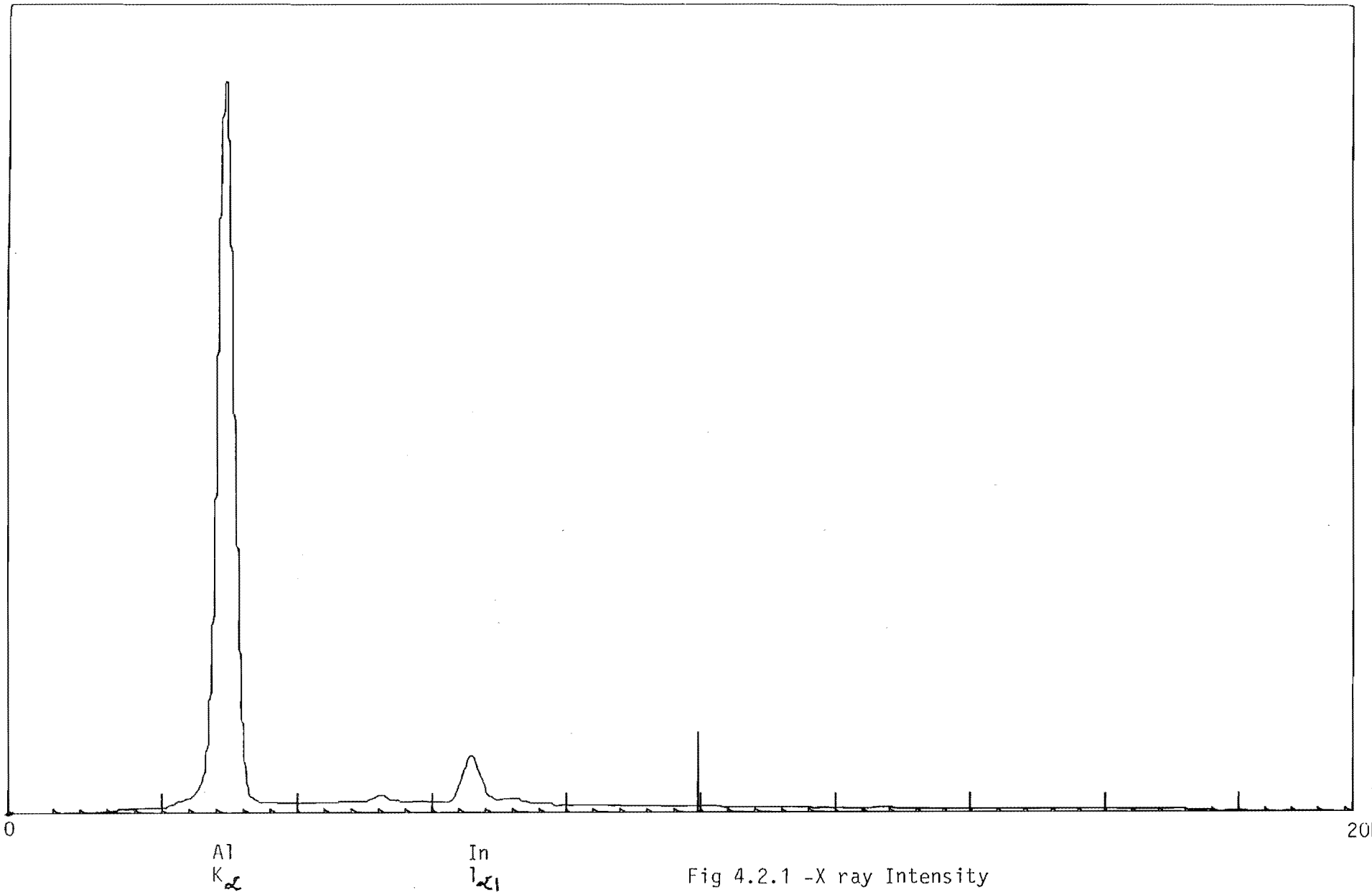

Fig 4.2.1 -X ray Intensity

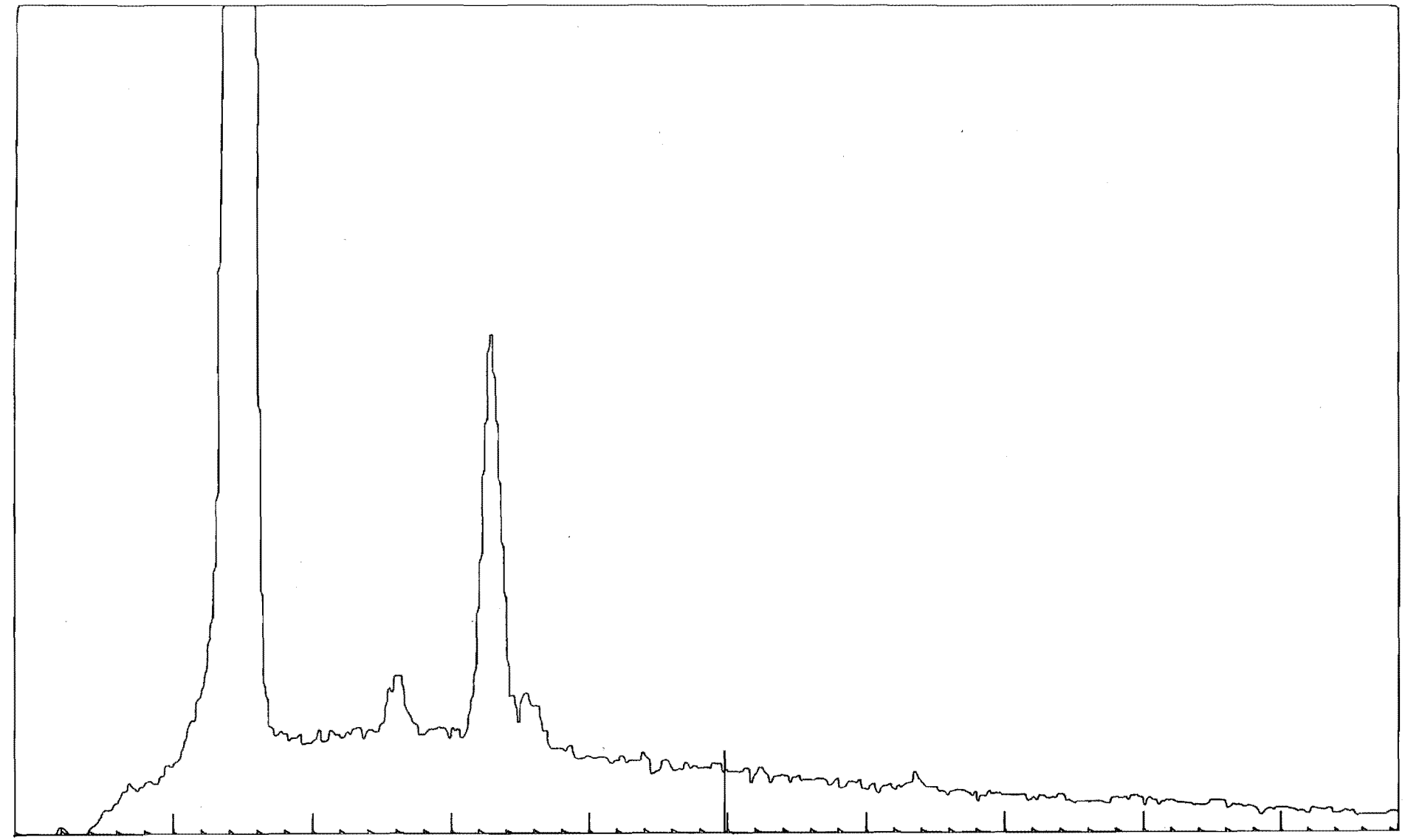

Fig 4.2.2 -X ray Intensity

A similar phenomenon of surface buildup was also found to occur for gallium, with the gallium preferentially concentrating at grain boundaries. The X-ray analyses for the Al - 0.046%Ga electrode in 4M KOH at 40°C are given in figure 4.2.3 and figure 4.2.4 below. The increased surface concentration of gallium for the etched sample is easily seen when comparing the two figures. The gallium forms local cathodes which increases the already high self corrosion rate, eventually leading to electrode disintegration. This effect has been observed by other workers (32,33,43), making gallium doubtful as a viable binary or higher order alloy for battery anodes.

Hunter (33) showed that gallium alloys dissolve via two mechanisms dependent on gallium concentration in the alloy. At high concentrations (2.3%Ga) he showed the alloy to undergo serious grain boundary etching, with no pit mechanism. The massive grain boundary dissolution eventually leads to disintegration of the anode surface. At low gallium content the alloys were pitted, with gallium present at the bottom of the pits and the surrounding areas being gallium free. The reaction surface was a dense network of pits, with merging pits creating discontinuities in the pit walls leaving isolated pillars of material.

The two photographs below illustrate the destructive effect that gallium provides. This electrode is a ternary alloy (Al - 0.085%In - 0.09%Ga), in 4M KOH + 9.5 g/l AlO_2^- at 60°C and 1.47 m/s flow velocity, which even with its indium content is aggressively attacked at the grain boundaries (Photo 4.2.15).

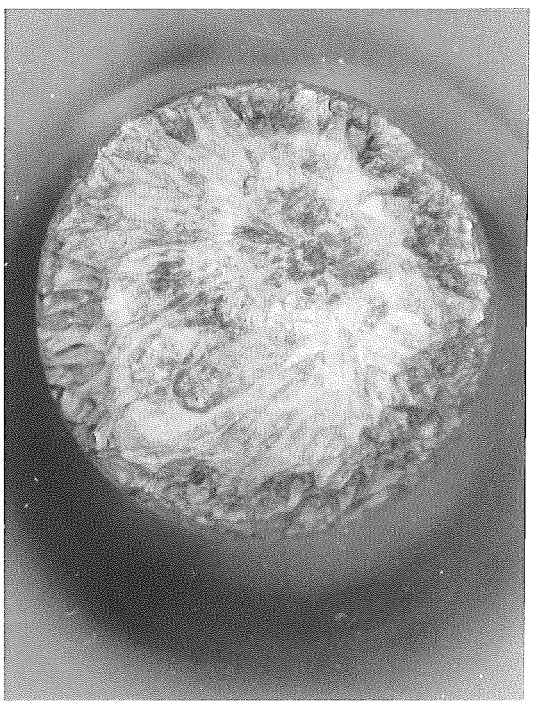

Photo.4.2.14

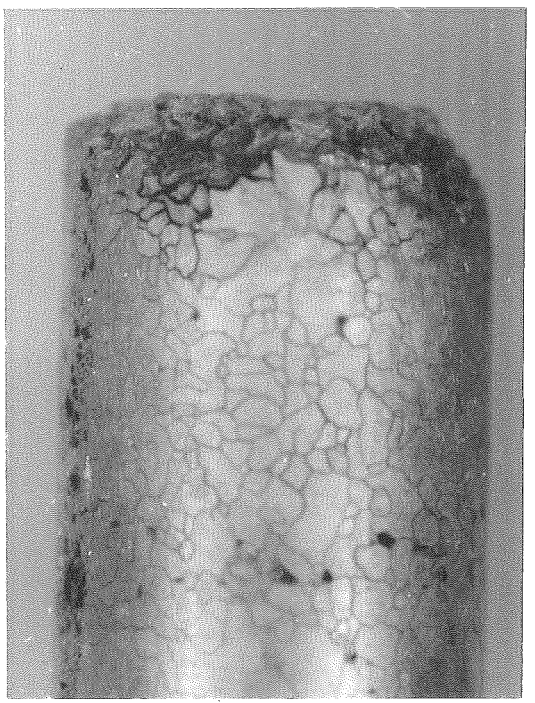

Photo.4.2.15

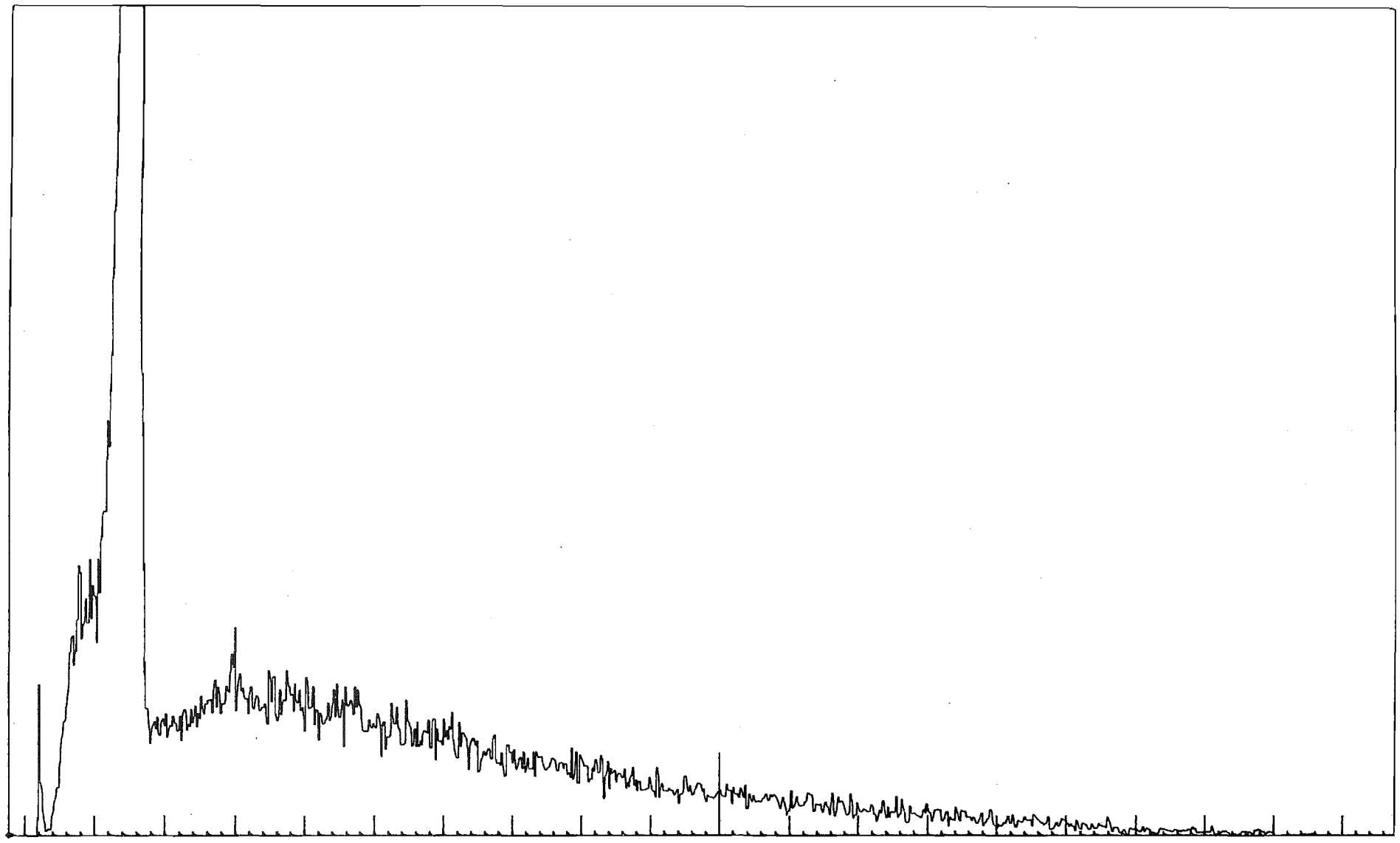

Fig 4.2.3 - Polished surface

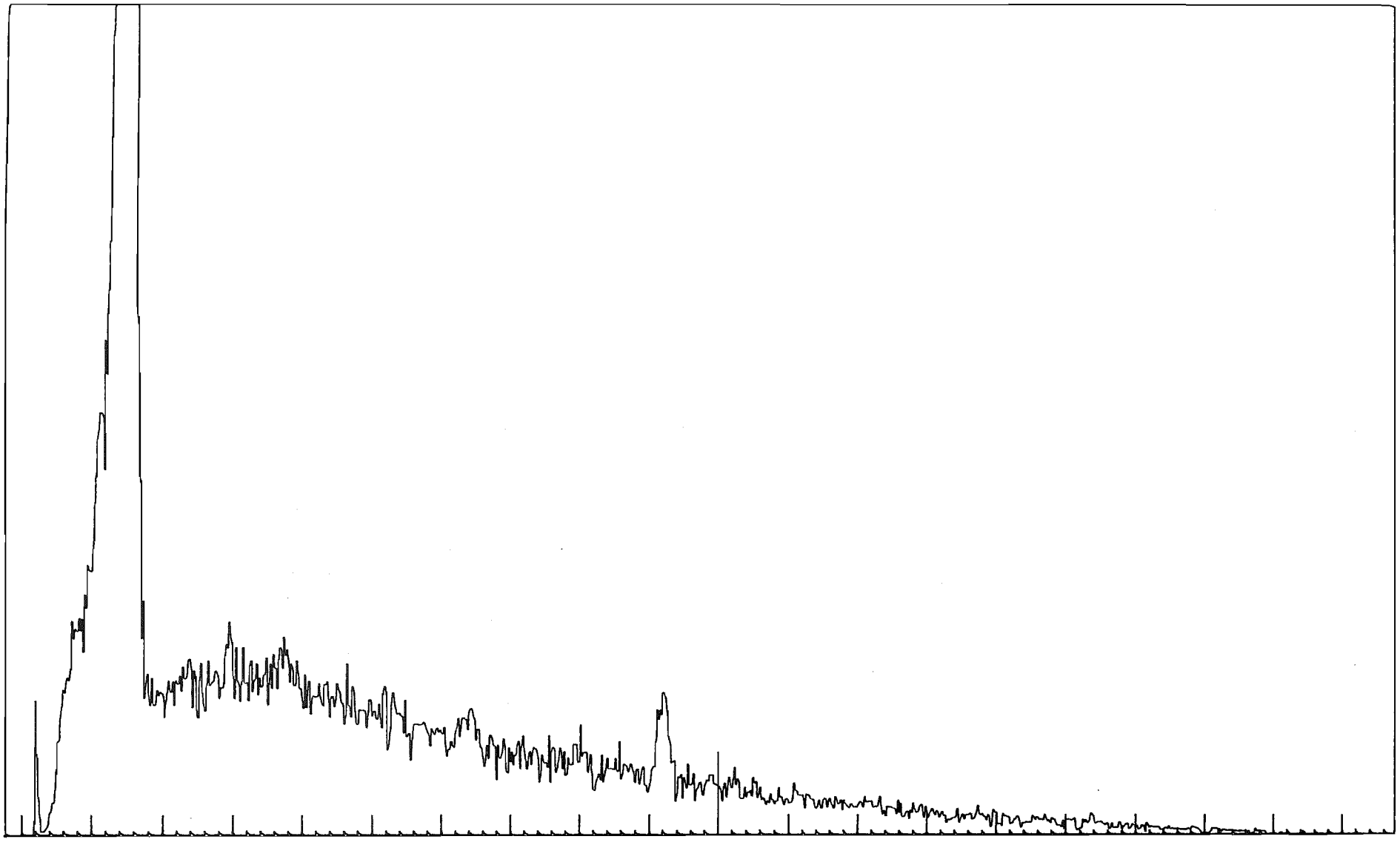

Fig 4.2.4 - Etched Surface

Even though it has been shown above that gallium concentrates at the grain boundary when polarised, photos 4.2.16 - 4.2.19 below show that there is very little segregation to the grain boundary in the as cast state for the Al - 0.0.085%In - 0.09%Ga and Al - 0.11%Ga alloys.

Photos 4.2.16 and 4.2.18 for the Al - In - Ga ternary alloy show that gallium increases the solubility of indium in the aluminium structure, giving a relatively homogeneous solid solution. The Al 0.11%Ga binary alloy (photos 4.2.17,4.2.19) shows a similar structure to that of the ternary alloy.

Given the homogeneous appearance of the gallium alloys (photos 4.2.16 - 4.2.19), it is clear that gallium has a high affinity for the grain boundary under polarising conditions (photos 4.2.14 - 4.2.15). This is supported by Hunter (33), who used homogenised electrodes, and found that gallium diffuses back into the aluminium bulk via grain boundaries, after having accumulated on the electrode surface during polarization. He found that gallium needed to be in direct contact with the aluminium bulk material, and that only the gallium accumulated during superactive discharge could diffuse back in the bulk material. He found no evidence that indium diffused back into the bulk material, which indicates that the grain boundary diffusion rate for indium is much lower than that of gallium, or that indium is more strongly bound to the electrode surface than gallium.

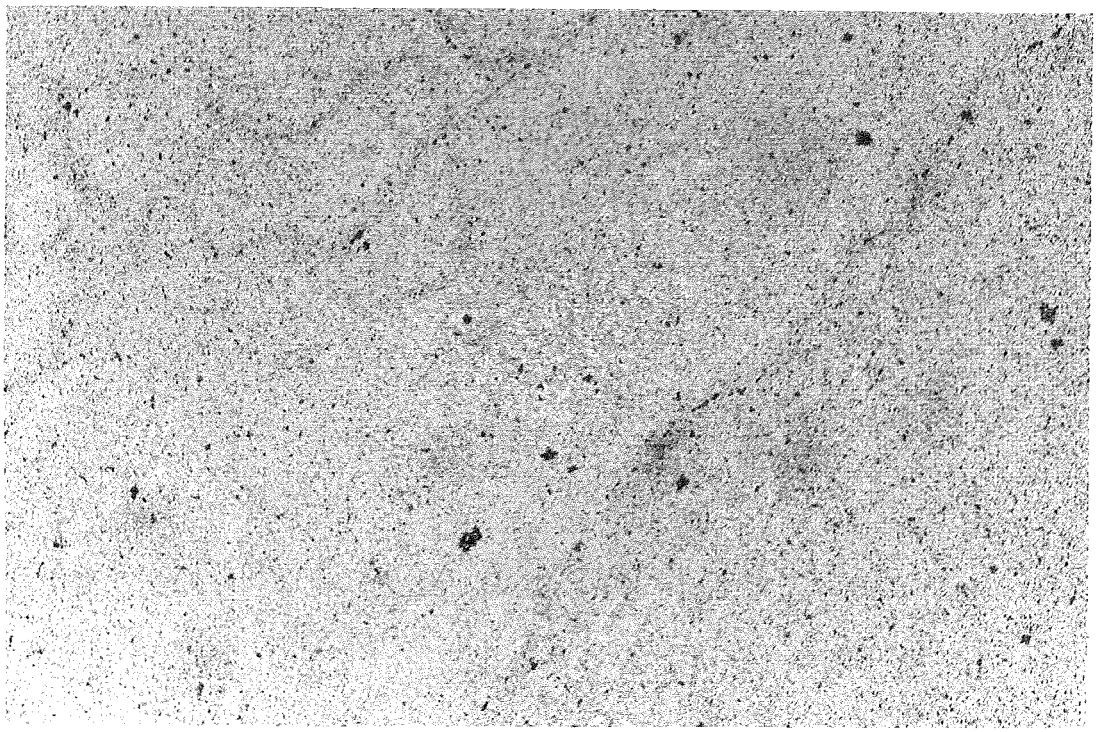

Photo 4.2.16 - Al - 0.85%In - 0.09%Ga
Magnification 130x

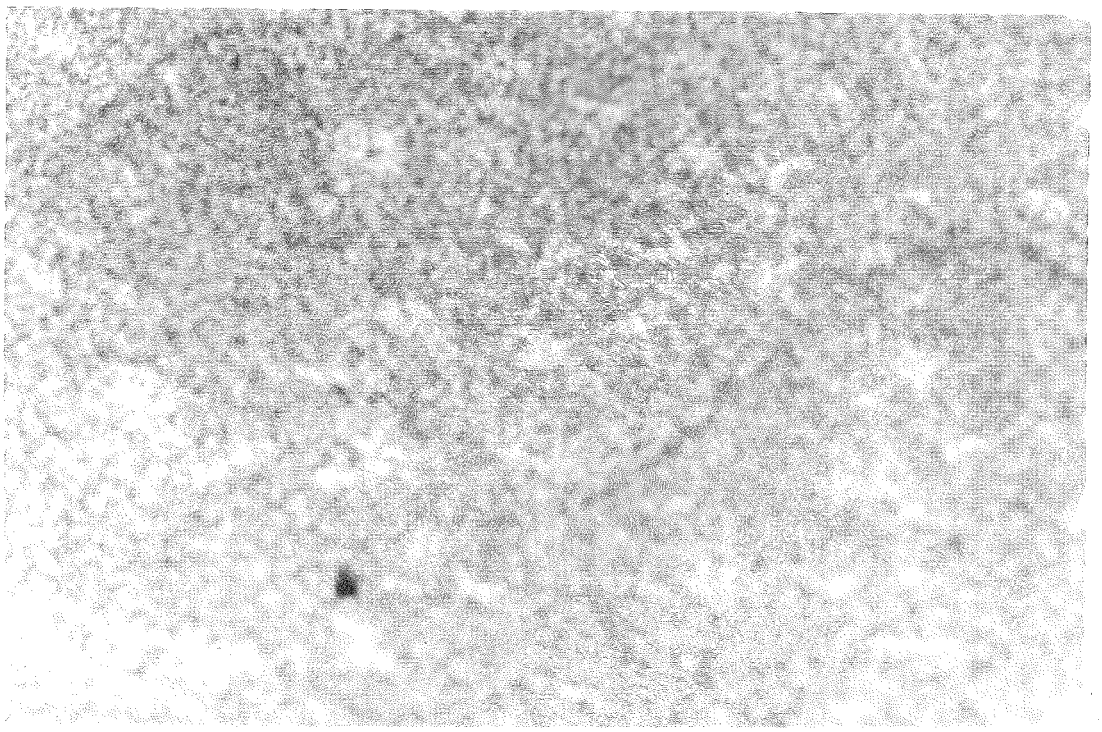

Photo 4.2.17 - Al - 0.11%Ga
magnification 130x

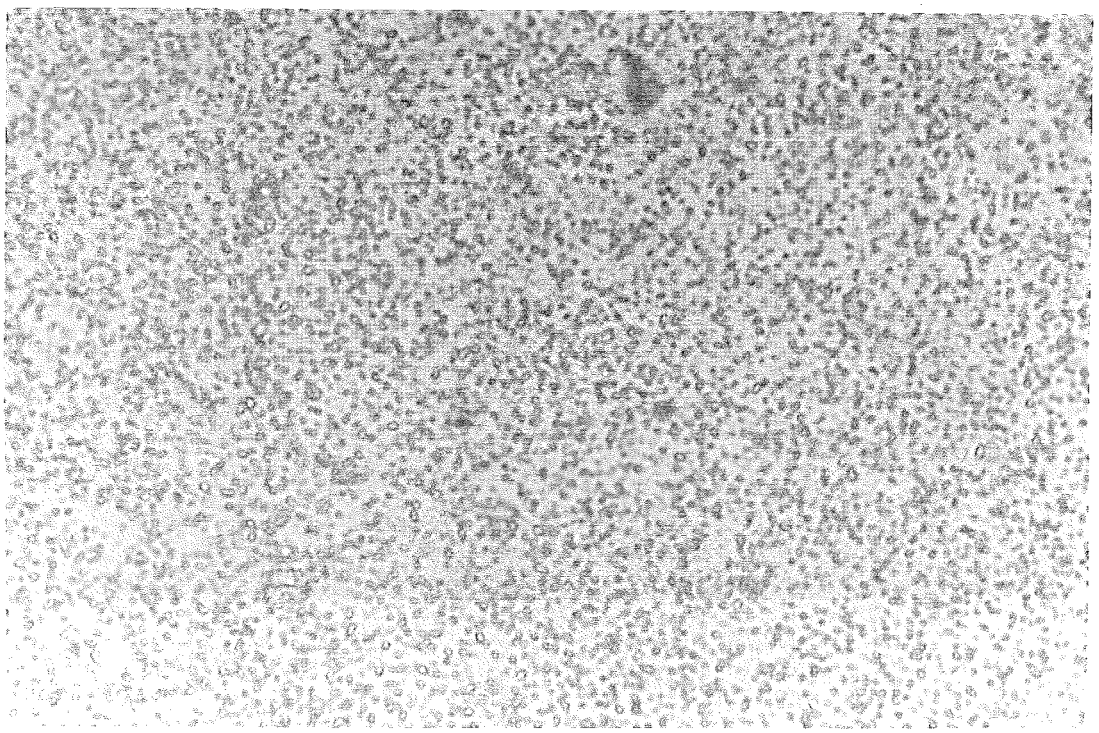

Photo 4.2.18 - Al - 0.085%In - 0.09%Ga
Magnification 1300x

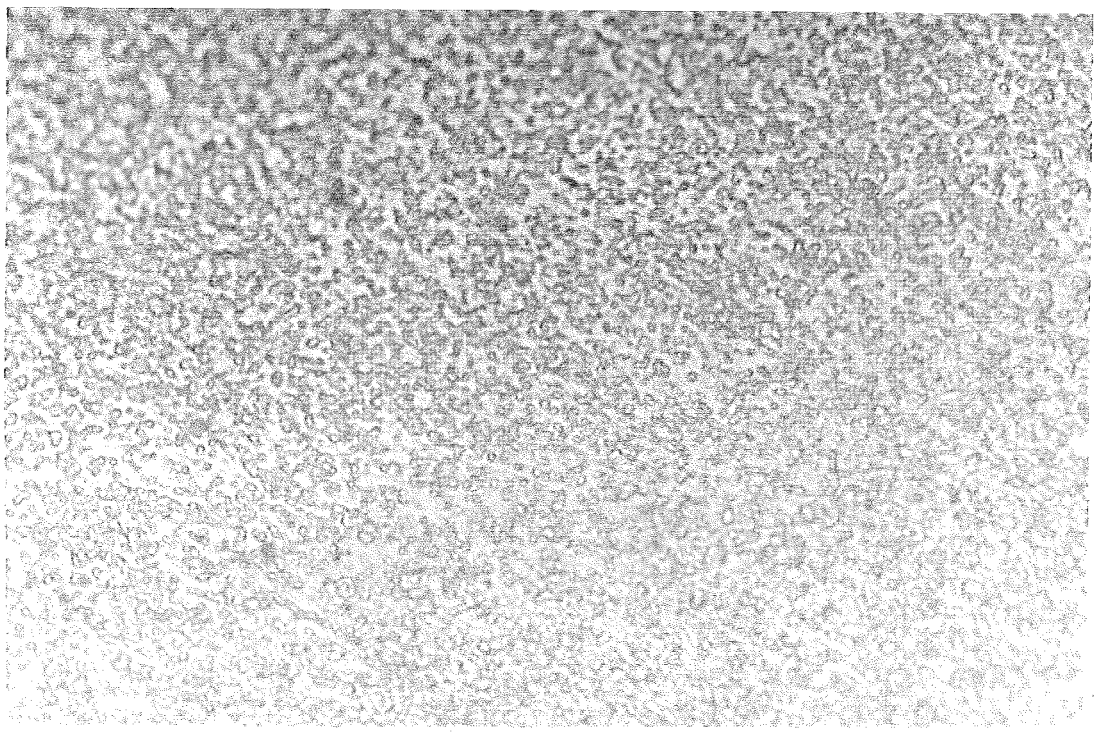

Photo 4.2.19 - Al - 0.11%Ga
magnification 1300x

4.3 Comparing results of other workers

The reliability of any new or modified piece of apparatus is often checked by comparing the results with those of other workers in the field where possible. Using the published results of two different sets of workers (27,32), a comparison of results at 25 and 50 °C for pure aluminium in 4M KOH is given below.

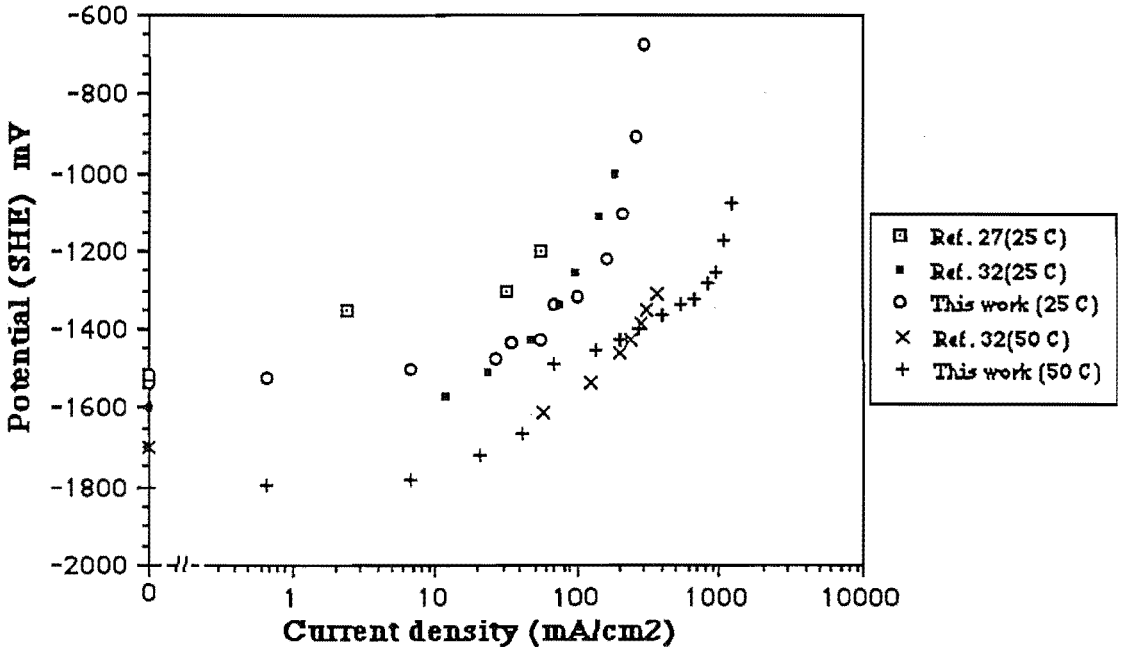

Graph 4.3.1 Comparison of Macdonald et al (ref. 32)
Brown & Whitley (ref. 27) with our data for
Pure aluminium in 4M KOH at 25 and 50°C

The results for this work agree more closely with those of Macdonald et al (32), with only minor differences being evident, which are possibly due to differences in experimental conditions.

The results of Brown and Whitley (27) are very different from both this work and Macdonald's results, thus suggesting that there were significant experimental differences.

For this work it was not thought necessary to have hydrogen continually passing through the solution to remove any free oxygen present. This was due to the continual hydrogen production at the electrode surface, at rest and to reasonably high current densities (100 - 1000 mA/cm^2), thus making it unlikely that oxygen would reach the electrode surface unreacted.

The graph below supports these assertions, showing that with or without oxygen removal the polarization curves are identical to within experimental error.

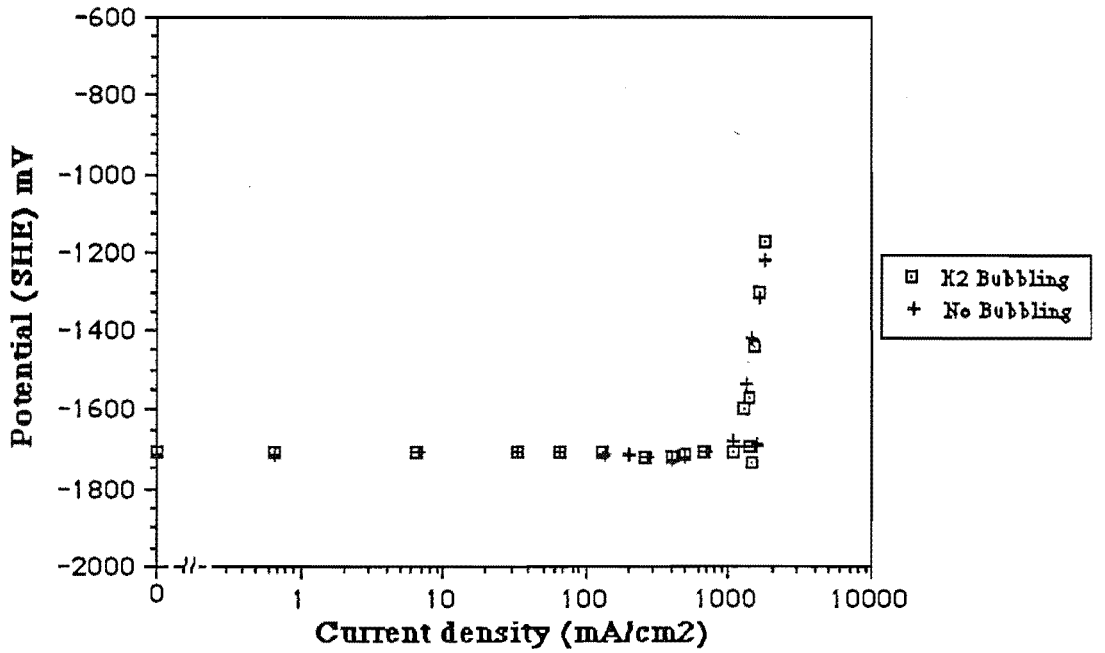

Graph 4.3.2 Polarization of Al - 0.1%Mg - 0.1%In in 6M KOH, at 60°C, with a flow velocity of 1.47 m/s with and without H_2 removal

Support is also provided by the closeness of these results to those of Macdonald et al (32), graph 4.3.1, given that Macdonald used oxygen free solutions.

4.4 Aluminium & In / Ga / Mg alloys

Only a selection of the polarization results are presented here to illustrate specific points. The remainder are given in appendix C.

It is shown in the following sections how the polarization characteristics of aluminium vary with environmental factors, and low level alloying. The purpose of this work is to identify the electrochemical behaviour of various aluminium alloys suitable for Al / Air battery systems.

Temperature effects

The polarization curves for pure aluminium with varying temperature are given below,

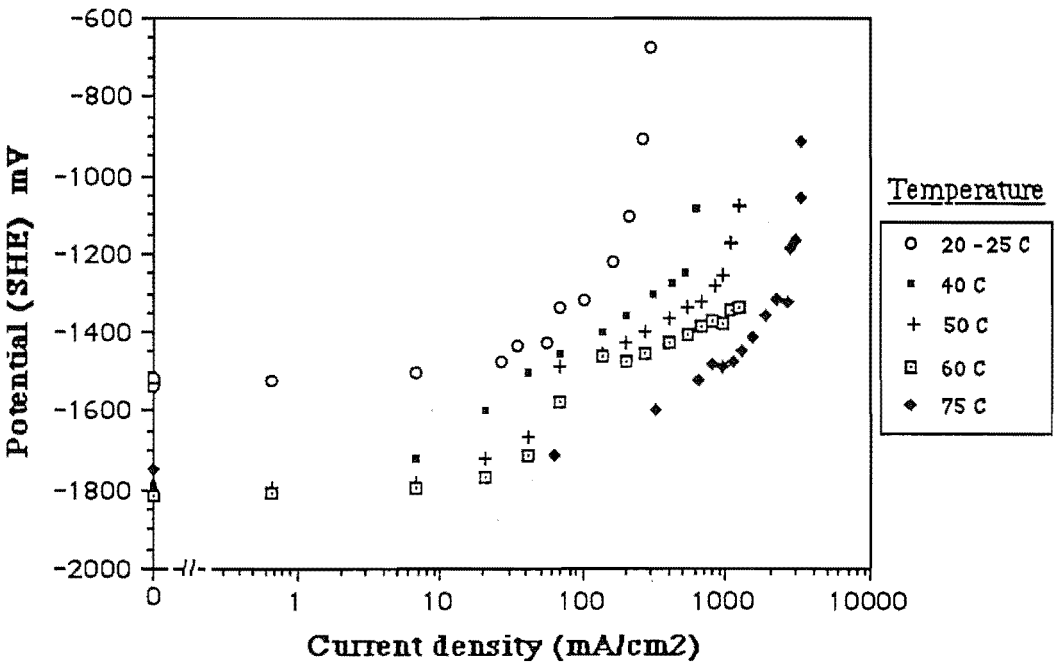

Graph 4.4.1 Polarization curves for Pure (5N) Aluminium in 4M KOH with a flow velocity of 1.47 m/s

The rest potential becomes significantly more negative for pure aluminium with an increase in temperature from 25 to 40 °C, but does not become increasingly more negative for further rises in temperature. This trend is opposite to that predicted by theory, for a metal / metal ion couple, as shown by Macdonald (73), but can be explained by an increase in oxide conductivity, and a thinning of the oxide layer, with increasing temperature. Some standard electrode potentials (vs SHE) for metal / metal ion couples, from (73), are:

Fe^{2+} / Fe -0.44V @ 25, -0.42V @150, -0.39V @300°C

Al^{3+} / Al -1.67V @ 25, -1.61V @150, -1.53V @300°C

CuO_2^{2-} / Cu 1.51V @ 25, 1.67V @150, 2.00V @300°C

all of which become more positive with increasing temperature.

The effect of temperature on the rest potential for aluminium and its alloys is best illustrated below (graph 4.4.2).

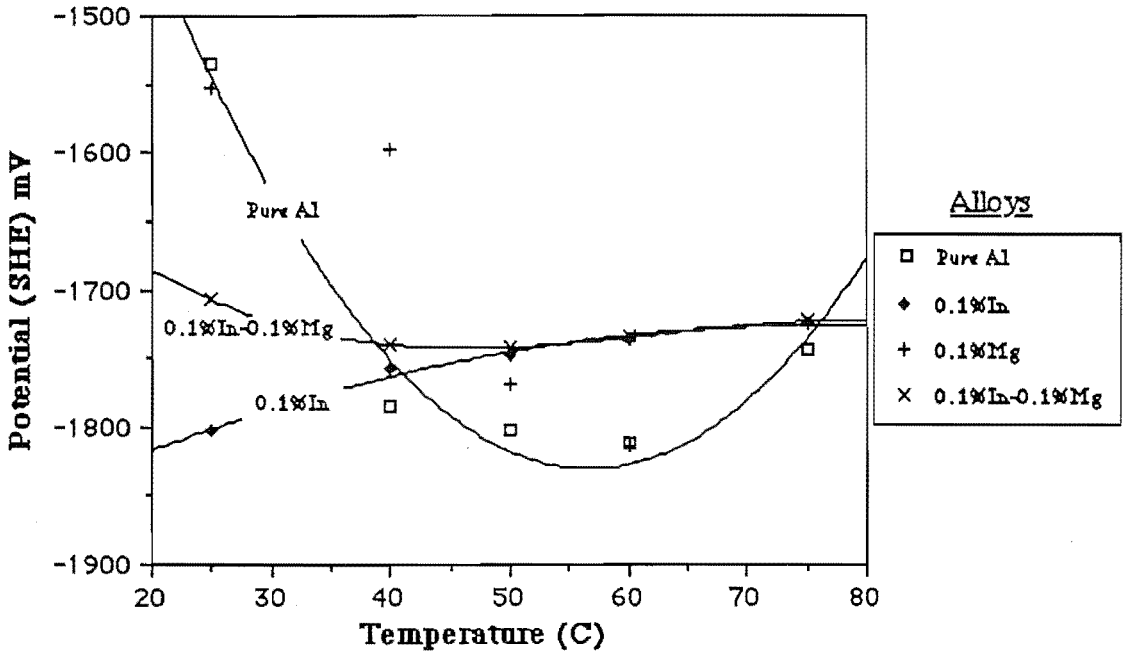

Graph 4.4.2 Rest potential dependence on temperature
in 4M KOH with flow velocity of 1.47 m/s

The above graph shows the significant effect on potential that occurs when small amounts of alloy are added to pure aluminium. It is interesting to note that the effect on potential bought about by the addition of magnesium to the binary Al - In alloy diminishes with increasing temperature, thus the ternary Al - Mg - In curve coincides with the binary Al - In curve above 50°C.

The pure aluminium curve shows a minimum at approximately 55°C, which is explained by a thinning of the oxide layer and an increase in hydrogen production with increasing temperature.

The Al - 0.1%In alloy rest potential becomes more positive with increasing temperature, due also to the increased hydrogen production with increasing temperature.

This trend of the potential becoming more negative with increasing temperature, as found for pure aluminium (graph 4.4.1), is also evident for the Al - 0.1%Mg alloy (graph 4.4.3 below), but is not present for the Al - 0.1%Mg - 0.1%In ternary alloy (graph 4.4.4 below). This indicates that the indium directly modifies the oxide layer, which is observed experimentally by the appearance of a black surface film, and that the magnesium is involved mainly in modifying the grain structure (i.e. grain refinement as shown in micrographs earlier).

The polarization curves for the Al - 0.1%Mg - 0.1%In alloy.(graph 4.4.4) shows the current density increasing with temperature as expected, but more significant is the independence of the rest potential. This independence of the rest potential also occurs for the indium containing binary alloys, which also form a black surface film in hydroxide solutions. The above trends have been observed to occur for hydroxide solutions with or without aluminate present.

The onset of significant polarization for the alloys generally coincides with the removal of this surface film (i.e. the black surface film disappears, leaving a metallic looking surface), after which the aluminium dissolution reaches its limiting current density, and the potential is positive enough that hydrogen production ceases. At this point the anode current efficiency is approximately 100%, as shown later in this chapter.

By contrast, observation of the pure aluminium electrodes showed that they undergo parasitic corrosion in alkaline solutions, which increases with increasing solution temperature. The gasing at the electrode increases with current density, this is the so called " Negative Difference Effect " (NDE) and has been observed by other workers (11,23). No quantitative measurements were made of the NDE, as this was not an experimental objective.

As predicted by theory (shown by Butler - Volmer equation in appendix .E) the current density obtainable for a particular overpotential is increased by increasing the solution temperature, which is attributed to an increase in the exchange current density, or the transfer coefficient (α) and diffusivity. This is best illustrated in graphs 4.4.3 and 4.4.4 below, and is discussed further in the "alloy effects" section.

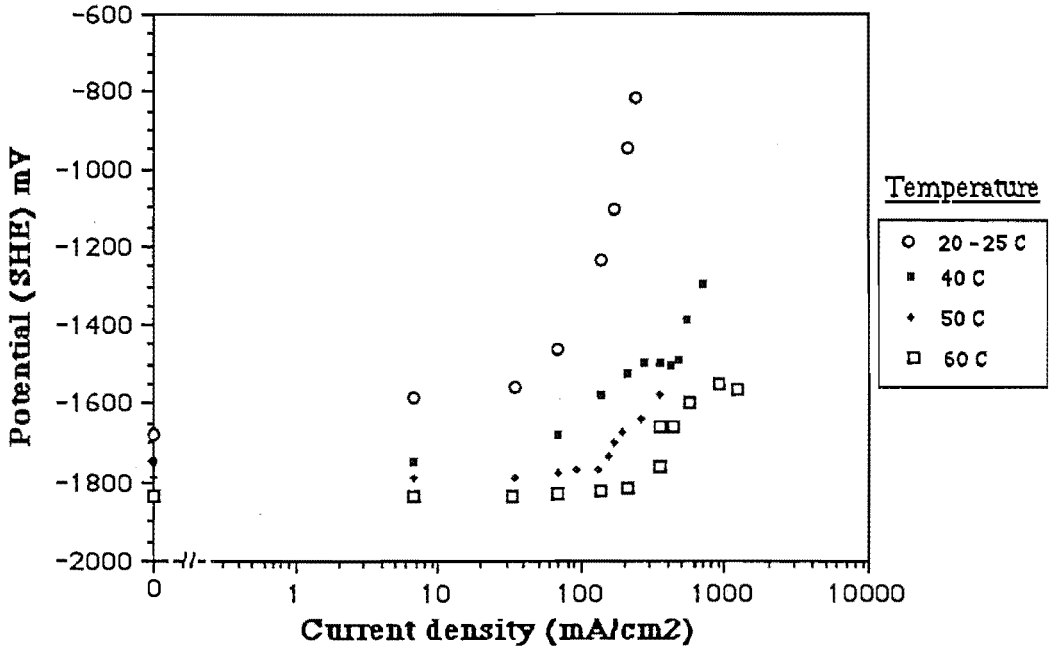

Graph 4.4.3 Al - 0.1%Mg polarization curves in 4M KOH + 9.5 g/l AlO_2^-, with a flow velocity of 1.47 m/s

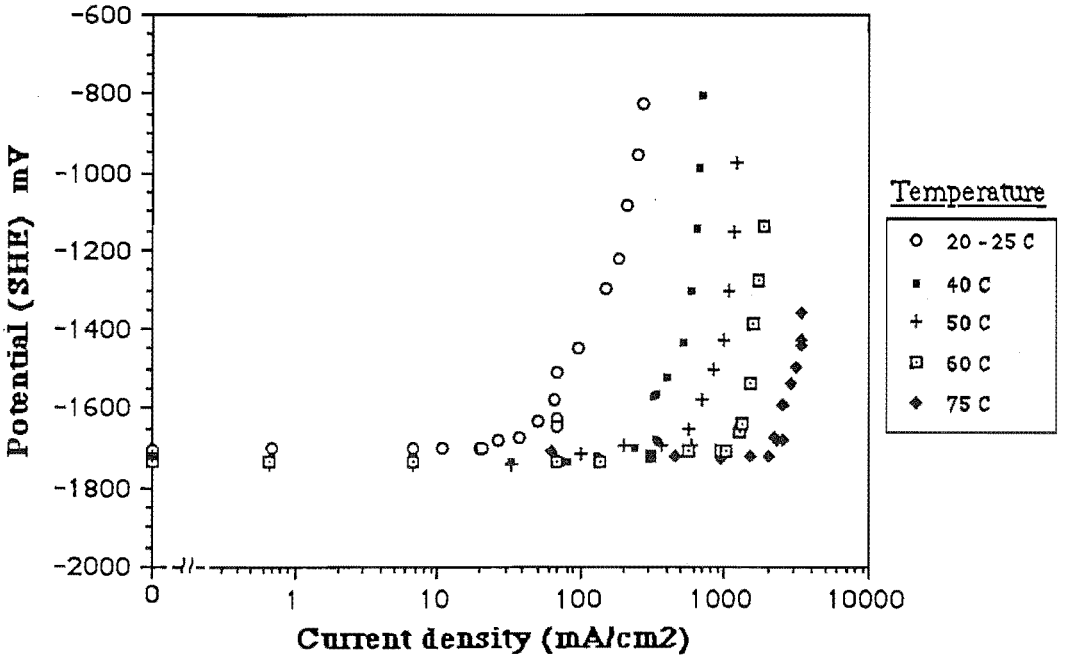

Graph 4.4.4 Al - 0.1%Mg - 0.1%In alloy polarization curves in 4M KOH with a flow velocity of 1.47 m/s

A short experimental program to investigate the anode efficiency and corrosion current (method of calculation given in appendix.G) for the Al - 0.1%Mg - 0.1%In and Al - 0.1%In alloys was undertaken. The electrodes were placed in the flowcell under no load conditions for 5 hours to obtain the corrosion current, via weight loss measurements.

Two one hour polarization stages were carried out using new electrodes for each stage, where the electrodes were polarised to as high a current density as possible without removing the surface film, and then to a very high current density, so dissolution was in the passive region, with no black surface film or visible gasing. The tables below show the results of this work.

Table 4.4.1 Anode efficiency at different current densities for Al -0.1%Mg -0.1%In

Temperature °C	H_2 I_{corr} mA / cm^2	Efficiency with film (@ -1750mV)	Efficiency without film (@ -1600mV)
50	65.6	92.5% @ 325 mA/cm^2	100% @ 600 mA/cm^2
60	44.2	80.7% @ 454 mA/cm^2	99.1% @ 1227 mA/cm^2
75	52.0	81.4% @ 785 mA/cm^2	97.2% @ 2164 mA/cm^2

Solution = 4M KOH + 70 g/l AlO_2^-

Table 4.4.2 Anode efficiency at different current densities for Al -0.1%In

Temperature °C	H_2 I_{corr} mA / cm^2	Efficiency with film (@ -1775mV)	Efficiency without film (@ -1600mV)
60	77.7	84.6% @ 738mA/cm^2	99% @ 1353mA/cm^2
75	62.6		

Solution = 4M KOH + 70 g/l AlO_2^-

Hunter (33) has investigated different grades of aluminium in 4N NaOH at 60°C, the table (4.4.3)below is a summary of his corrosion results.

Table 4.4.3 Hunter's Corrosion Results

Aluminium Purity %	H_2 I_{corr} mA / cm^2	Efficiency @ 300 mA / cm^2
99.999	118.1	79.3 %
99.99	286.4	71.6 %
99.9	407.5	60.3 %

The above tables 4.4.1 - 4.4.3 show the significant improvement that can be obtained by using small amounts of alloys in the aluminium bulk. The ternary alloy (table 4.4.1) shows a minimum in parasitic corrosion at 60°C and a no load corrosion current lower than for the Al - 0.1%In alloy at the same temperature. The ternary alloy and the Al - In alloy have the same rest potential at 60°C, with the ternary alloy having a no load corrosion rate of 44.2 mA/cm^2 and the binary indium alloy that of 77.7 mA/cm^2. This represents a 43% reduction in corrosion rate, thus illustrating the beneficial effect of magnesium, and supporting assertions made by Macdonald et al (32) and Jeffery & Halliop (34) that magnesium is a corrosion reducer.

From the three tables above the effect of the alloying components on pure (5N) aluminium can be seen. The addition of 0.1% indium to aluminium reduces the corrosion current from 118 mA/cm^2 to 77.7 mA/cm^2, whilst the addition of 0.1%Mg to this binary Al - In alloy further reduces the corrosion current to 44.2 mA/cm^2,which is 37% that of the original value for pure aluminium.

Table 4.4.3 illustrates the significance of aluminium purity, showing the corrosion current to be greatly decreased, and the anode efficiency to be increased, as the aluminium purity increases.

Wasteful corrosion, which can be measured by the amount of hydrogen produced, is not of real concern from a safety point of view in an operating Al / air cell, as the cell gases will be exhausted with the excess air that passes through the cell. It does however represent a drop in anode efficiency.

Of major importance in any battery system is the continuous power availability, which is measured by the power density obtainable for any particular electrode.

The maximum attainable power density , as seen in graph 4.4.5, increases with increasing temperature. The initial slope of each curve is the same, which indicates that although the reaction rate is changing with temperature, the rate determining step for the Al - Mg - In alloy is still the same. This is supported by the observation that the surface film remains to higher current densities as the temperature increases.

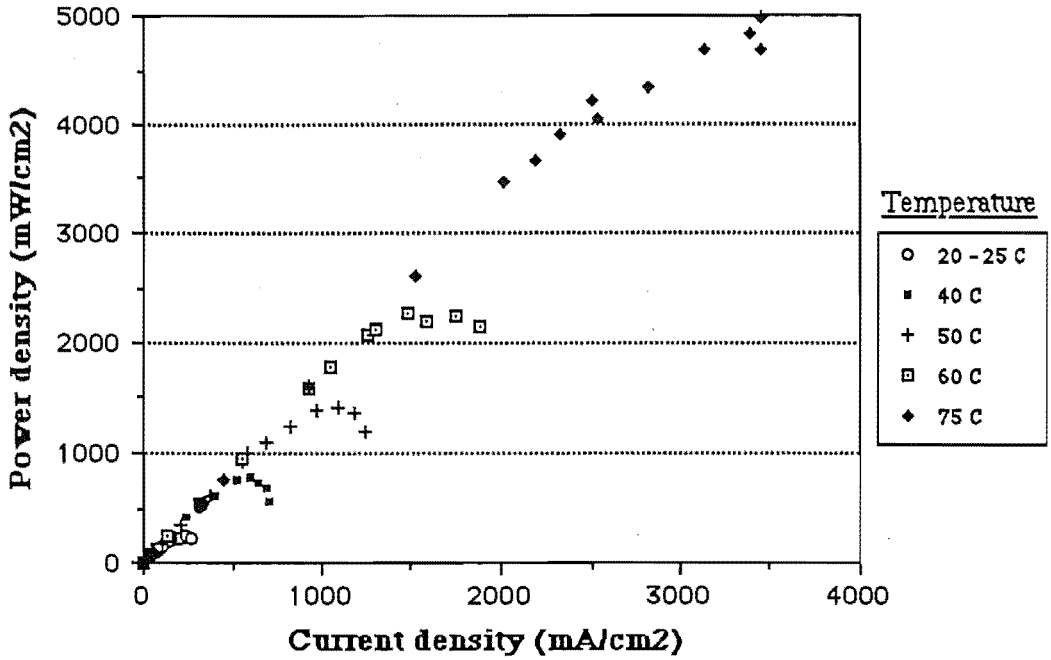

Graph 4.4.5 Power output dependence on temperature for Al - 0.1%Mg - 0.1%In anodes, in 4M KOH, with a flow velocity of 1.47 m/s

Alloy effects

How each alloying component contributes to the power density is also of interest and is illustrated below in graph 4.4.6 .

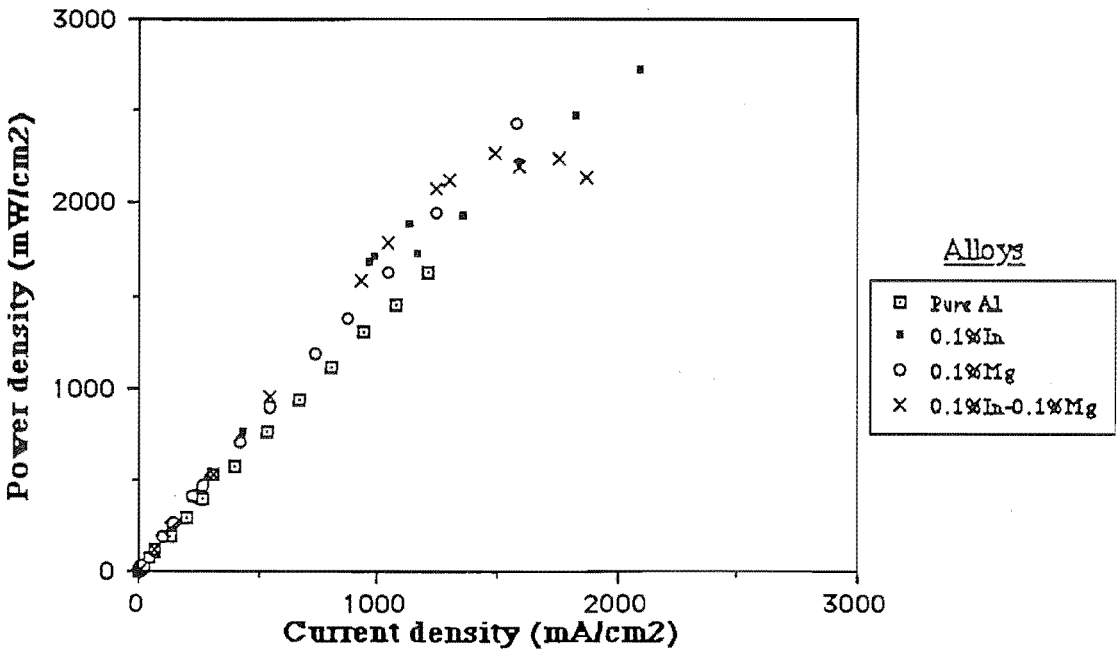

Graph 4.4.6 Power density for various alloys at 60°C, in 4M KOH, with a flow velocity of 1.47 m/s

The power density of aluminium is improved with indium and magnesium whether in the binary or ternary alloy. The maximum power density attainable for the two binary alloys is however greater than that of the ternary alloy. The ternary alloy generally follows the same curve as the indium alloy, with a deviation which apparently coincides with the removal of the surface film. After the film has been removed the ternary alloy tends to behave in a similar manner to the Al - Mg binary alloy, until its maximum power density is reached.

The slope of the power density curve clearly becomes steeper by addition of either alloy. This is due to the alloying elements modifying the polarization characteristics of aluminium, and inhibiting the cathodic hydrogen evolution reaction.

The effect of the indium alloying component on aluminium is illustrated in the graph below.

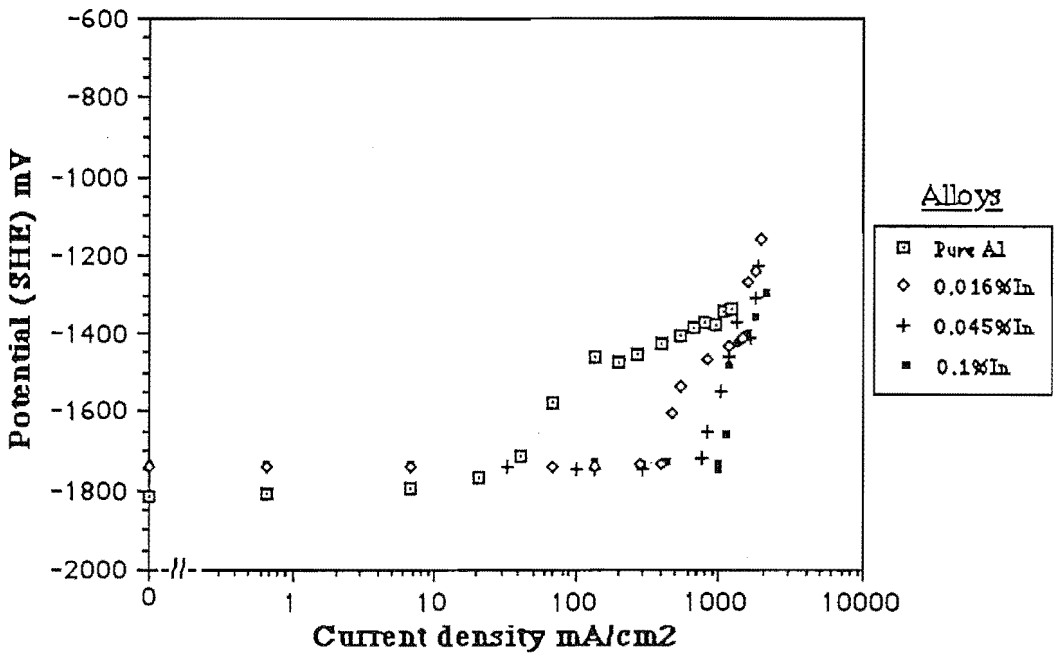

Graph 4.4.7 Indium alloy polarization curves at 60°C, in 4M KOH, with a flow velocity of 1.47 m/s

Very little indium is required to effect the polarization characteristics of aluminium. The polarization curves for all the indium alloys above are the same at low current densities (<400 mA/cm^2), possibly due to the presence of this black surface film, which appeared on all the indium containing alloys, and was independent of the indium content in the alloy. However the maximum current density attainable, without significant polarization occurring, for each alloy is dependent on the indium content of the alloy. As the potential shifts away from its no load condition the effectiveness of the alloying component diminishes, until eventually the pure aluminium and the alloy current - voltage curves coincide.

Graph 4.4.8 below illustrates the effect of indium at a specific overpotential. This graph shows the dramatic improvement associated with adding indium, but more importantly that there is little difference in attainable current density between 0.016% In and 0.1% In once the electrode significantly polarizes.

The current density - temperature dependence of the polarized alloy electrodes is shown in graph 4.4.9 below. This illustrates the improvement of the alloys over pure aluminium in the 20 to 80 °C range, and the need for magnesium shown by the improvement of the ternary alloy over the binary indium alloys at 75°C. This also shows that simple rate law theory (74) applies, given that in general the current approximately doubles for a 10 degree change in temperature. The Al - 0.1%In electrodes deviates from this simple theory above 70°C.

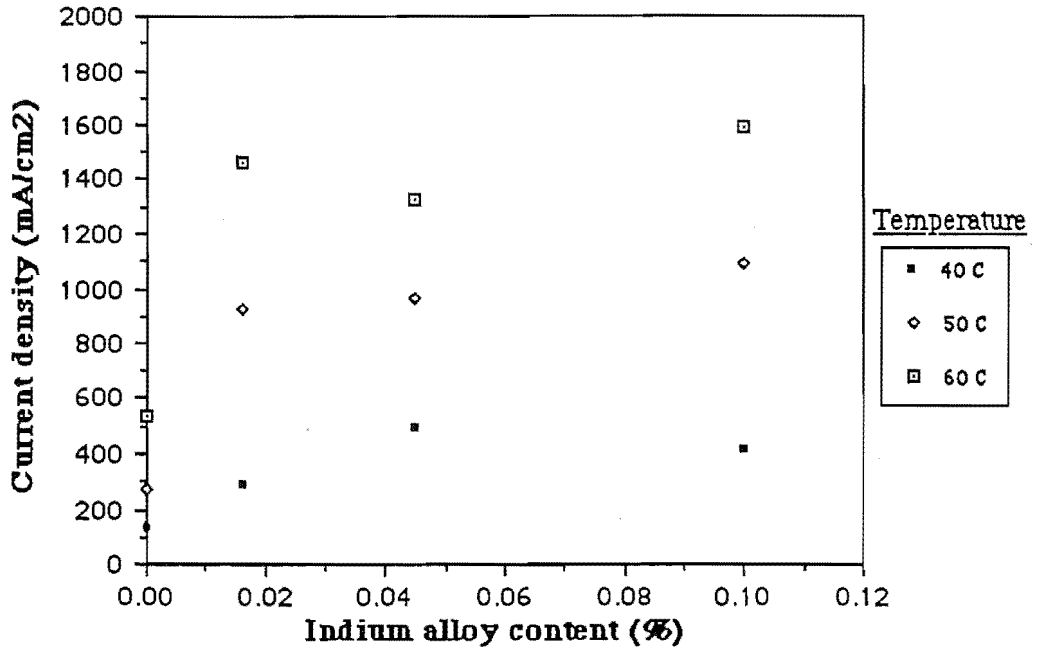

Graph 4.4.8 Indium temperature dependence
in 4M KOH, @ -1400mV vs SHE

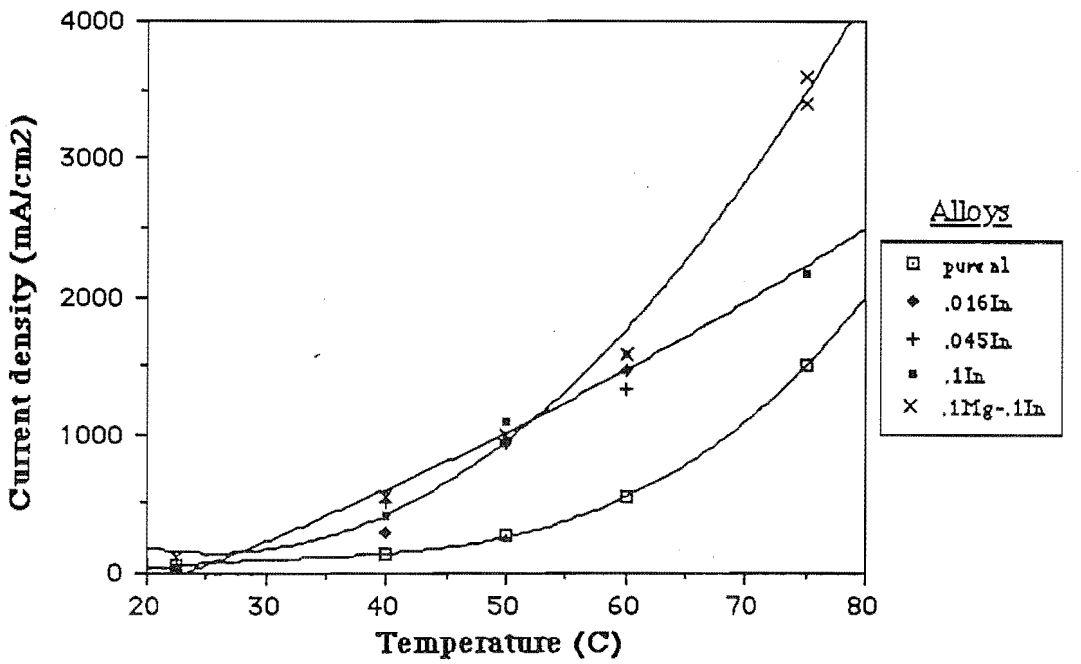

Graph 4.4.9 Alloy current density dependence
on temperature in 4M KOH @ -1400mV vs SHE

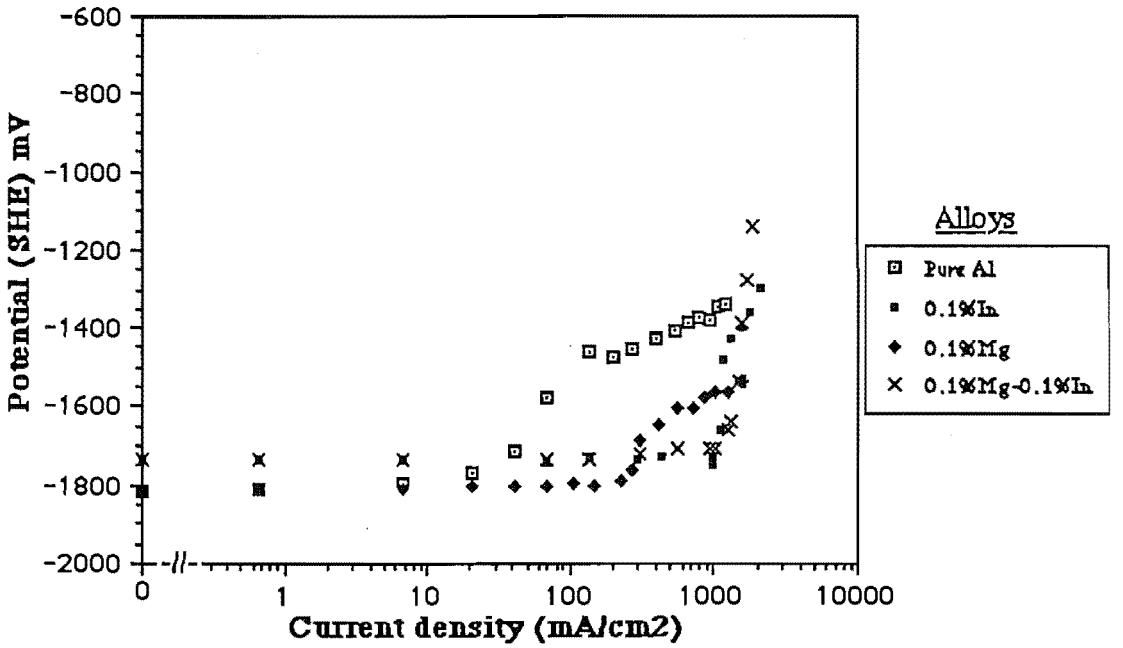

Graph 4.4.10 Al - 0.1%Mg, Al - 0.1%In and
Al - 0.1%Mg - 0.1%In alloy polarization curves
at 60°C,in 4M KOH, with a flow velocity of 1.47 m/s

Indium is clearly the dominant alloy in the ternary form, with magnesium having little effect on the polarization characteristic.

Magnesium alone as an alloying component tends to shift the aluminium polarization curve to higher current densities, which is obviously beneficial in a working cell. This is due to magnesium inhibiting the parasitic corrosion reaction as shown by tables 4.4.1 and 4.4.2, which is consistent with other workers observations (32,34), and increasing the exchange current density for aluminium discharge.

Even though the indium containing alloys shown in graph 4.4.10 have very negative rest potentials, it is clearly seen that these alloys have a more positive rest potential to that of pure aluminium. This is expected given that the theoretical indium reversible potential is positive to that of aluminium.

The maximum current density attainable is increased when indium is present, this could be due to a change in the exchange current density or transfer coefficient for aluminium dissolution and / or the hydrogen evolution reaction.

It has been suggested by Mosley (52) that an operating cell would operate in a current density range of 100 - 200 mA/cm^2, although this work clearly shows that 1000 mA/cm^2 would be quite acceptable. This means that there would be a potential advantage of approximately 60 mV by using the binary Al - Mg alloy, as compared to the ternary alloy.

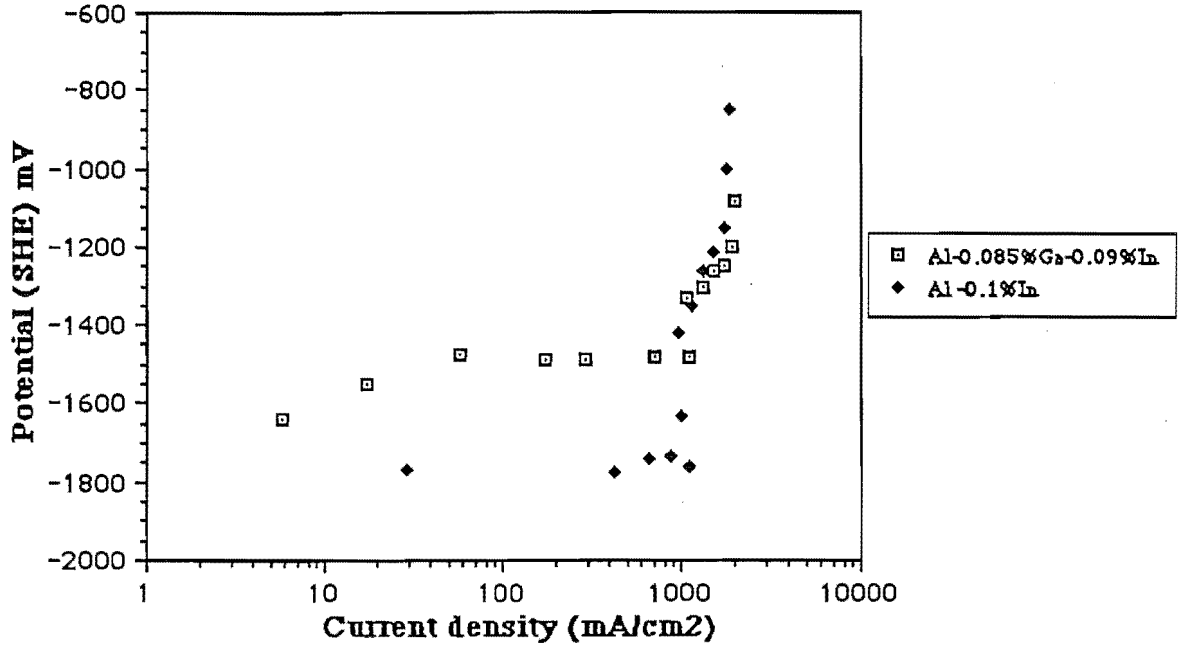

Graph 4.2.1 Gallium - indium polarization curves in 4M KOH + 9.5 g/l AlO_2^-, at 60 °C and a flow velocity of 1.47 m/s

Comparing the polarization characteristic for the Al-Ga-In ternary alloy to that of the Al - 0.1%In alloy clearly shows that it is the gallium that causes the rapid polarization of the ternary alloy in the low current density range. The only advantage that this has is that there is negligible gasing from this electrode once polarised. At the very high current densities the electrode behaves as if it were a binary Al-In alloy. This only partly agrees with Hunter's assertions that the indium alloying component is dominant over the other low level alloys (Mg, Ga, Tl). Any improvement in current - voltage characteristics for gallium containing alloys is likely to be due to grain boundary dissolution, which vastly increases the surface area of the electrode and consequently leads to its destruction.

The results observed here for gallium alloys effectively eliminate it as an alloying component for any battery applications.

Solution effects

The use of different cation species; varying the hydroxyl ion concentration, and the buildup of aluminate in the electrolyte with and without hydroxyl ion adjustment are three aspects of solution modification which have been investigated.

Despic et al (23) have investigated the cation effect on parasitic hydrogen production, and found that the NDE depended to some extent on the ionic radius of the cation, with the ammonium ion, which has a larger atomic radius than potassium or sodium, giving the lowest loss of aluminium due to parasitic corrosion. Roebuck & Pritchett (37) also found that the cations in solution can have a significant effect on the corrosion rate.

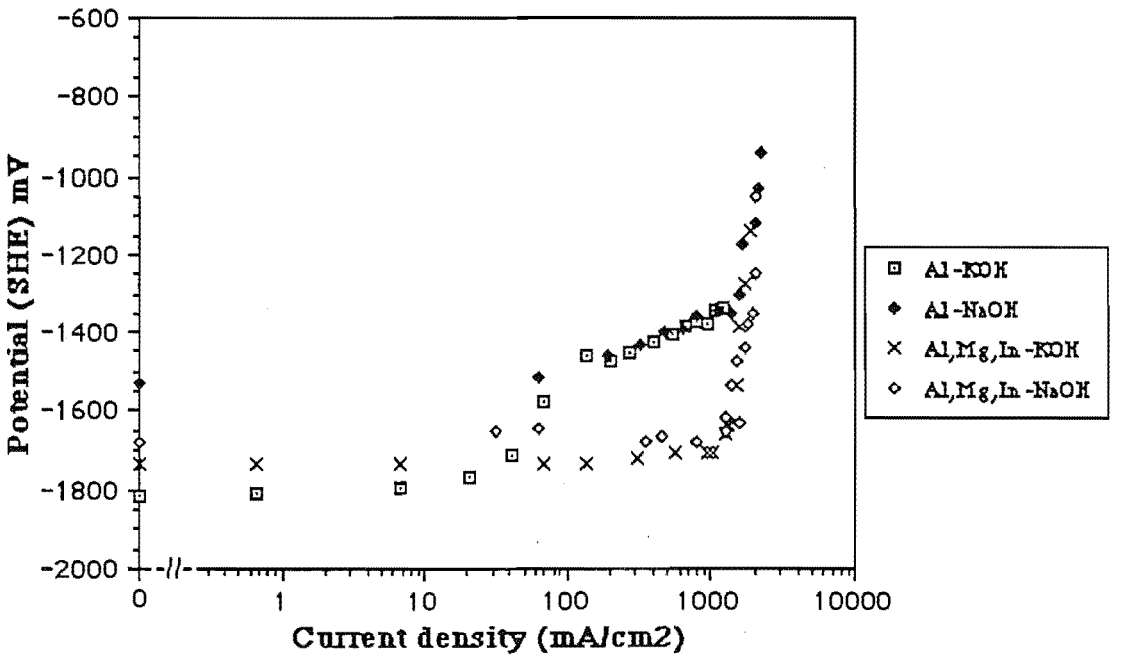

Graph 4.4.11 Comparison of Pure Aluminium and Al - 0.1%Mg - 0.1%In, in 4M KOH and 4M NaOH at 60°C, with a flow velocity of 1.47 m/s

In this work NaOH has been compared to KOH, and found to give no significant difference in polarization behaviour (graph 4.4.11). Any differences been the two solutions for the pure aluminium electrode can be attributed to solution impurities, of which the effects become insignificant at current densities above 50 mA/cm^2 due to aluminium dissolution predominating. There was no detectable cation effect on polarization for either the ternary alloy or the pure aluminium electrode as shown in the graph above.

Graph 4.4.12 below shows that the trends already established for the various alloys in KOH solution, hold similarly for the NaOH solution (i.e. similarity between the binary and ternary alloys, and the improvement obtained over pure aluminium when alloying).

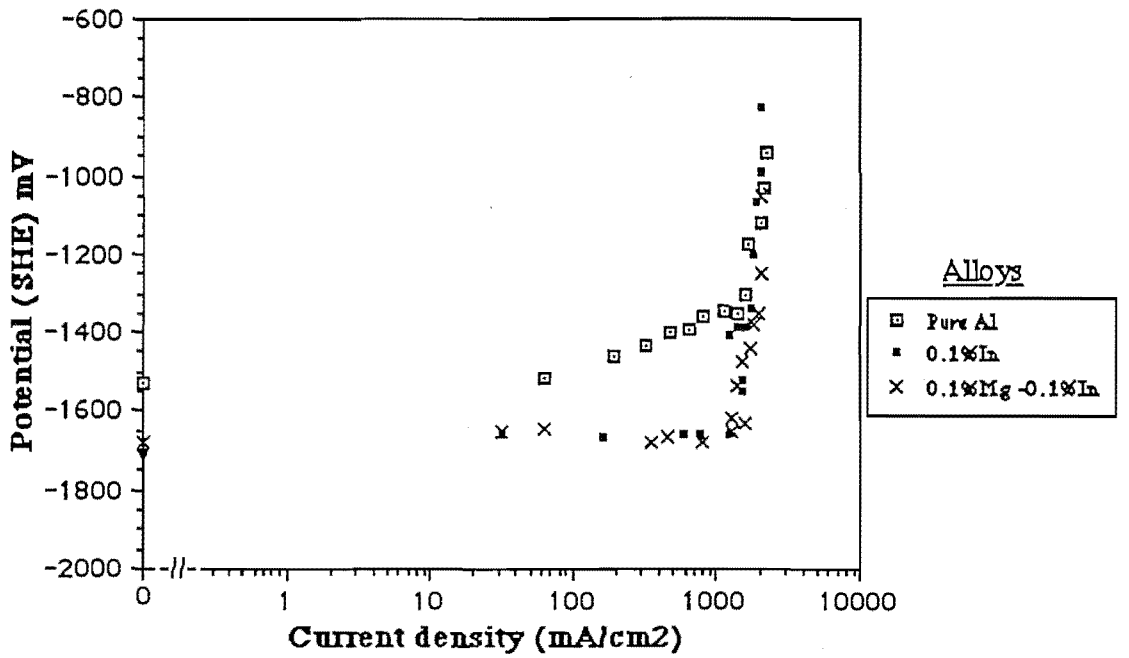

Graph 4.4.12 Aluminium alloy polarization curves
in 4M NaOH, at 60°C, with a flow velocity of 1.47 m/s

The effect of increasing hydroxyl ion concentration has also been investigated, and a significant difference in trend between the ternary alloy and pure aluminium has been found. The polarization curves for pure aluminium (shown below, graph 4.4.13) move to slightly higher current densities with increasing concentration. This is in agreement with Macdonald's (17) stepwise dissolution mechanism, where the rate controlling step, and the current density, are dependent on the availability of hydroxyl ions.

The ternary alloy (graph 4.4.14 below) behaves quite differently, showing a marked dependence on the concentration of hydroxyl ions. The curve for the 2M KOH is polarized at a markedly lower current density, whereas the 4M KOH and 6M KOH curves are virtually indistinguishable. This trend indicates that the surface film is concentration dependent for KOH concentrations below 4 $mol.l^{-1}$, with no significant advantage in using solutions of greater than 4 $mol.l^{-1}$ for the ternary alloy.

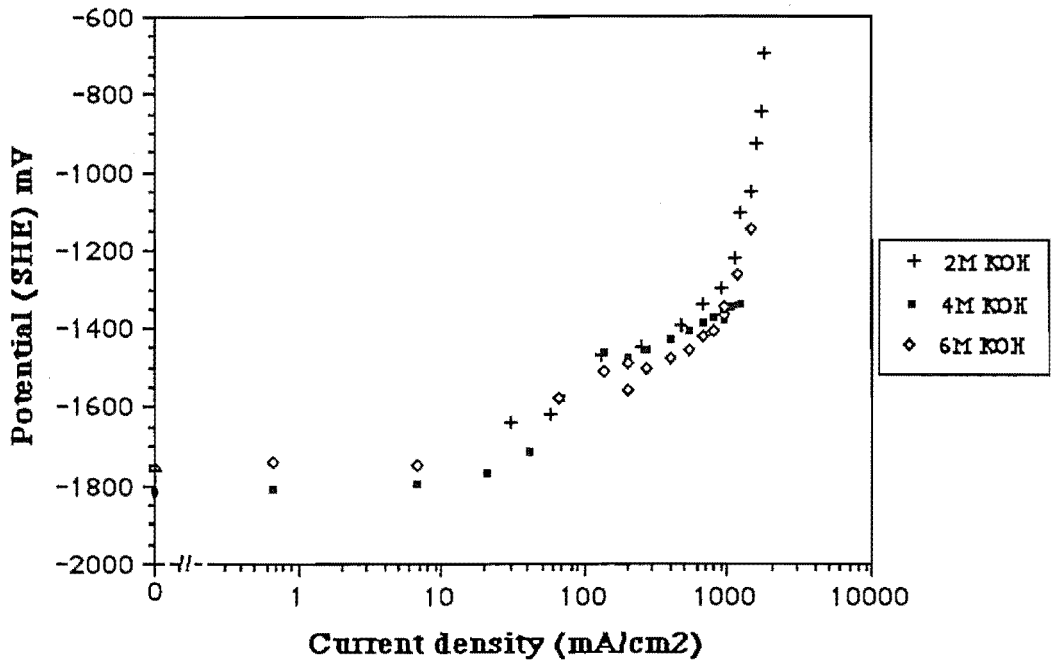

Graph 4.4.13 Solution concentration influence on polarization for pure aluminium at 60°C, with a flow velocity of 1.47 m/s

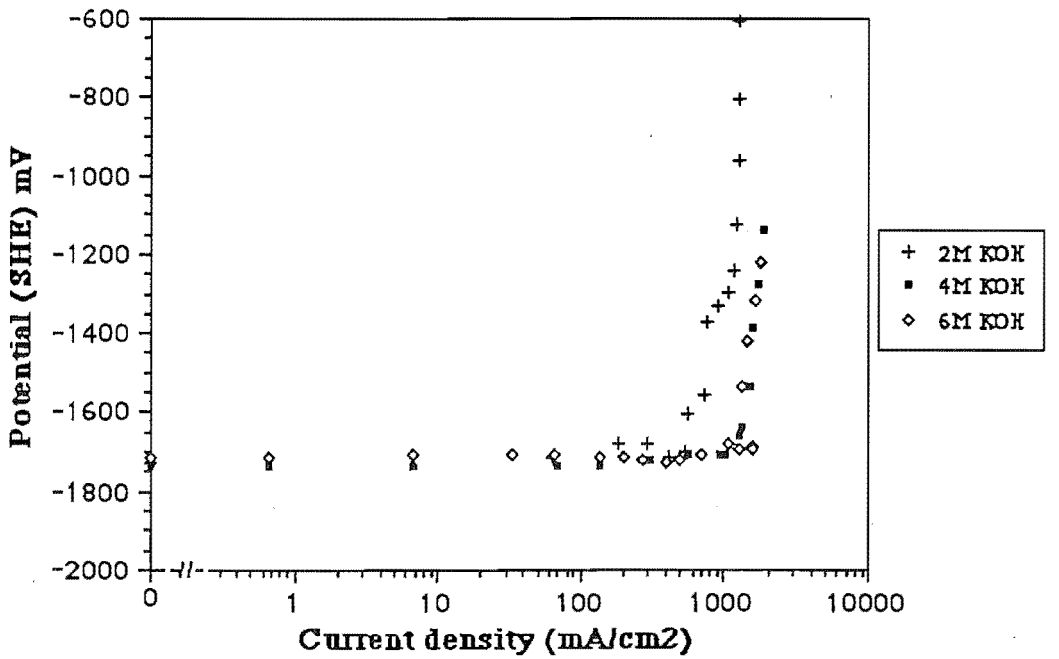

Graph 4.4.14 Solution concentration influence on polarization for Al - 0.1%Mg - 0.1%In at 60°C, with a flow velocity of 1.47 m/s

A comparison of how the current density varies for a specific overpotential is illustrated in graph 4.4.15 below This graph shows an optimum concentration of approximately 4M KOH for the two alloys. Pure aluminium on the other hand does not show this behaviour. The fast cut results (chapter.3) also suggest this. There is little difference between the Al-0.1%In binary alloy and the Al-0.1%Mg-0.1%In ternary alloy. The steady increase in the aluminium current density with concentration, observed here, has also been reported by Koshel et al (18).

The power density for the ternary alloy at varying KOH concentrations (graph 4.4.16) shows the same trends as for current density, with a discontinuity for each curve corresponding to the disappearance of the black surface film. The change from 2M to 4M KOH represents an increase in the maximum power density attainable from 1.2 watt/cm^2 to 2.2 watt/cm^2, but there is no significant increase in going from 4M KOH to 6M KOH.

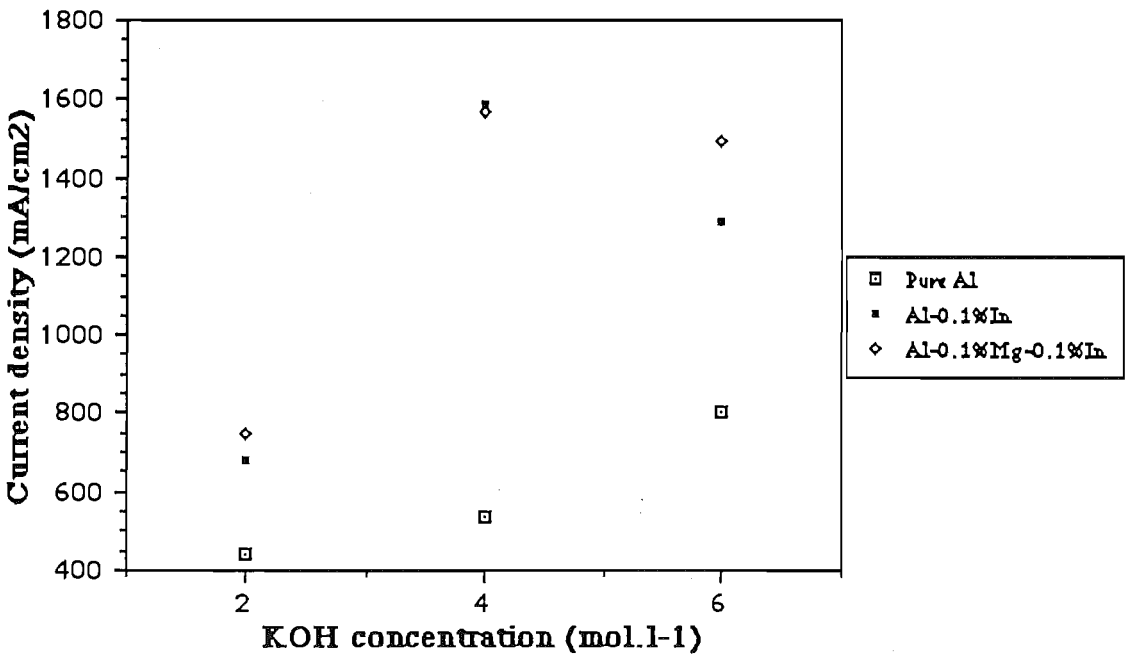

Graph 4.4.15 Solution concentration influence on aluminium alloys at 60°C, @ -1400mV vs SHE, with a flow velocity of 1.47 m/s

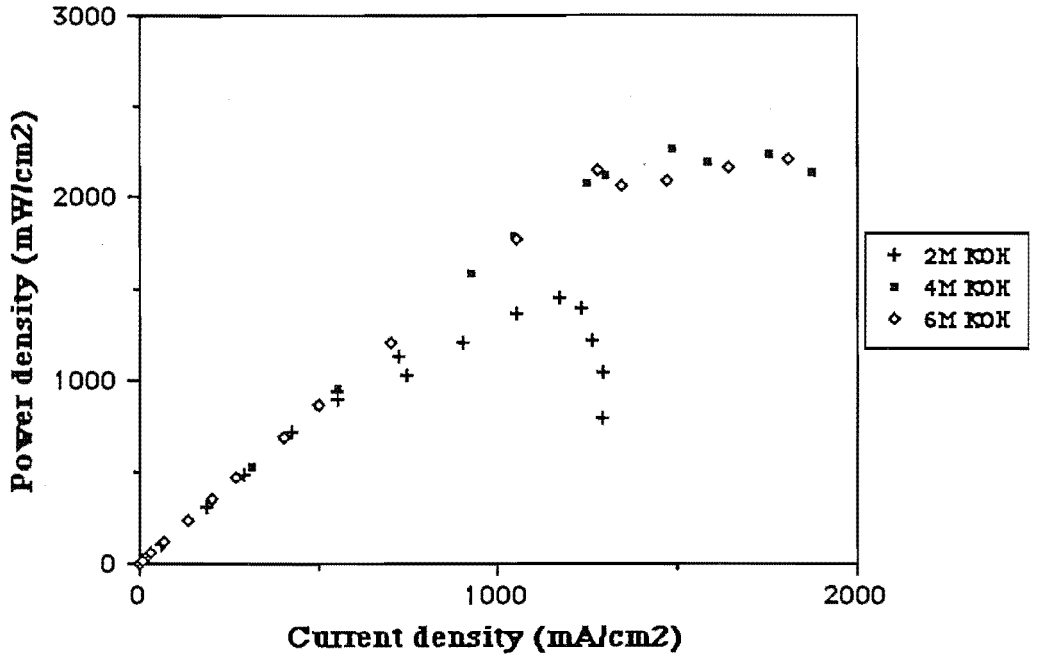

Graph 4.4.16 Al - 0.1%Mg - 0.1%In power density dependence on KOH concentration, at 60°C, with a flow velocity of 1.47 m/s

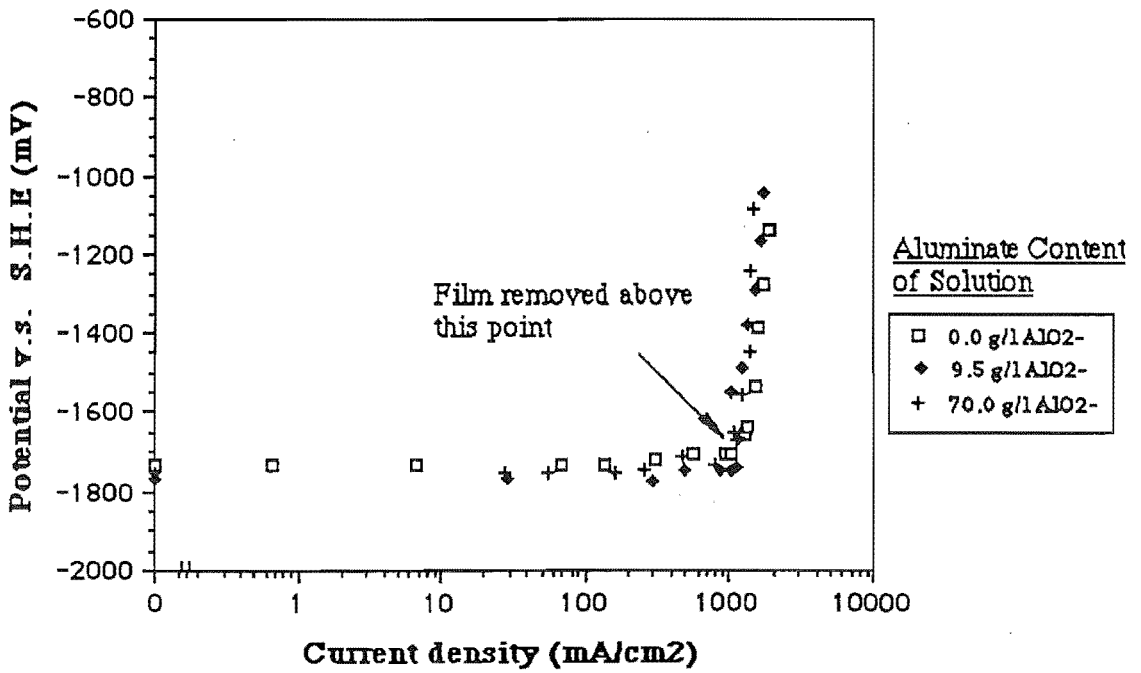

Graph 4.4.17 Al - 0.1%Mg - 0.1%In aluminate dependence in 4M KOH, at 60°C, with a flow velocity of 1.47 m/s

The effect of aluminate has been investigated in two ways, so that an Al / air cell with and without hydroxyl ion regeneration can be represented. The regeneration of hydroxyl ions in the Al / air electrolyte normally occurs by seeding the aluminium hydroxide solution, thus causing further precipitation of aluminium hydroxide. The precipitation reaction is as follows:

$$Al(OH)_4^-{}_{(aq)} \quad \text{-----} > \quad Al(OH)_{3\,(sol)} \quad + \quad OH^-{}_{(aq)}$$

The release of the single hydroxide ion helps maintain the solution alkalinity.

The film covered ternary alloy (Al - 0.1%Mg - 0.1%In) in 4M KOH solution with aluminate and hydroxyl ion adjustment (graph 4.4.17) shows no distinguishable change on the electrode potential due to the aluminate in solution. Once the surface film has been removed there is a significant difference in polarization curves. The polarization curves for the 9.5 g/l (0.16M) and 70 g/l AlO_2^- (1.18M) solutions are within experimental error, and have shifted to lower current densities (approximately 100 mA/cm^2@ -1400mV) to that of the curve for the pure KOH solution.

The trend of a shift in polarization curves with aluminate concentration found for the hydroxyl ion adjusted solutions (i.e. solutions with regeneration), has been found to also apply to the solutions non-adjusted for hydroxyl ion depletion due to aluminium dissolution (Graph 4.4.18). This graph shows that the polarization curves are shifted to lower current densities as the aluminate concentration increases. The observed shift is greater in the non - adjusted solutions due to a decrease in hydroxyl ion concentration, e.g. the KOH solution was initially at 4M, but after dissolution of aluminium to obtain 70 g/l aluminate the hydroxyl ion concentration has fallen to 2.8M.

A direct comparison of the adjusted and non-adjusted hydroxyl ion solutions is given in Graph 4.4.19. As expected there is no difference between the polarization curves when the surface film is present. The current - voltage characteristic for the non-adjusted solution polarizes at a slightly lower current density to the adjusted solution. At the upper polarization limit (> -1400 mV) the curves for the aluminate containing solutions coincide, however the current - voltage curve for the aluminate free solution is more favourable in all cases.

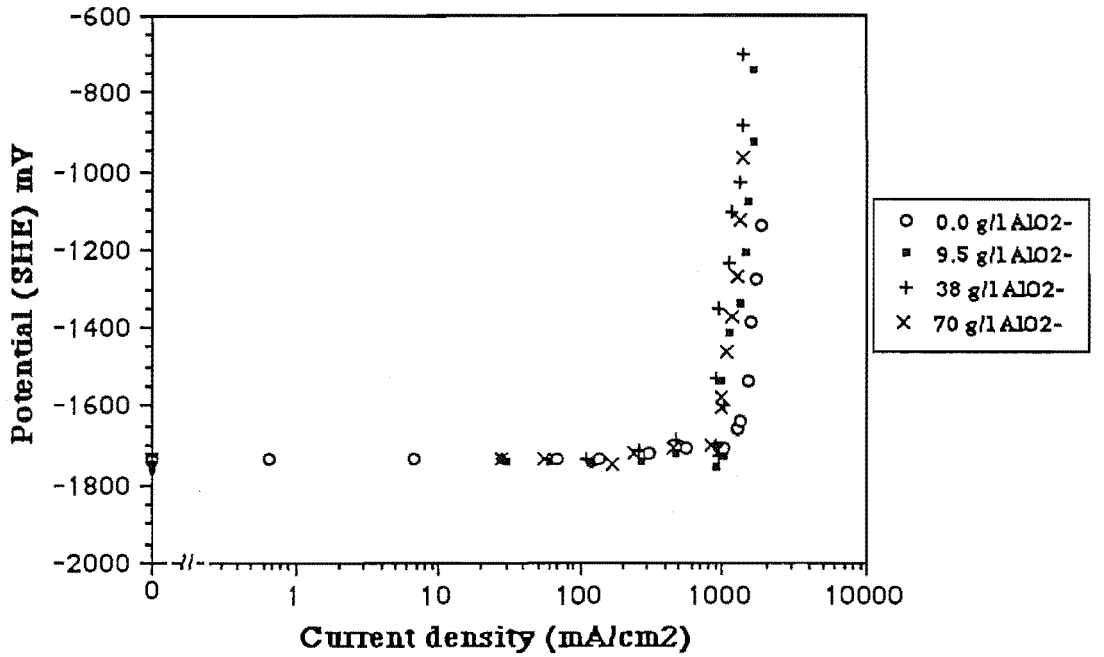

Graph 4.4.18 Aluminate influence on Al - 0.1%Mg - 0.1%In polarization, for solutions not adjusted for hydroxyl ion depletion Solution initially at 4M KOH, at 60°C,with a flow velocity of 1.47 m/s

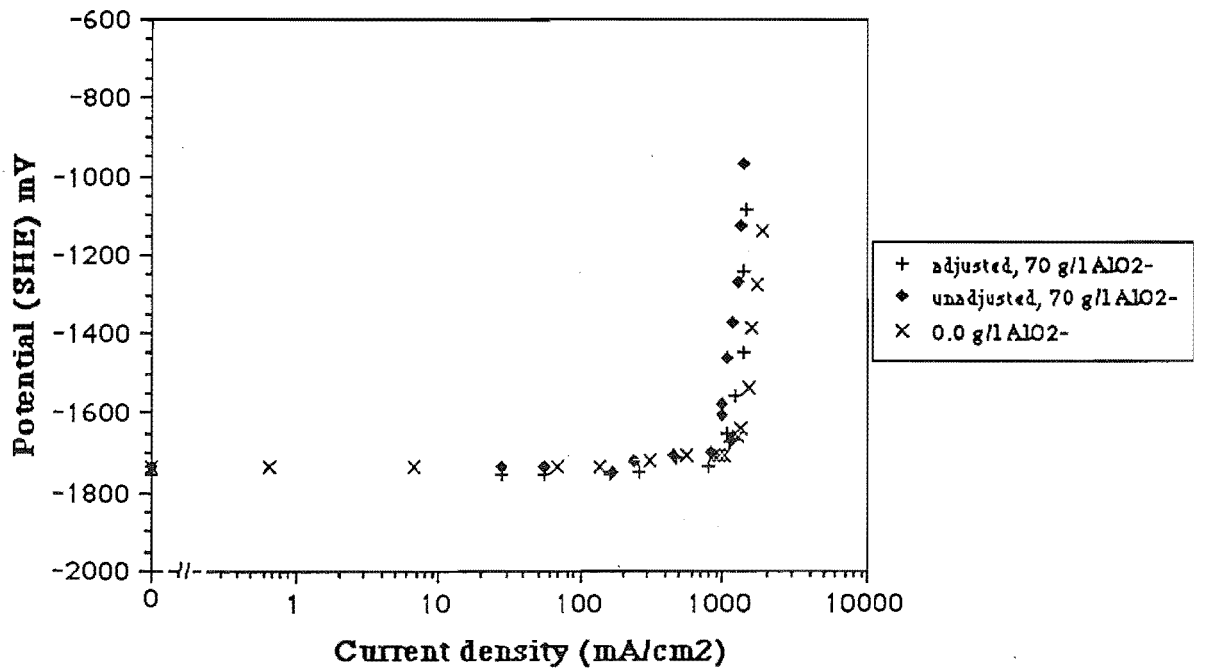

Graph 4.4.19 Al - 0.1%Mg - 0.1%In polarization dependence in 4M KOH, with and without hydroxyl ion adjustment and / or aluminate, at 60°C, with a flow velocity of 1.47 m/s

Flowrate effects

Varying the flowrate has the effect of changing the boundary layer thickness over the electrode surface, which effects the rate at which the reaction products are removed from the electrode surface.

The influence of flowrate on pure (5N) aluminium (Graph 4.4.20) shows little difference in polarization characteristics in the low (< 40 mA/cm^2) current density region, but as shown by the curve for the 4M NaOH solution the limiting current density is increased with increasing flowrate.

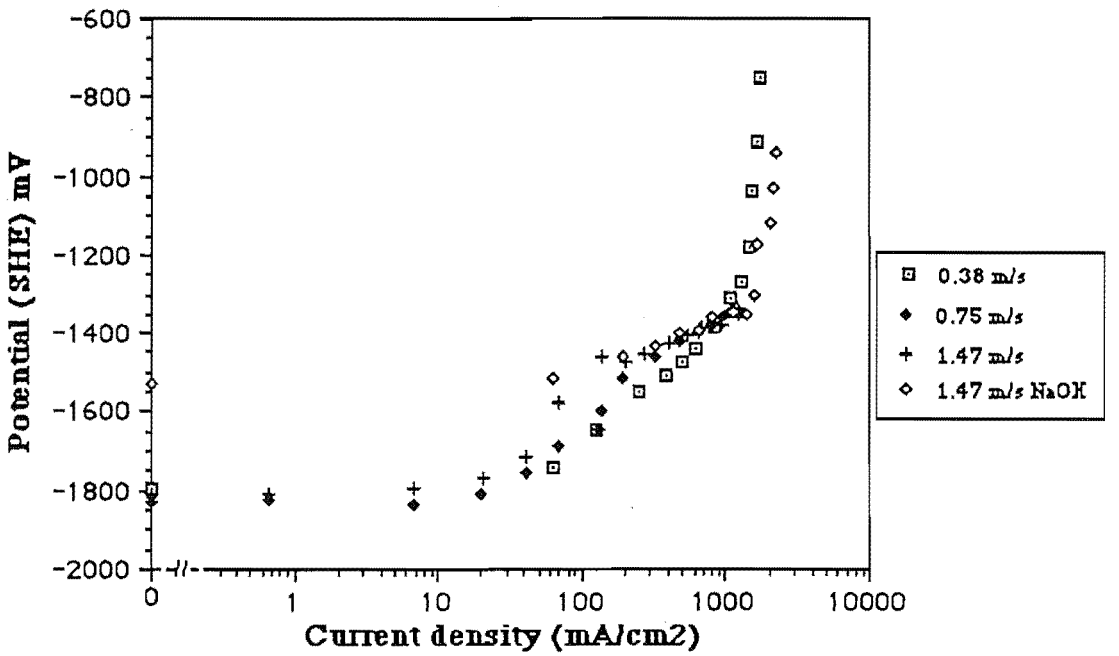

Graph 4.4.20 Flowrate influence on pure aluminium polarization in 4M KOH, at 60°C

However the difference in polarization curves over the current density range of 40 - 800 mA/cm^2 is greater than can be explained by any error in the correction of the solution potential drop, thus is attributed to varying rates of hydrogen gas removal from the reaction surface. The hydrogen gas removal is coupled to the increase in hydrogen evolution with increasing current density, which cathodically polarises the electrode.

The gas bubbles coming off the electrode surface at the low flowrate (0.38 m/s) were observed to be much larger than those at the high flowrate (1.47 m/s), thus the flowrate effects the degree of coalescence on the electrode surface.

The power density curves for the pure aluminium electrode (Graph 4.4.21 below) do not show any significant variation with flowrate, even though the current - voltage curves (graph 4.4.20) have a distinct deviation. This shows that the power density is less sensitive to changes in polarization characteristics.

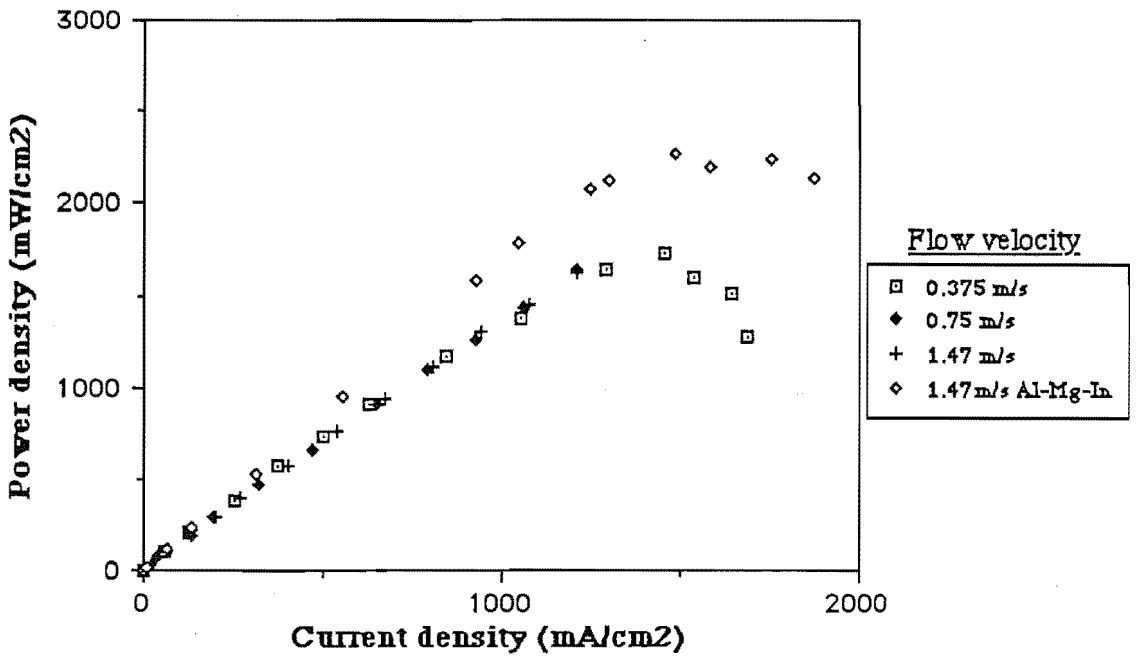

Graph 4.4.21 Pure aluminium power density dependence on flow velocity, in 4M KOH, at 60°C

The power density curve for the ternary Al - 0.1%Mg - 0.1%In alloy is shown in the above graph, illustrating the significant improvement that is attainable by adding small amounts of alloy to pure aluminium.

The polarization curves, showing flowrate dependence, for the indium containing alloys (Graph 4.4.22) are quite different to those of pure aluminium. These curves show a polarization independence on flowrate while the surface film is present, and a higher polarization at lower current densities for the lower flowrate (0.38 m/s) after the surface film has been removed. It would appear that within experimental error it is unneccessary to use flowrates greater than 0.75 m/s for the ternary alloy.

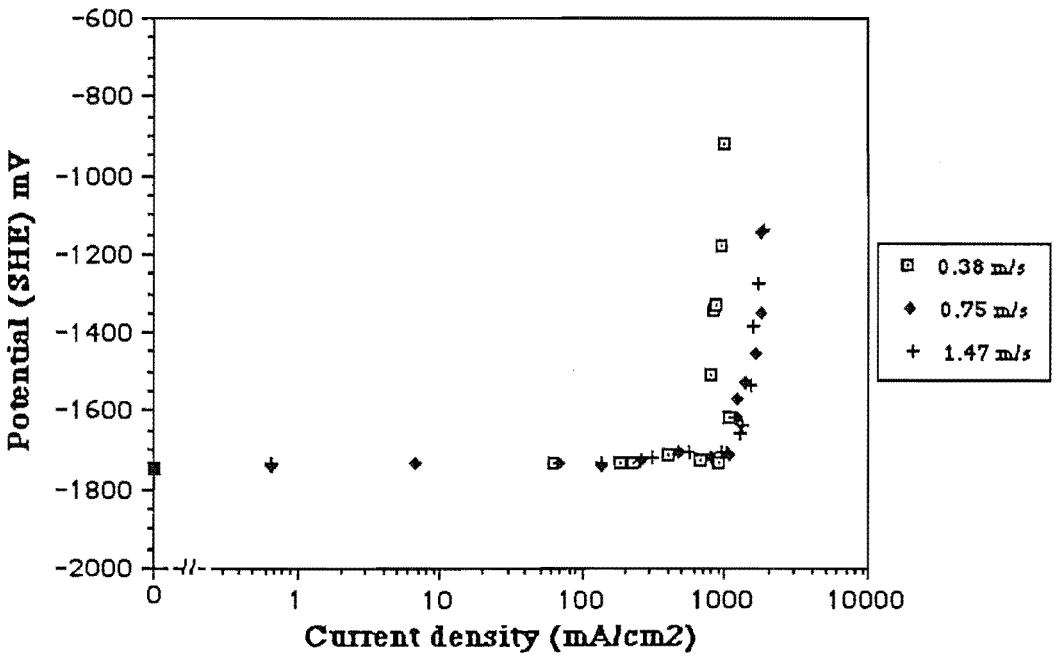

Graph 4.4.22 Flowrate influence
on Al - 0.1%Mg - 0.1%In polarization,
in 4M KOH, at 60°C

It can be concluded that for flowrates above 0.75 m/s, the dissolution of aluminium is activation controlled, and not diffusion controlled.

Chapter.5
Conclusions & Recommendations

General:

The purpose of this work has been to investigate the dissolution behaviour of aluminium and its alloys in hydroxide solutions at elevated temperatures, and to identify the parameters that will most effect an operating Al / air battery system.

It is quite clear that the addition of small amounts of indium, magnesium and gallium to aluminium shifts the rest potential in a negative direction. This is also accompanied, in the case of indium and magnesium, by a decrease in the cathodic hydrogen evolution reaction.

All the alloys used in this work have been used in the as - cast condition, and have shown various amounts of segregation to grain boundaries, and a radial appearance on etching of the surface. Most workers to date have used heat treated alloys to maintain the alloying elements at their maximum solubility in the aluminium bulk (homogenized). The significance of whether an electrode is used in the as - cast or homogenized condition needs to be further clarified, especially for the higher order alloys. The results of this work show that many of the alloys investigated here are suitable for use as anodes in an electrochemical cell. It is clearly advantageous, from cost considerations, if an alloy can be used in the as - cast state.

Many workers (15,25,33,39,41,42) have investigated alloys made using lower than 99.99% aluminium, and have found that any beneficial alloy effects are reduced with increasing impurity level. It is recommended that only aluminium of greater than 99.999% purity be used to make the alloy anodes.

The alloy dominance effect reported by Hunter (33) can not be supported from these results, which suggest that this effect may be heat treatment related, given that Hunter used homogenized alloys.

Even though gallium aids in the solvation of indium into the aluminium lattice, its high affinity to the grain boundary, which results in the eventual destruction of the electrode, means that it is most unsuitable as an alloying constituent for anodes.

Fast cut work:

The use of the fast cut technique showed the measured peak potential to be a transient mixed potential, which was more positive (approx. -1960 mV) than the expected theoretical value (-2370 mV @ pH=14). This is due to immediate onset of the cathodic hydrogen evolution reaction in alkaline solutions, after cutting of the electrode.

It has been found that the peak potential is independent of indium concentration for indium alloys of less than 0.1%In, but dependent on the gallium concentration, shown to become more negative with increasing gallium content (upto the 0.11% level tested).

It was found that the steady state / mixed potential data obtained from the fast cut results for the Al - In alloys corresponded well with the rest potentials measured using the flowcell. The results showed that there is a logarithmic relationship for the mixed potential with indium content of the binary alloys, and that there is little advantage in using an indium content of greater than 0.04%.

The fast cut results showed that the hydroxide concentration should be greater than $1 mol.l^{-1}$ and less than $6 mol.l^{-1}$. The flowcell results showed there to be an optimal hydroxide concentration of approximately $4 mol.l^{-1}$.

Flowcell work:

The flowcell that was developed to investigate the polarization behaviour of the alloys at elevated temperatures, also showed that the construction materials used (ABS plastic, teflon and perspex) would be suitable for use as a construction material for an operating battery system.

A black film covered the surface of the indium containing alloys, which remained to high current densities, and the onset of significant polarization coinciding with its removal. Once the electrode has significantly polarised (approximately 400 - 500mV) from its rest potential the effects of the alloys are greatly diminished, with the electrode behaviour tending toward that of pure aluminium.

X - ray analysis showed that there is a buildup of alloy component on the electrode surface during polarization for both the indium and gallium alloys. This is consistent with the dissolution mechanism proposed by Macdonald (32), and supported by Pickering et al (75,76), who investigated the dissolution behaviour of binary alloys.

It has been shown that the rest potential for pure aluminium has a minimum or most negative potential of -1830 mV at about 55°C, wheres the rest potential for the indium containing alloys is only weakly temperature dependent .

The dissolution current density was shown to increase with increasing temperature, which is predicted by the Butler - Volmer equation (appendix .E), and shown to follow simple rate law kinetics. It follows from this that the power density of the electrodes also increased with increasing temperature, with the power density of the

indium and magnesium containing alloys increasing at a faster rate than pure aluminium anodes.

It was discovered that magnesium caused a finer grain structure to develop in the ternary Al - 0.1%Mg - 0.1%In alloy, as compared to its binary Al - In counterpart, but also had an accumulation of low melting point species near the centre of the electrode. The no load or rest potential for the ternary alloy at 60°C was the same as that of the binary Al - 0.1%In alloy, but it had a corrosion current 43% lower, showing magnesium to be a corrosion reducer and hence a valuable alloying constituent.

KOH and NaOH solutions have been used to investigate possible cation effects on polarization, but no significant difference could be found. Following Despic's work (23) improvements in potential might be made by using ammonium hydroxide.

Following the dissolution mechanism of hydroxyl ions interacting directly with aluminium, it would be expected that an increase in hydroxyl ion concentration would increase the aluminium dissolution current density. This was found to be the case for the pure aluminium electrode, however the ternary Al - Mg - In alloy only showed a dependence on hydroxyl ion concentration upto 4mol.l^{-1}. This was also reflected in the maximum power density attainable for the ternary alloy going from 1.2 watts/cm^2 (2M KOH) to 2.2 watts/cm^2 (4M KOH), with no further improvement at higher concentrations.

The use of aluminate solutions, with and without adjustment for the depleted hydroxyl ion concentration after aluminium has been dissolved into the solution, was to simulate an operating cell with and without regeneration of the electrolyte. In all cases the polarization curves for the solutions containing aluminate were shifted to lower current densities (e.g. 70 g/l AlO_2^- solution with hydroxyl adjustment is approximately 100 mA/cm^2 lower at -1400mV to the aluminate free solution curve). The curves for the unadjusted hydroxyl ion solutions were shifted to lower current densities than those of the adjusted solutions (e.g. approx. 100 mA/cm^2 lower at -1400mV for the 70 g/l AlO_2^- solution).

It has been shown that the film covered indium containing alloys are independent of aluminate concentration.

An increase in flowrate has been shown to increase the dissolution current density for aluminium. The shape of pure aluminium polarization curve changes markedly, due to an increased cathodic polarization effect with increased hydrogen removal from the electrode surface as flowrate increases. The ternary alloy polarization curve on the other hand was independent of flowrate when the surface film was present, and showed no increase in dissolution current density for flowrates above 0.75 m/s when the surface film had been removed, this indicates that the dissolution at this point is activation controlled.

Al / Air Batteries:

Before an Al / air battery system can be built consideration must be given to the current loading at which the cell will be operated. The cell design is dependent on whether the current loading is low (< 100 mA/cm^2), medium (>100, <1000 mA/cm^2) or high (>1000 mA/cm^2).

In all cases it is recommended that the cell has regeneration of the electrolyte by precipitation of aluminium hydroxide; if not to give a more advantageous polarization characteristic, then to avoid precipitation of aluminium hydroxide between the cell plates, which would eventually block the electrolyte flowpath. An electrolyte concentration of $4mol.l^{-1}$ is also recommended, with the possible use of a corrosion inhibitor in solution.

The choice of anode alloy at the low current loading will be a matter of preference, but it would be recommended from these results to use an alloy containing indium. The cell temperature can also be reduced at the low current density level, which will reduce the amount of parasitic corrosion. A flow velocity of less than 0.375 m/s is recommended, but this is dependent on the anode alloy chosen.

The medium current density range would require the cell to be operated at about 60°C with an anode with indium content . A flow velocity of about 0.375 m/s is required.

The high current density cell should be operated using an Al - Mg - In alloy at a temperature of 60°C or greater. The flow velocity should be atleast 0.75 m/s, with regeneration of the cell electrolyte being essential.

Further work in this field:

The recommendations for further work are:

(1) An in depth investigation into the effect of heat treatment on the low level aluminium alloys used in or envisaged for Al / Air fuel cells, and how the heat treatment effects their electrochemical behaviour is suggested.

(2) Further investigation into solutions containing corrosion inhibitors, and the effect they have on the polarization behaviour of aluminium alloy electrodes.

(3) The construction of an aluminium / air fuel cell system, and its modelling using the Kwong -Yu Chen & Savinell (56) model, later be extended to aluminium alloy anodes, would be very beneficial in obtaining information for further improved cell design.

(4) The extension of Macdonald's work (31) with bismuth as a alloying component is suggested, as this element showed promising results, but was unable to be investigated in this work.

(5) The investigation of the role of manganese, when it is added to binary and higher order alloys.

Chapter .6 - References

Aluminium in acid to neutral solutions:

(1) T.Hagyard and W.B.Earl
" Potential of Aluminium in Aqueous Chloride solutions "
J.Electrochem.Soc., **114**, 694 (1967)

(2) T.Hagyard and J.R.Williams
Trans. Far. Soc., **57**, 2288 (1961)

(3) W.Cheng
" Effects of surface additives on the performance of Li - Al electrodes "
J.Electrochem.Soc., **126**, 483 (1979)

(4) M.Garreau and P.L.Bonora
" On the role of the anions on the anomalous anodic dissolution of Aluminium "
J.Appl.Electrochem.,**7** (1977) 197-209

(5) P.A.Brook
" Potential - pH diagrams at elevated temperatures "
Corrosion Science.,**12** , 297 (1972)

(6) G.A.Dibari and H.J.Read
" Electrochemical behaviour of high purity Aluminium in chloride containing solutions "
Corrosion, **27**, 483 (1971)

(7) J.Kunze
" Untersuchungen zur elektrochemischen Polarisation von Aluminium in gepuffter Natriumchloridlösung "
Corrosion Science, **7**, 273 (1967)

(8) D.D.Macdonald and P.Butler
" The thermodynamics of the Aluminum - Water system at elevated temperatures "
Corrosion Science, **13**, 259 (1973)

(9) W.B.Earl
" The Aluminium electrode potential "
Ph.D thesis, Univ. of Cant., N.Z., (1965)

(10) W.B.Earl
" The Aluminium Electrode Potential in Chloride solutions "
B.E. thesis, Univ. of Cant., N.Z., (1960)

(11) K.J.Kirkpatrick
" The anodic behaviour of Aluminium in aqueous solutions "
Ph.D thesis, Univ. of Cant., N.Z., (1967)

(12) I.G. Watson
Private communication
Dept. Chem. Eng , Univ. of Cant., N.Z.,

Aluminium in alkaline solutions:

(13) K.E.Heusler and T.Valand
" Reactions at the oxide - electrolyte interface of anodic oxide films on Aluminium"
J.Electroanal.Chem., **149**, 71 (1983)

(14) R.C.Plumb and J.W.Swaine Jr
" Oxide coated electrodes - II. Aluminium in alkaline solutions and the nature of the aluminate ion "
J.Phys.Chem., **68** , 2057 (1964)

(15) D.Belitskus
" Reaction of Aluminium with sodium hydroxide solution as a source of hydrogen "
J.Electrochem.Soc., **117** , 1097 (1970)

(16) K.E.Heusler and W.Allgaier
" Die Kinetik der Auflösung von Aluminium in alkalischen Lösungen "
Werkstoffe und Korrosion, 22. Jahrgang, Heft 4 / 1971, 297

(17) D.D.Macdonald,S. Real, S.I.Smedley and M.Urquidi - Macdonald
" Evaluation of alloy anodes for Al - Air batteries -
IV. Electrochemical Impedance Analysis of pure Al in 4M KOH @ 25°C "
J.Electrochem.Soc., **135**, 2410 (1988)

(18) N.D.Koshel, A.N.Verba and O.S.Ksenzhek
" Macrokinetics of the electrochemical dissolution of Aluminium in a slit cell with flowing electrolyte "
Élektrokhimya, **12** , 1615 (1976)

(19) D.D.Macdonald, S.Real and M.Urqidi - Macdonald
" Development and evaluation of anode alloys for Al - Air batteries "
Abstract No.135, Electrochem.Soc., 172nd Fall Meeting, Honolulu, 87-2, October 18 - 23, (1987) 194-5

(20) M.G.Khedr & A.M.S Lashein
" Corrosion behaviour of Aluminium in presence of accelerating metal cations and inhibition "
J.Electrochem.Soc., **136**, 968 (1989)

Aluminium alloys in acid to neutral solutions:

(21) D.S.Keir, M.J.Pryor and P.R.Sperry
" The influence of ternary alloying additions on the galvanic behaviour of Al - Sn alloys "
J.Electrochem.Soc., **116**, 319 (1969)

(22) D.S.Keir, M.J.Pryor and P.R.Sperry
" Galvanic corrosion characteristics of Aluminium alloyed with group IV metals "
J.Electrochem.Soc., **114**, 777 (1967)

(23) A.R.Despic, D.M.Drazic, M.M.Purenovic and N.Cikovic
" Electrochemical properties of Aluminium alloys containing In, Ga and Tl "
J.Appl.Electrochem., **6** , 527(1976)

(24) A.Mance, D.Cerovic and A.Mihajlovic
" The effect of gallium and phosphorous on the corrosion behaviour of Aluminium in NaCl solutions "
J.Appl.Electrochem., **15** , 415 (1985)

(25) A.Mance, D.Cerovic and A.Mihajlovic
" The effect of small additions of indium and thallium on the corrosion behaviour of Aluminium in sea water "
J.Appl.Electrochem., **14** , 459 (1984)

(26) Y.Hori, J.Takao and H.Shomon
" Aluminium alloys for Aluminium primary cell "
Electrochimica Acta, **30**, 1121 (1985)

Aluminium alloys in alkaline solutions:

(27) O.R.Brown and J.S.Whitley
" Electrochemical behaviour of Aluminium in aqueous caustic solutions "
Electrochemica Acta, **32**, 545 (1987)

(28) D.D.Macdonald,S. Real and M.Urquidi - Macdonald
" Evalution of alloy anodes for Al - Air batteries - II. Delineation of anodic and cathodic partial reactions "
J.Electrochem.Soc., **135**, 1633 (1988)

(29) D.D.Macdonald and M.Urquidi - Macdonald
" Application of Kramers - Kronig transforms in the analysis of electrochemical systems - I. Polarisation resistance "
J.Electrochem.Soc., **132**, 2316 (1985)

(30) D.D.Macdonald,S. Real and M.Urquidi - Macdonald
" Application of Kramers - Kronig transforms in the analysis of electrochemical systems - II. Transformations in the complex plane "
J.Electrochem.Soc., **133**, 2018 (1986)

(31) D.D.Macdonald, K.H.Lee, A.Moccari and D.Harrington
" Evalution of alloy anodes for Al - Air batteries - Corrosion Studies "
Corrosion - Nace, **44**, 652 (1988)

(32) D.D.Macdonald,S. Real and M.Urquidi - Macdonald
" Evalution of alloy anodes for Al - Air batteries - III. Mechanisms of activation, passivation and hydrogen evolution "
J.Electrochem.Soc., **135**, 2397 (1988)

(33) Hunter
" The Anodic Behaviour of Aluminium Alloys in Alkaline Electrolytes "
Ph.D thesis, Oxford, England, (1989)

(34) P.W.Jeffery and W.Halliop
" Aluminium anodes with indium activation for alkaline electrolyte primary batteries "
Electrochemical Soc., 172nd Fall meeting, Extended Abstract, Honolulu, Hawaii, 87-2, October 18 - 23, (1987)193

Aluminium in ion adjusted solutions:

(35) D.D.Macdonald and C.English
" Development of anodes for Al - Air batteries - solution phase inhibition of corrosion "
J.Appl.Electrochem., **20**, 405 (1990)

(36) G.Burri, W.Luedi and O.Haas
" Electrochemical properties of Aluminium in weakly acid NaCl solutions - Part .1 Influence of the electroyte additions of In^{3+} and Zn^{2+} "
J.Electrochem.Soc., **136**, 2167 (1989)

(37) A.H.Roebuck and T.R.Pritchett
" Corrosin inhibitors for alumiunium "
Materials Protection , July 1966, pp 16

(38) P.J.Zanzucchi and J.H.Thomas III
" Corrosion inhibitors for Al - films "
J.Electrochem.Soc., **135**, 1370 (1988)

(39) I.J.Albert, M.Anbu Kulandainathan, M.Ganesan and V.Kapali
" Characteristion of different grades of commercially pure Aluminium as prospective galvanic anodes in saline and alkaline battery electrolyte"
J.Appl.Electrochem., **19**, 547 (1989)

(40) T. Hirai, J.Yamaki,T.Okada and A.Yamaji
" Inhibiting effects of Al corrosion by polymer ammonium chlorides in alkaline electrolytes "
Electrochimica Acta, **30**, 61 (1985)

(41) M.Paramasivam, G.Suresh, B.Muthuramalingam, S.Venkatakrishna iyer, V.Kapali
" Different commercial grades of Aluminium as galvanic anodes in alkaline zincate solutions "
J.Appl.Electrochem., **21**, 452 (1991)

(42) K.B.Sarangapani, V.Balaramachandran, V.Kapali, S.Venkatakrishna iyer, M.G.Potdar, K.S.Rajagopalan
" Aluminium as anode in primary alkaline batteries - Influence of additions on the corrosion and anodic behaviour of 2S Aluminium in alkaline citrate solution "
J.Appl.Electrochem., **14**, 475 (1984)

(43) W.Böhstedt
" The influence of electrolyte additives of the anodic dissolution of Aluminium in alkaline solutions "
Journal of Power Sources, **5**, 245 (1980)

(44) L.Bockstie, D.Trevethan and S.Zaromb
" Control of Aluminium corrosion in caustic solutions "
J.Electrochem.Soc., **110** , 267 (1963)

Battery Technology:

(45) D.Katryniok,J.Ruch and P.Schmöde
" Hochleistungsbatterien auf der Basis von Al - Sauerstoff - Zellen "
, etz Bd. 102 (1981) Heft 21

(46) S.Zaromb and R.A.Foust, Jr
" Feasibility of electrolyte regeneration in Al batteries "
J.Electrochem.Soc., **109**, 1191 (1962)

(47) A.Despic, E.Budevski, I.Iliev, A.Kaisheva and K.Krsmanovic
" Investigation of a large - capacity medium - power saline Al - Air battery "
J.Appl.Electrochem., **19** , 323 (1989)

(48) S.Zaromb
" The use and behaviour of Aluminium anodes in alkaline primary batteries "
J.electrochem.Soc., **109** , 1125 (1962)

(49) G.Scamans
Advances in battery technolgy - Development of the Al / Air battery
A paper presented at the Electrochemical Technology Group of the SCI,
London, 8 October 1985

(50) N.P.Fitzpatrick, F.N.Smith and P.W.Jeffrey
The Aluminium - Air Battery
SAE Technical Paper 830290

(51) P.Dvorak
" The shocking truth about electric vehicles "
Machine Design, sept 1989, pp 86

(52) K.Mosley
" The aluminium - air fuel cell "
Transactions of the I.P.E.N.Z., **13** , 155 (1986)

(53) K.F.Blurton and A.F.Sammells
" Metal / Air batteries : Their status and potential - A review "
Journal of Power Sources, **4**, 263 (1979)

(54) J.F.Equey, S.Müller, A.Tsukada and O.Haas
" Al / Cl_2 battery with slightly acidic NaCl electrolyte -
I. porous graphite chlorine cathodes "
J.Appl.Electrochem., **19**, 65 (1989)

(55) J.J .Stokes,Jr and D.Belitskus
" Chapter .3 - Aluminium Cells "
"Primary Batteries" , N.C.Cahoon and G.W.Heise eds,
New York - 1976

(56) Kwong - Yu Chen & R.F.Savinell
" Modelling Calculations of an Al - Air Cell "
J.Electrochem.Soc.,**138**, 1976 (1991)

(57) A.Maimoni
" Al / Air Power Cell - A progress report "
20th IECEC Conference, Miami Beach, Florida, Aug 18 - 23, 1985
Preprint UCRL - 92281

(58) Design News , Nov 7, 1988, " Design Feature "
Cahners publishing company

(59) KRDC Update special
3 August 1988, pp 1 - 4

(60) Machine design
Sept 21, 1982, pp 86 - 94

(61) G.M.Scamans et al
" Further developments of Aluminium Batteries "
Electric Vehicle Development, Vol 8, No.1,
Butterworth & Co, Feb 1989

(62) Materials edge
July / August 1989
" Alcan air battery - further down road "

(63) N.P.Fitzpatrick and G. Scamans
New Scientist, 17th July 1986
" Aluminium is a fuel for tomorrow "

General:

(64) C.D.S.Tuck et al
J.Electrochem.Soc., **134**, No.12 (1987)

(65) M.Stern and A.L.Geary
" Electrochemical Polarization -
I. A theoretical analysis of the shape of polarization curves "
J.Electrochem.Soc., **104**, 56 (1957)

(66) " The measurement and correction of Electrolyte resistance in Electrochemical tests "
Scribers / Taylor editors, ASTM - STP 1056, 1990

(67) M.Pourbaix
" Atlas of Electrochemical Equilibria in aqueous solutions "
Pergamon Press,(1966)

(68) Smithells - Metals Reference Book, 6th Ed
Editor E.A.Brandes
Butterworth & Co. (Publishers) Ltd, (1983)

(69) CRC - Handbook of Chemistry & Physics, 61st Ed
CRC Press (1980 -1981)

(70) J.L.Murray
Bull. Alloy Phase diagrams, 4(3) Nov 1983

(71) Materials Science & Engineering Series -
Hansens - Constitution of Binary alloys, 2nd Ed
Mcgraw - Hill book company (1958)

(72) Aluminium Alloys, Structure & Properties
Mondolfo L.F,
Butterworths (1976)

(73) D.D.Macdonald
" The Electrochemistry of metals in aqueous systems at elevated temperatures "
Modern aspects of Electrochemistry, No.11, Chapter.4,
Edited by B.E.Conway & J.O'M.Bockris
Plenum Press, New York, 1975

(74) P.W.Atkins
Physical Chemistry 2nd Ed
Oxford University Press, 1982

(75) H.W.Pickering & C.Wagner
" Electrolytic Dissolution of Binary Alloys Containing a Noble Metal "
J.Electrochem.Soc., **114**, 698 (1967)

(76) H.W.Pickering & P.J.Byrne
" On Preferential Anodic Dissolution of Alloys in the Low - Current Region and the Nature of the Critical Potential "
J.Electrochem.Soc., **118**, 209, (1971)

(77) R. Greef & C.F.W. Norman
" Ellipsometry of the Growth and Dissolution of Anodic Oxide Films on Aluminium in alkaline solution "
J.Electrochem.Soc., **132**, 2362 (1985)

(78) Vogel's Textbook of Quantitative Inorganic Analysis 4th Ed
Longman Group Ltd
London
Pages 301-305

(79) ibid, pages 316-320

(80) J.R.Williams
" The static potential of the aluminium electrode in chloride solutions"
B.E. thesis, Univ. of Cant., N.Z., (1959)

CHAPTER.7
APPENDICES

APPENDIX.A

Notation & Symbols

Notation:

SCE = Saturated Calomel Electrode
Potential of 245mV v.s. S.H.E at 25°C

SHE = Standard Hydrogen Electrode

NDE = Negative Difference Effect

EDTA = Ethylene diammine tetra - acetate

IR = solution resistive voltage drop

rds = rate determining step

Symbols:

i_o = Exchange current density (mA/cm^2)

$\Delta\Phi$ = the potential difference between the metal and solution (volts)

$\Delta\Phi_e$ = the equilibrium between the metal and solution with respect to the reference electrode (volts)

η = $\Delta\Phi - \Delta\Phi_e$ (volts)

R = Universal gas constant (8.314 $J.mol^{-1}.K^{-1}$)

F = Faraday's constant (96485 $C.mol^{-1}$)

α = kinetic transfer coefficient $(0 < \alpha < 1)$

E^o = equilibrium potential with respect to SHE (The potential IUPAC 1953)

E_o^o = standard equilibrium potential @25°C

μ = chemical potential

I = current density (mA/cm^2)

Z = number of electrons transferred in the anodic reaction

T = absolute temperature (K)

APPENDIX.B

List of Graphs:

All graphs not given in the main text of chapter.3

B1.1 and B1.2 are different representations of the same data, and serve to illustrate that there is no significant difference in plotting the original data, given as potential versus KOH concentration, as potential versus pH. As there is no advantage in changing the KOH concentration to 'pH' the data has been left in its original form.

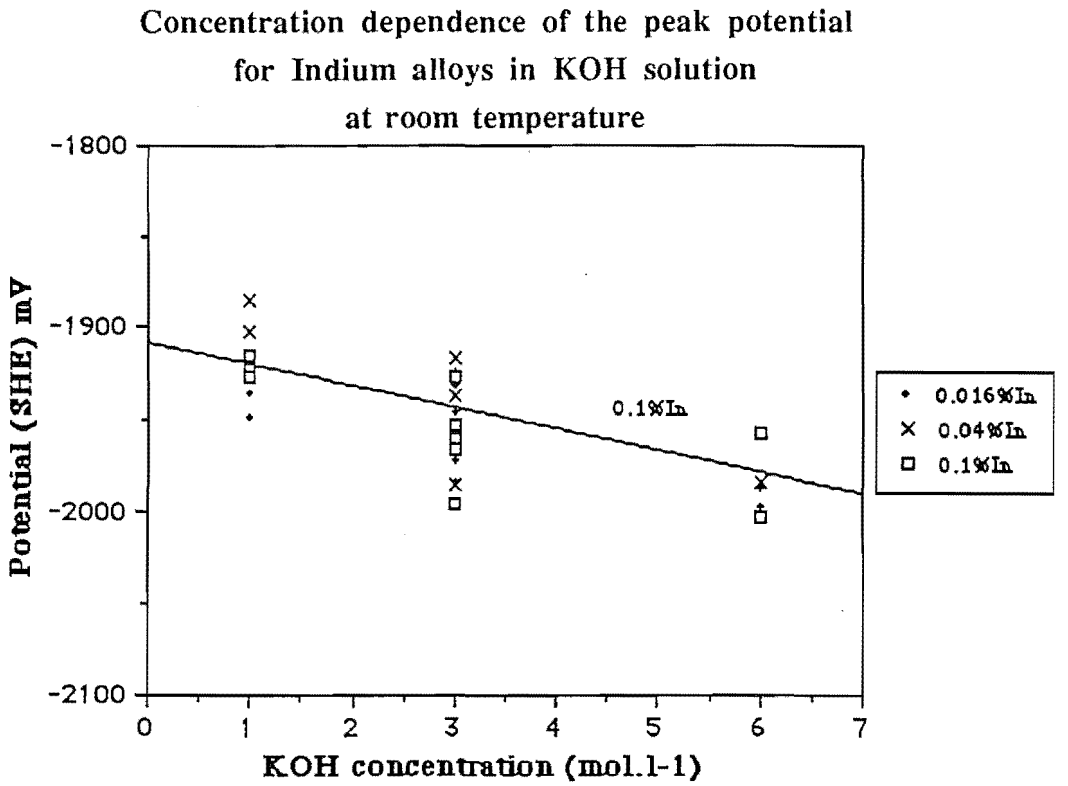
Concentration dependence of the peak potential
for Indium alloys in KOH solution
at room temperature
Potential (SHE) mV
-1800
-1900
-2000
-2100
0
1
2
3
4
5
6
7
KOH concentration (mol.l-1)
0.1%In
0.016%In
0.04%In
0.1%In

B1.1

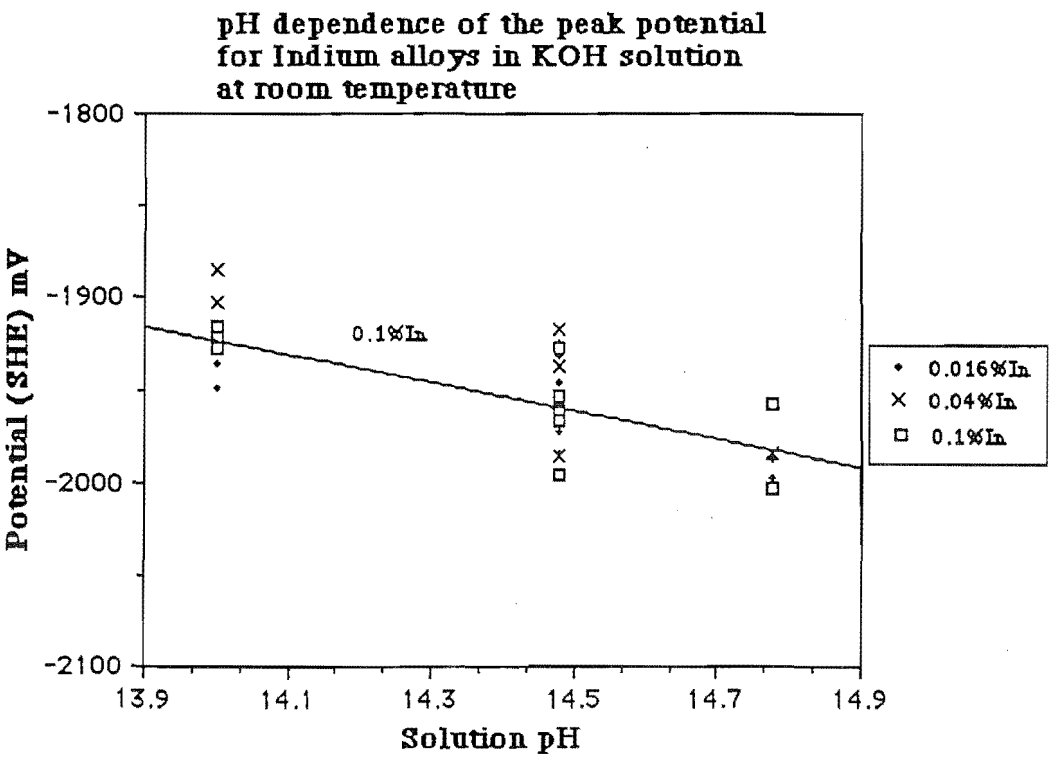
pH dependence of the peak potential
for Indium alloys in KOH solution
at room temperature
Potential (SHE) mV
-1800
-1900
-2000
-2100
13.9
14.1
14.3
14.5
14.7
14.9
Solution pH
0.1%In
0.016%In
0.04%In
0.1%In

B1.2

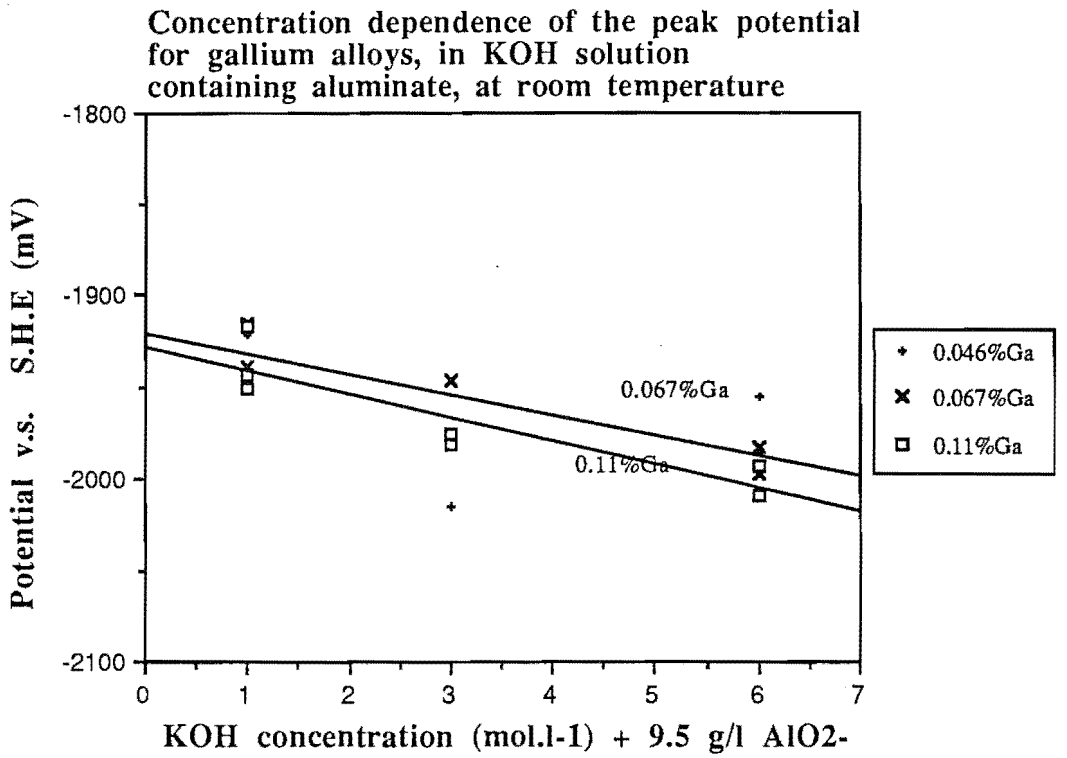
Concentration dependence of the peak potential
for gallium alloys, in KOH solution
containing aluminate, at room temperature
Potential v.s. S.H.E (mV)
-1800
-1900
-2000
-2100
0
1
2
3
4
5
6
7
0.067%Ga
0.11%Ga
0.046%Ga
0.067%Ga
0.11%Ga
KOH concentration (mol.l-1) + 9.5 g/l AlO2-

B2.1

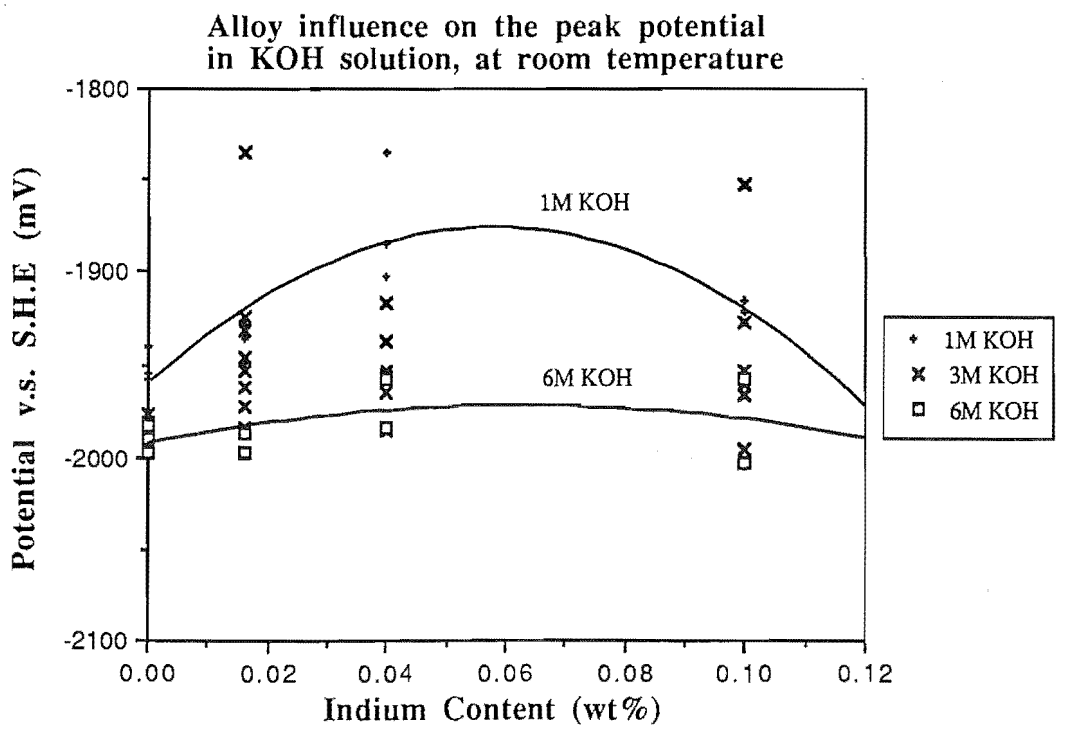
Alloy influence on the peak potential
in KOH solution, at room temperature
Potential v.s. S.H.E (mV)
-1800
-1900
-2000
-2100
0.00
0.02
0.04
0.06
0.08
0.10
0.12
1M KOH
6M KOH
1M KOH
3M KOH
6M KOH
Indium Content (wt%)

B2.2

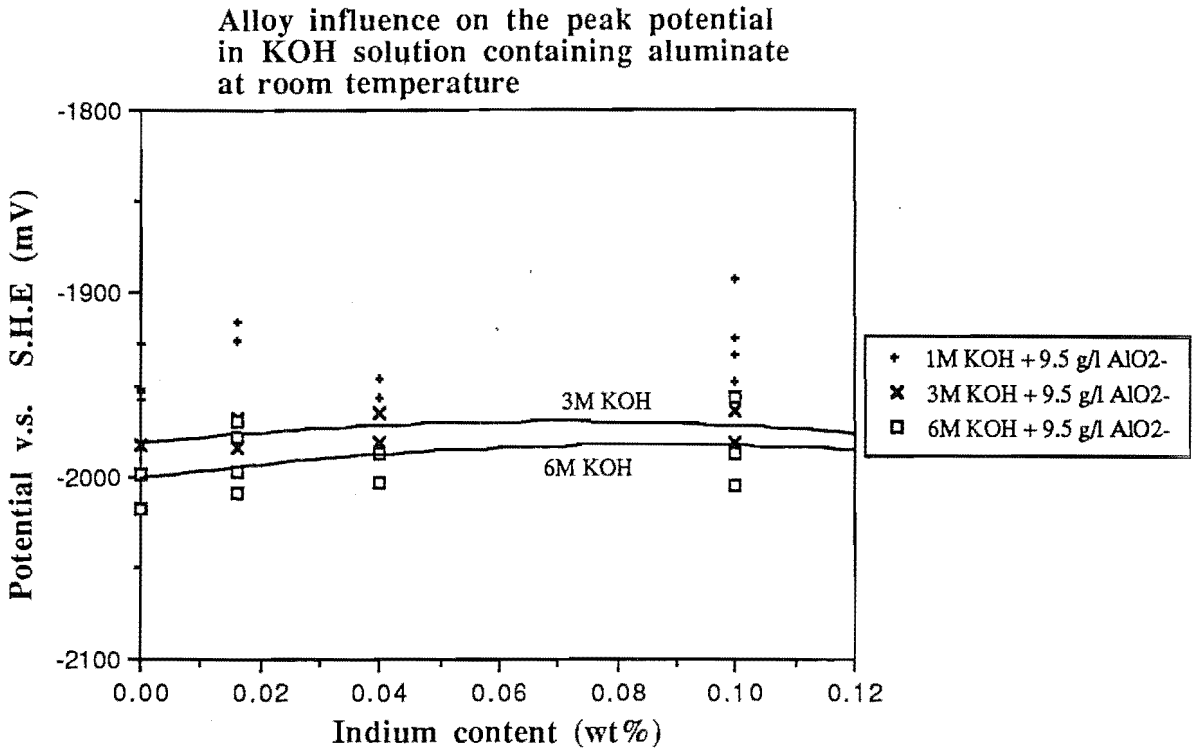
Alloy influence on the peak potential
in KOH solution containing aluminate
at room temperature
Potential v.s. S.H.E (mV)
-1800
-1900
-2000
-2100
0.00
0.02
0.04
0.06
0.08
0.10
0.12
Indium content (wt%)
3M KOH
6M KOH
1M KOH + 9.5 g/l AlO2-
3M KOH + 9.5 g/l AlO2-
6M KOH + 9.5 g/l AlO2-

B3.1

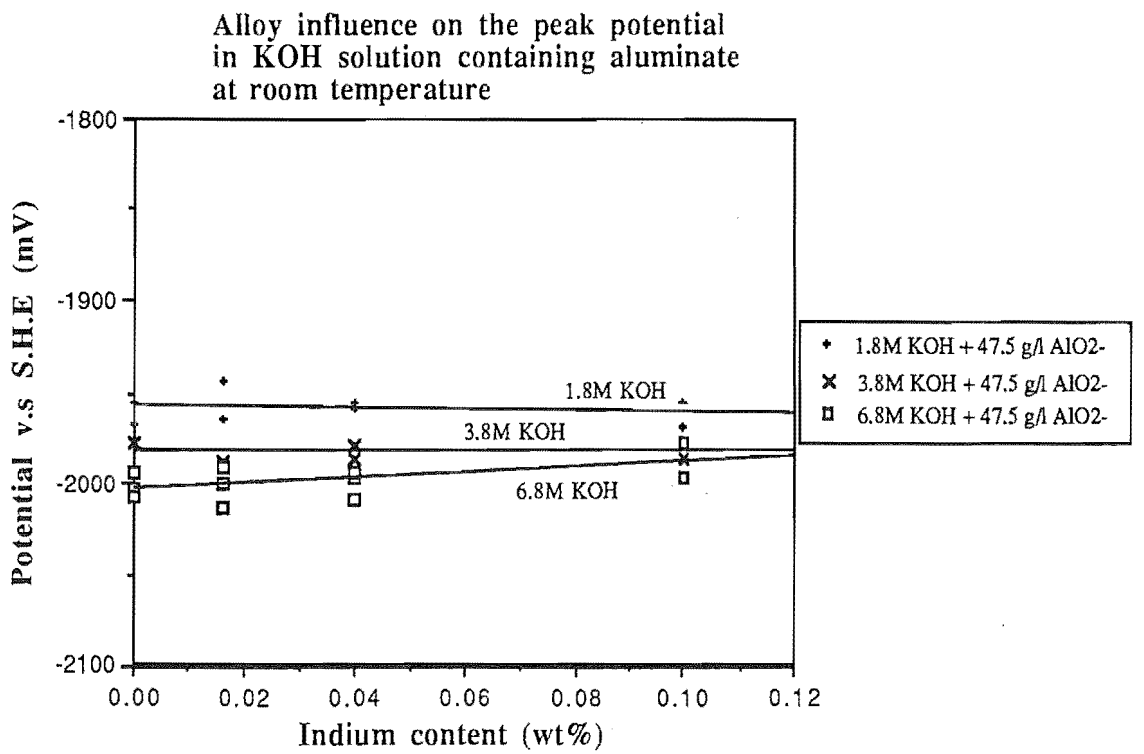
Alloy influence on the peak potential
in KOH solution containing aluminate
at room temperature
Potential v.s S.H.E (mV)
-1800
-1900
-2000
-2100
0.00
0.02
0.04
0.06
0.08
0.10
0.12
Indium content (wt%)
1.8M KOH
3.8M KOH
6.8M KOH
1.8M KOH + 47.5 g/l AlO2-
3.8M KOH + 47.5 g/l AlO2-
6.8M KOH + 47.5 g/l AlO2-

B3.2

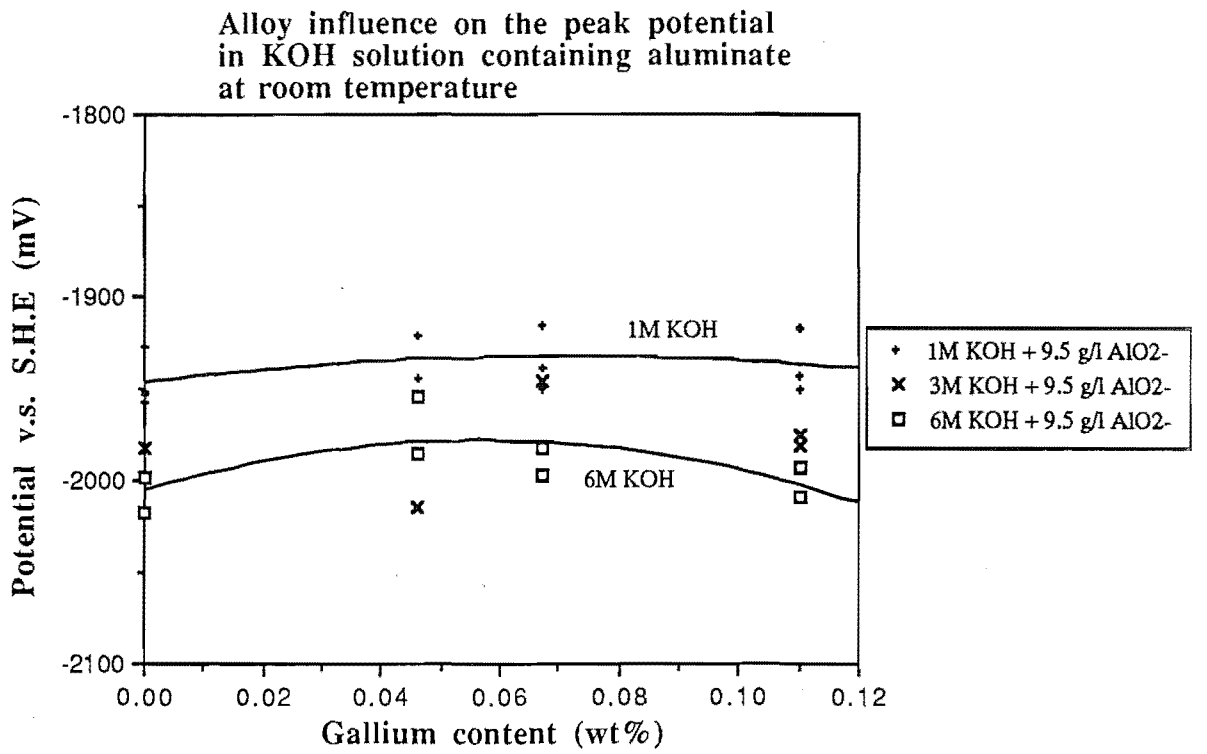
Alloy influence on the peak potential
in KOH solution containing aluminate
at room temperature
Potential v.s. S.H.E (mV)
-1800
-1900
-2000
-2100
1M KOH
6M KOH
0.00
0.02
0.04
0.06
0.08
0.10
0.12
Gallium content (wt%)
1M KOH + 9.5 g/l AlO2-
3M KOH + 9.5 g/l AlO2-
6M KOH + 9.5 g/l AlO2-

B4.1

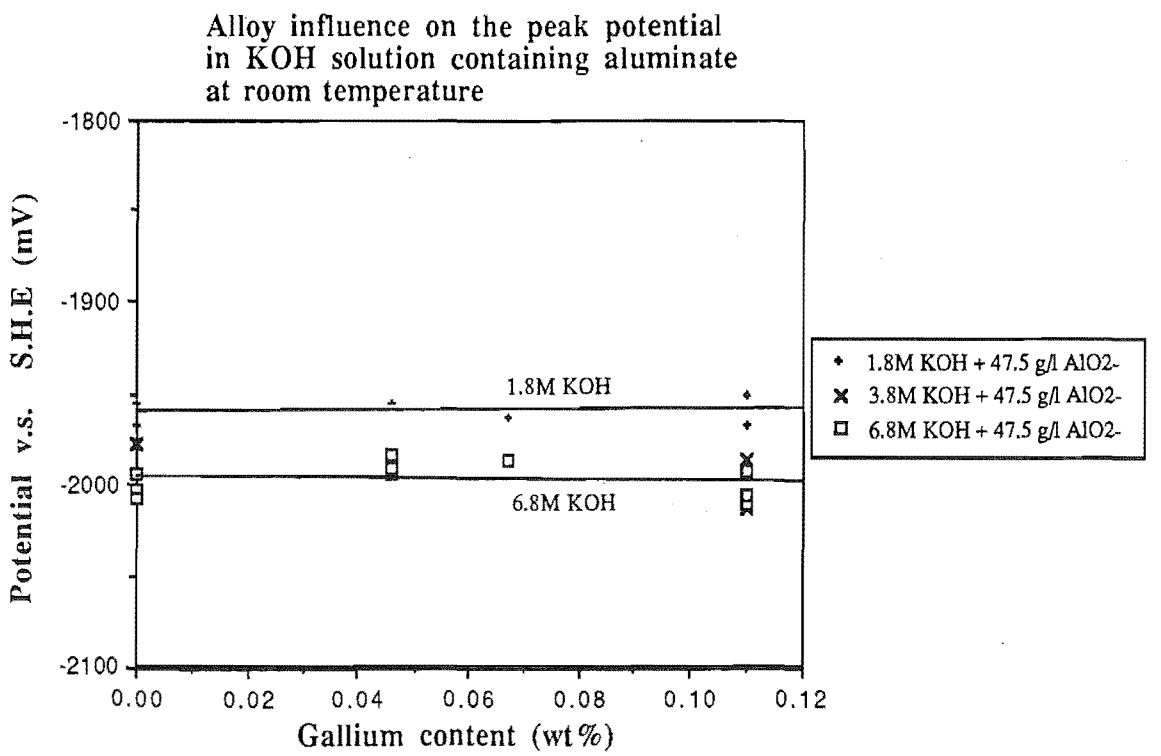
Alloy influence on the peak potential
in KOH solution containing aluminate
at room temperature
Potential v.s. S.H.E (mV)
-1800
-1900
-2000
-2100
1.8M KOH
6.8M KOH
0.00
0.02
0.04
0.06
0.08
0.10
0.12
Gallium content (wt%)
1.8M KOH + 47.5 g/l AlO2-
3.8M KOH + 47.5 g/l AlO2-
6.8M KOH + 47.5 g/l AlO2-

B4.2

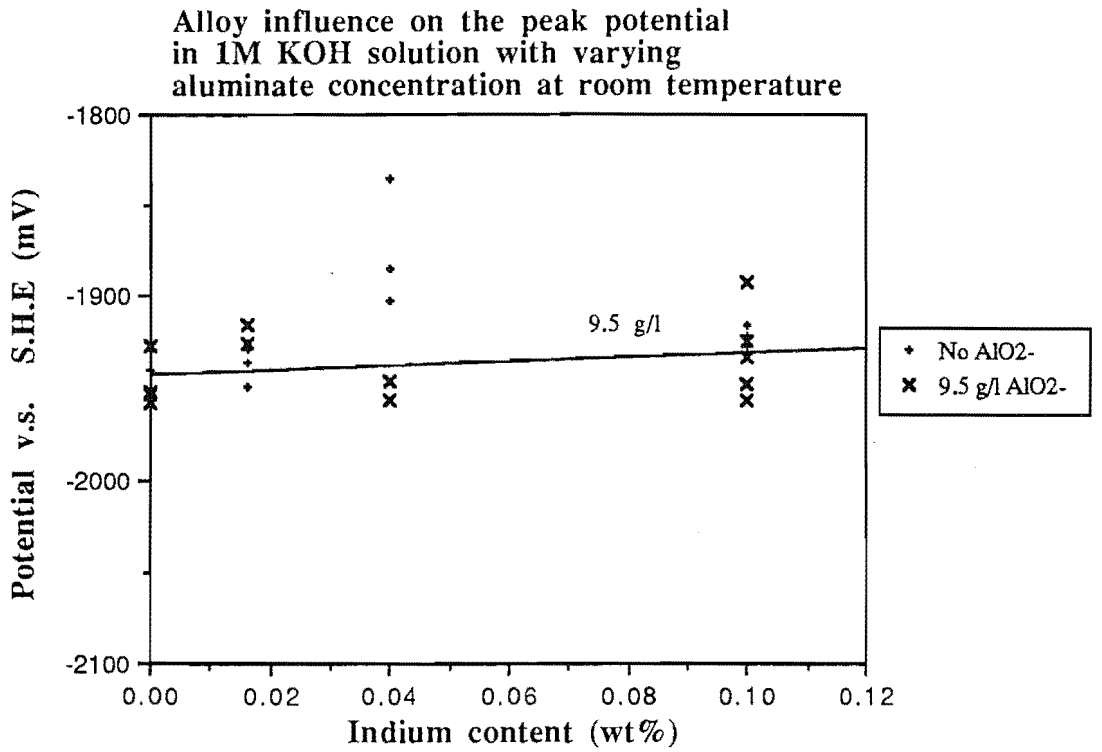
Alloy influence on the peak potential
in 1M KOH solution with varying
aluminate concentration at room temperature
Potential v.s. S.H.E (mV)
-1800
-1900
-2000
-2100
9.5 g/l
No AlO2-
9.5 g/l AlO2-
0.00
0.02
0.04
0.06
0.08
0.10
0.12
Indium content (wt%)

B5.1

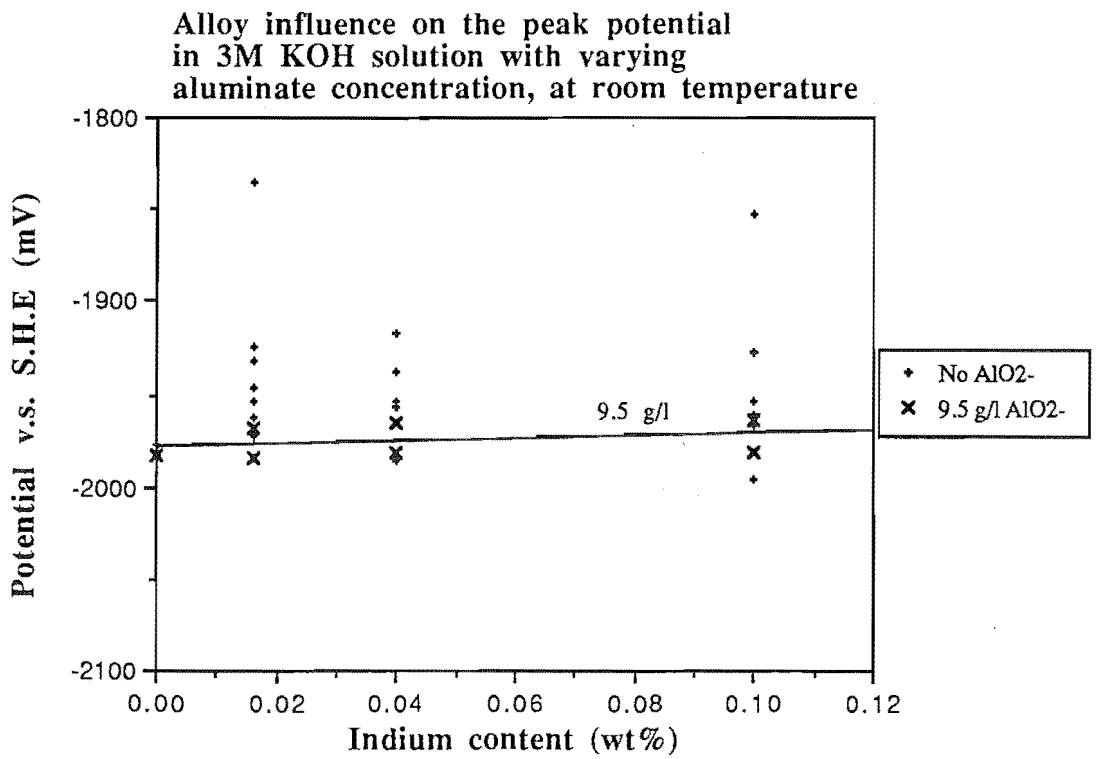
Alloy influence on the peak potential
in 3M KOH solution with varying
aluminate concentration, at room temperature
Potential v.s. S.H.E (mV)
-1800
-1900
-2000
-2100
9.5 g/l
No AlO2-
9.5 g/l AlO2-
0.00
0.02
0.04
0.06
0.08
0.10
0.12
Indium content (wt%)

B5.2

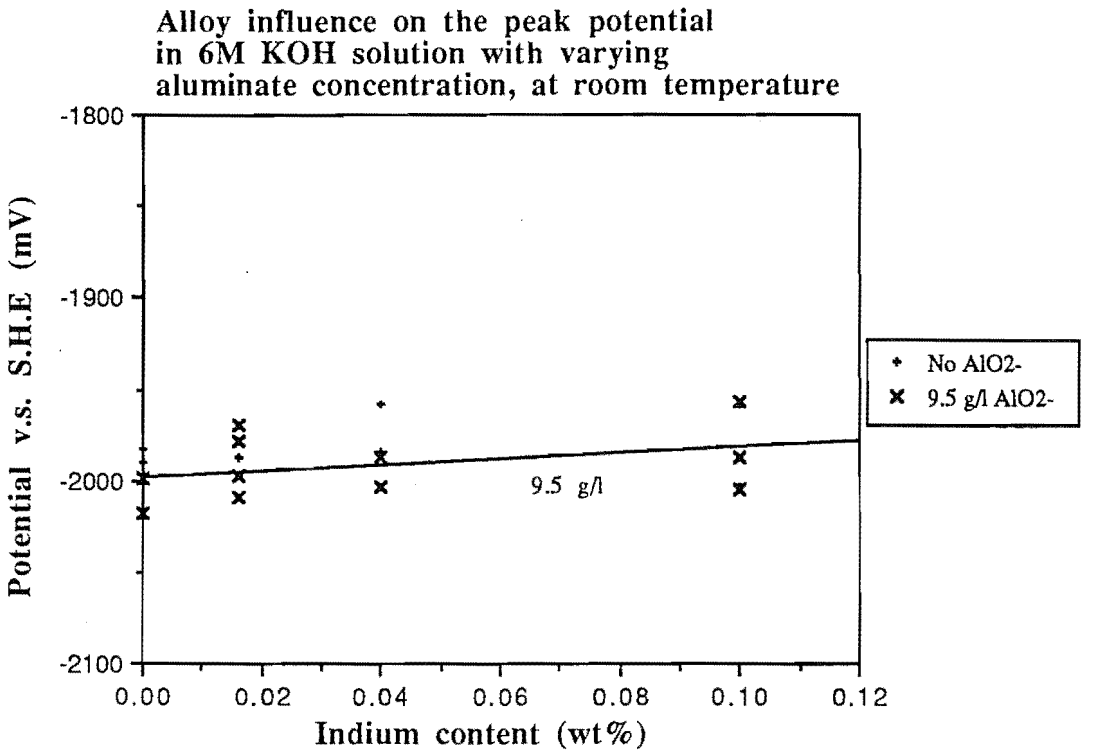
Alloy influence on the peak potential
in 6M KOH solution with varying
aluminate concentration, at room temperature
Potential v.s. S.H.E (mV)
-1800
-1900
-2000
-2100
9.5 g/l
No AlO2-
9.5 g/l AlO2-
0.00
0.02
0.04
0.06
0.08
0.10
0.12
Indium content (wt%)

B6.1

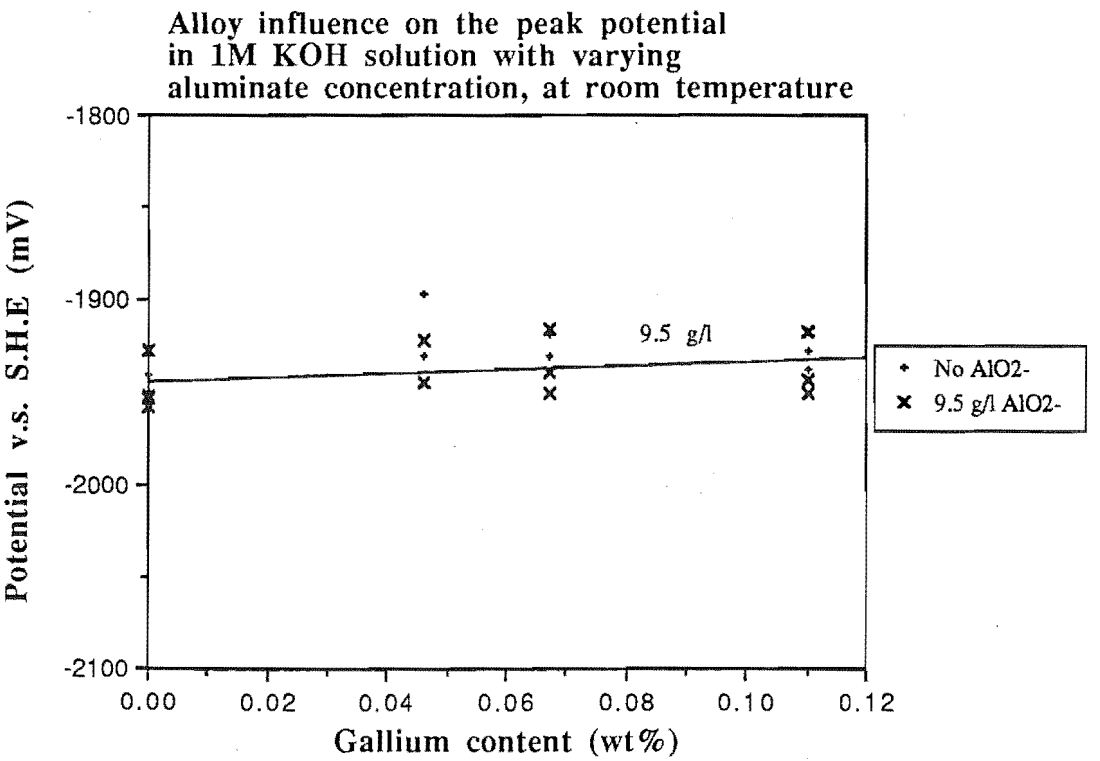
Alloy influence on the peak potential
in 1M KOH solution with varying
aluminate concentration, at room temperature
Potential v.s. S.H.E (mV)
-1800
-1900
-2000
-2100
9.5 g/l
No AlO2-
9.5 g/l AlO2-
0.00
0.02
0.04
0.06
0.08
0.10
0.12
Gallium content (wt%)

B6.2

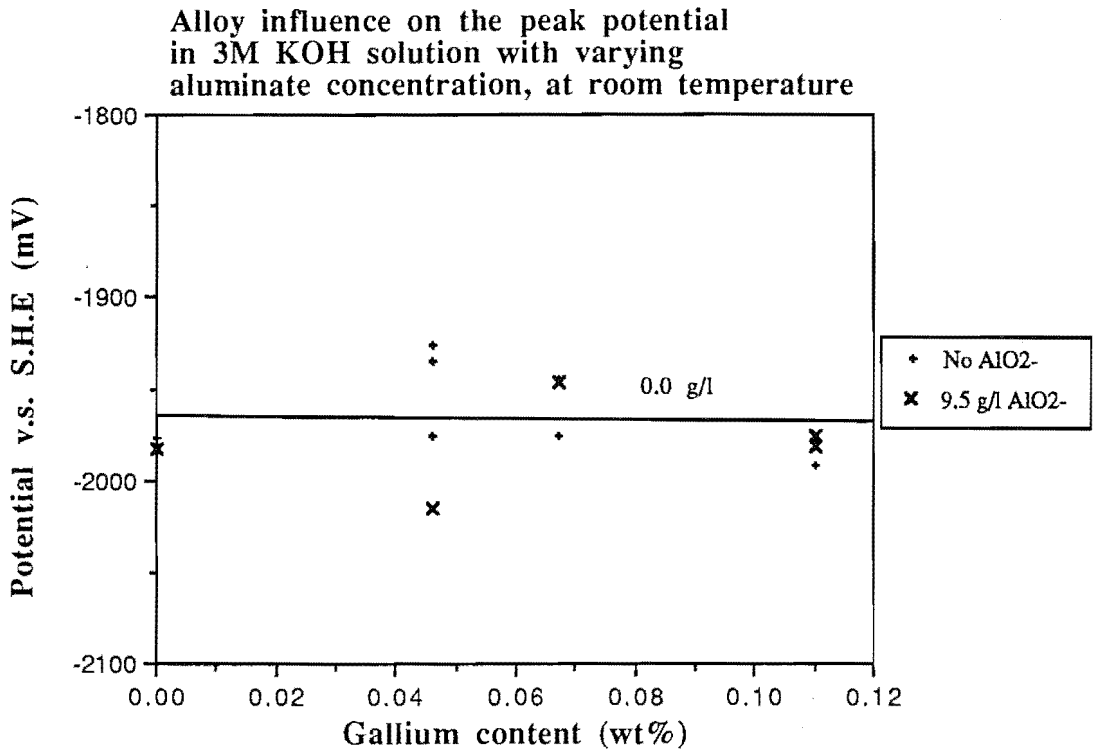
Alloy influence on the peak potential
in 3M KOH solution with varying
aluminate concentration, at room temperature
Potential v.s. S.H.E (mV)
-1800
-1900
-2000
-2100
0.0 g/l
No AlO2-
9.5 g/l AlO2-
0.00
0.02
0.04
0.06
0.08
0.10
0.12
Gallium content (wt%)

B7.1

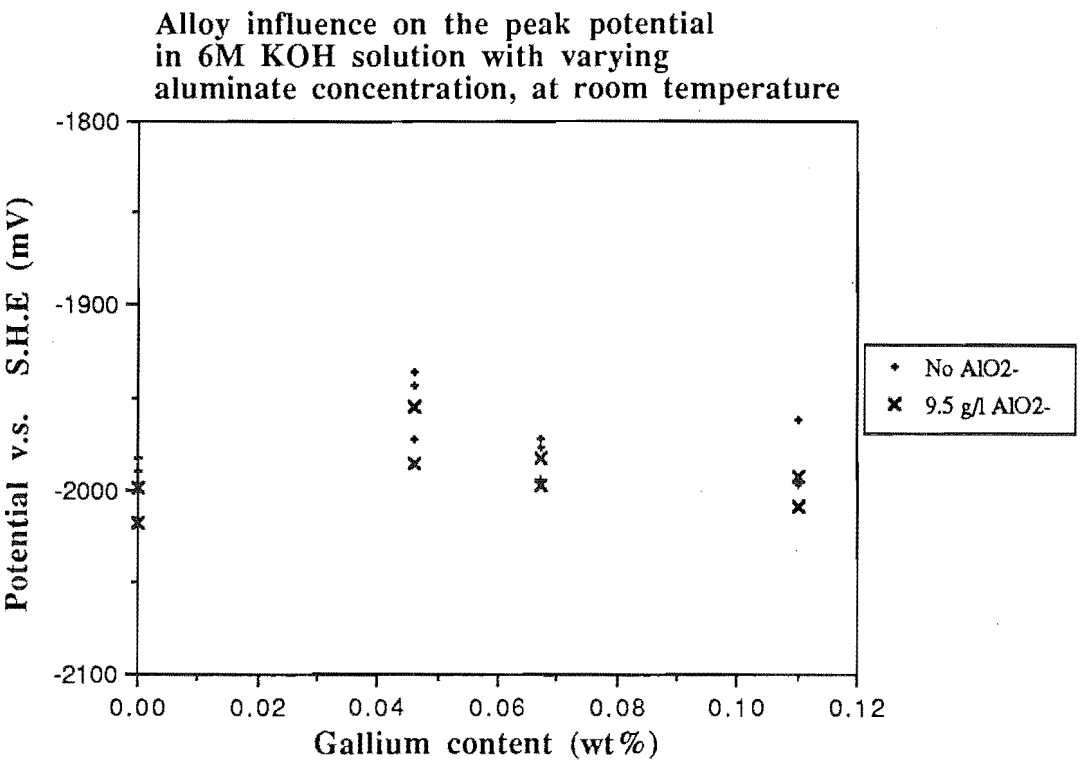
Alloy influence on the peak potential
in 6M KOH solution with varying
aluminate concentration, at room temperature
Potential v.s. S.H.E (mV)
-1800
-1900
-2000
-2100
No AlO2-
9.5 g/l AlO2-
0.00
0.02
0.04
0.06
0.08
0.10
0.12
Gallium content (wt%)

B7.2

Concentration dependence of the 3 minute potential
for Indium alloys, in KOH solution
containing aluminate, at room temperature

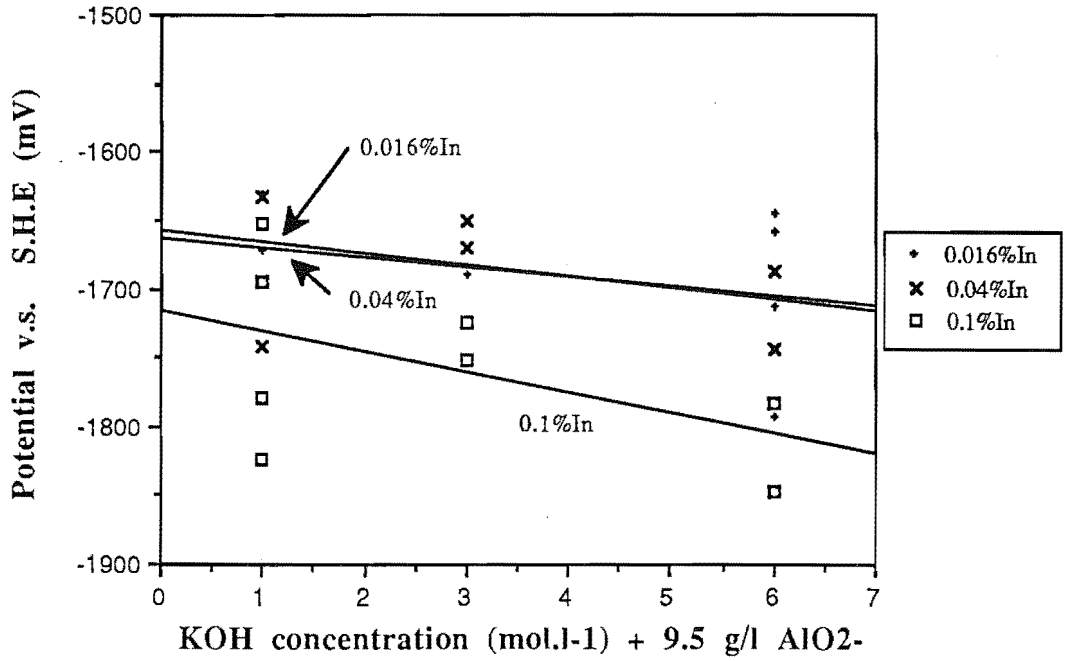

B8.1

Concentration dependence of the 3 minute potential
for Indium alloys, in KOH solution
containing aluminate, at room temperature

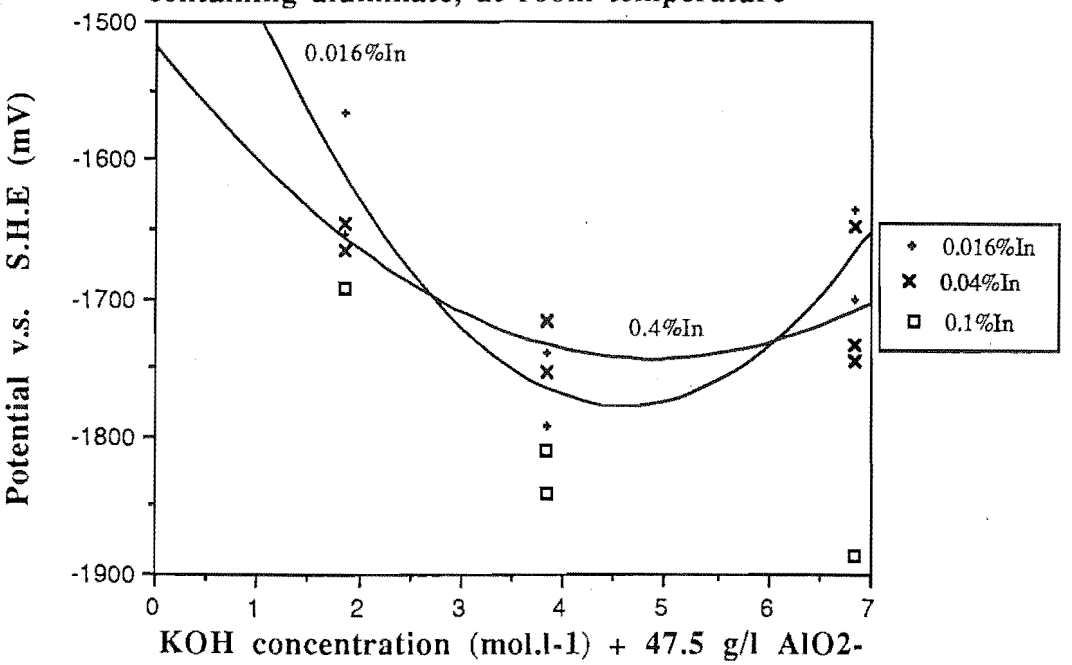

B8.2

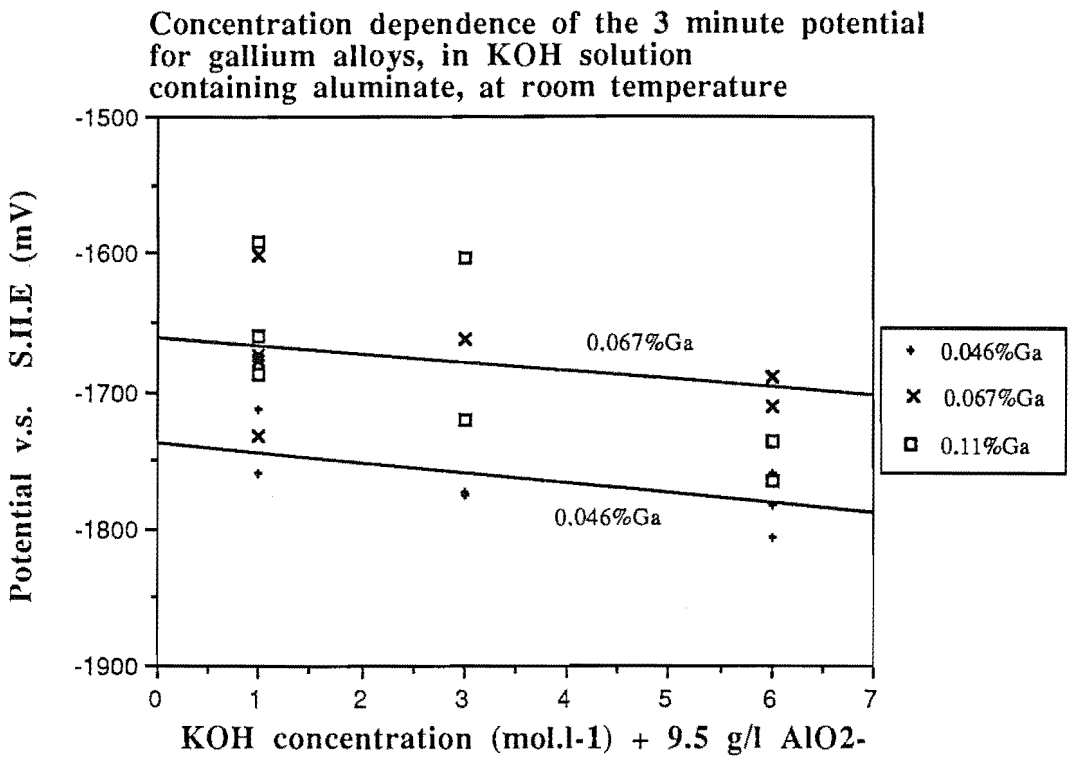
Concentration dependence of the 3 minute potential
for gallium alloys, in KOH solution
containing aluminate, at room temperature
Potential v.s. S.H.E (mV)
-1500
-1600
-1700
-1800
-1900
0.067%Ga
0.046%Ga
0.046%Ga
0.067%Ga
0.11%Ga
0
1
2
3
4
5
6
7
KOH concentration (mol.l-1) + 9.5 g/l AlO2-

B9.1

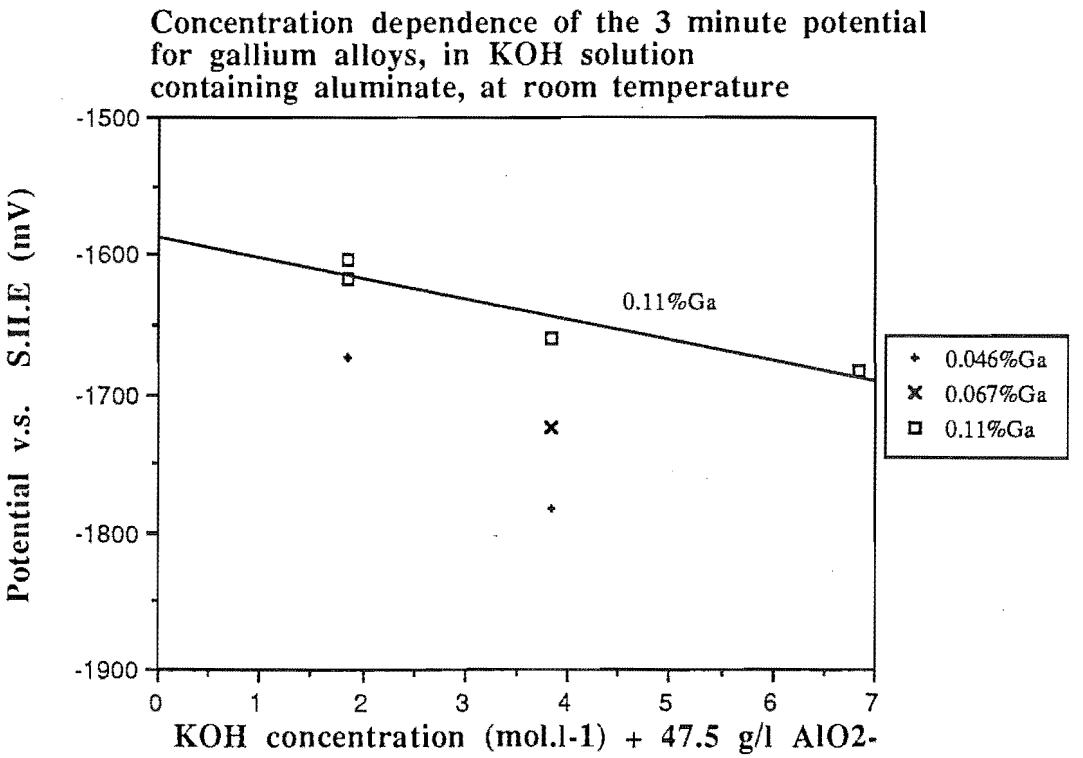
Concentration dependence of the 3 minute potential
for gallium alloys, in KOH solution
containing aluminate, at room temperature
Potential v.s. S.H.E (mV)
-1500
-1600
-1700
-1800
-1900
0.11%Ga
0.046%Ga
0.067%Ga
0.11%Ga
0
1
2
3
4
5
6
7
KOH concentration (mol.l-1) + 47.5 g/l AlO2-

B9.2

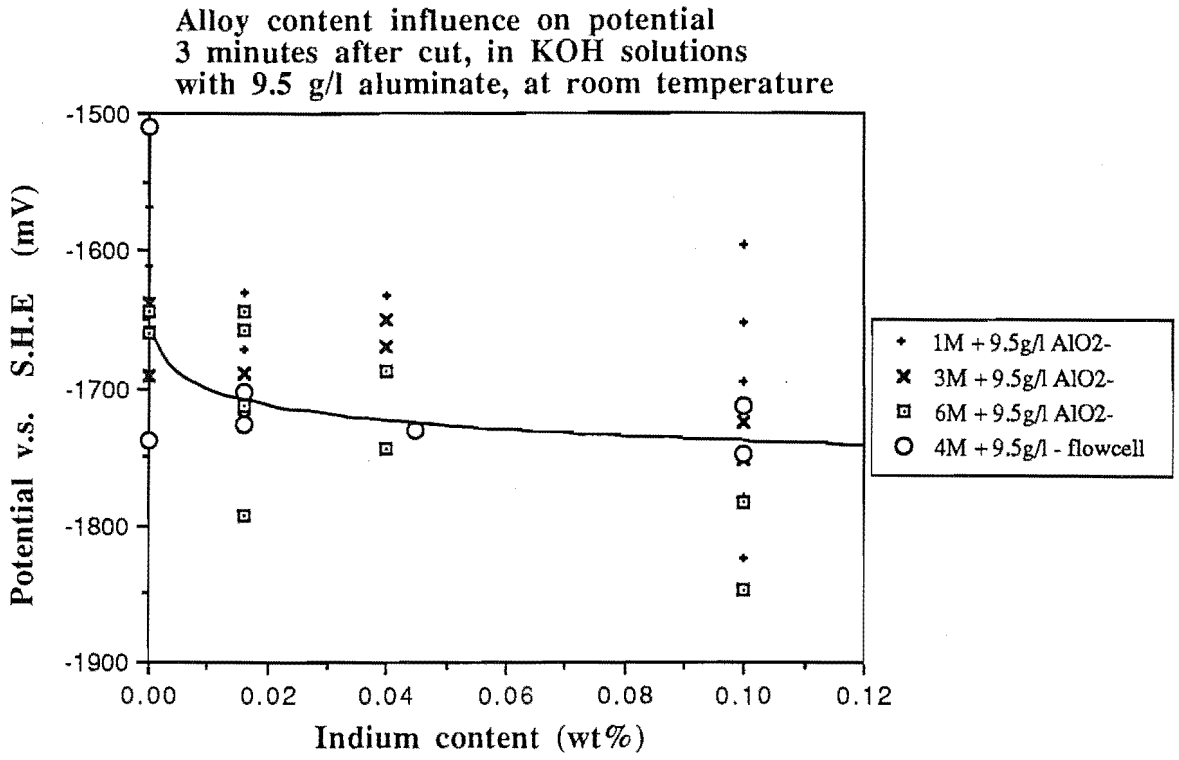
Alloy content influence on potential
3 minutes after cut, in KOH solutions
with 9.5 g/l aluminate, at room temperature
Potential v.s. S.H.E (mV)
-1500
-1600
-1700
-1800
-1900
0.00
0.02
0.04
0.06
0.08
0.10
0.12
Indium content (wt%)
1M + 9.5g/l AlO2-
3M + 9.5g/l AlO2-
6M + 9.5g/l AlO2-
4M + 9.5g/l - flowcell

B10.1

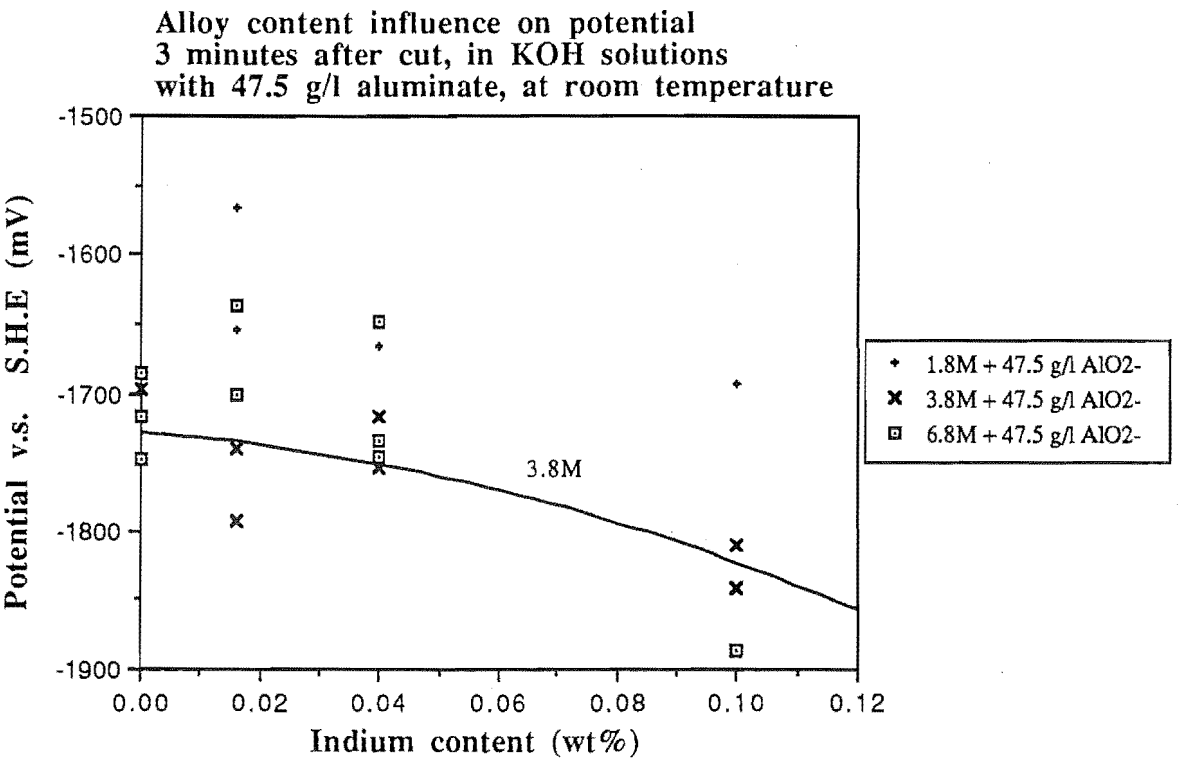
Alloy content influence on potential
3 minutes after cut, in KOH solutions
with 47.5 g/l aluminate, at room temperature
Potential v.s. S.H.E (mV)
-1500
-1600
-1700
-1800
-1900
0.00
0.02
0.04
0.06
0.08
0.10
0.12
Indium content (wt%)
3.8M
1.8M + 47.5 g/l AlO2-
3.8M + 47.5 g/l AlO2-
6.8M + 47.5 g/l AlO2-

B10.2

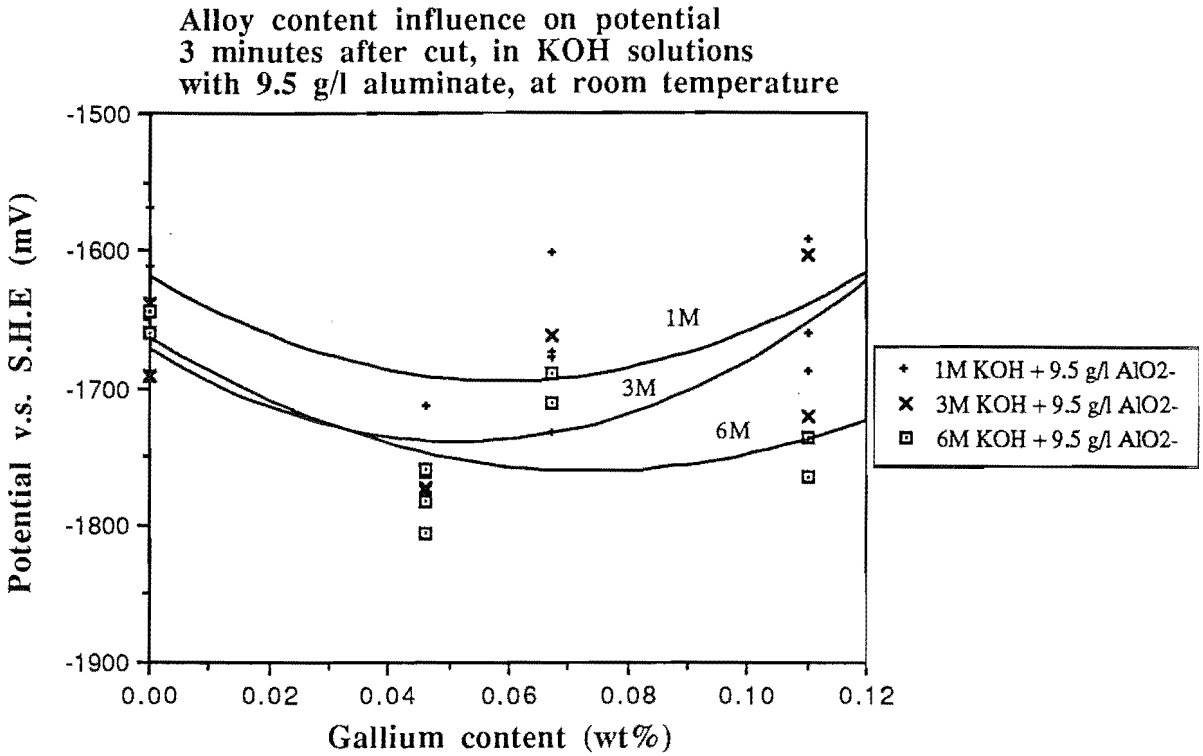
Alloy content influence on potential
3 minutes after cut, in KOH solutions
with 9.5 g/l aluminate, at room temperature
Potential v.s. S.H.E (mV)
-1500
-1600
-1700
-1800
-1900
0.00
0.02
0.04
0.06
0.08
0.10
0.12
Gallium content (wt%)
1M
3M
6M
1M KOH + 9.5 g/l AlO2-
3M KOH + 9.5 g/l AlO2-
6M KOH + 9.5 g/l AlO2-

B11.1

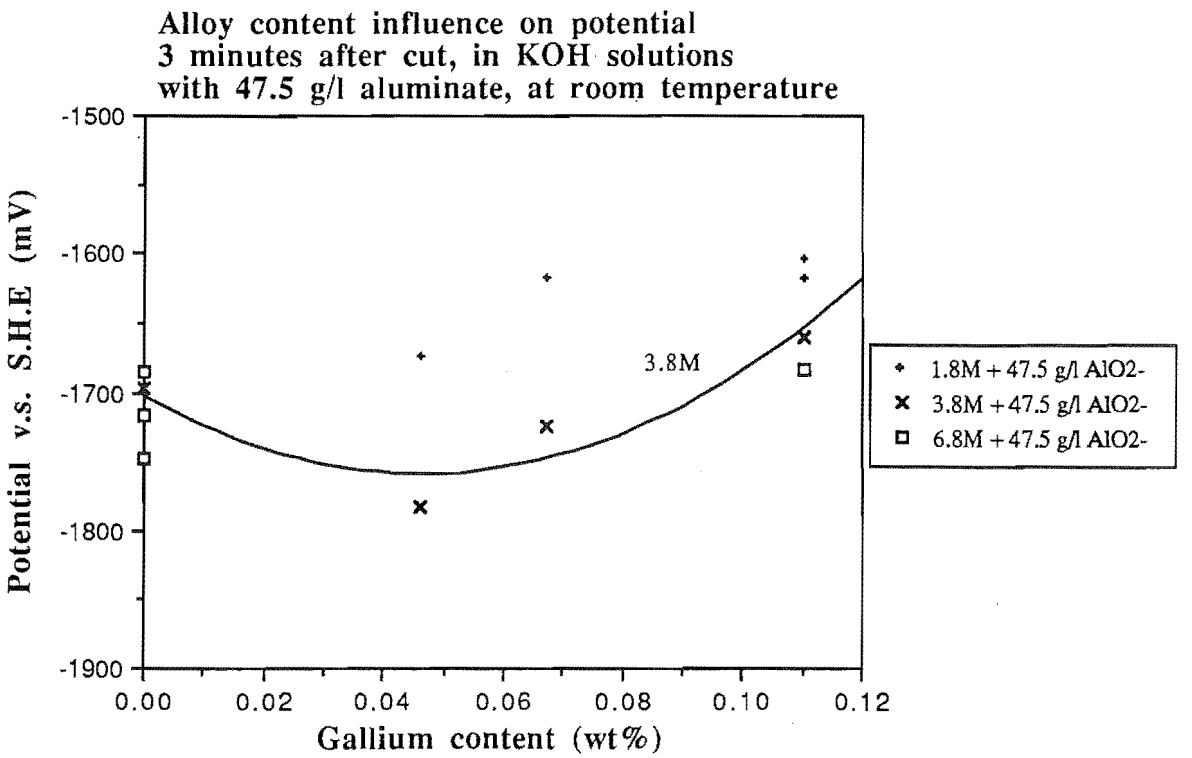
Alloy content influence on potential
3 minutes after cut, in KOH solutions
with 47.5 g/l aluminate, at room temperature
Potential v.s. S.H.E (mV)
-1500
-1600
-1700
-1800
-1900
0.00
0.02
0.04
0.06
0.08
0.10
0.12
Gallium content (wt%)
3.8M
1.8M + 47.5 g/l AlO2-
3.8M + 47.5 g/l AlO2-
6.8M + 47.5 g/l AlO2-

B11.2

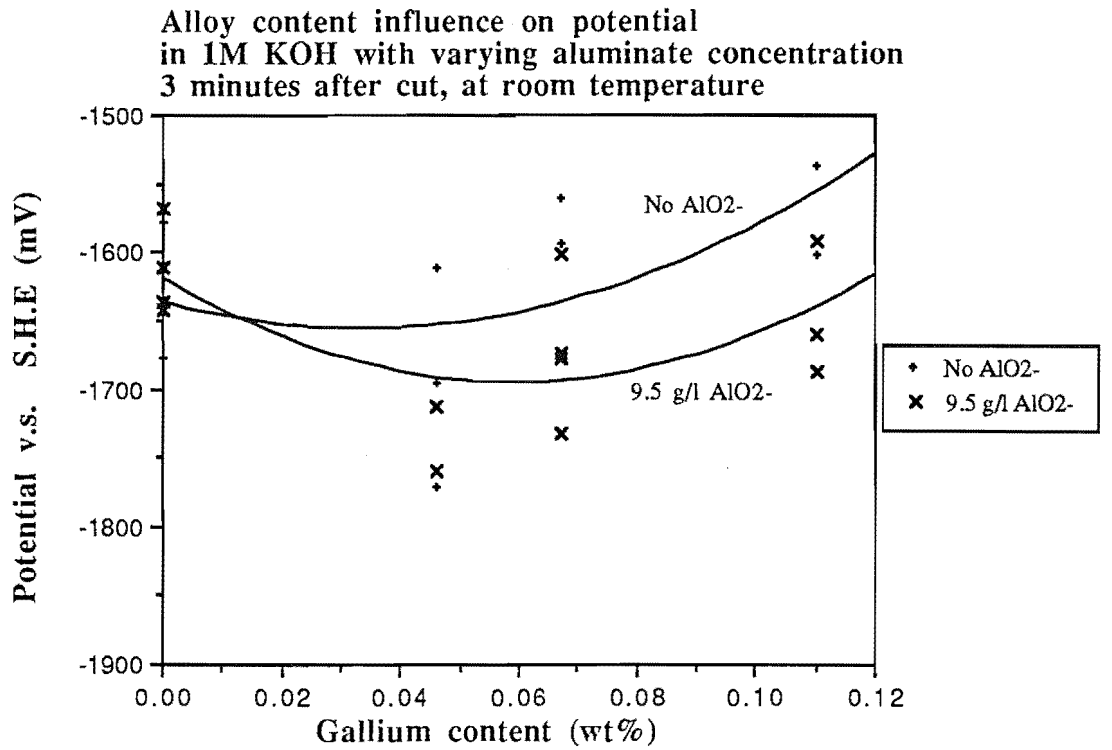
Alloy content influence on potential
in 1M KOH with varying aluminate concentration
3 minutes after cut, at room temperature
Potential v.s. S.H.E (mV)
-1500
-1600
-1700
-1800
-1900
0.00
0.02
0.04
0.06
0.08
0.10
0.12
Gallium content (wt%)
No AlO2-
9.5 g/l AlO2-
No AlO2-
9.5 g/l AlO2-

B12.1

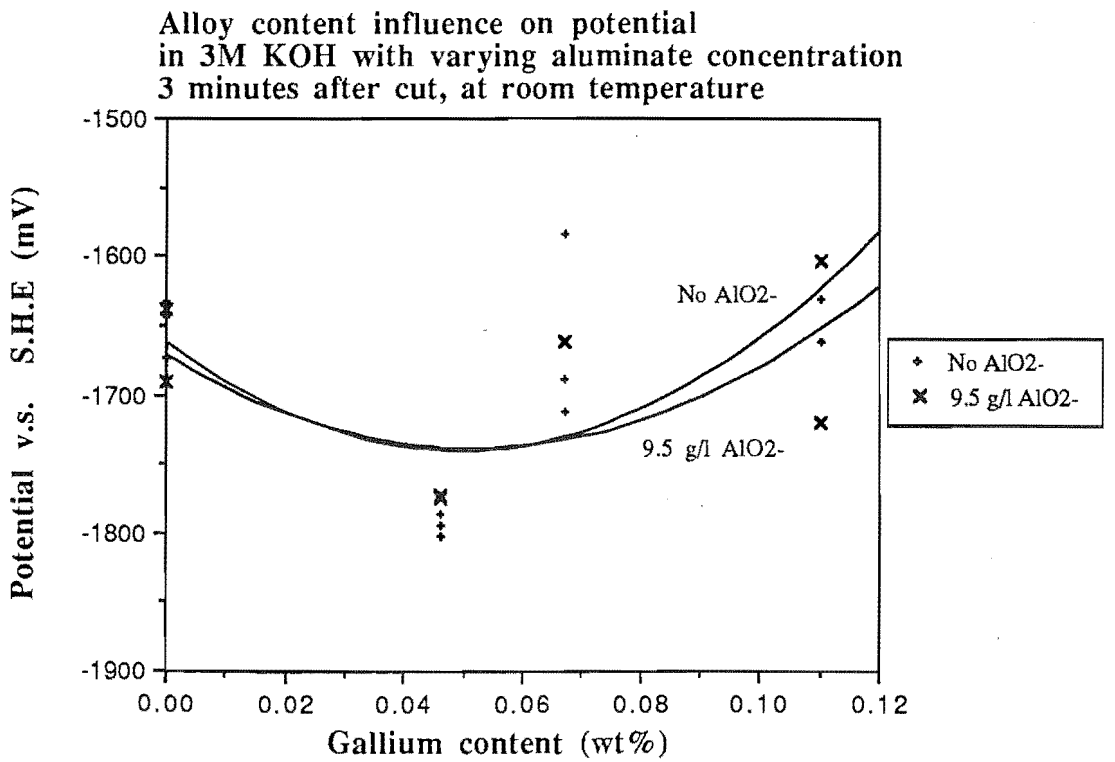
Alloy content influence on potential
in 3M KOH with varying aluminate concentration
3 minutes after cut, at room temperature
Potential v.s. S.H.E (mV)
-1500
-1600
-1700
-1800
-1900
0.00
0.02
0.04
0.06
0.08
0.10
0.12
Gallium content (wt%)
No AlO2-
9.5 g/l AlO2-
No AlO2-
9.5 g/l AlO2-

B12.2

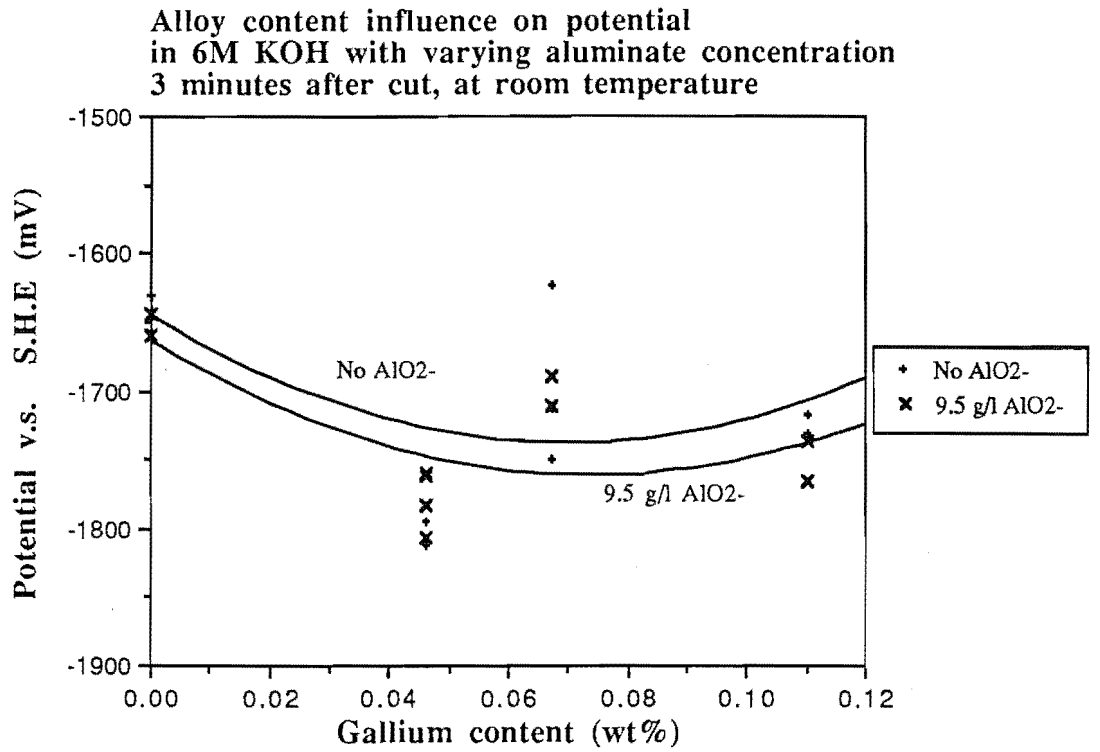
Alloy content influence on potential
in 6M KOH with varying aluminate concentration
3 minutes after cut, at room temperature
Potential v.s. S.H.E (mV)
-1500
-1600
-1700
-1800
-1900
No AlO2-
9.5 g/l AlO2-
0.00
0.02
0.04
0.06
0.08
0.10
0.12
Gallium content (wt%)
No AlO2-
9.5 g/l AlO2-

B13.1

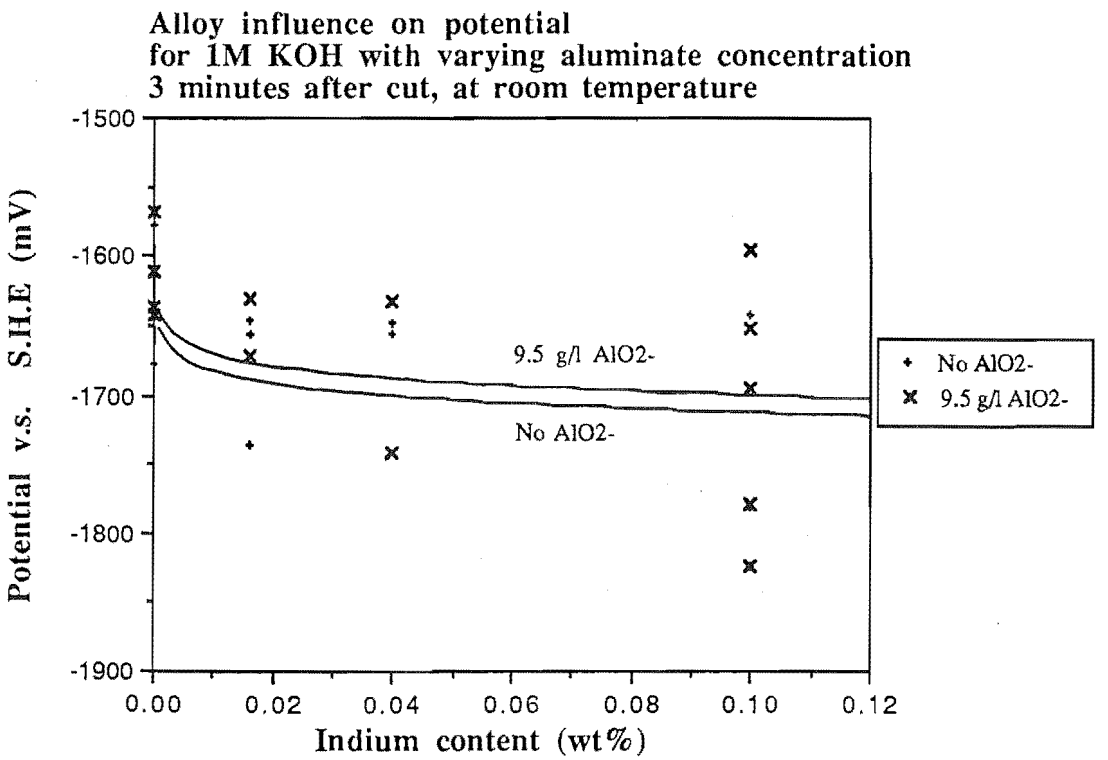
Alloy influence on potential
for 1M KOH with varying aluminate concentration
3 minutes after cut, at room temperature
Potential v.s. S.H.E (mV)
-1500
-1600
-1700
-1800
-1900
9.5 g/l AlO2-
No AlO2-
0.00
0.02
0.04
0.06
0.08
0.10
0.12
Indium content (wt%)
No AlO2-
9.5 g/l AlO2-

B13.2

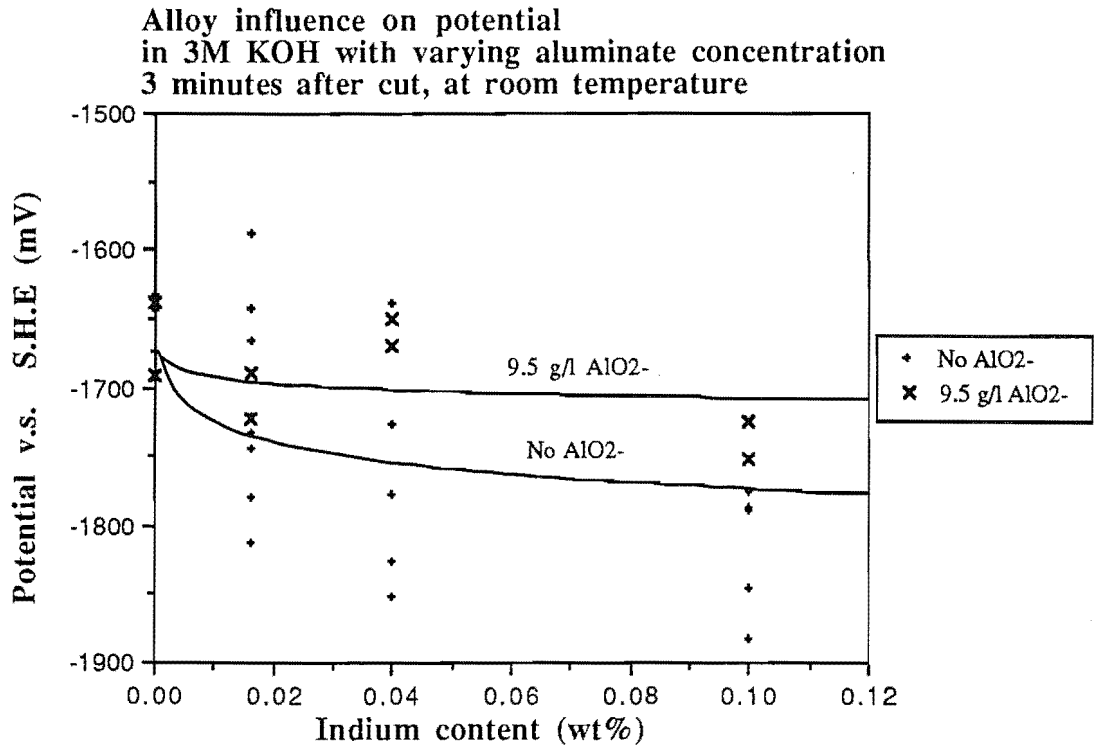
Alloy influence on potential
in 3M KOH with varying aluminate concentration
3 minutes after cut, at room temperature
Potential v.s. S.H.E (mV)
-1500
-1600
-1700
-1800
-1900
0.00
0.02
0.04
0.06
0.08
0.10
0.12
Indium content (wt%)
9.5 g/l AlO2-
No AlO2-
No AlO2-
9.5 g/l AlO2-

B14.1

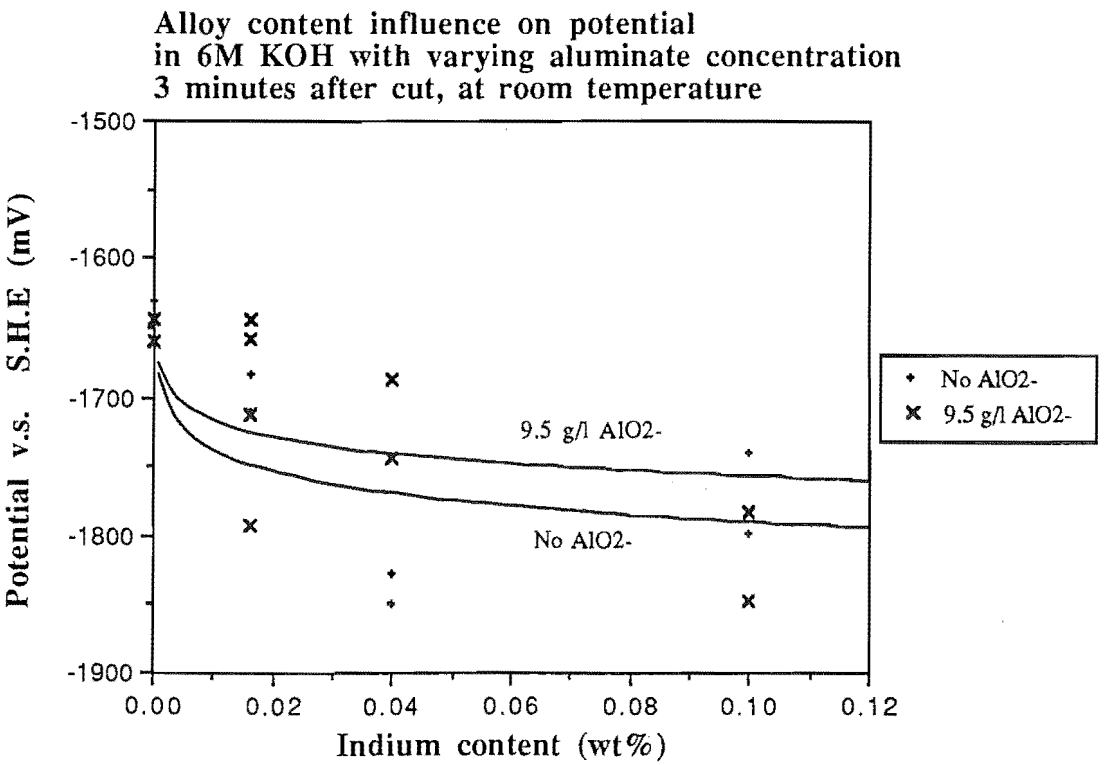
Alloy content influence on potential
in 6M KOH with varying aluminate concentration
3 minutes after cut, at room temperature
Potential v.s. S.H.E (mV)
-1500
-1600
-1700
-1800
-1900
0.00
0.02
0.04
0.06
0.08
0.10
0.12
Indium content (wt%)
9.5 g/l AlO2-
No AlO2-
No AlO2-
9.5 g/l AlO2-

B14.2

Concentration dependence of the peak potential for gallium alloys, in KOH solution containing aluminate, at room temperature

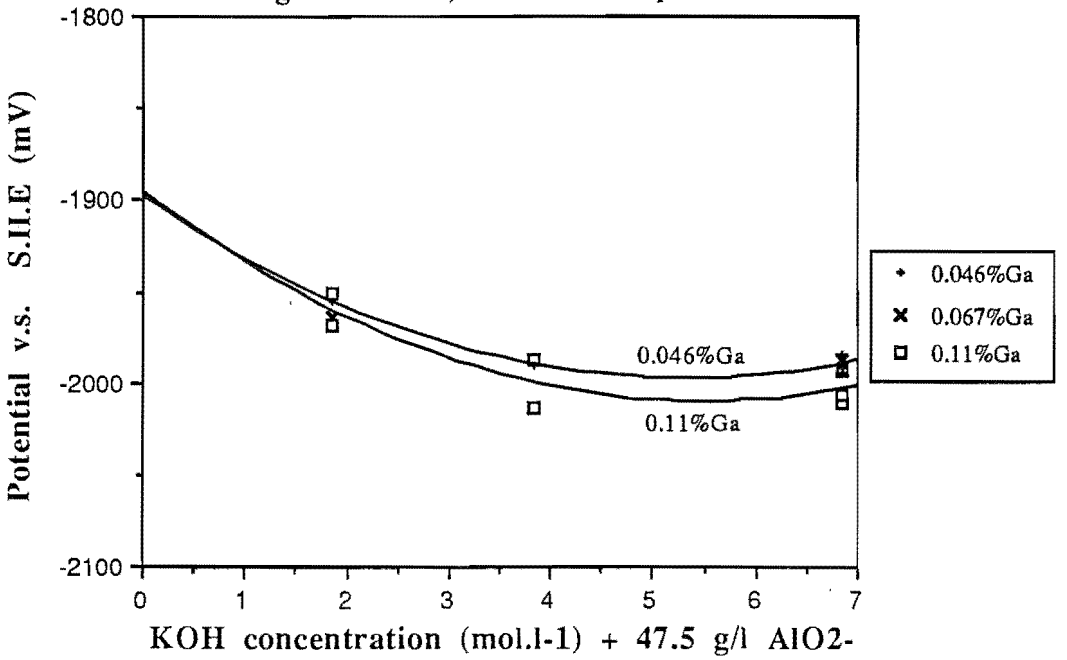

B15.1

Concentration dependence of the peak potential for Indium alloys in KOH solution with 9.5 g/l aluminate, at room temperature

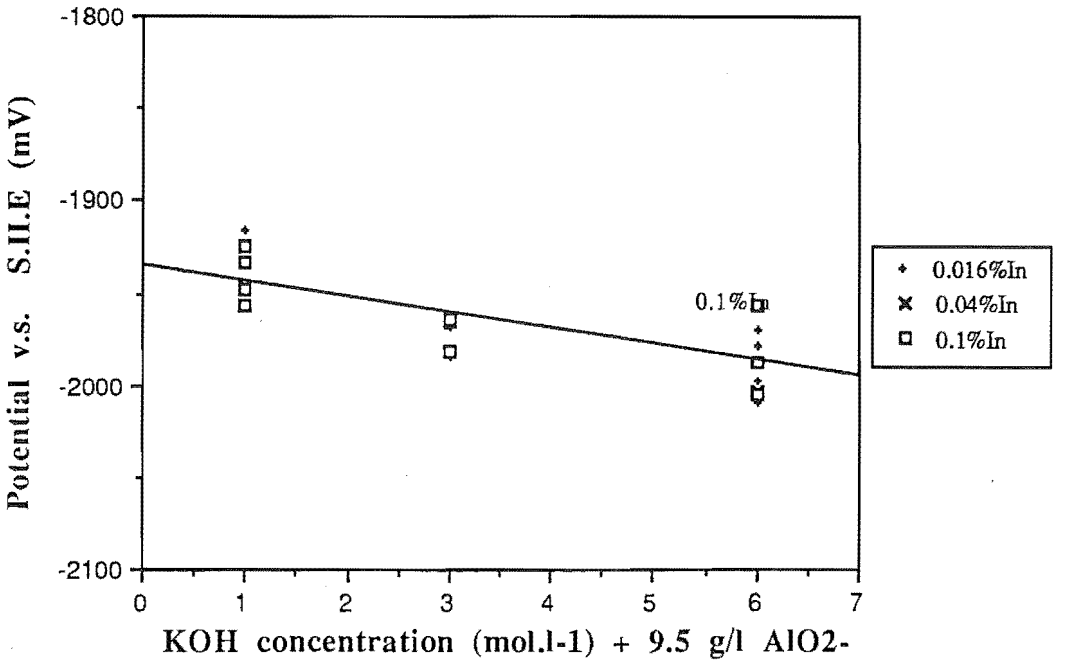

B15.2

APPENDIX.C

List of Graphs:

Polarization curves for:

Flowrate of 1.47 m / s

Flowrate of 0.375 m / s

C 12.2 Pure Aluminium temperature dependence (4M KOH)

C 13.1 Al - 0.1%Mg - 0.1%In alloy temperature dependence (4M KOH)

Flowrate of 0.75 m / s

C 13.2 Pure Aluminium temperature dependence (4M KOH)

C 14.1 Al - 0.1%Mg alloy temperature dependence (4M KOH)

C 14.2 Al - 0.1%In alloy temperature dependence (4M KOH)

C 15.1 Al - 0.1%Mg - 0.1%In alloy temperature dependence (4M KOH)

Sundry graphs

C 15.2 Polarization curves for 0.1%In with KOH concentration at 60°C

C 16.1 Polarization curves for 0.1%In with AlO_2^- concentration at 60°C and 4M KOH

C 16.2 Alloy current density dependence

C 17.1 Alloy current density dependence with temperature @ -1400mV

C 17.2 Pure aluminium power density dependence with temperature

C 18.1 Al - 0.1%Mg - 0.1%In power density dependence with flowrate at 60°C

C 18.2 Alloy power density dependence at 60°C, 4M KOH and 1.47 m / s

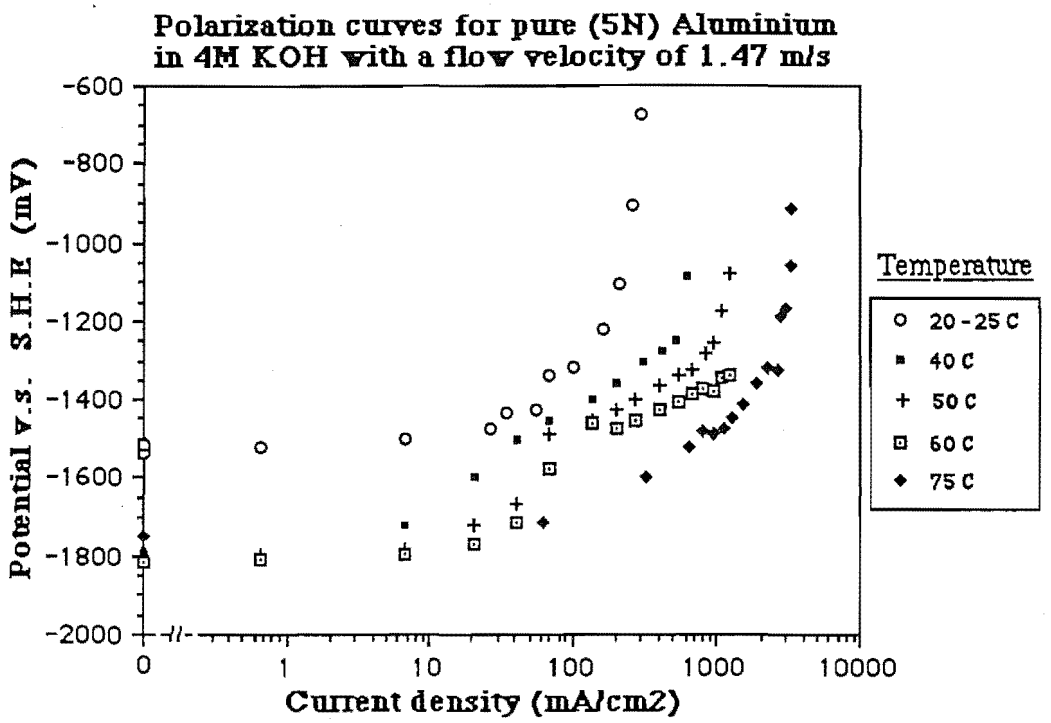
Polarization curves for pure (5N) Aluminium
in 4M KOH with a flow velocity of 1.47 m/s
Potential v.s. S.H.E (mV)
-600
-800
-1000
-1200
-1400
-1600
-1800
-2000
0
1
10
100
1000
10000
Current density (mA/cm2)
Temperature
20-25 C
40 C
50 C
60 C
75 C

C 1.1

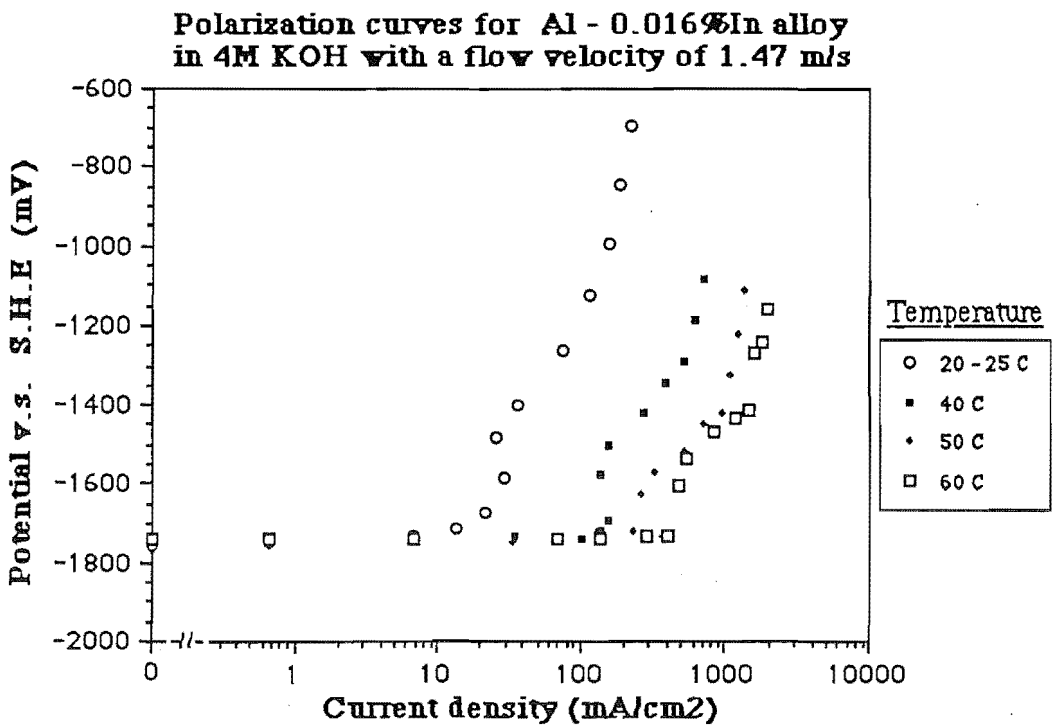
Polarization curves for Al - 0.016%In alloy
in 4M KOH with a flow velocity of 1.47 m/s
Potential v.s. S.H.E (mV)
-600
-800
-1000
-1200
-1400
-1600
-1800
-2000
0
1
10
100
1000
10000
Current density (mA/cm2)
Temperature
20-25 C
40 C
50 C
60 C

C 1.2

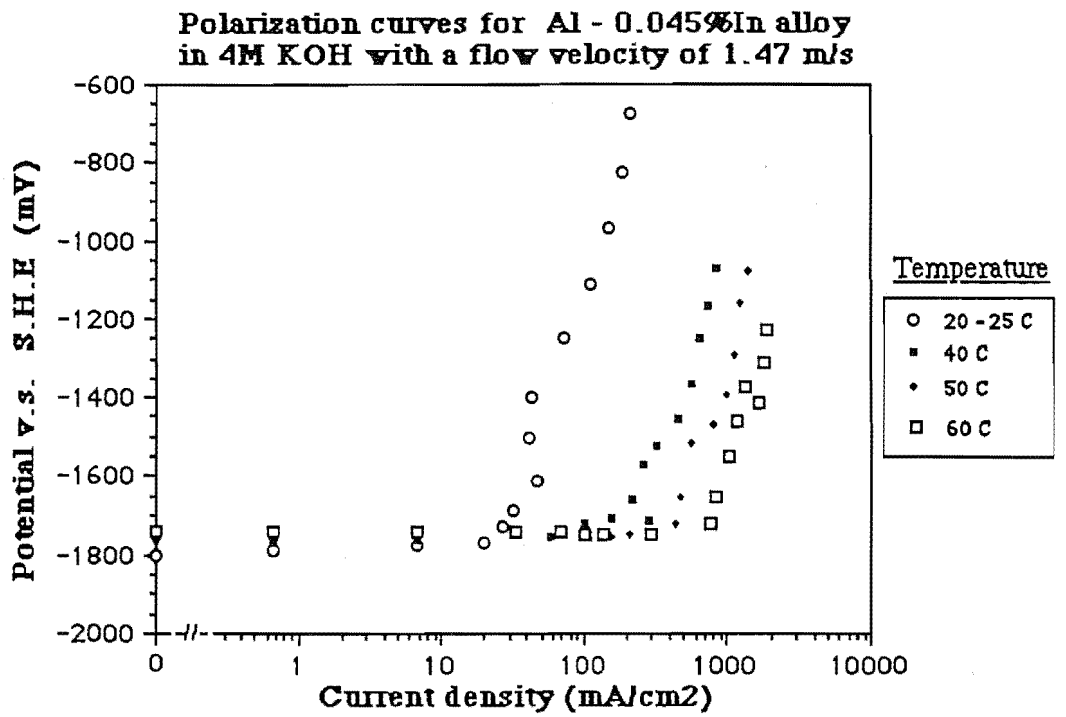
Polarization curves for Al - 0.045%In alloy
in 4M KOH with a flow velocity of 1.47 m/s
Potential v.s. S.H.E (mV)
-600
-800
-1000
-1200
-1400
-1600
-1800
-2000
0
1
10
100
1000
10000
Current density (mA/cm2)
Temperature
20 - 25 C
40 C
50 C
60 C

C 2.1

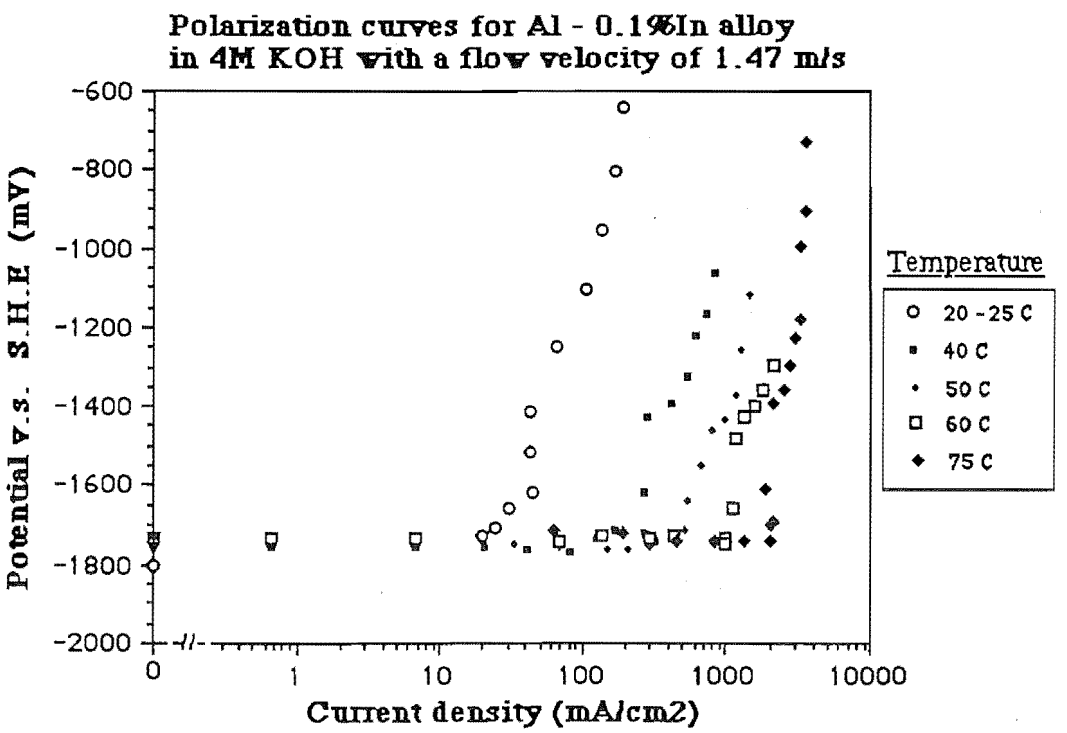
Polarization curves for Al - 0.1%In alloy
in 4M KOH with a flow velocity of 1.47 m/s
Potential v.s. S.H.E (mV)
-600
-800
-1000
-1200
-1400
-1600
-1800
-2000
0
1
10
100
1000
10000
Current density (mA/cm2)
Temperature
20 - 25 C
40 C
50 C
60 C
75 C

C 2.2

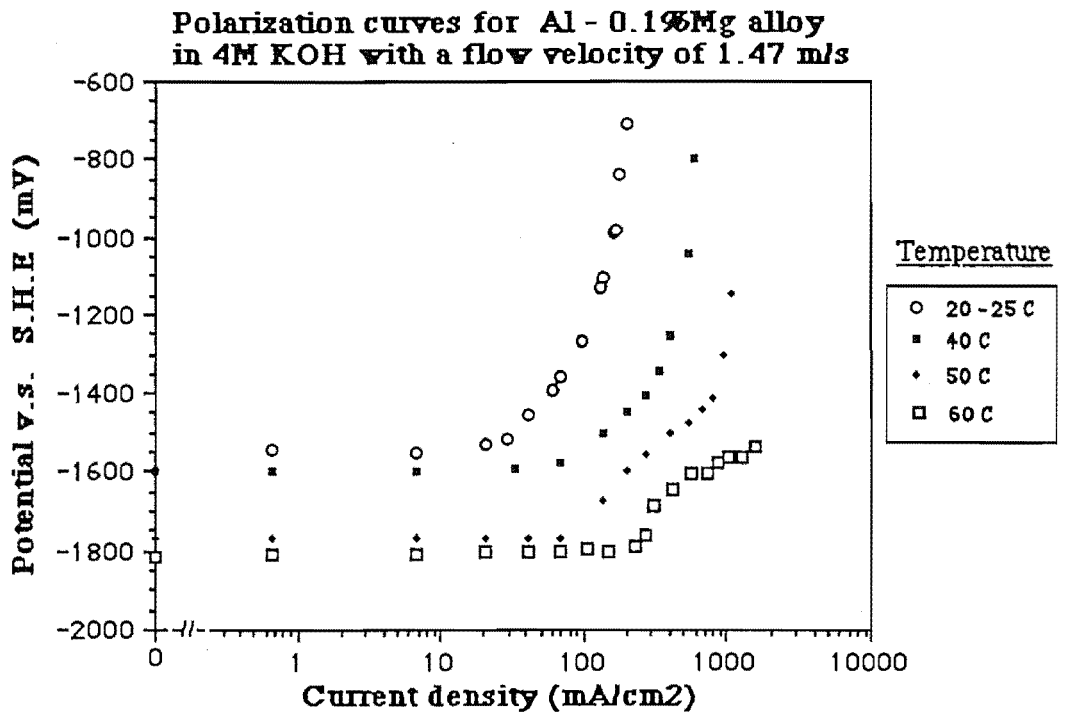
Polarization curves for Al - 0.1%Mg alloy
in 4M KOH with a flow velocity of 1.47 m/s
Potential v.s. S.H.E (mV)
-600
-800
-1000
-1200
-1400
-1600
-1800
-2000
0
1
10
100
1000
10000
Current density (mA/cm2)
Temperature
20 - 25 C
40 C
50 C
60 C

C 3.1

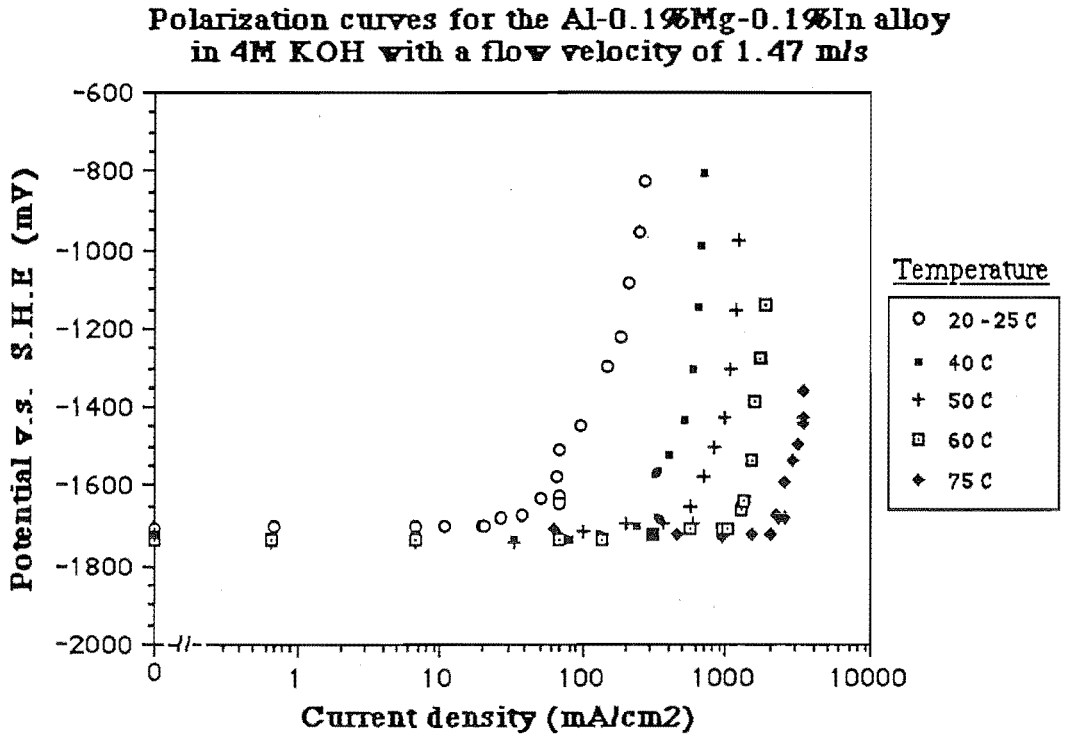
Polarization curves for the Al-0.1%Mg-0.1%In alloy
in 4M KOH with a flow velocity of 1.47 m/s
Potential v.s. S.H.E (mV)
-600
-800
-1000
-1200
-1400
-1600
-1800
-2000
0
1
10
100
1000
10000
Current density (mA/cm2)
Temperature
20 - 25 C
40 C
50 C
60 C
75 C

C 3.2

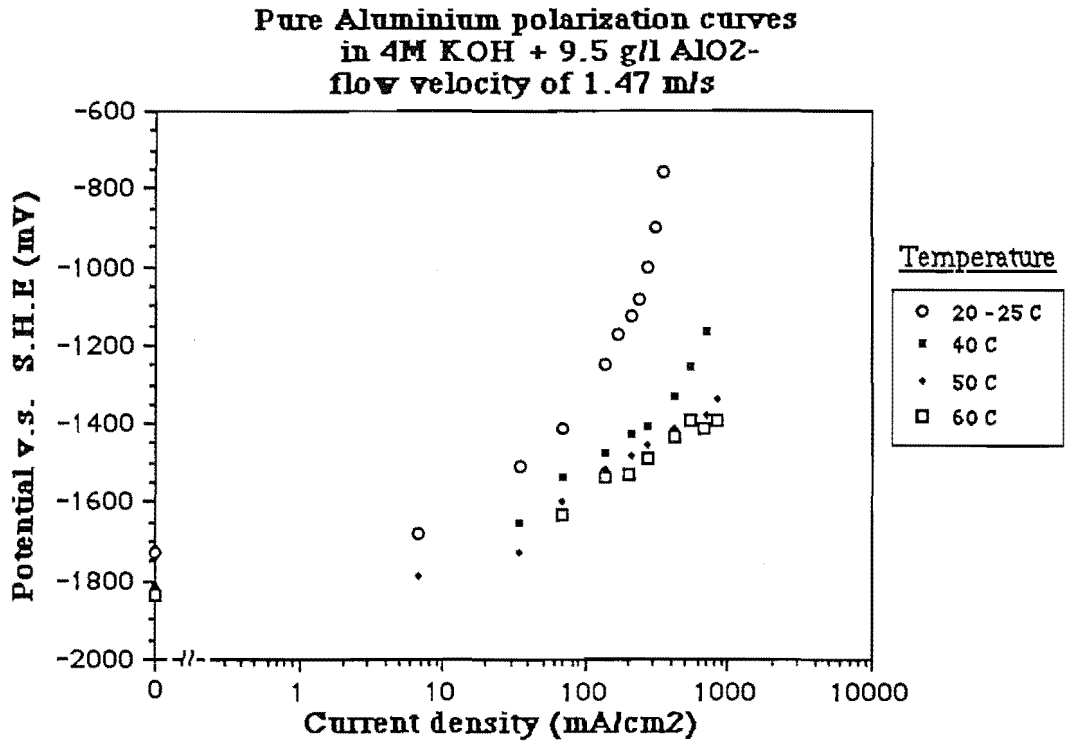
Pure Aluminium polarization curves
in 4M KOH + 9.5 g/l AlO2-
flow velocity of 1.47 m/s
Potential v.s. S.H.E (mV)
-600
-800
-1000
-1200
-1400
-1600
-1800
-2000
0
1
10
100
1000
10000
Current density (mA/cm2)
Temperature
20 - 25 C
40 C
50 C
60 C

C 4.1

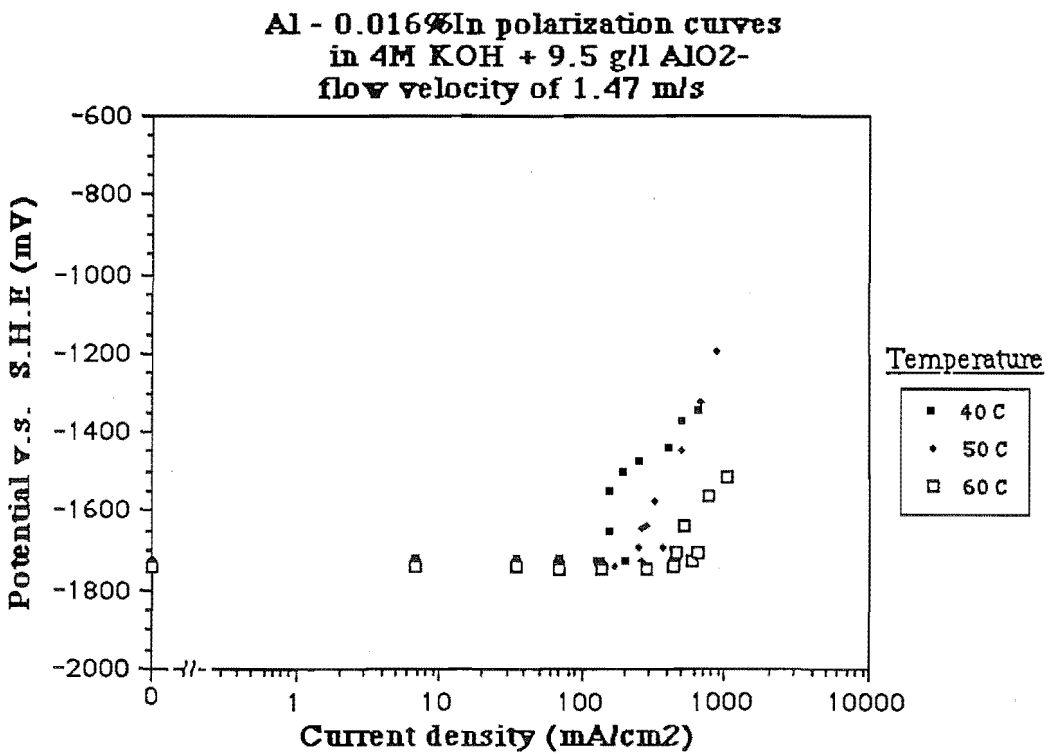
Al - 0.016%In polarization curves
in 4M KOH + 9.5 g/l AlO2-
flow velocity of 1.47 m/s
Potential v.s. S.H.E (mV)
-600
-800
-1000
-1200
-1400
-1600
-1800
-2000
0
1
10
100
1000
10000
Current density (mA/cm2)
Temperature
40 C
50 C
60 C

C 4.2

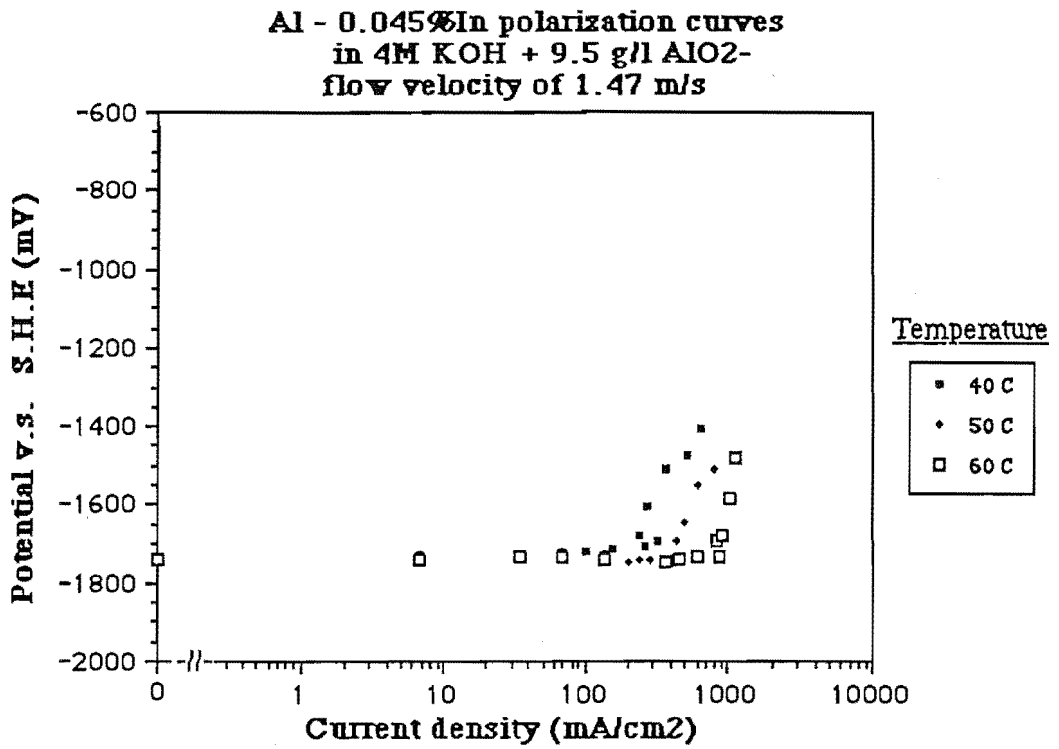
Al - 0.045%In polarization curves
in 4M KOH + 9.5 g/l AlO2-
flow velocity of 1.47 m/s
Potential v.s. S.H.E (mV)
-600
-800
-1000
-1200
-1400
-1600
-1800
-2000
0
1
10
100
1000
10000
Current density (mA/cm2)
Temperature
40 C
50 C
60 C

C 5.1

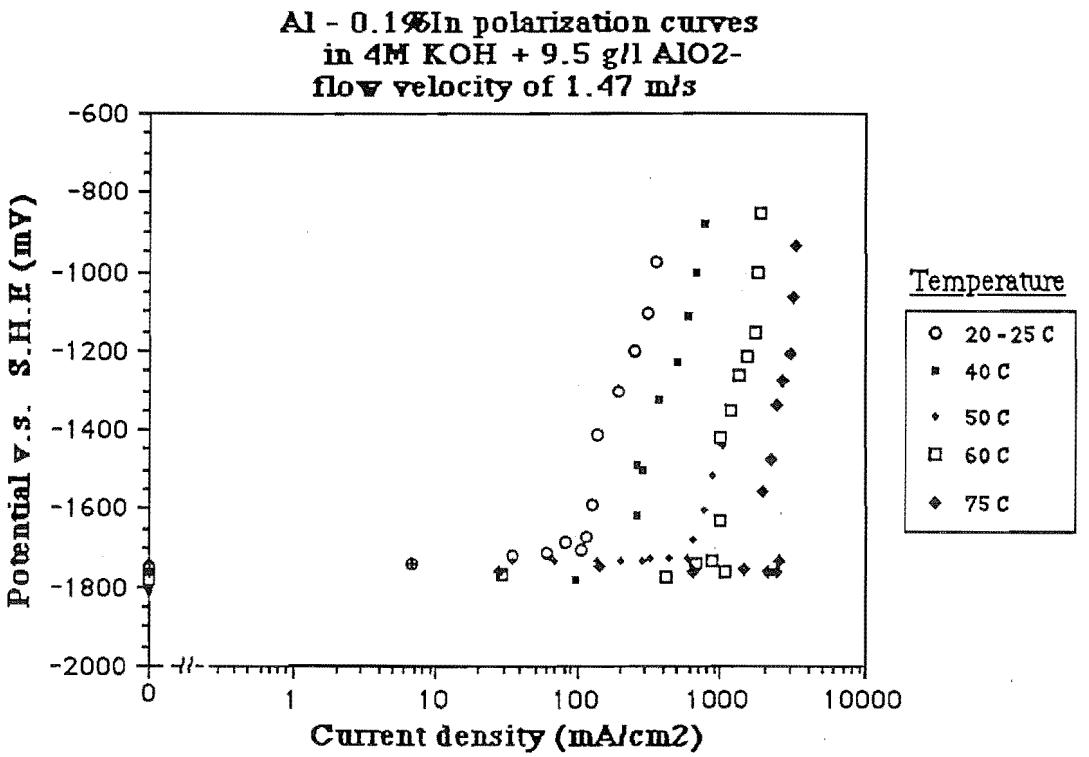
Al - 0.1%In polarization curves
in 4M KOH + 9.5 g/l AlO2-
flow velocity of 1.47 m/s
Potential v.s. S.H.E (mV)
-600
-800
-1000
-1200
-1400
-1600
-1800
-2000
0
1
10
100
1000
10000
Current density (mA/cm2)
Temperature
20 - 25 C
40 C
50 C
60 C
75 C

C 5.2

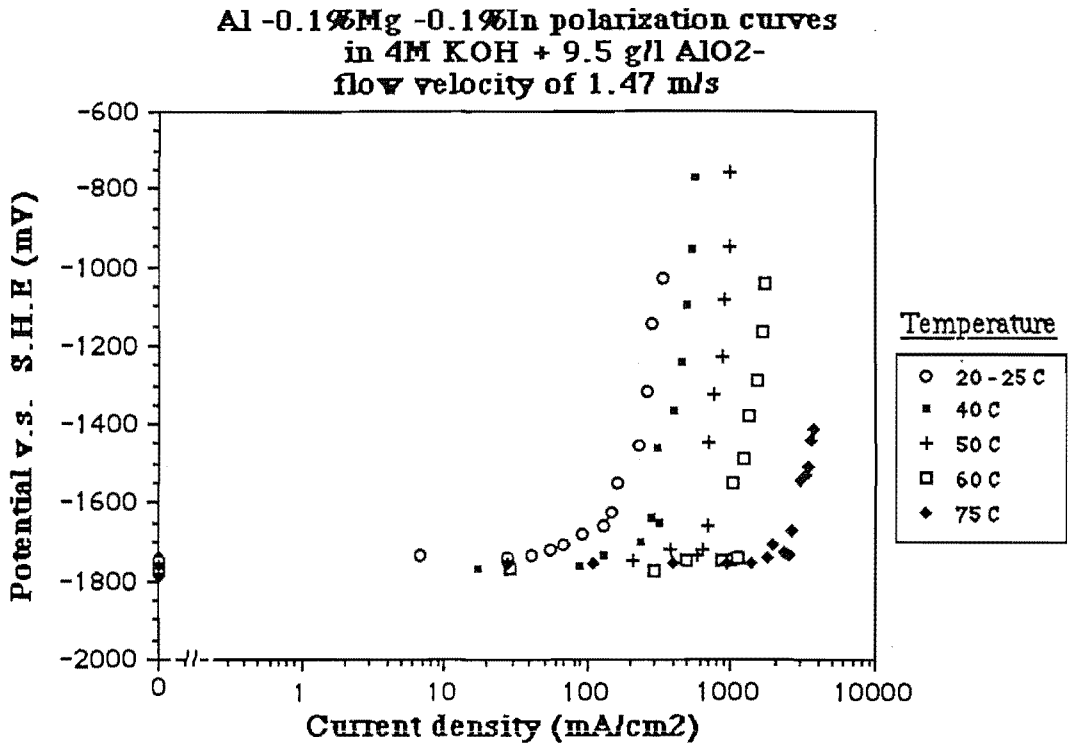
Al -0.1%Mg -0.1%In polarization curves
in 4M KOH + 9.5 g/l AlO2-
flow velocity of 1.47 m/s
Potential v.s. S.H.E (mV)
-600
-800
-1000
-1200
-1400
-1600
-1800
-2000
0
1
10
100
1000
10000
Current density (mA/cm2)
Temperature
20 - 25 C
40 C
50 C
60 C
75 C

C 6.1

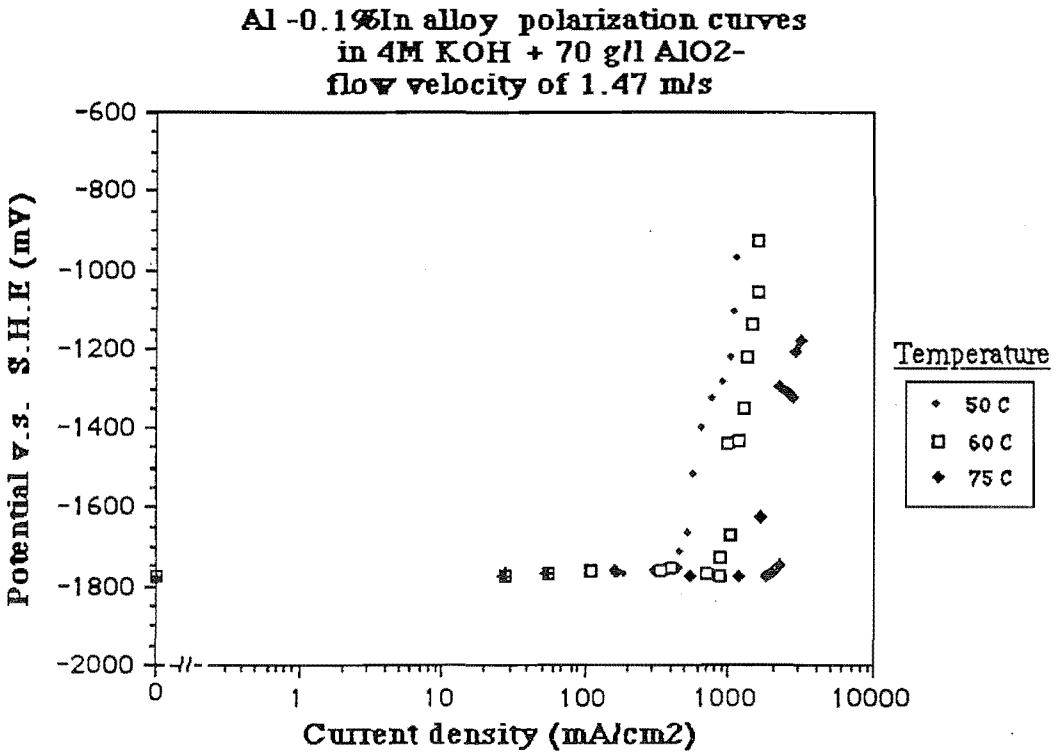
Al -0.1%In alloy polarization curves
in 4M KOH + 70 g/l AlO2-
flow velocity of 1.47 m/s
Potential v.s. S.H.E (mV)
-600
-800
-1000
-1200
-1400
-1600
-1800
-2000
0
1
10
100
1000
10000
Current density (mA/cm2)
Temperature
50 C
60 C
75 C

C 6.2

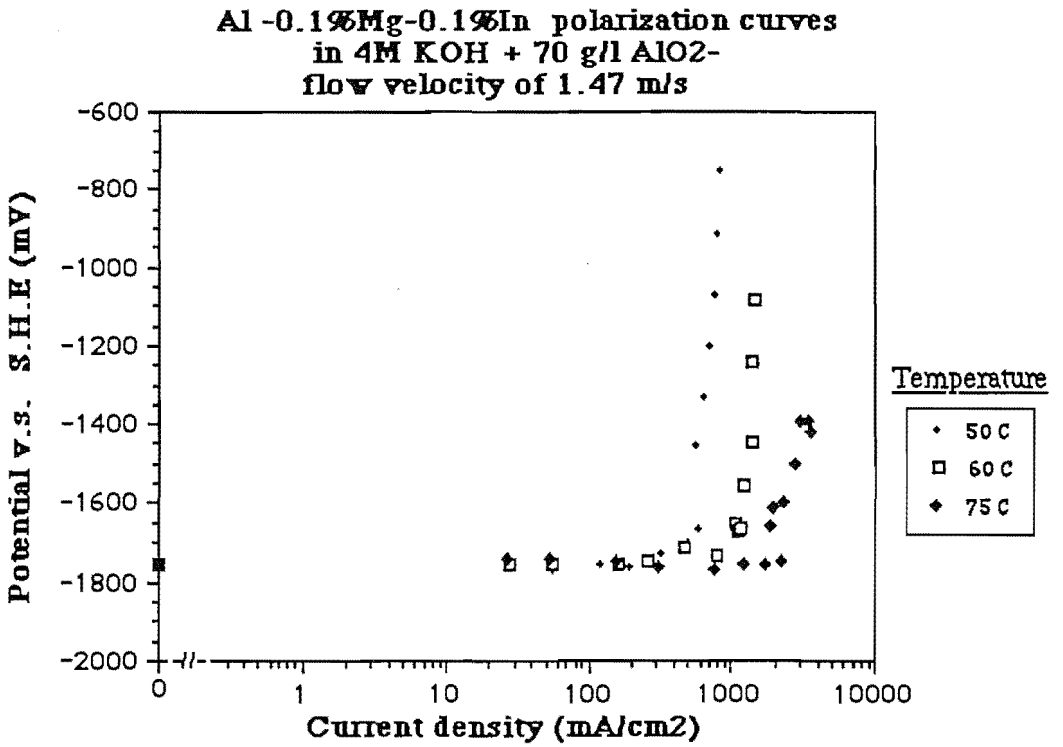
Al -0.1%Mg-0.1%In polarization curves
in 4M KOH + 70 g/l AlO2-
flow velocity of 1.47 m/s
Potential v.s. S.H.E (mV)
-600
-800
-1000
-1200
-1400
-1600
-1800
-2000
0
1
10
100
1000
10000
Current density (mA/cm2)
Temperature
50 C
60 C
75 C

C 7.1

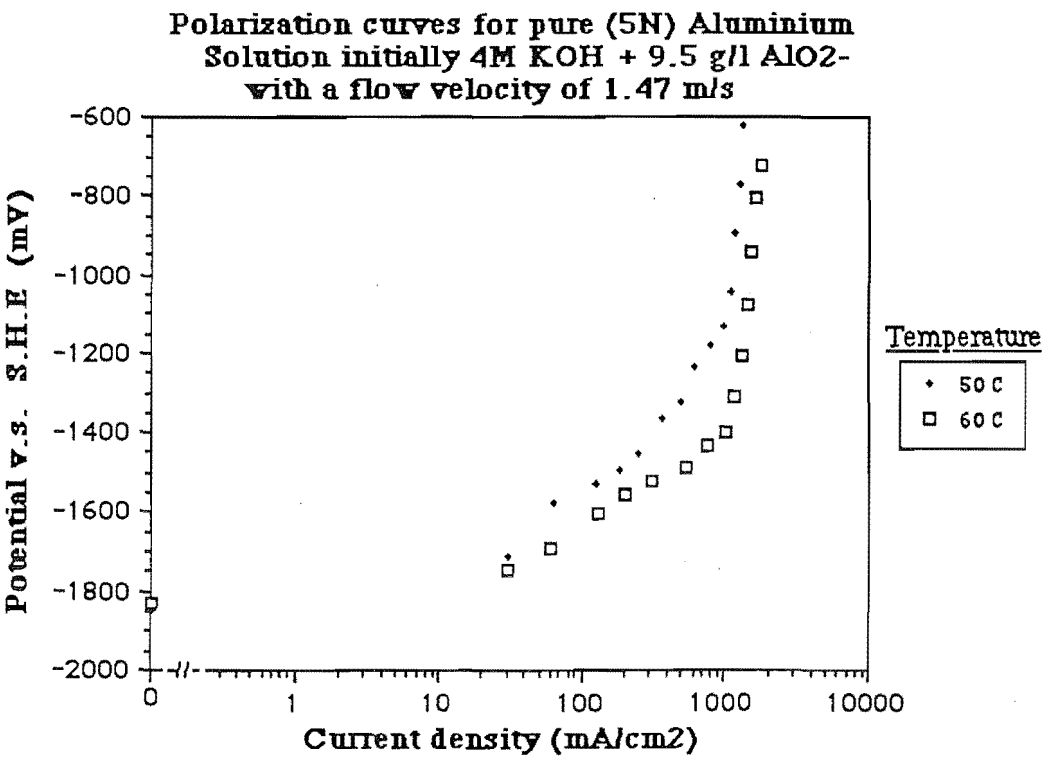
Polarization curves for pure (5N) Aluminium
Solution initially 4M KOH + 9.5 g/l AlO2-
with a flow velocity of 1.47 m/s
Potential v.s. S.H.E (mV)
-600
-800
-1000
-1200
-1400
-1600
-1800
-2000
0
1
10
100
1000
10000
Current density (mA/cm2)
Temperature
50 C
60 C

C 7.2

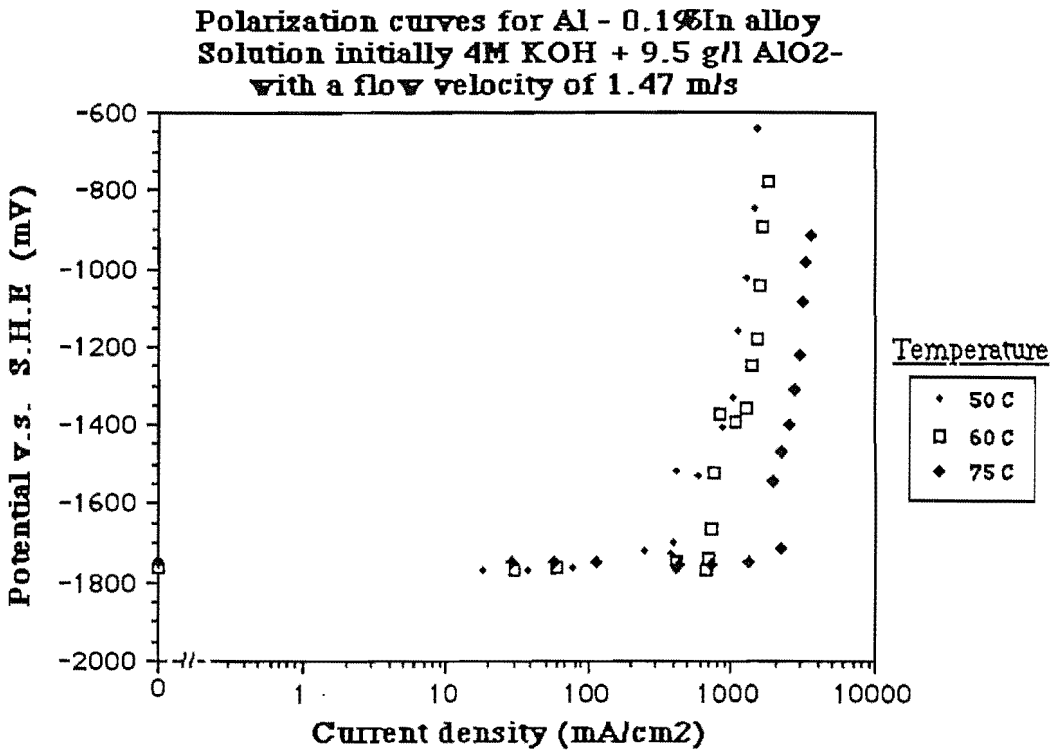
Polarization curves for Al - 0.1%In alloy
Solution initially 4M KOH + 9.5 g/l AlO2-
with a flow velocity of 1.47 m/s
Potential v.s. S.H.E (mV)
-600
-800
-1000
-1200
-1400
-1600
-1800
-2000
0
1
10
100
1000
10000
Current density (mA/cm2)
Temperature
50 C
60 C
75 C

C 8.1

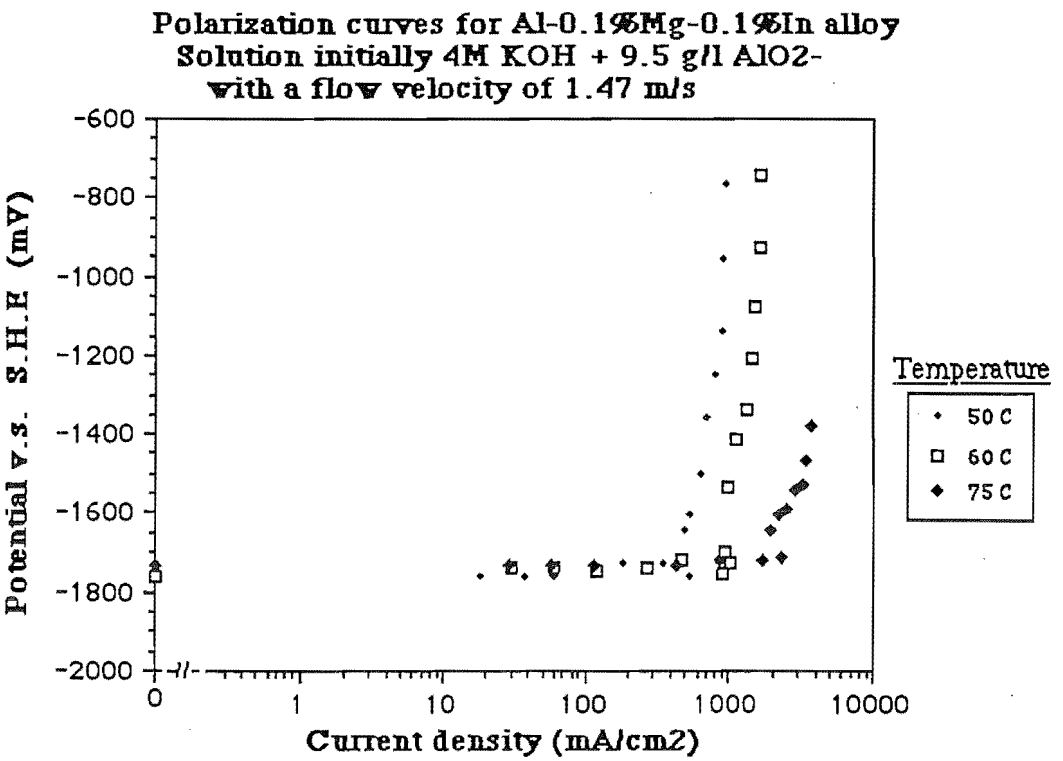
Polarization curves for Al-0.1%Mg-0.1%In alloy
Solution initially 4M KOH + 9.5 g/l AlO2-
with a flow velocity of 1.47 m/s
Potential v.s. S.H.E (mV)
-600
-800
-1000
-1200
-1400
-1600
-1800
-2000
0
1
10
100
1000
10000
Current density (mA/cm2)
Temperature
50 C
60 C
75 C

C 8.2

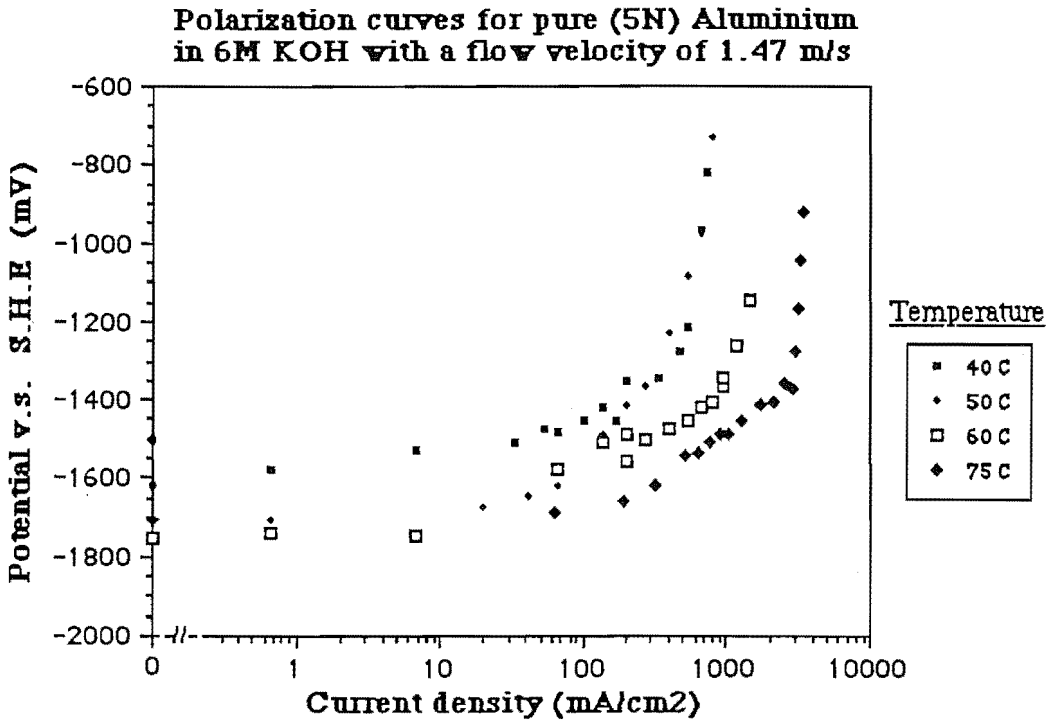
Polarization curves for pure (5N) Aluminium
in 6M KOH with a flow velocity of 1.47 m/s
Potential v.s. S.H.E (mV)
-600
-800
-1000
-1200
-1400
-1600
-1800
-2000
0
1
10
100
1000
10000
Current density (mA/cm2)
Temperature
40 C
50 C
60 C
75 C

C 9.1

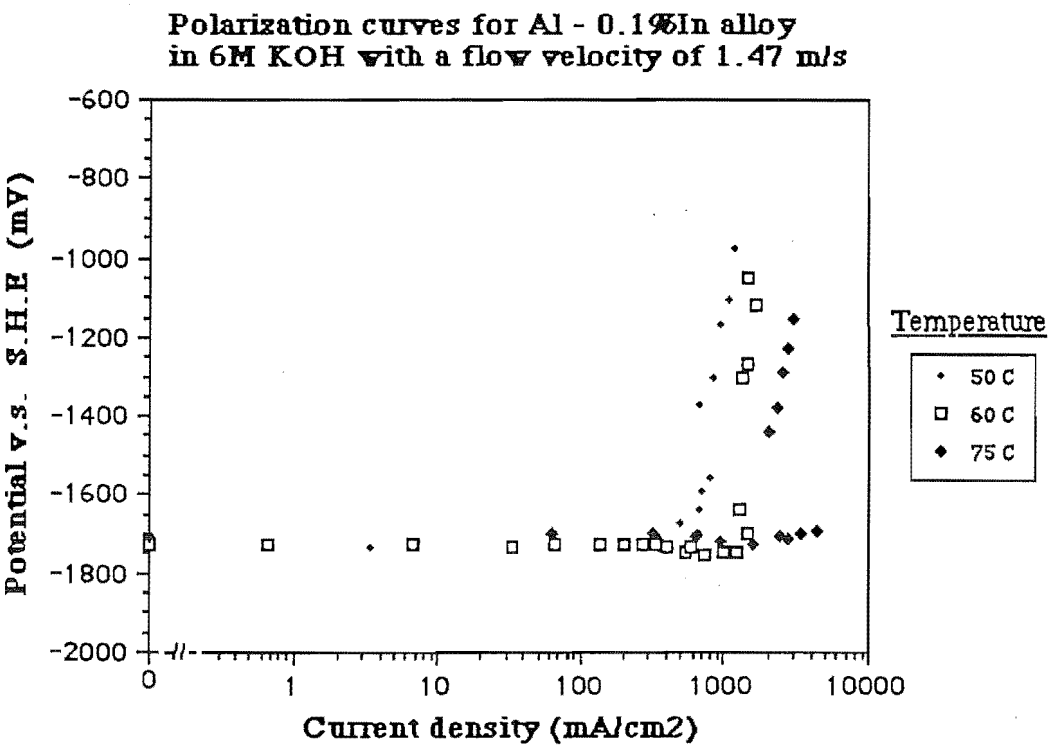
Polarization curves for Al - 0.1%In alloy
in 6M KOH with a flow velocity of 1.47 m/s
Potential v.s. S.H.E (mV)
-600
-800
-1000
-1200
-1400
-1600
-1800
-2000
0
1
10
100
1000
10000
Current density (mA/cm2)
Temperature
50 C
60 C
75 C

C 9.2

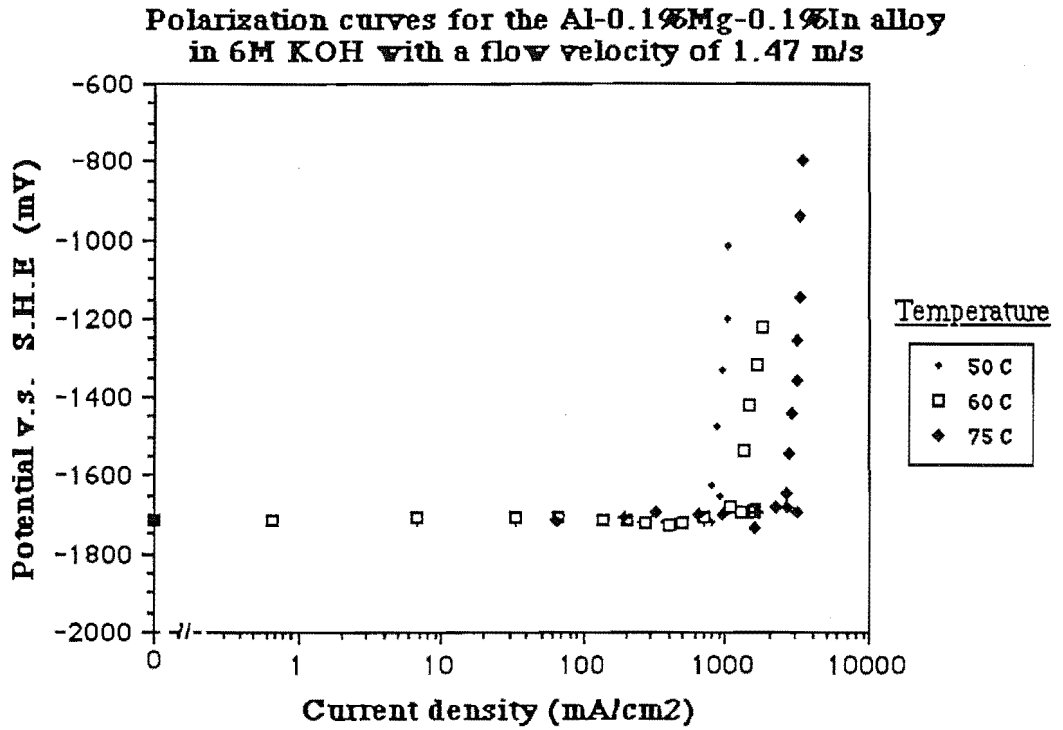
Polarization curves for the Al-0.1%Mg-0.1%In alloy
in 6M KOH with a flow velocity of 1.47 m/s
Potential v.s. S.H.E (mV)
-600
-800
-1000
-1200
-1400
-1600
-1800
-2000
0
1
10
100
1000
10000
Current density (mA/cm2)
Temperature
50 C
60 C
75 C

C 10.1

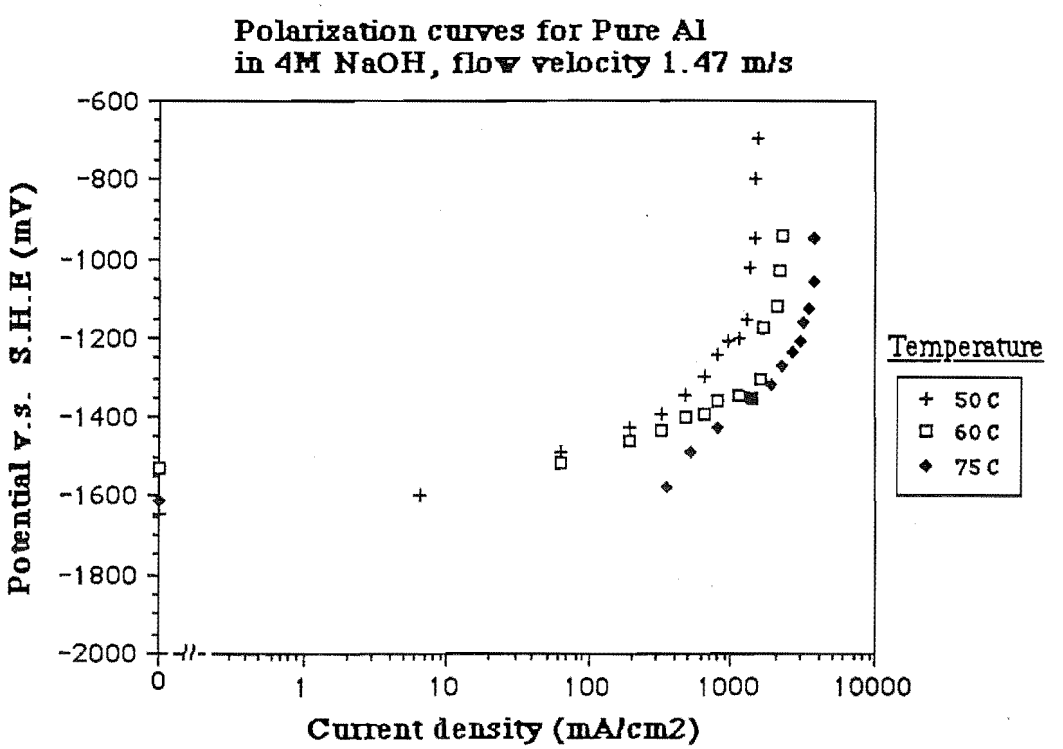
Polarization curves for Pure Al
in 4M NaOH, flow velocity 1.47 m/s
Potential v.s. S.H.E (mV)
-600
-800
-1000
-1200
-1400
-1600
-1800
-2000
0
1
10
100
1000
10000
Current density (mA/cm2)
Temperature
50 C
60 C
75 C

C 10.2

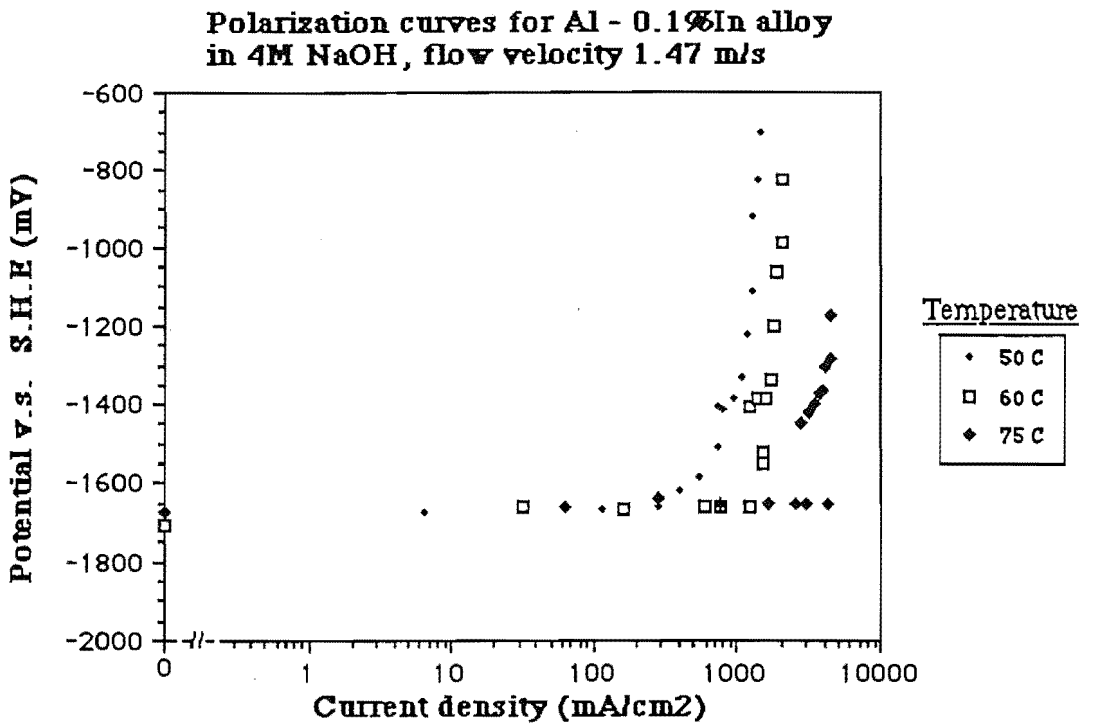
Polarization curves for Al - 0.1%In alloy
in 4M NaOH, flow velocity 1.47 m/s
Potential v.s. S.H.E (mV)
-600
-800
-1000
-1200
-1400
-1600
-1800
-2000
0
1
10
100
1000
10000
Current density (mA/cm2)
Temperature
50 C
60 C
75 C

C 11.1

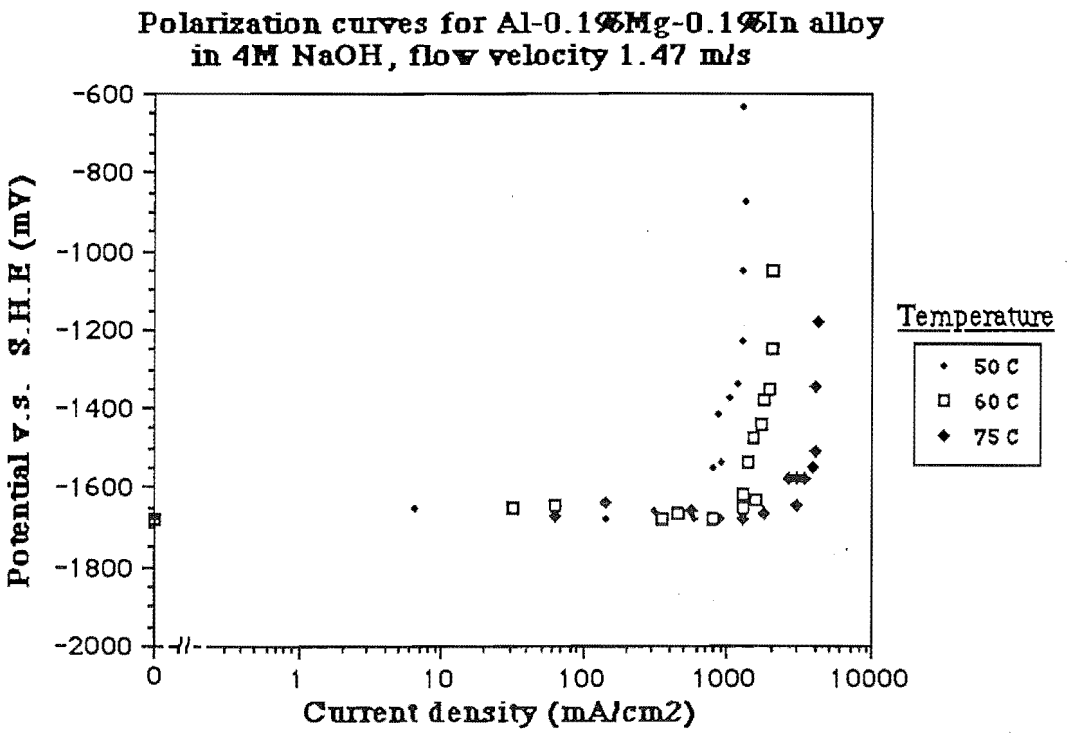
Polarization curves for Al-0.1%Mg-0.1%In alloy
in 4M NaOH, flow velocity 1.47 m/s
Potential v.s. S.H.E (mV)
-600
-800
-1000
-1200
-1400
-1600
-1800
-2000
0
1
10
100
1000
10000
Current density (mA/cm2)
Temperature
50 C
60 C
75 C

C 11.2

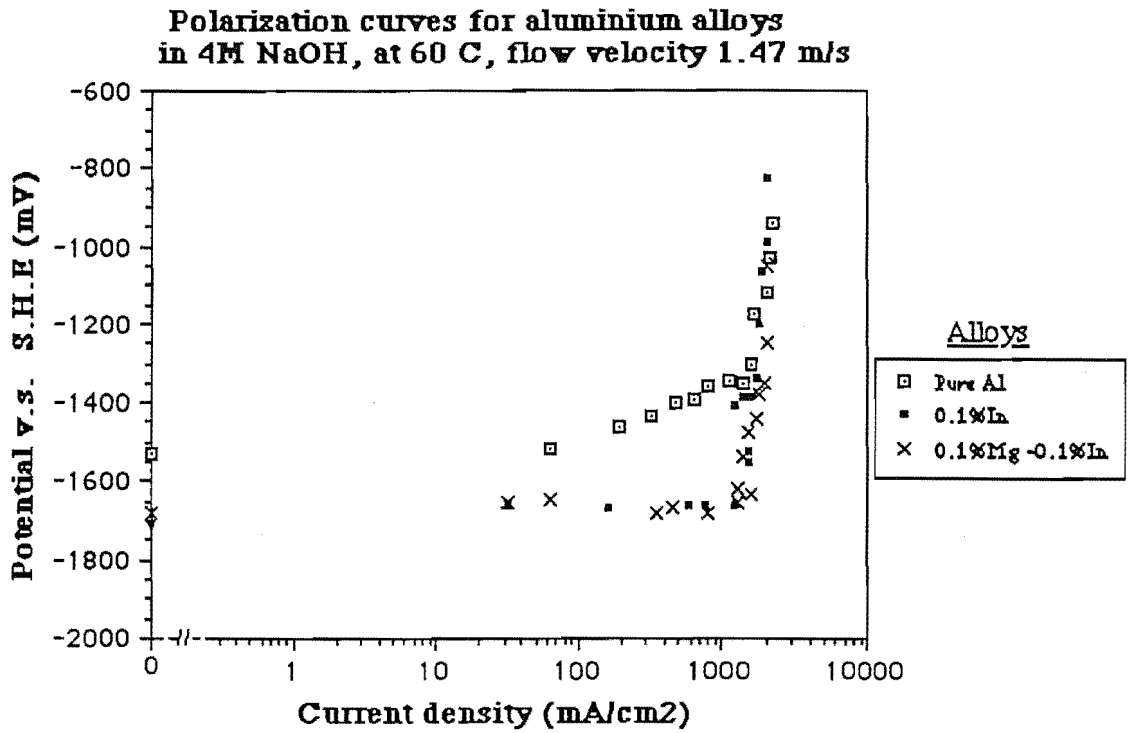
Polarization curves for aluminium alloys
in 4M NaOH, at 60 C, flow velocity 1.47 m/s
Potential v.s. S.H.E (mV)
-600
-800
-1000
-1200
-1400
-1600
-1800
-2000
0
1
10
100
1000
10000
Current density (mA/cm2)
Alloys
Pure Al
0.1%In
0.1%Mg -0.1%In

C 12.1

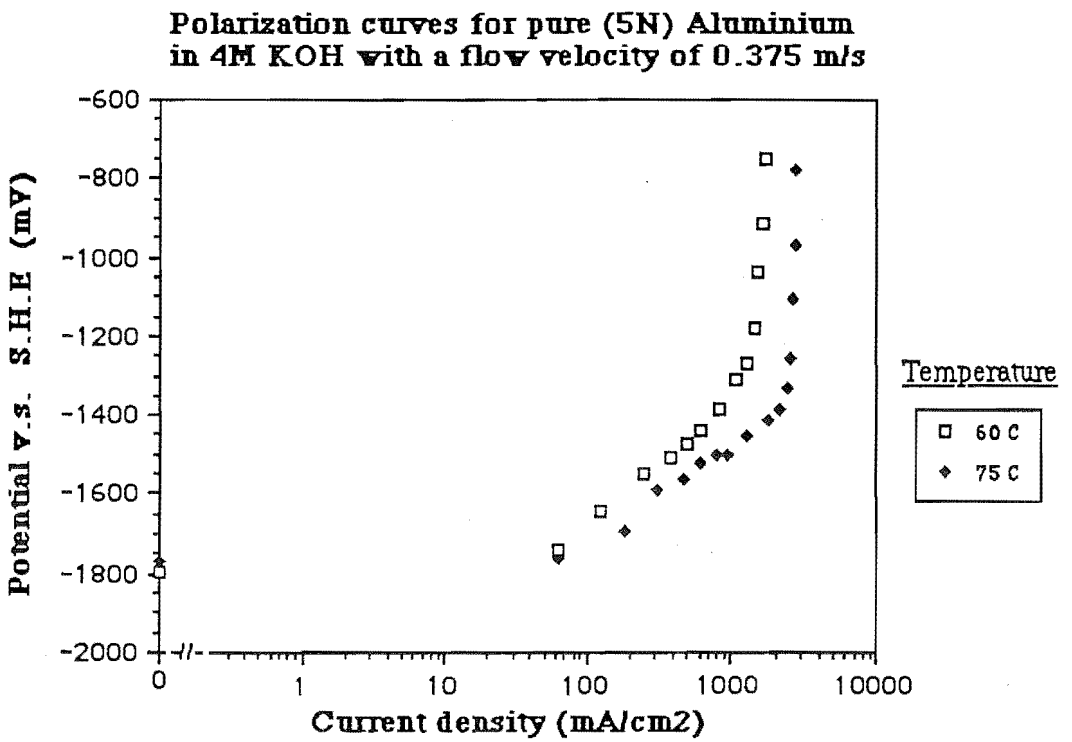
Polarization curves for pure (5N) Aluminium
in 4M KOH with a flow velocity of 0.375 m/s
Potential v.s. S.H.E (mV)
-600
-800
-1000
-1200
-1400
-1600
-1800
-2000
0
1
10
100
1000
10000
Current density (mA/cm2)
Temperature
60 C
75 C

C 12.2

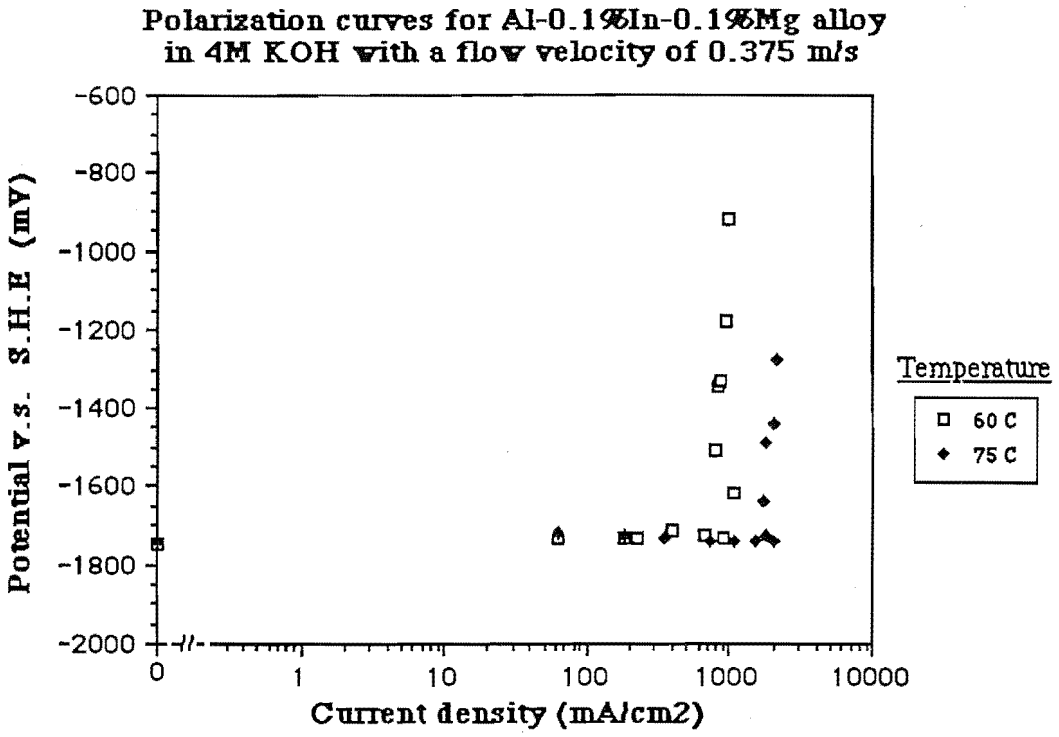
Polarization curves for Al-0.1%In-0.1%Mg alloy
in 4M KOH with a flow velocity of 0.375 m/s
Potential v.s. S.H.E (mV)
-600
-800
-1000
-1200
-1400
-1600
-1800
-2000
0
1
10
100
1000
10000
Current density (mA/cm2)
Temperature
60 C
75 C

C 13.1

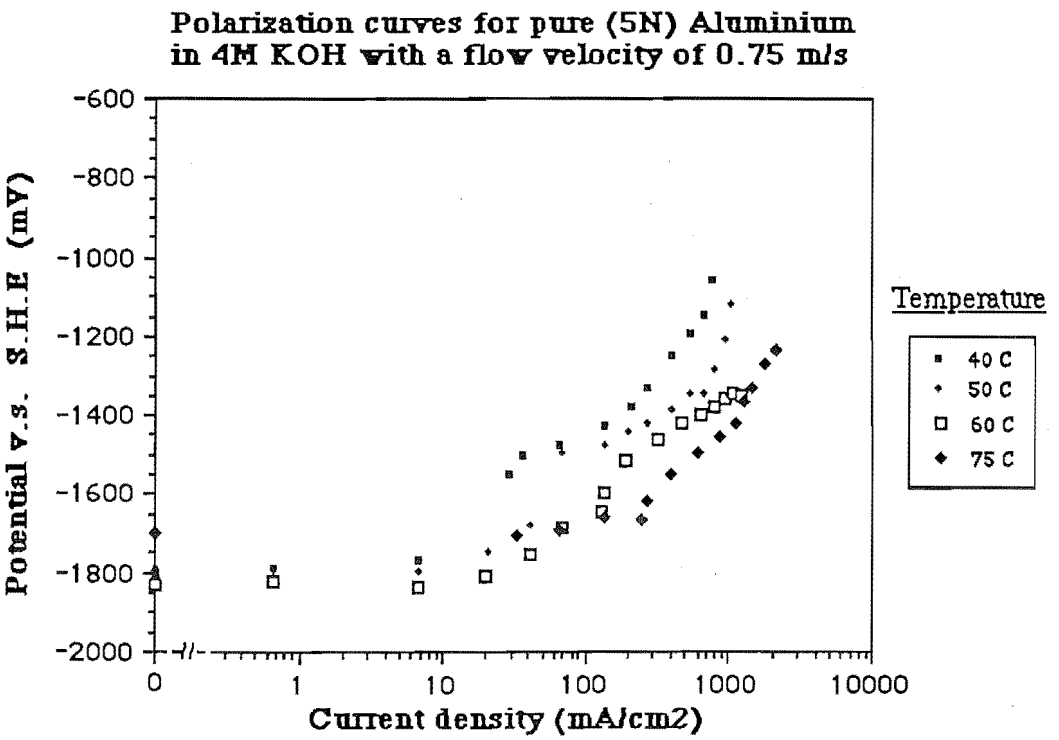
Polarization curves for pure (5N) Aluminium
in 4M KOH with a flow velocity of 0.75 m/s
Potential v.s. S.H.E (mV)
-600
-800
-1000
-1200
-1400
-1600
-1800
-2000
0
1
10
100
1000
10000
Current density (mA/cm2)
Temperature
40 C
50 C
60 C
75 C

C 13.2

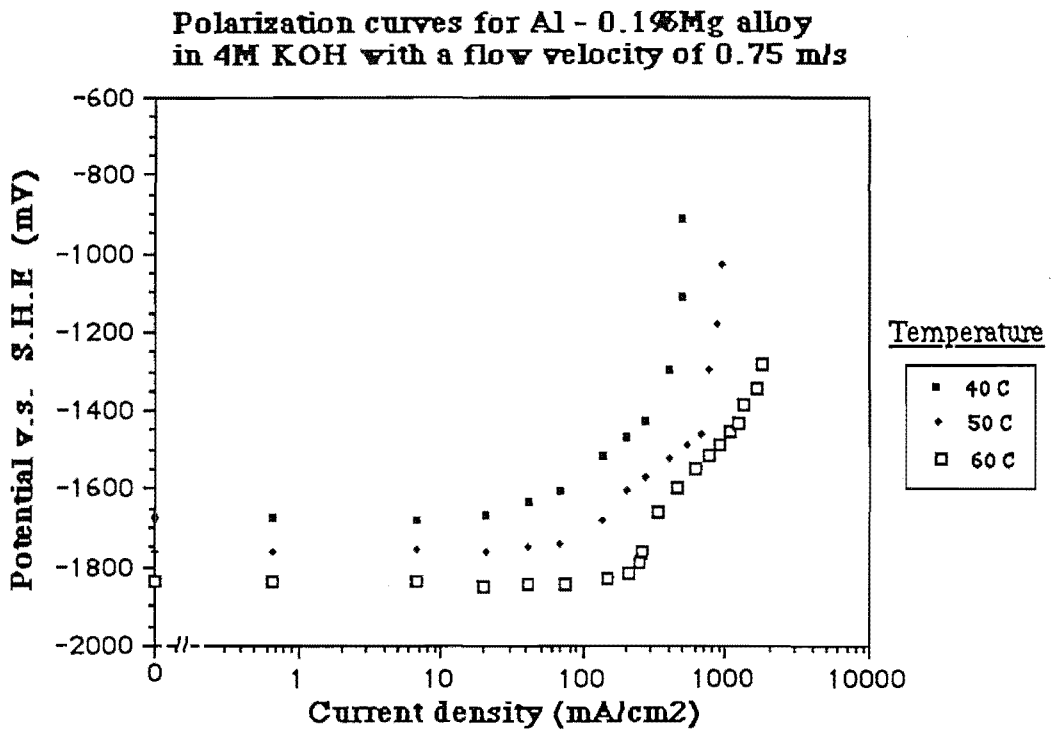
Polarization curves for Al - 0.1%Mg alloy
in 4M KOH with a flow velocity of 0.75 m/s
Potential v.s. S.H.E (mV)
-600
-800
-1000
-1200
-1400
-1600
-1800
-2000
0
1
10
100
1000
10000
Current density (mA/cm2)
Temperature
40 C
50 C
60 C

C 14.1

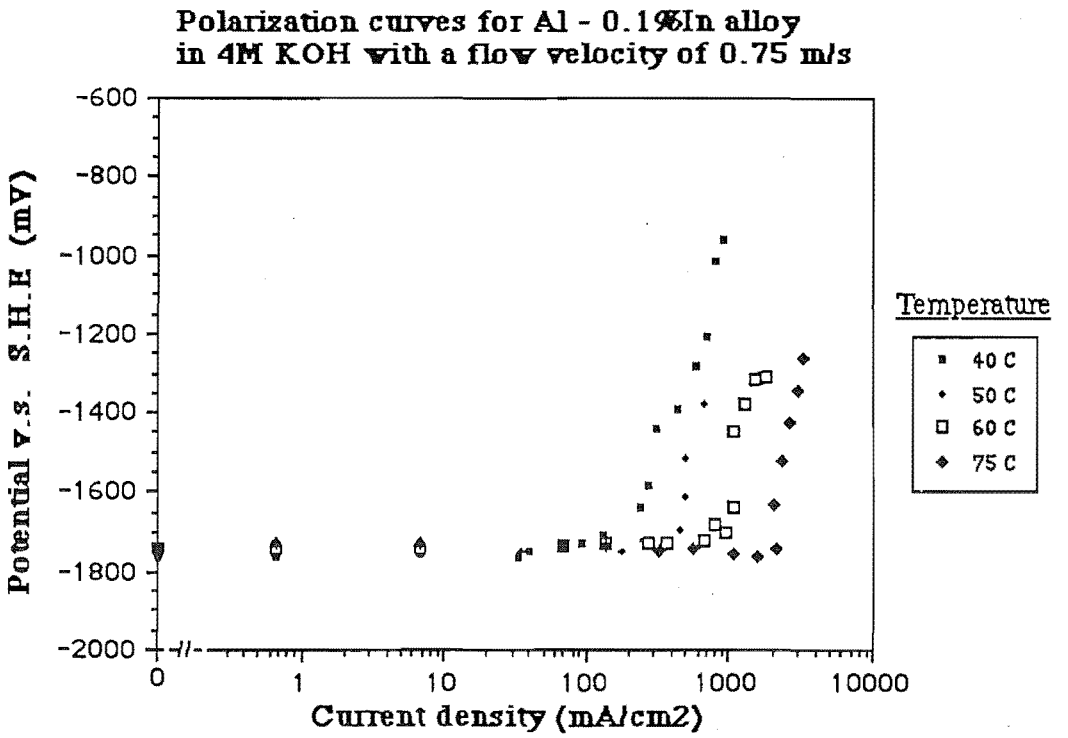
Polarization curves for Al - 0.1%In alloy
in 4M KOH with a flow velocity of 0.75 m/s
Potential v.s. S.H.E (mV)
-600
-800
-1000
-1200
-1400
-1600
-1800
-2000
0
1
10
100
1000
10000
Current density (mA/cm2)
Temperature
40 C
50 C
60 C
75 C

C 14.2

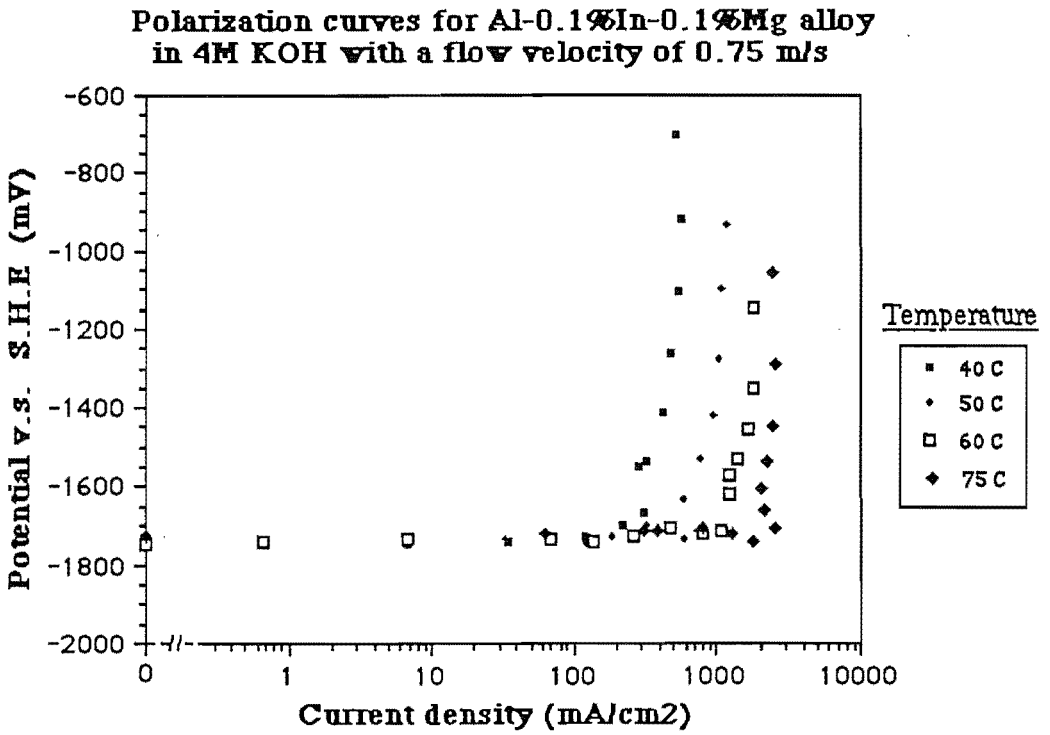
Polarization curves for Al-0.1%In-0.1%Mg alloy
in 4M KOH with a flow velocity of 0.75 m/s
Potential v.s. S.H.E (mV)
-600
-800
-1000
-1200
-1400
-1600
-1800
-2000
0
1
10
100
1000
10000
Current density (mA/cm2)
Temperature
40 C
50 C
60 C
75 C

C 15.2

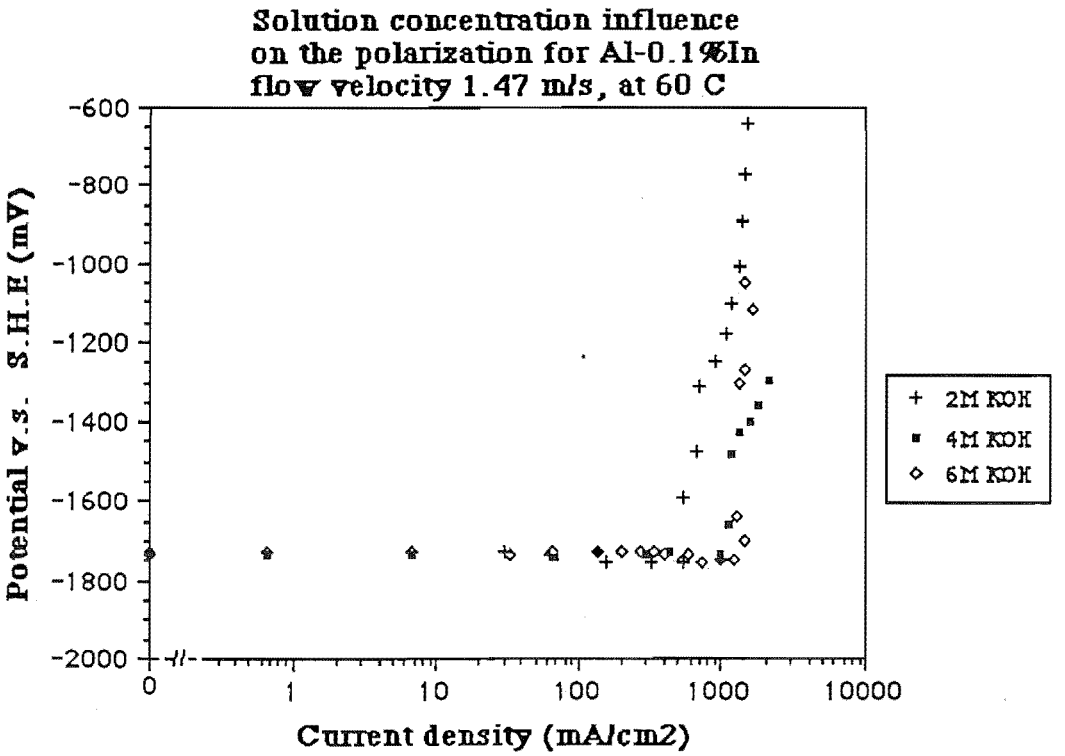
Solution concentration influence
on the polarization for Al-0.1%In
flow velocity 1.47 m/s, at 60 C
Potential v.s. S.H.E (mV)
-600
-800
-1000
-1200
-1400
-1600
-1800
-2000
0
1
10
100
1000
10000
Current density (mA/cm2)
2M KOH
4M KOH
6M KOH

C 15.2

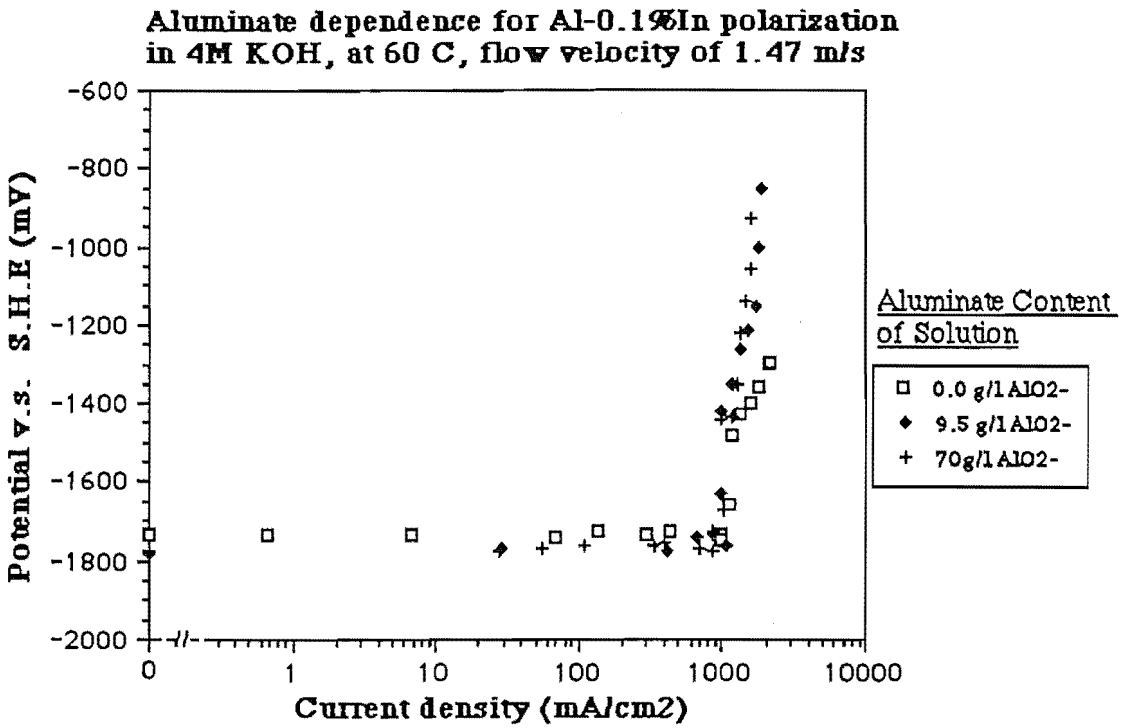
Aluminate dependence for Al-0.1%In polarization
in 4M KOH, at 60 C, flow velocity of 1.47 m/s
Potential v.s. S.H.E (mV)
-600
-800
-1000
-1200
-1400
-1600
-1800
-2000
0
1
10
100
1000
10000
Current density (mA/cm2)
Aluminate Content of Solution
0.0 g/l AlO2-
9.5 g/l AlO2-
70g/l AlO2-

C 16.1

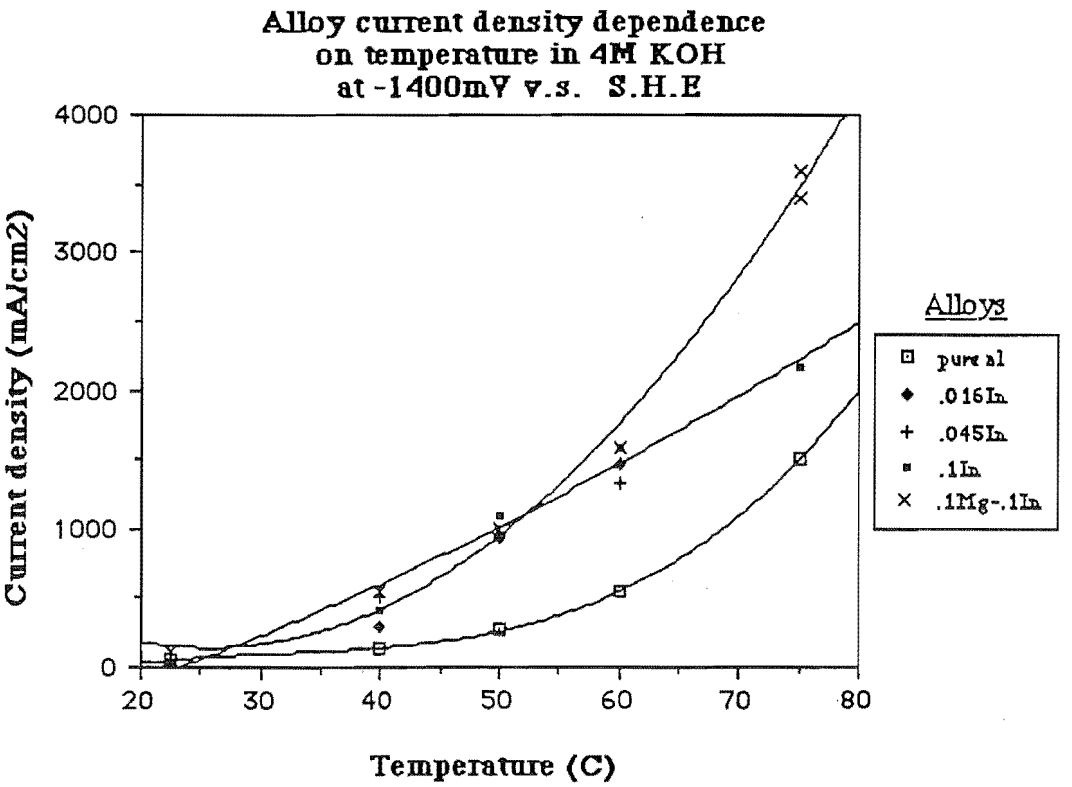
Alloy current density dependence
on temperature in 4M KOH
at -1400mV v.s. S.H.E
Current density (mA/cm2)
4000
3000
2000
1000
0
20
30
40
50
60
70
80
Temperature (C)
Alloys
pure al
.016In
.045In
.1In
.1Mg-.1In

C 16.2

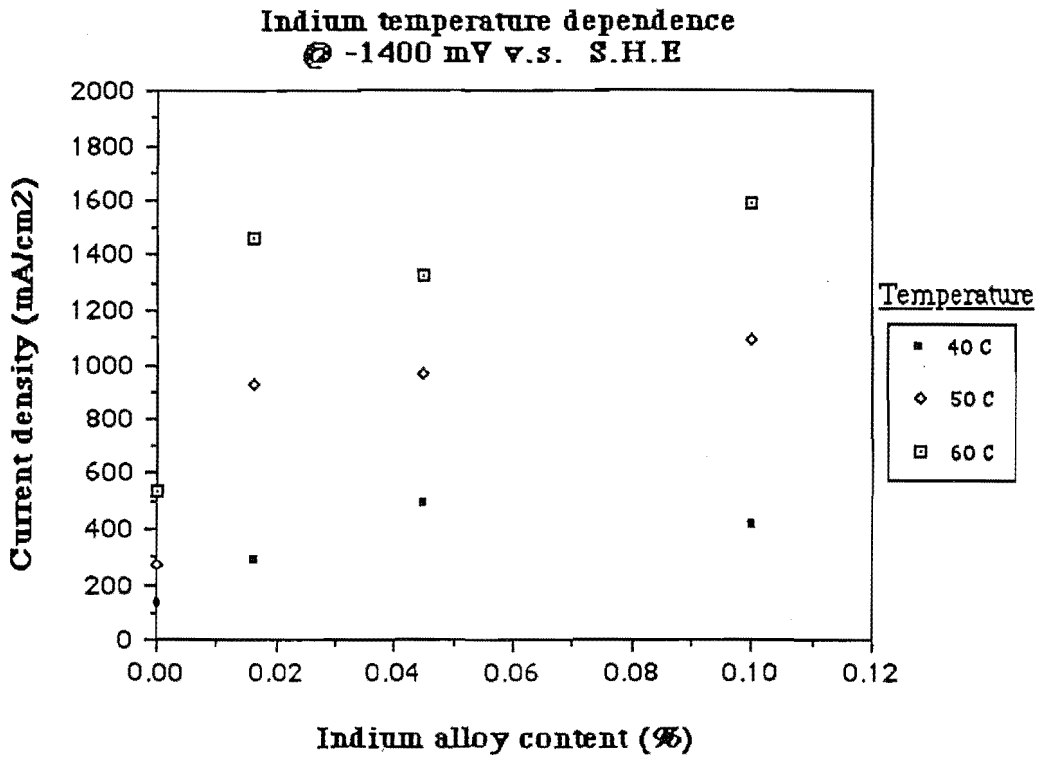
Indium temperature dependence
@ -1400 mV v.s. S.H.E
Current density (mA/cm2)
2000
1800
1600
1400
1200
1000
800
600
400
200
0
0.00
0.02
0.04
0.06
0.08
0.10
0.12
Indium alloy content (%)
Temperature
40 C
50 C
60 C

C 17.1

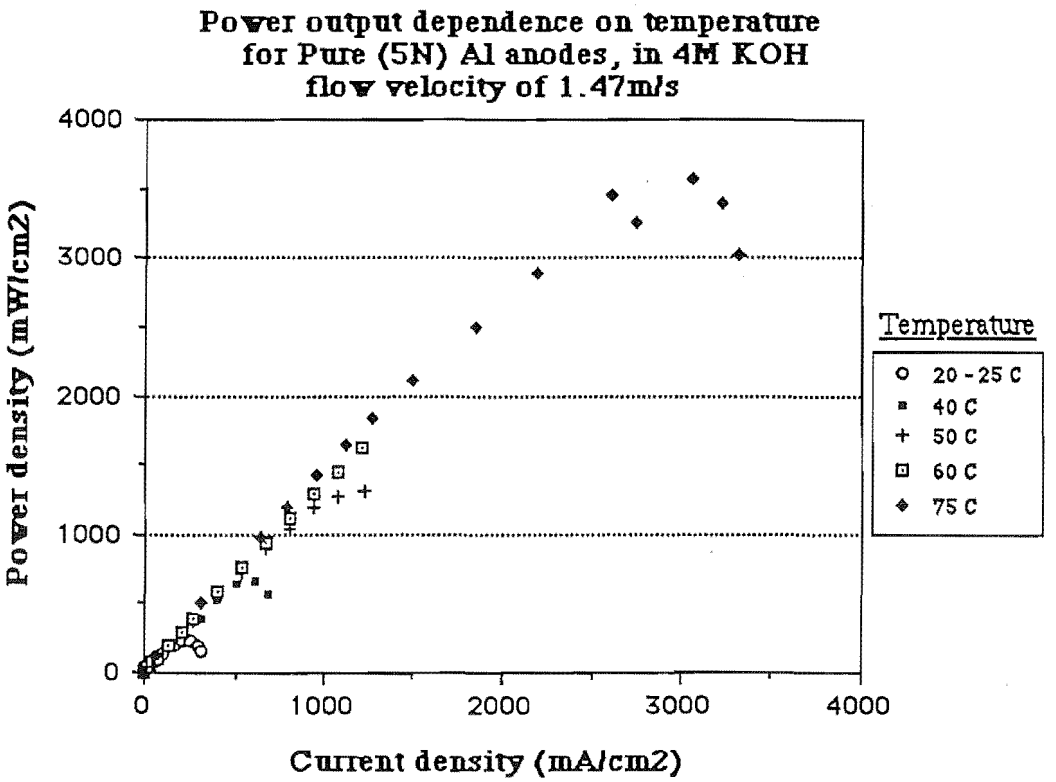
Power output dependence on temperature
for Pure (5N) Al anodes, in 4M KOH
flow velocity of 1.47m/s
Power density (mW/cm2)
4000
3000
2000
1000
0
0
1000
2000
3000
4000
Current density (mA/cm2)
Temperature
20 - 25 C
40 C
50 C
60 C
75 C

C 17.2

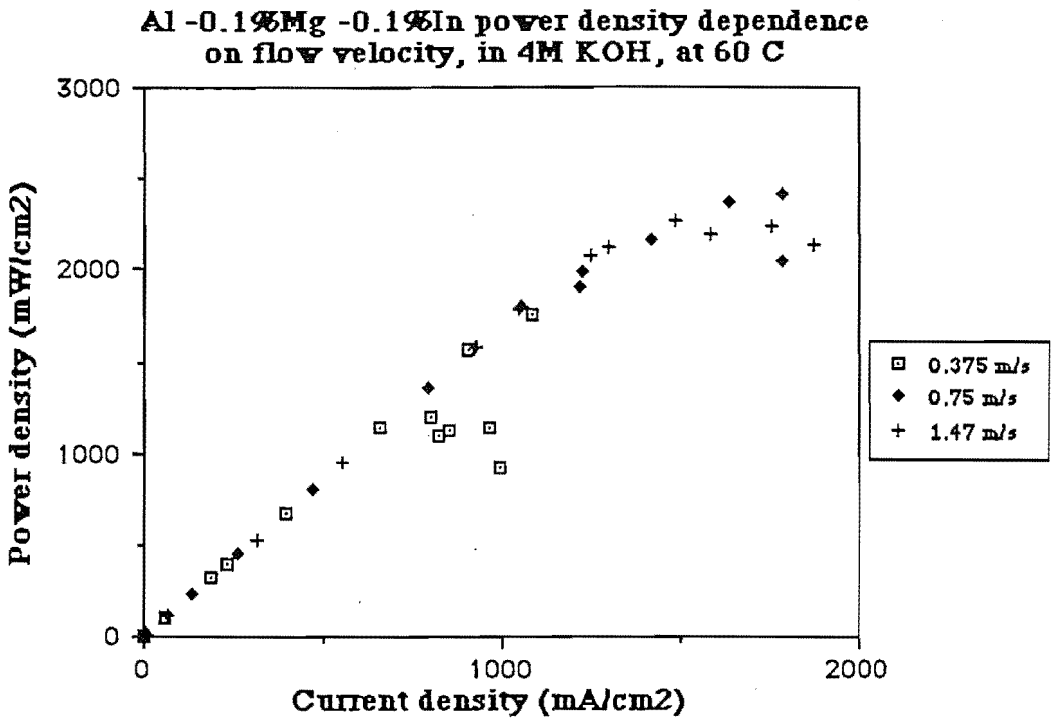
Al -0.1%Mg -0.1%In power density dependence
on flow velocity, in 4M KOH, at 60 C
Power density (mW/cm2)
Current density (mA/cm2)
0
1000
2000
3000
0.375 m/s
0.75 m/s
1.47 m/s

C 18.1

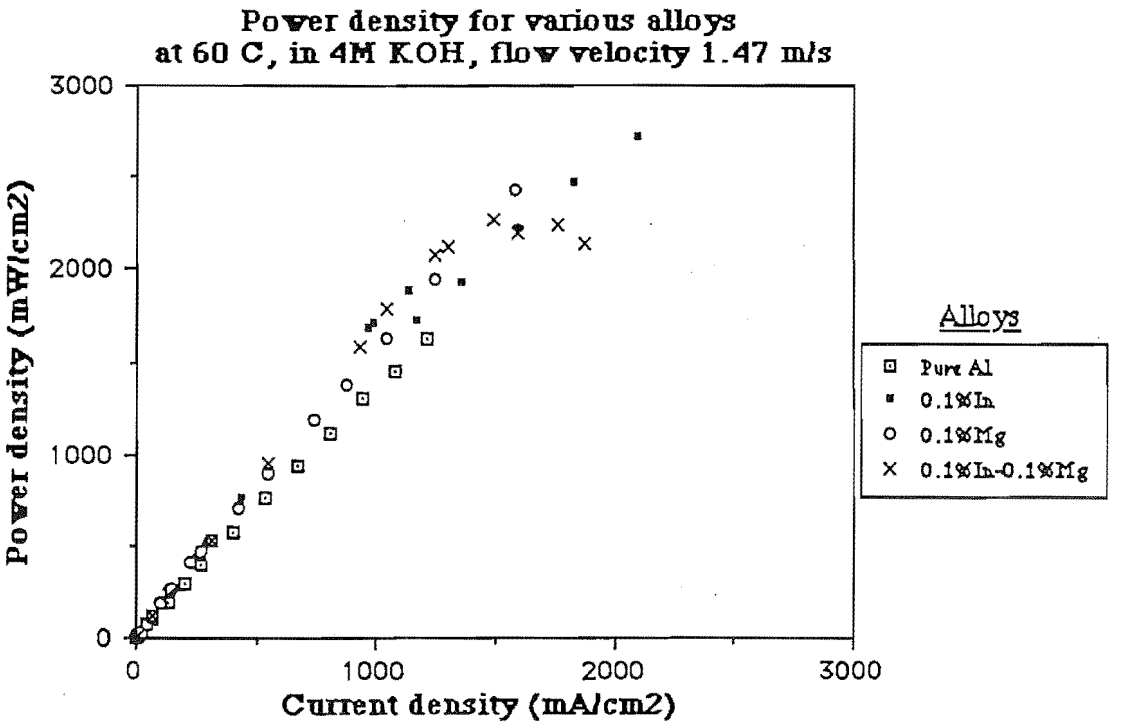
Power density for various alloys
at 60 C, in 4M KOH, flow velocity 1.47 m/s
Power density (mW/cm2)
Current density (mA/cm2)
0
1000
2000
3000
Alloys
Pure Al
0.1%In
0.1%Mg
0.1%In-0.1%Mg

C 18.2

APPENDIX.D

PERIODIC TABLE OF THE ELEMENTS

Table of Radioactive Isotopes

Naturally occurring radioactive isotopes are indicated by a blue mass number. Half lives are in parentheses where s, m, h, d and y stand for seconds, minutes, hours, days and years respectively. The symbols describing the mode of decay and resulting radiation are defined as follows:

α	alpha particle	L	L-electron capture
β^-	beta particle	SF	spontaneous fission
β^+	positron	γ	gamma ray
K	K-electron capture	e^-	internal electron conversion

Ac 227(22y)β^-,α
Ag 110(24s)β^-,γ 111(7.5d)β^-,γ
Am 241(458y)α,γ,e^- 242(16.0h)β^-,K,α,γ 243(8000y)α,γ
As 76(26.7h)β^-,γ 77(39h)β^-,γ
At 210(8.3h)K,α,γ 211(7.2h),Kα,γ
Au 198(2.69d)β^-,γ
Ba 131(12d)K,γ 133(7.2y)K,γ,e^-
Bi 210(5d)β^-,α
Bk 245(4.9d)K,α,γ 249(314d)β^-,α,SF
Br 82(36h)β^-,γ
C 14(5700 y)β^-
Ca 41(8x10^{4}y)K 45(165d)β^- 47(4.5d)β^-,γ
Cd 115(43d)β^-,γ
Ce 141(32d)β^-,γ 143(33h)β^-,γ 144(285d)β^-,γ
Cf 246(35h)α,γ,SF 249(360 y)α,γ,SF 251(800 y)γ
Cl 36(3x10^{5}y)β^-
Cm 243(35y),α,γ 245(9300y),α,γ 247(10^{7}y)
Co 58(71d),K,β^+,γ 60(5.27y)β^-,γ
Cr 51(27d),K,γ
Cs 134(2.0y)β^-,γ 135(3x10^{6}y)β^- 137(30y)β^-,γ
Cu 64(12.8h)K,β^-,β^+,γ
Es 253(20d)α,γ,SF 254(1y)α,SF
Eu 154(16y)β^-,γ 155(1.8y)β^-,γ
Fe 55(2.6y)K 59(45d)β^-,γ
Fm 255(20h)α
Fr 223(22m)β^-,γ,α
Ga 72(14.1h),β^-,γ
Gd 153(236d)K,γ,e^- 159(18h)β^-,γ
Ge 71(11d)K
H 3(12.3y)β^-
Hf 181(45d)β^-,γ,e^-
Hg 197(65h)K,γ,e^- 203(47d)β^-,γ,e^-
Ho 166(27.3h)β^-,γ
I 129(10^{7}y)β^+,γ,e 131(8.05d)β^-,γ
In 114(50d)γ
Ir 192(74.4d)β^-,γ
K 40(10^{9}y)β^+,K,γ 42(12.4h),β^-,γ
La 140(40.2h)β^-,γ
Lu 176(10^{10}y)β^-,K,γ 177(6.8d)β^-,γ
Md 256(90m)K,SF
Mo 99(67h)β^-,γ
Na 22(2.6y)β^+,K,γ 24(15h)β^-,γ
Nd 147(11.1d)β^-,γ
Ni 63(125y)β^- 59(8x10^{4}y),K
Np 237(2.2x10^{6}y)α,γ 239(2.33d)β^-,γ
Os 191(15d)β^-,γ,e^-
P 32(14.2d)β^-
Pa 231(34000y)α,γ
Pb 210(19.4y)β^-,γ,e^- 202(10^{5}y)L
Pd 103(17d)K,γ
Pm 147(2.6y)β^-
Po 210(138.4d)α,γ 209(103y)α,K,γ
Pr 143(13.8d)β^-
Pt 197(18h)β^-,γ
Pu 242(3.8 x 10^{5}y)α,SF 241(13y)β^-,α,γ 239(24300y)α,γ,SF
Ra 226(1620y)α,γ
Rb 86(18.6d)β^-,γ
Re 188(16.7h)β^-,γ 186(3.7d)β^-,γ
Rn 222(3.82d)α
Ru 103(40d)β^-,γ 97(2.9d),K,γ,e^-
S 35(88d)β^-
Sb 122(2.8d)β^-,K,β^+,γ 124(60d)β^-,γ
Sc 46(84d)β^-,γ
Se 75(120 d)K,γ
Sm 153(47h)β^-,γ 145(340d)K,γ
Sn 113(119d)K,L,γ,e^-
Sr 90(28y)β^- 89(51d)β^-,γ 85(64d)K,γ
Ta 182(115d)β^-,γ
Tb 160(73d)$\beta^-\gamma$
Tc 99(2x10^{5}y)β^- 97(10^{6}y)K
Te 127(9.3h)β^-
Th 232(1.4x10^{10}y)α,γ,SF 228(1.91y)β^-
Tl 204(3.81y)β^-,K
Tm 170(134d)β^-,γ,e^-
U 238(4.5x10^{9}y)α,γ,SF 234(2.5x10^{5}y)α,γ,SF 235(7.1x10^{8}y)α,γ,SF 233(1.6x10^{5}y)α,γ
W 185(75d)β^-
Y 90(64h)β^-,e^-
Yb 175(4.2d)β^-,γ 169(31d)K,γ,e^-
Zn 65(245d)K,β^+,γ
Zr 95(65d)β^-,γ,e^- 93(9x10^{5}y)β^-,γ

GROUP IA | IIA | IIIB | IVB | VB | VIB | VIIB | VIII | IB | IIB | IIIA | IVA | VA | VIA | VIIA | VIIIA

1 1.00797 −252.7 −259.2 0.071 1 **H** $1s^1$ Hydrogen																	2 4.0026 −268.9 −269.7 0.126 1 **He** $1s^1$ Helium
3 6.939 1330 180.5 0.53 1 **Li** $1s^2\,2s^1$ Lithium	4 9.0122 2770 1277 1.85 2 **Be** $1s^2\,2s^2$ Beryllium										5 10.811 — (2030) 2.34 3 **B** $1s^2\,2s^2\,2p^1$ Boron	6 12.01115 4830 3727 g 2.26 ±4,2 **C** $1s^2\,2s^2\,2p^2$ Carbon	7 14.0067 −195.8 −210 0.81 ±3,5,4,2 **N** $1s^2\,2s^2\,2p^3$ Nitrogen	8 15.9994 −183 −218.8 1.14 −2 **O** $1s^2\,2s^2\,2p^4$ Oxygen	9 18.9984 −188.2 −219.6 1.505 −1 **F** $1s^2\,2s^2\,2p^5$ Fluorine	10 20.183 −246 −248.6 1.20 **Ne** $1s^2\,2s^2\,2p^6$ Neon
11 22.9898 892 97.8 0.97 1 **Na** [Ne]$3s^1$ Sodium	12 24.312 1107 650 1.74 2 **Mg** [Ne]$3s^2$ Magnesium										13 26.9815 2450 660 2.70 3 **Al** [Ne]$3s^2 3p^1$ Aluminum	14 28.086 2680 1410 2.33 4 **Si** [Ne]$3s^2 3p^2$ Silicon	15 30.9738 280w 44.2w 1.82w ±3,5,4 **P** [Ne]$3s^2 3p^3$ Phosphorus	16 32.064 444.6 119.0 2.07 ±2,4,6 **S** [Ne]$3s^2 3p^4$ Sulfur	17 35.453 −34.7 −101.0 1.56 ±1,3,5,7 **Cl** [Ne]$3s^2 3p^5$ Chlorine	18 39.948 −185.8 −189.4 1.40 **Ar** [Ne]$3s^2 3p^6$ Neon
19 39.102 760 63.7 0.86 1 **K** [Ar]$4s^1$ Potassium	20 40.08 1440 838 1.55 2 **Ca** [Ar]$4s^2$ Calcium	21 44.956 2730 1539 3.0 3 **Sc** [Ar]$3d^1 4s^2$ Scandium	22 47.90 3260 1668 4.51 4,3 **Ti** [Ar]$3d^2 4s^2$ Titanium	23 50.942 3450 1900 6.1 5,4,3,2, **V** [Ar]$3d^3 4s^2$ Vanadium	24 51.996 2665 1875 7.19 6,3,2 **Cr** [Ar]$3d^5 4s^1$ Chromium	25 54.938 2150 1245 7.43 7,6,4,2,3 **Mn** [Ar]$3d^5 4s^2$ Manganese	26 55.847 3000 1536 7.86 2, 3 **Fe** [Ar]$3d^6 4s^2$ Iron	27 58.933 2900 1495 8.9 2, 3 **Co** [Ar]$3d^7 4s^2$ Cobalt	28 58.71 2730 1453 8.9 2,3 **Ni** [Ar]$3d^8 4s^2$ Nickel	29 63.54 2595 1083 8.96 2,1 **Cu** [Ar]$3d^{10} 4s^1$ Copper	30 65.37 906 419.5 7.14 2 **Zn** [Ar]$3d^{10} 4s^2$ Zinc	31 69.72 2237 29.8 5.91 3 **Ga** [Ar]$3d^{10} 4s^2 4p^1$ Gallium	32 72.59 2830 937.4 5.32 4 **Ge** [Ar]$3d^{10} 4s^2 4p^2$ Germanium	33 74.922 613s 817 5.72 ±3,5 **As** [Ar]$3d^{10} 4s^2 4p^3$ Arsenic	34 78.96 685 217 4.79 −2,4,6 **Se** [Ar]$3d^{10} 4s^2 4p^4$ Selenium	35 79.909 58 −7.2 3.12 ±1,5 **Br** [Ar]$3d^{10} 4s^2 4p^5$ Bromine	36 83.80 −152 −157.3 2.6 **Kr** [Ar]$3d^{10} 4s^2 4p^6$ Krypton
37 85.47 688 38.9 1.53 1 **Rb** [Kr]$5s^1$ Rubidium	38 87.62 1380 768 2.6 2 **Sr** [Kr]$5s^2$ Strontium	39 88.905 2927 1509 4.47 3 **Y** [Kr]$4d^1 5s^2$ Yttrium	40 91.22 3580 1852 6.49 4 **Zr** [Kr]$4d^2 5s^2$ Zirconium	41 92.906 3300 2468 8.4 5,3 **Nb** [Kr]$4d^4 5s^1$ Niobium	42 95.94 5560 2610 10.2 6,5,4,3,2 **Mo** [Kr]$4d^5 5s^1$ Molybdenum	43 (98) — 2140 11.5 7 **Tc** [Kr]$4d^5 5s^2$ Technetium	44 101.07 4900 2500 12.2 2,3,4,6,8 **Ru** [Kr]$4d^7 5s^1$ Ruthenium	45 102.905 4500 1966 12.4 2,3,4 **Rh** [Kr]$4d^8 5s^1$ Rhodium	46 106.4 3980 1552 12.0 2,4 **Pd** [Kr]$4d^{10} 5s^0$ Palladium	47 107.870 2210 960.8 10.5 1 **Ag** [Kr]$4d^{10} 5s^1$ Silver	48 112.40 765 320.9 8.65 2 **Cd** [Kr]$4d^{10} 5s^2$ Cadmium	49 114.82 2000 156.2 7.31 3 **In** [Kr]$4d^{10} 5s^2 5p^1$ Indium	50 118.69 2270 231.9 7.30 4,2 **Sn** [Kr]$4d^{10} 5s^2 5p^2$ Tin	51 121.75 1380 630.5 6.62 ±3,5 **Sb** [Kr]$4d^{10} 5s^2 5p^3$ Antimony	52 127.60 989.8 449.5 6.24 −2,4,6 **Te** [Kr]$4d^{10} 5s^2 5p^4$ Tellurium	53 126.904 183 113.7 4.94 ±1,5,7 **I** [Kr]$4d^{10} 5s^2 5p^5$ Iodine	54 131.30 −108.0 −111.9 3.06 **Xe** [Kr]$4d^{10} 5s^2 5p^6$ Xenon
55 132.905 690 28.7 1.90 1 **Cs** [Xe]$6s^1$ Cesium	56 137.34 1640 714 3.5 2 **Ba** [Xe]$6s^2$ Barium	57 138.91 3470 920 6.17 3 ★ **La** [Xe]$5d^1 6s^2$ Lanthanum	72 178.49 5400 2222 13.1 4 **Hf** [Xe]$4f^{14} 5d^2 6s^2$ Hafnium	73 180.948 5425 2996 16.6 5 **Ta** [Xe]$4f^{14} 5d^3 6s^2$ Tantalum	74 183.85 5930 3410 19.3 6,5,4,3,2 **W** [Xe]$4f^{14} 5d^4 6s^2$ Wolfram	75 186.2 5900 3180 21.0 7,6,4,2,−1 **Re** [Xe]$4f^{14} 5d^5 6s^2$ Rhenium	76 190.2 5500 3000 22.6 2,3,4,6,8 **Os** [Xe] $4f^{14} 5d^6 6s^2$ Osmium	77 192.2 5300 2454 22.5 2,3,4,6 **Ir** [Xe]$4f^{14} 5d^7 6s^2$ Iridium	78 195.09 4530 1769 21.4 2, 4 **Pt** [Xe] $4f^{14}\ 5d^9\ 6s^1$ Platinum	79 196.967 2970 1063 19.3 3,1 **Au** [Xe]$4f^{14} 5d^{10} 6s^1$ Gold	80 200.59 357 −38.4 13.6 2,1 **Hg** [Xe]$4f^{14} 5d^{10} 6s^2$ Mercury	81 204.37 1457 303 11.85 3, 1 **Tl** [Xe]$4f^{14} 5d^{10} 6s^2 6p^1$ Thallium	82 207.19 1725 327.4 11.4 4, 2 **Pb** [Xe]$4f^{14} 5d^{10} 6s^2 6p^2$ Lead	83 208.980 1560 271.3 9.8 3,5 **Bi** [Xe]$4f^{14} 5d^{10} 6s^2 6p^3$ Bismuth	84 (210) — 254 (9.2) 2,4 **Po** [Xe]$4f^{14} 5d^{10} 6s^2 6p^4$ Polonium	85 (210) — (302) — ±1,3,5,7 **At** [Xe]$4f^{14} 5d^{10} 6s^2 6p^5$ Astatine	86 (222) — (−61.8) (−71) — **Rn** [Xe]$4f^{14} 5d^{10} 6s^2 6p^6$ Radon
87 (223) — (27) — 1 **Fr** [Rn]$7s^1$ Francium	88 (226) — 700 5.0 2 **Ra** [Rn]$7s^2$ Radium	89 (227) — 1050 — 3 ★★ **Ac** [Rn]$6d^1 7s^2$ Actinium	104														

★	58 140.12 3468 795 6.67 3,4 **Ce** [Xe]$4f^2 5d^0 6s^2$ Cerium	59 140.907 3127 935 6.77 3,4 **Pr** [Xe] $4f^3 5d^0 6s^2$ Praseodymium	60 144.24 3027 1024 7.00 3 **Nd** [Xe] $4f^4 5d^0 6s^2$ Neodymium	61 (147) — (1027) 3 **Pm** [Xe] $4f^5 5d^0 6s^2$ Promethium	62 150.35 1900 1072 7.54 3,2 **Sm** [Xe] $4f^6 5d^0 6s^2$ Samarium	63 151.96 1439 826 5.26 3,2 **Eu** [Xe] $4f^7 5d^0 6s^2$ Europium	64 157.25 3000 1312 7.89 3 **Gd** [Xe]$4f^7 5d^1 6s^2$ Gadolinium	65 158.924 2800 1356 8.27 3,4 **Tb** [Xe]$4f^9 5d^0 6s^2$ Terbium	66 162.50 2600 1407 8.54 3 **Dy** [Xe] $4f^{10} 5d^0 6s^2$ Dysprosium	67 164.930 2600 1461 8.80 3 **Ho** [Xe]$4f^{11} 5d^0 6s^2$ Holmium	68 167.26 2900 1497 9.05 3 **Er** [Xe] $4f^{12} 5d^0 6s^2$ Erbium	69 168.934 1727 1545 9.33 3,2 **Tm** [Xe]$4f^{13} 5d^0 6s^2$ Thulium	70 173.04 1427 824 6.98 3,2 **Yb** [Xe]$4f^{14} 5d^0 6s^2$ Ytterbium	71 174.97 3327 1652 9.84 3 **Lu** [Xe] $4f^{14} 5d^1\ 6s^2$ Lutetium
★★	90 232.038 3850 1750 11.7 4 **Th** [Rn] $5f^0\ 6d^2\ 7s^2$ Thorium	91 (231) — (1230) 15.4 5,4 **Pa** [Rn]$5f^2 6d^1 7s^2$ Protactinium	92 238.03 3818 1132 19.07 6,5,4,3 **U** [Rn]$5f^3 6d^1 7s^2$ Uranium	93 (237) — 637 19.5 6,5,4,3 **Np** [Rn] $5f^4\ 6d^1\ 7s^2$ Neptunium	94 (242) — 3235 640 — 6,5,4,3 **Pu** [Rn]$5f^6 6d^0 7s^2$ Plutonium	95 (243) — — 11.7 6,5,4, 3 **Am** [Rn]$5f^7 6d^0 7s^2$ Americium	96 (247) — — — 3 **Cm** [Rn]$5f^7 6d^1 7s^2$ Curium	97 (247) — — — 4,3 **Bk** [Rn] $5f^9\ 6d^0\ 7s^2$ Berkelium	98 (249) — — — 3 **Cf** [Rn] $5f^{10}\ 6d^0\ 7s^2$ Californium	99 (254) — — — — **Es** [Rn] $5f^{11}\ 6d^0\ 7s^2$ Einsteinium	100 (253) — — — — **Fm** [Rn] $5f^{12}\ 6d^0\ 7s^2$ Fermium	101 (256) — — — — **Md** [Rn] $5f^{13}\ 6d^0\ 7s^2$ Mendelevium	102 (254) — — — — **No** [Rn] $5f^{14}\ 6d^0\ 7s^2$ Nobelium	103 (257) — — — — **Lw** [Rn] $5f^{14}\ 6d^1\ 7s^2$ Lawrencium

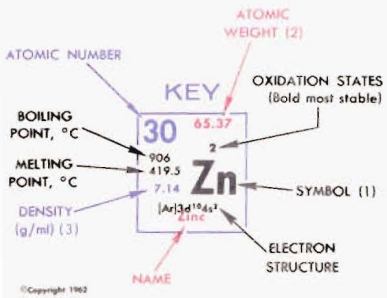

NOTES:

(1) Black — solid.
Red — gas.
Blue — liquid.
Outline — synthetically prepared.

(2) Based upon carbon – 12. ( ) indicates most stable or best known isotope.

(3) Values for gaseous elements are for liquids at the boiling point.

SARGENT-WELCH
SARGENT-WELCH SCIENTIFIC COMPANY
7300 LINDER AVENUE, SKOKIE, ILLINOIS 60076
CHICAGO • CINCINNATI • CLEVELAND • DETROIT • DALLAS • DENVER

TABLE OF PERIODIC PROPERTIES OF THE ELEMENTS

Percent Ionic Character of a Single Chemical Bond

Difference in electronegativity	0.1	0.2	0.3	0.4	0.5	0.6	0.7	0.8	0.9	1.0	1.1	1.2	1.3	1.4	1.5	1.6	1.7	1.8	1.9	2.0	2.1	2.2	2.3	2.4	2.5	2.6	2.7	2.8	2.9	3.0	3.1	3.2
Percent ionic character %	0.5	1	2	4	6	9	12	15	19	22	26	30	34	39	43	47	51	55	59	63	67	70	74	76	79	82	84	86	88	89	91	92

Sub-Atomic Particles

	Electron	Positron	Proton	Neutron	Photon	Neutrino	Meson					Hyperon				
Symbol	e^-, β^-	e^+, β^+	p	n	γ	ν	$\mu^\pm$	$\pi^\pm$	π^0	K^+	K^0	Λ^0	Σ^+	Σ^-	Ξ^-	Ω^-
Mass*	1	1	1836.12	1838.65	0	~0	206.84	273.23	264.4	966.6	974.4	2181.4	2327.7	2343.2	2584	1686
Charge**	−1	+1	+1	0	0	0	±1	±1	0	+1	0	0	+1	−1	−1	−1
Spin	½	½	½	½	1	½	½	0	0	0	0	½	½-integral	½-integral	½-integral	
Magnetic Moment	1.00 B.m.	1.00 B.m.	2.793 n.m.	−1.913 n.m.	0	~0		0	0							
Mean Life (sec.)	stable	stable	stable	1.11×10^{3}	stable	stable	2.22×10^{-6}	2.54×10^{-8}	$\sim10^{-15}$	$\sim10^{-8}$	$\sim10^{-10}$–10^{-7}	2.8×10^{-10}	$\sim5\times10^{-11}$	$\sim10^{-10}$	$\sim10^{-10}$	$\sim10^{-9}$
Decay Modes				$\rightarrow p+e^-+\bar{\nu}$			$\rightarrow e^\pm+\nu+\bar{\nu}$	$\rightarrow\mu^\pm+\nu$	$\rightarrow\gamma+\gamma$ $\rightarrow e^+ + e^- + \gamma$	complex	complex	$\rightarrow p+\pi^-$ $\rightarrow n+\pi^0$	$\rightarrow p+\pi^0$ $\rightarrow n+\pi^+$	$\rightarrow n+\pi^-$	$\rightarrow\Lambda^0+\pi^-$	$\pi^-+\Xi$

B.m. = Bohr magneton n.m. = Nuclear magneton *In units of 9.1083×10^{-31} kg. **In units of 4.80286×10^{-10} esu. †Exists as an antiparticle not listed.

GROUP IA	IIA	IIIB	IVB	VB	VIB	VIIB	VIII			IB	IIB	IIIA	IVA	VA	VIA	VIIA	VIIIA
H												B	C	N	O	F	He
Li	Be	Sc	Ti	V	Cr	Mn	Fe	Co	Ni	Cu	Zn	Ga	Ge	As	Se	Br	Ne
Na	Mg											Al	Si	P	S	Cl	Ar
K	Ca	Sc	Ti	V	Cr	Mn	Fe	Co	Ni	Cu	Zn	Ga	Ge	As	Se	Br	Kr
Rb	Sr	Y	Zr	Nb	Mo	Tc	Ru	Rh	Pd	Ag	Cd	In	Sn	Sb	Te	I	Xe
Cs	Ba	La	Hf	Ta	W	Re	Os	Ir	Pt	Au	Hg	Tl	Pb	Bi	Po	At	Rn
Fr	Ra	Ac**															

★	Ce	Pr	Nd	Pm	Sm	Eu	Gd	Tb	Dy	Ho	Er	Tm	Yb	Lu
★★	Th	Pa	U	NP	Pu	Am	Cm	Bk	Cf	Es	Fm	Md	No	Lw

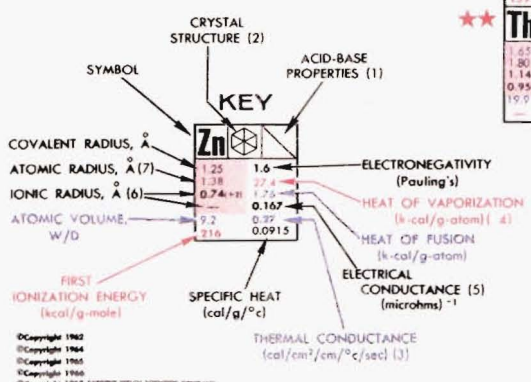

NOTES:

(1) For representative oxides (higher valence) of group. Oxide is acidic if color is red, basic if color is blue and amphoteric if both colors are shown. Intensity of color indicates relative strength.

(2) Cubic, face centered; cubic, body centered; diamond; cubic; hexagonal; rhombohedral; tetragonal; orthorhombic; monoclinic.

(3) At room temperature. (4) At boiling point. (5) From 0° to 20°C.

(6) Ionic (crystal) radii for coordination number 6.

(7) Metallic radii for coordination number of 12.

SARGENT-WELCH
SARGENT-WELCH SCIENTIFIC COMPANY
7300 LINDER AVENUE, SKOKIE, ILLINOIS 60076
CHICAGO • CINCINNATI • CLEVELAND • DETROIT • DALLAS • DENVER
BIRMINGHAM • SPRINGFIELD, N. J. • ANAHEIM, CALIF. • TORONTO, CANADA

Catalog Number S-18806 SIDE 2

APPENDIX.E

The Butler - Volmer Equation Derivation:

The following derivation is similiar to that given by Atkins (74). Assumptions in this derivation are, the rate determining step is a single electron transfer process, and that the charge transfer is described via a Boltzmann distribution.

$$k = A.\exp(\frac{-E_a}{RT}) \qquad \text{eqn (1)}$$

Starting with the Arrhenius rate law equation for the reaction of chemicals at a specific temperature, an analogy can be drawn. E_a , the activation energy for reaction changes to ΔG^*_m the molar Gibbs function for activation (i.e. * indicates the transition state), and the constant 'A' changes to constant 'B' which will be defined later in this appendix.

$$k = B.\exp(\frac{-\Delta G^*_m}{RT}) \qquad \text{eqn (2)}$$

[Ox],[Red] = concentration of the oxidised and reduced species in the bulk solution.

For a **single** electron transfer the charge passed for a unit amount of product is $e^-.L = F$ (Faraday's constant 96520 Coul / mol)

Current density forward reaction $(I_{for}) = F.k_{red}.[Ox]$
Current density reverse reaction $(I_{rev}) = F.k_{ox}.[Red]$

Let $k_{red} = k_c$ ('c' for cathodic reaction)
and $k_{ox} = k_a$ ('a' for anodic reaction)

Net current density (I) $= I_{for} - I_{rev}$ eqn (3)
$= F.k_{red}.[Ox] - F.k_{ox}.[Red]$

substituting for 'k'

$$I = B_c\, F[Ox].\exp(\frac{-\Delta G^*_{m.c}}{RT}) - B_a\, F[Red].\exp(\frac{-\Delta G^*_{m.a}}{RT}) \qquad \text{eqn (4)}$$

This is the net current density with no potential difference between the solution and metal surface.

Let $\Phi(m)$ = the potential of the metal
and $\Phi(s)$ = the potential of the solution.
Therefore $\Delta\Phi = \Phi(m) - \Phi(s)$: the potential difference across the double layer.

The work required to bring one electron across the charged double layer = $e^{-}.\Delta\Phi$
Therefore the work for unit amount of product = $F.\Delta\Phi$

Let it be assumed that $\Delta\Phi > 0$, thus required to do work to bring the oxidised species to the transition state within the double layer.
α = the transfer coefficient or symmetry factor
if $\alpha = 0$ the transition state is at the outer boundary of the double layer,
if $\alpha = 1$ the transition state is at the electrode surface.

Thus the Activation Gibbs function for reduction is increased by $\alpha .F.\Delta\Phi$
and that for the oxidation is increased by $((1-\alpha).(-F.\Delta\Phi))$
adding these into equation (4) gives

$$I = B_c F[Ox]\exp\left(\frac{-(\Delta G^{*}_{m.c} + \alpha .F.\Delta\Phi)}{RT}\right) - B_a F[Red].\exp\left(\frac{-(\Delta G^{*}_{m.a} + (1-\alpha)(-F.\Delta\Phi))}{RT}\right) \qquad \text{eqn (5)}$$

at equilibrium $\Delta\Phi = \Delta\Phi_e$ and $I = 0$
therefore $I_{c,e} = I_{a,e} = I_o$ (the exchange current density)

$$I_o = B_a F[Red].\exp\left(\frac{-(\Delta G^{*}_{m.a} + (1-\alpha)(-F.\Delta\Phi_e))}{RT}\right) \qquad \text{eqn (6)}$$

$$= B_c F[Ox]\exp\left(\frac{-(\Delta G^{*}_{m.c} + \alpha .F.\Delta\Phi_e)}{RT}\right) \qquad \text{eqn (7)}$$

If a Boltzmann distribution has been assumed, it is found that
$B_a = B_c = \frac{kT}{h}$ where

k is Boltzmann's constant
T is the absolute temperature
h is Planck's constant

Thus I_o increases proportionally with any increase in temperature, which directly increases 'I', given that $\Delta\Phi$ is held constant.

I_o will also increase as temperature increases given the (-1/T) exponential relationship with temperature that also exists.

Let $\eta = \Delta\Phi - \Delta\Phi_e$ = overpotential

thus rearranging the above equation to give $\Delta\Phi = \eta + \Delta\Phi_e$

and substituting this into equation (5).

$$I = I_o.[\exp(\frac{-(\alpha .F.\eta)}{RT}) - .\exp(\frac{((1-\alpha).F.\eta)}{RT})] \qquad \text{eqn (8)}$$

for a single electron transfer.

If 'z' is the number of electrons transfered in the reaction the equation (8) becomes:

$$I = I_o.[\exp(\frac{-(\alpha.z.F.\eta)}{RT}) - .\exp(\frac{((1-\alpha).z.F.\eta)}{RT})] \qquad \text{eqn (9)}$$

for a multiple electron transfer.

APPENDIX.F

The equilibrium Potential Equation Derivation

This derivation follows that of Pourbaix (67) for the establishment of pH - potential diagrams. The standard dissolution reaction for aluminium in alkaline solutions is

$$Al + 4\,OH^- \longrightarrow Al(OH)_4^- + 3e^- \qquad \text{eqn (1)}$$

but in establishing the potential - pH relationship it is better to represent the above equation in the following way

$$Al + 2H_2O \longrightarrow AlO_2^- + 4H^+ + 3e^- \qquad \text{eqn (2)}$$

It is assumed that the potential is measured with respect to the standard hydrogen electrode.
By definition the equilibrium reaction potential is

$E^o = \frac{A^*}{zF}$ where 'A^*' is the chemical affinity of the reaction
'z' is the number of electrons transferred
'F' is faradays constant

$A^* = -\sum \nu\mu$ 'ν' is the stoichiometric reaction coefficient
'μ' is the chemical potential

Now calculating the potential equation via eqn (2)

$$E^o = - \frac{(\mu_{Al} + 2\mu_{H2O} - \mu_{AlO2-} - 4\mu_{H+} + (3\mu_{H+} - \frac{3}{2}\mu_{H2}))}{3F} \qquad \text{eqn(3)}$$

$$\mu_i = \mu_i^o(T,p) + RT \ln A_i \qquad \text{eqn(4)}$$
$$= \mu_i^o(T,p) + 2.3RT \log A_i \qquad \text{eqn(5)}$$

By convention $2\mu_{H+} - \mu_{H2} = 0$ at all temperatures
but at 25°C $\mu^o_{H+} = 0$, $\mu^o_{H2} = 0$.
It is also noted that for any element in its normal molecular state at 25°C $\mu = 0$; therefore $\mu_{Al} = 0$.

$$A_{H2O} = \frac{\text{vap. pressure solution}}{\text{vap. pressure solvent}} \cong 1; \qquad A_{Al} \cong 1$$

Substituting eqn (5) into eqn (3), and applying the appropriate conditions

$$E^o = \frac{\mu^o_{AlO2^-} - 2\mu^o_{H2O}}{3F} + \frac{2.3RT}{3F} \log A_{AlO2^-} . A^4_{H+} \qquad \text{eqn(6)}$$

$$E^o_o = \frac{\mu^o_{AlO2^-} - 2\mu^o_{H2O}}{3F}$$ the standard equilibrium potential

$$= \frac{-839770\ J - 2 * -237191\ J}{96487\ Coul.mol^{-1} * 3\ mol\ e^-\text{'s}}$$

$$= -1.262V$$

as $pH = -\log A_{H+}$ and $\frac{2.3RT}{F} = 0.059V$ @ 25°C

$$E^o = E^o_o + \frac{2.3RT}{3F} \log A_{AlO2^-} - \frac{9.2RT}{3F} pH \qquad \text{eqn (7)}$$

This equation predicts the effect on the equilibrium potential for changing AlO_2^- concentration, pH and temperature.

APPENDIX.G

The Corrosion Current & Current Efficiency Calculation

Corrosion Current:

The corrosion current is calculated from weight loss measurements of the electrode which has been placed in the flowcell apparatus under no load conditions.

Weight loss (g) = weight of electrode before - weight of electrode after

It is assumed that 3 electrons are liberated per aluminium atom that goes into solution.

$$\text{Corrosion Current (amp)} = \frac{\text{weight loss}}{\text{Mr (Al)}} * \frac{3 \text{ e's}}{\text{mol Al}} * \frac{96500 \text{ Coul}}{\text{mol e's}} * \frac{1}{\text{expt duration (s)}}$$

This can be divided by the surface area of the electrode to give the result in terms of current density.

Current Efficiency:

The current efficiency is calculated by firstly calculating the charge passed to the electrode over the duration of the experiment from measurements of the applied current, then comparing this with the faradaic charge required from the weight loss measurements.

$$\text{Charge from weight loss (coul)} = \frac{\text{weight loss (g)}}{\text{Mr (Al)}} * \frac{3 \text{ e's}}{\text{mol Al}} * \frac{96500 \text{ Coul}}{\text{mol e's}}$$

$$\text{Actual charge passed (coul)} = \sum (\text{Current (amp)} * \text{duration of current application (s)})$$

N.B. Over a single experimental run the current might be varied over several orders of magnitude for various lengths of time.

$$\text{Current Efficiency (\%)} = \frac{\text{Actual charge passed}}{\text{Charge from weight loss}} * 100$$